2016

The Role of Upper Ocean Heat Content and Sea Surface Temperature on Northeast Pacific Hurricane Evolution during Average and Active Years

Victoria Lauren Ford
Louisiana State University and Agricultural and Mechanical College

THE ROLE OF UPPER OCEAN HEAT CONTENT AND SEA SURFACE TEMPERATURE ON NORTHEAST PACIFIC HURRICANE EVOLUTION DURING AVERAGE AND ACTIVE YEARS

A Thesis

Submitted to the Graduate Faculty of the
Louisiana State University and
Agricultural and Mechanical College
in partial fulfillment of the
requirements for the degree of
Master of Science

in

The Department of Oceanography and Coastal Sciences

by
Victoria Lauren Ford
B.S., University of Oklahoma, 2014
August 2016

Acknowledgments

I am indebted to my advisor, Dr. Nan Walker, for her guidance and understanding throughout the course of this research. In our time working together, via coursework and laboratory research, she has become both mentor and friend. My sincerest thanks go to Dr. Jill Trepanier and Dr. Chunyun Li for their keen insight, helpful suggestions, and guidance with two separate programming languages.

I cannot thank Mr. Ric Haag enough for teaching computer programming fundamentals and inspiring the use of Python in all of my research work, thesis related or otherwise, even if only lending a kind ear and a cup of hot tea. To the students and researchers at the Louisiana State University Earth Scan Laboratory for providing a fun work environment and an unending fascination with severe weather and satellite imagery. I must thank Dr. Iam-Fei Pun of the National Taiwan University for graciously providing the dataset utilized in this research and for answering many questions.

To my family, for their unyielding faith, encouragement, love, and support throughout my academic career. And to BH, EK, LC, MM, KC, and RH, who inspire me in innumerable ways each and every day, and for whom I am forever grateful for their friendship.

I could not have done this without you. Thank you.

Table of Contents

List of Tables

List of Figures

List of Abbreviations and Symbols

CCE	Cold Core Eddy
CPHC	Central Pacific Hurricane Center
D26	Depth of the 26°C Isotherm (m)
ENSO	El Niño Southern Oscillation
HURDAT2	HURricane DATabase 2
LISA	Local Indicator of Spatial Association
NHC	National Hurricane Center
NPO	Northeast Pacific Ocean
OLR	Outgoing Longwave Radiation
ONI	Oceanic Niño Index
OTS	Ocean Thermal Structure
REGWNP	Regression for the Western North Pacific
SOI	Southern Oscillation Index
SSHA	Sea Surface Height Anomaly (cm)
SST	Sea Surface Temperature (°C)
SSTA	Sea Surface Temperature Anomaly (°C)
TC	Tropical Cyclone
TLM	Two-Layer Reduced Gravity Model
UOHC	Upper Ocean Heat Content (kJ cm^{-2})
WCE	Warm Core Eddy
U_H	Translation Speed of Storm (ms^{-1})
U_z	Maximum Sustained Wind Speed (ms^{-1})
c_p	Heat Capacity of Water at Constant Pressure (J kg^{-1} $°C^{-1}$)
ρ	Average Density of Water in the Upper Ocean (kg m^{-3})
$\Delta T(z)$	Temperature Difference between T(z) and 26°C at Depth z (°C)

Abstract

Upon comparison to typical neutral-ENSO conditions in the Northeast Pacific Ocean, the 2014 hurricane season has been identified as highly anomalous in both tropical cyclone frequency and intensity. This thesis seeks to investigate the influence of sea surface temperatures (SSTs) and upper ocean heat content (UOHC), defined as the excess of heat present above 26°C, upon the upper ocean thermal structure, mesoscale features, and anomalies that led to an active hurricane season in the Northeast Pacific. The 2012 Northeast Pacific hurricane season was selected as a 'normal' season to fully quantify the anomalous 2014 hurricane season. Data sets utilized in this work included optimally interpolated SSTs, UOHC, and the National Hurricane Center's post-storm observation database. Oceanic variables were extracted nearest-pixel to the hurricane path and were scrutinized through the use of along-track time series analysis, gridded UOHC fields, and a complex scheme of linear regression models. In order to quantify intensity modulation throughout a hurricane, enthalpy flux was calculated along-track for the duration of the storm with atmospheric model data, as well as from in-situ dropsonde observations.

Results suggest that variable SSTs and UOHC were critical in tropical cyclone genesis, duration, and maximum intensity. A minimum requirement of 30 kJ cm^{-2} of UOHC was found at genesis for all storms. At least 7 of the major hurricanes interacted with a warm oceanic mesoscale feature either at genesis or along-track that induced rapid intensification periods, including one high-end Category-5 hurricane. Cool wake signatures from deep upwelling along-track were detected within gridded UOHC and were also found to be influential in subsequent hurricane trajectories. Linear regressions suggested that storm-specific models, and not season-specific models, were optimal for estimating the influence of oceanic and environmental parameters within the intensification phase. Specifically, regressions for Hurricanes Emilia (2012) and Odile (2014) performed extremely well, indicating that a combination of oceanic parameters, storm position, and storm translation speed could ex-

plain 98% of along-track intensity variability. Along-track enthalpy fluxes peaked at 1234 W m^{-2} as the hurricane attained maximum intensity, while dropsonde-derived enthalpy emphasized stronger enthalpy fluxes within the northeast quadrants of the hurricane.

Chapter 1
Introduction

1.1 Background

A tropical cyclone is an intense atmospheric vortex that forms over warm ocean waters at low latitudes (Palmén, 1948; Emmanuel, 1988). These powerful systems occur on an annual basis in almost every ocean basin globally, and go by many names. The Northeast Pacific Ocean basin, in particular, is the most cyclonically active basin per unit area and per unit time worldwide (Molinari et al., 2000). Tropical cyclones require a number of pre-existing conditions, including but not limited to, an initial disturbance, weak vertical shear of horizontal winds, a deep thermocline associated with high sea surface temperatures, and considerable relative humidity in the lower and middle troposphere (Palmén, 1948; Gray, 1968).

Due to the potentially destructive and deadly nature of these powerful storms, a further understanding of their genesis and life cycles is imperative. Of the many associated risks, storm surge, high winds, tornadoes, torrential rainfall, and flooding pose the greatest threat to public health and life. As a direct result of the 2014 Northeast Pacific hurricane season, twenty-seven people lost their lives and over USD $1.02 billion in damages occurred (Berg, 2015). Storms stranded thousands of tourists in Cabo San Lucas, Mexico (Cangialosi and Kimberlain, 2015) and alarmed residents of the Island of Hawai'i, which had never been directly struck before by a tropical cyclone in history.

Although tropical cyclones are influenced by both atmospheric and oceanic forcings, this body of work will primarily focus on the oceanic parameters involved in tropical cyclone generation and maintenance. Early in the 2014 season, atmospheric scientists, oceanographers, and climate scientists detected widespread, abnormally high sea surface tempera-

tures across the Northeast Pacific Ocean and accurately predicted a highly active tropical cyclone season. Perhaps of even greater importance than high sea surface temperatures is a sufficiently deep upper ocean thermal structure, which is theorized to energize and intensify tropical cyclones. In this study, upper ocean heat content is used as a metric to quantify the oceanic thermal structure. By assessing the interactions between these complex oceanic parameters and the atmosphere, this thesis seeks to provide additional insight into the Northeast Pacific air-sea-tropical cyclone relationship.

1.2 Research Objectives and Hypotheses

This thesis investigates the relationships between the extent of anomalous sea surface temperatures, oceanic heat content, tropical cyclogenesis, and wind speed intensity for major hurricanes throughout the Northeast Pacific Ocean basin in 2014. A typical hurricane season/neutral El Niño year, 2012, was statistically chosen to serve as a measure of the abnormal activity of 2014. By combining satellite-retrieved sea surface temperatures, model-derived upper ocean heat content, and the National Hurricane Center's tropical cyclone best-track observation database, this thesis utilizes a wealth of data to conduct an in-depth analysis of Northeast Pacific oceanic conditions in 2014. Specifically, this thesis seeks to answer the following key research questions:

1. When, where, and to what spatial extent were sea surface temperatures anomalous in 2014?

2. How precisely did tropical cyclone genesis locations and tracks correspond with sea surface temperature anomalies?

3. How precisely did tropical cyclone genesis locations and tracks correspond to varying upper ocean heat content values?

4. How did sea surface temperatures correlate to tropical cyclone intensification in 2014?

5. How did latent and sensible heat fluxes influence intensification in 2014?

1.3 Study Area

This thesis reviews the major hurricanes ($\geq 50\ ms^{-1}$) of two Northeast Pacific Ocean (NPO) tropical cyclone seasons. Throughout this work, the NPO comprises the region bounded by the Equator to the south, the western coastline of the Americas to the east, and the International Date Line (180°) to the west (Figure 1.1). The NPO consist of two subset areas: the East Pacific, the region east of 140°W (East NPO), and the Central Pacific, the region west of 140°W (Central NPO). Naming conventions are specific to the appropriate subset region throughout.

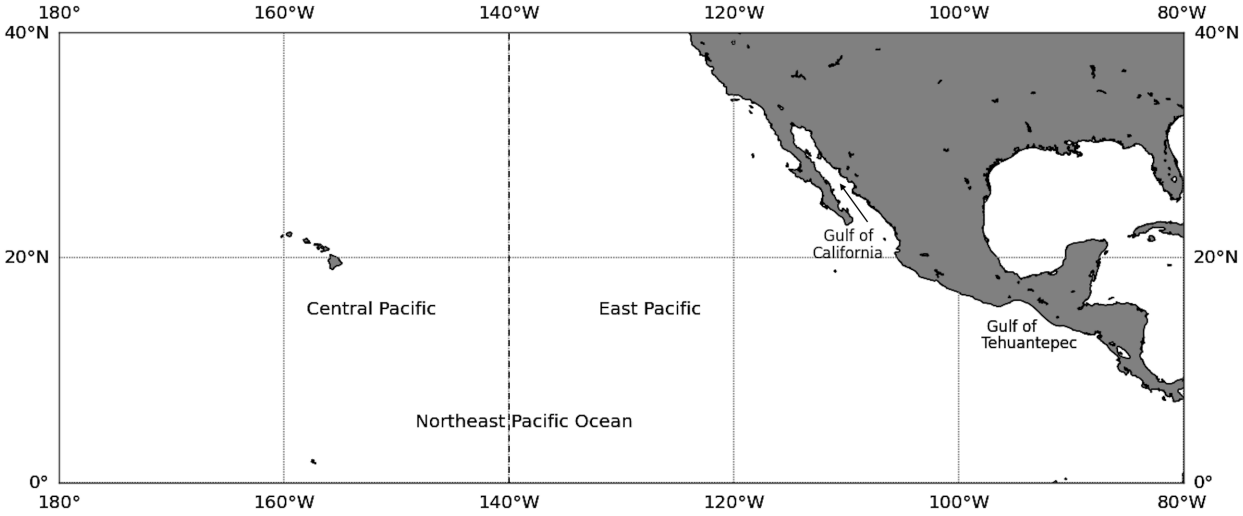

Figure 1.1: Map of the NPO basin study area.

1.3.1 The 2014 Northeast Pacific Hurricane Season

By several measures, the 2014 NPO hurricane season was the most active since the early 1990s (Berg, 2015). From a total of 20 tropical storms, 16 became hurricanes, 9 attained major hurricane status (Category-3 and greater on the Saffir-Simpson scale), and 3 became landfalling storms. Thus, the 2014 season is ranked as the second[1] most intense season behind the 1992 NPO season. The major hurricanes of the 2014 season are depicted in Figure 1.2.

[1]This record was subsequently broken by the 2015 NPO hurricane season. The 2014 NPO season currently stands as the third most active season.

Of basin records broken, several important events have been selected to discuss. The NPO experienced the strongest May and August tropical cyclones ever (Amanda; Marie), the earliest first and second Category-4 tropical cyclones (Amanda; Cristina), and a tropical cyclone to track across all three Pacific Ocean basins (Genevieve). Of particular interest to this thesis is Hurricane Iselle, which made a rare landfall on the Island of Hawai'i in early August, resulting in a federal major disaster declaration[2]. This study investigates whether high sea surface temperatures and upper ocean heat content were partially responsible for each of these exceptional events.

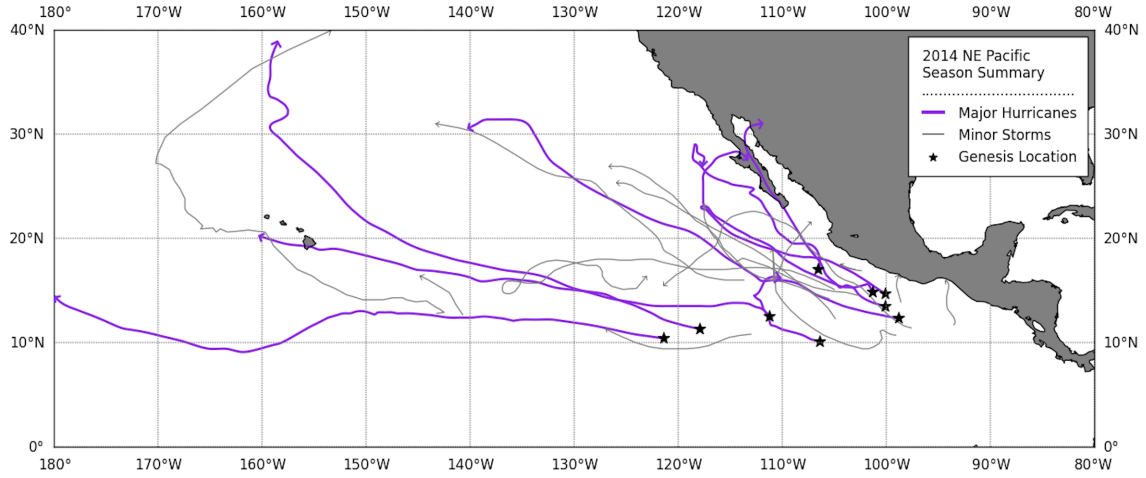

Figure 1.2: Major hurricanes of the 2014 NPO hurricane season.

1.3.2 The 2012 Northeast Pacific Hurricane Season

In regards to activity, the 2012 NPO hurricane season is considered near average with a total of 17 tropical storms, 10 hurricanes, and 5 major hurricanes (Pasch, 2014). According to the National Hurricane Center (NHC), the 1981-2010 averages for the NPO are 15 tropical storms, 8 hurricanes, and 4 major hurricanes, which align very well with the 2012 totals. Storm activity remained primarily off shore, as is considered normal for the NPO, with three storms making landfall in Mexico. Most notable is Hurricane Paul, which made landfall in Baja California Sur as a post-tropical cyclone, resulting in over

[2]Federal Emergency Management Agency Disaster Declaration DR-4194

USD $16.6 million in damages. With the exception of Hurricanes Daniel and Emilia, which moved westward, tropical cyclones remained on primarily meridional (north-south) paths in 2012 (Pasch, 2014). Tracks for the 2012 major hurricanes are shown in Figure 1.3.

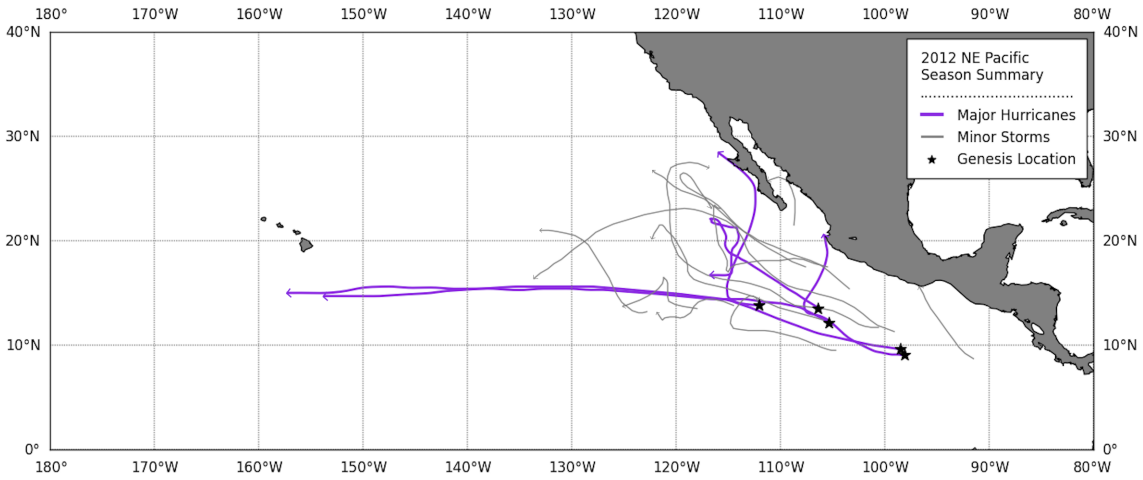

Figure 1.3: Major hurricanes of the 2012 NPO hurricane season.

1.4 Significance of Proposed Research

This thesis comprehensively investigates potential controls of intensity variation in the NPO. Although the NPO experiences more tropical cyclones than other basins, there is significantly less attention paid to the NPO in literature and the media, as those storms make fewer landfalls (Chu, 2004). All major hurricanes of the 2012 and 2014 NPO tropical cyclone season will be discussed in depth in this work. Sea surface temperatures and upper ocean heat content are scrutinized as mechanisms for cyclogenesis, tropical storm maintenance or intensity changes, and energy exchange between the ocean and atmosphere. In order to better provide for those impacted by tropical cyclones globally, a greater understanding of oceanic conditions prior-, during, and post-event is critical. Specifically, by researching the complex influence upper ocean heat content has on intensification in the NPO, forecasts may be improved for tropical cyclone warnings and landfall preparations. In cases of unexpected rapid intensification, improved intensity forecasting may potentially be the difference between lives lost and lives saved.

Chapter 2
Literature Review

2.1 Conducive Oceanic Parameters for Cyclogenesis

2.1.1 Sea Surface Temperature and Depth of the 26°C Isotherm

For decades, scientific literature has provided convincing evidence that the temperature of the sea surface is fundamental to the genesis and evolution of tropical cyclones (TCs) (Wentz et al., 2000). Leipper and Volgenau (1972) found that hurricanes only form over warm seas, and that their intensity is greater where sea surface temperatures (SSTs) are highest, often tracking over tongues of warm water. The required minimum temperature to support cyclogenesis has been discussed extensively and is widely agreed to be very high SSTs, typically 26 – 27°C (*i.e.* Palmén (1948); Fisher (1958); Perlroth (1967); Dare and McBride (2011)). Leipper and Volgenau (1972) state that 26°C is important for two reasons: it is the sea surface temperature below which hurricanes do not form, and it is the air surface temperature for the mean tropical atmosphere in the hurricane season.

However, in the tropics, SSTs regularly exceed 26°C. Thus, the depth to which the 26°C isotherm (D26) extends is also vital. Pun et al. (2011) state that D26 at low latitudes (10 to 15°N) can be as much as 160 m in depth, whereas at higher latitudes (30 to 35°N) D26 may only be 20 – 30 m in depth. As such, D26 represents the volume of available oceanic heat for air-sea-hurricane exchange, rather than a one-dimensional sea surface parameter.

It is acknowledged that SST is just one of several environmental parameters influencing the formation and maintenance of TCs. DeMaria and Kaplan (1994) and Whitney and Hobgood (1997) found that SST acts as an upper bound on the maximum potential intensity of a TC, but indicate that other environmental factors ultimately determine the actual intensity of any given TC. Thus, rather than a finite threshold of 26°C, the necessary

SST required for cyclogenesis may be relative to extant conditions at the time of formation. Dare and McBride (2011) support this with evidence that approximately 2% of global genesis locations occur over SSTs less than 25.5°C. The authors found that given a generalized poleward heading where SSTs are cooler, approximately 12.5% of TC observations occur over SSTs less than 25.5°C. The importance of this inference relative to the NPO will be discussed within this text.

2.1.2 Upper Ocean Heat Content and Oceanic Mesoscale Features

Recent literature has indicated that evaluating the ocean condition mandates the need for both surface and subsurface temperature structure. For the subsurface, D26 and upper ocean heat content (UOHC) are appropriate diagnostic parameters (Lin et al., 2009). Leipper and Volgenau (1972) coined 'hurricane heat potential' as the excess of heat in waters above the 26°C isotherm. UOHC and hurricane heat potential (Goni and Trinanes, 2003) are used interchangeably in the literature. For temperatures above this threshold, UOHC provides a vertically integrated estimate of stored energy within the upper ocean (Cione, 2015). It is important to note that heat content is a relative quantity, and any sub-surface isotherm could be used as a reference. This study uses 26°C as the reference isotherm in determining UOHC values. By calculating the initial heat content of the ocean, the number of days in which a hurricane might be supported can be estimated (Leipper and Volgenau, 1972). Emmanuel (1988) stated that hurricane intensity is very sensitive to the nature of the underlying ocean surface. Thus, the deeper the D26 and resulting UOHC, the longer a TC may be sustained. UOHC can be calculated with the following equation:

$$UOHC = c_p \rho \int_0^{D26} \Delta T(z) dz \tag{2.1}$$

where c_p represents the heat capacity of water at constant pressure (4178 J kg^{-1} °C^{-1}), ρ

is the average density of the upper ocean (1026 kg m^{-3}), and $\Delta T(z)$ is the temperature difference between the surface and 26°C at depth z (Pun et al., 2011). It is evident that UOHC is only positive when SST exceeds 26°C (Cione, 2015).

Several studies investigate the importance of UOHC on subsequent intensity changes (e.g. in the Gulf of Mexico (Shay et al., 2000), the North Atlantic Ocean (Mainelli et al., 2008), and the NPO (Shay and Brewster, 2010)). Lin et al. (2009) state the criticality of the ocean thermal structure in controlling intensity, especially for the most intense Western NPO storms and those that move slowly. Research on the upper ocean response to a moving hurricane has largely focused on the upwelling and entrainment of cool, deep waters which leads to a reduction in enthalpy fluxes, the primary energy source for TC maintenance (e.g. (Price, 1981). A 2 – 3°C cooling within the hurricane inner core is sufficient to shut down the entire energy production of a storm (Emmanuel, 1988; Lin et al., 2009). Hurricane Ivan (2004) experienced rapid negative feedback from two large cool core eddies (CCEs) where cool-wake SSTs of 20 – 26°C evolved rapidly, immediately decreasing hurricane intensity (Walker et al., 2005). Similarly, major Hurricanes Katrina and Rita both weakened in intensity over low SSTs within TC-intensified CCEs along their tracks (Jaimes and Shay, 2009). Walker et al. (2014) observed the rapid weakening of Hurricane Kenneth (2005) to tropical storm status as the hurricane stalled over a weak cyclonic eddy, cooling SSTs by 8 – 9°C in Kenneth's cool wake.

Conversely, the presence of warm oceanic mesoscale features can lead to a positive influence on TC intensification. Emmanuel (1988) emphasized the presence of a warm core eddy (WCE) at about the time of maximum intensification in Hurricane Opal (1995). In fact, Shay et al. (2000) found that Opal rapidly intensified from 35 ms^{-1} to greater than 60 ms^{-1} in the 14-hour period after tracking directly over a WCE in the Gulf of Mexico. WCEs are mainly characterized by a deepening of isotherms towards their centers (Goni

and Trinanes, 2003), thus representing abnormally high UOHC values. An evaluation of ocean thermal structure during the intensification phase of 32 of the 36 strongest North Atlantic TCs determined that intensification could be associated with storm passage over regions with at least 20 kJ cm^{-2} of increased UOHC along track (Goni and Trinanes, 2003). Cione (2015) observed that the energy required to maintain a non-stationary TC is 2 – 8% (depending on storm motion and intensity) of the available UOHC. Shay and Brewster (2010) developed a hurricane-season climatology of East NPO UOHC, and defined a 'basin equivalent' UOHC parameter, empirically derived from stratification of the mixed layer, and allows for comparison of UOHC between different ocean basins.

In their studies of the Western NPO, Lin et al. (2009) and Pun et al. (2011) found that 30% of Category-5 typhoons (>70 ms^{-1}) intensified due to warm ocean features, such as WCEs. Mainelli et al. (2008) observed that UOHC fluctuations have a small, but positive impact on intensity forecasts of Atlantic storms. The authors stress that the effect of UOHC is far more significant for intense Category-5 storms, suggestive of the importance on rapid intensification. Inclusion of UOHC in statistical prediction models decreased errors of average intensity forecasts by 20% for all storms and 5% in Category-5 storms (Mainelli et al., 2008). UOHC is thus considered a factor that requires further study as it could further greatly enhance prediction of tropical cyclone intensification (Goni and Trinanes, 2003).

2.2 Conducive Atmospheric Parameters for Cyclogenesis

There is considerable agreement that TC intensity is the result of subtle interactions between dynamic storm processes and the influence of the external environment. Wu and Chu (2007) state that the atmospheric parameters most influential in tropical cyclogenesis are the Coriolis force, low-level cyclonic vorticity, vertical shear of horizontal winds, moist instability, and moderately high relative humidity in the middle troposphere. In regards to

intensification, favorable atmospheric conditions include trough interactions (steering motion) and weak vertical wind shear leading to good outflow aloft (Goni et al., 2002). Vertical wind shear is calculated as the difference between the 200- and 850-mb atmospheric levels. Environmental relative humidity is averaged between the 700- and 850-mb levels. Boucheral et al. (2016) suggest that both of these parameters are critical for individual storm tracking and can be as important as oceanic control on season activity. Hobgood (1998) states that faster storm translation speed is often in conjunction with increased, unfavorable vertical wind shear, and thus associated with a decreased maximum wind speed. An exhaustive review of atmospheric forcing in the Northeastern Pacific is provided in Amador et al. (2006).

In this research study, basin-wide sea level pressure, 200- and 850-mb winds, and the depth of the 20°C isotherm were scrutinized from the Climate Prediction Center Climate Diagnostics Bulletins[1] for January – December 2012 and 2014. Analysis and discussion of these environmental parameters are not included within this text. Instead, the influence of the atmospheric environment is briefly discussed on a storm-specific basis in Chapter 4.

2.3 Enthalpy Fluxes and Intensification

Energy exchange at the air-sea boundary has been identified as one of the major physical processes governing hurricane intensity (Fisher, 1958; Wroe and Barnes, 2003; Hsu, 1988; Pun et al., 2016). Fluxes of momentum, moisture, and heat provide the necessary energy to establish and maintain deep convection over the ocean (Large and Pond, 1982; Cione and Uhlhorn, 2003; Pun et al., 2014). Latent heat is released when water vapor condenses during the formation of clouds and is important within synoptic- and climatic-scale atmospheric patterns, and is often the largest term in upper-ocean heat balance (DeCosmo et al., 1996). However, sensible (temperature) and latent (moisture) heat fluxes have rarely been measured successfully over the ocean in moderate to strong wind conditions, and the

[1] Available online: http://www.cpc.ncep.noaa.gov/products/CDB/CDB_Archive_html/CDB_archive.shtml

underlying physics between the exchange process and rough seas is poorly understood (DeCosmo et al., 1996; Powell et al., 2003; Zhang et al., 2008). Numerical attempts to verify the ocean environment rely on pre-storm ambient SSTs ahead of the storm track, as well as post-event cold wake SSTs.

Based on *in-situ* TC buoy measurements over a 27-year period (Cione et al., 2000), Cione and Uhlhorn (2003) found that within a hurricane, much of the ocean-to-atmosphere exchange of energy occurs within a relatively dense area near the eyewall. Analyses of inner-eyewall thermodynamics document well-mixed layers of specific humidity and potential temperature, consistent with well-developed boundary layers and in which a neutral stability surface layer is controlled by surface roughness. Routinely obtaining an accurate, direct, and continuous representation of atmospheric and near-surface ocean conditions, including temperature and sea surface roughness, remains a challenge to scientific research (Cione and Uhlhorn, 2003).

Hurricane track models have made substantial progress in recent decades, and yet forecasting hurricane intensity near and at landfall continue to show little advancement. The hurricane component of the Coupled Boundary Layer Air-Sea Transfer (CBLAST) experiment specifically targeted experimental observations of exchange fluxes in high wind conditions that would be suitable for improving both hurricane track and intensity model physics (Black et al., 2007). By routinely calculating enthalpy flux in a hurricane environment, observations governing intensity fluctuations, including rapid intensification, may lead to a greater understanding of the extreme hurricane environment. Research utilizing *in-situ* TC buoy measurements (Cione et al., 2000) has shown that surface values of hurricane inner-core enthalpy flux range from 700 – 2500 Wm^{-2}, with an average total surface enthalpy flux approximating to 1300 Wm^{-2} within a Category-1 hurricane on the Saffir-Simpson scale (Cione and Uhlhorn, 2003).

2.4 East Pacific Tropical Cyclone Climatology

To understand the significance of the highly active 2014 NPO hurricane season, a climatology of TC activity in the basin is essential. In regards to the number of genesis events per unit area and per unit time, the NPO is the most active tropical cyclone region on earth (Molinari et al., 2000). The NPO basin is split into two separate administrative regions for the issuance of watches, warnings, advisories, and forecasts, delineated by the 140°W meridian. The East NPO spans from the Americas western coastline to 140°W and is under the jurisdiction of the National Hurricane Center (NHC) in Miami, FL. The Central NPO spans the region 140°W to 180° (the International Date Line) and is monitored by the Central Pacific Hurricane Center in Honolulu, HI. Both the East and Central NPO hurricane seasons officially start 15 May and end 30 November, and are collectively known as the NPO hurricane season.

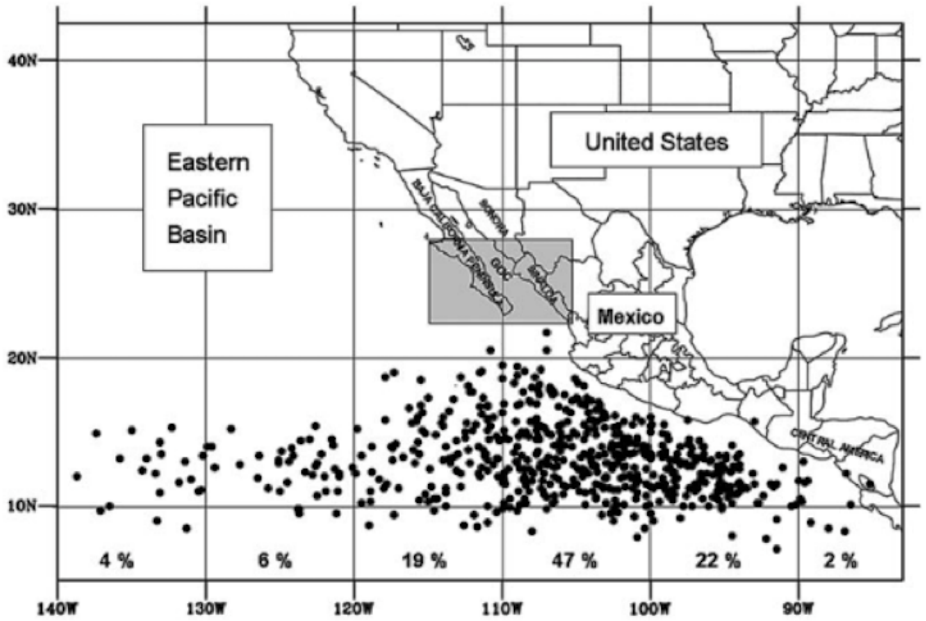

Figure 2.1: Genesis locations (dots) of East Pacific TCs 1980 – 2009. Numbers indicate percentage for genesis within 10° and longitude bins. From Farfán (2012).

Presented here is a brief combination of two separate East NPO climatologies: 1966-1980 (Allard, 1984) and 1980-2009 (Farfán, 2012), effectively creating a 43-year record.

Allard (1984) found an average of 14.3 TCs per season, with 7.2 storms achieving hurricane status (>32 ms^{-1}). Farfán (2012) determined a long-term annual average of 15.3 TCs per season, which agrees well with Allard's result. When dividing the entire season into 10 to 11 day periods, August 16 – 31 had the highest frequency of storms, resulting from both a maximum in SSTs and the northernmost position of the Intertropical Convergence Zone at this time (Allard, 1984). Hobgood (1998) calculated that the average hurricane duration is between 6.3 and 6.9 days, with a translation speed of 4.5 ms^{-1}. TCs are most likely to develop within a specific band, confined to 5°N and 20°N (Figure 2.1). Storm genesis positions in 2012 and 2014 align reasonably and extremely well, respectively, with the longitude bins presented in (Farfán, 2012). Few TCs will form south of 10°N, due to the reduced Coriolis force, or north of 20°N, due to the unlikelihood of necessary SST values for cyclogenesis (Farfán, 2012). A minimum in TC activity was found in the years 1977 and 1996, both of which had 8 storms only. A maximum in activity with 27 named storms occurred in 1992, which holds the historical record for the most active NPO season (Farfán, 2012). The most typical trajectory is oriented towards the west-northwest, leading to TCs that in most circumstances do not affect land (Camargo et al., 2008). Allard found that only 14% of East NPO TCs make landfall.

2.5 Central Pacific Tropical Cyclone Climatology

To assess the nature of two Central NPO TCs in 2014, a TC climatology was developed in the course of this study for the Central NPO region, as genesis in this basin is scarcely discussed in literature. Central NPO cyclogenesis positions and subsequent observations were obtained using the NE/NC HURDAT2 database (to be discussed in Section 3.1.3). Of the 67 Central NPO TCs listed in HURDAT2, 64 are considered in this brief climatology. Three TCs were excluded[2] due to genesis positions east of 140°W, despite their HURDAT2 classification as Central NPO storms. For the remaining 64 storms, genesis position in

[2]Tropical Depression 3-C (1997), Tropical Storm Alika (2002), and Tropical Depression 1-C (2003)

latitude and longitude coordinates, intensity at genesis, date of genesis, duration, maximum intensity, name, and landfall impacts were recorded. TC genesis is defined as the first observation at or above Tropical Depression status.

The spatial distribution of initial detection of TCs, assumed to be the genesis location, is shown in Figure 2.2. Most of these positions are confined between 5°N and 20°N, similar to that in the East NPO. Few TCs formed north of 18°N or south of 8°N. Of particular interest are the rare TCs that formed above 25°N, as SSTs are generally insufficient to support TC genesis so far north. It is broadly hypothesized that these few northern TCs resulted from very warm SSTs emanating from the eastern edge of the Western NPO basin, which is generally warmer than the East and Central NPO basins (Lin et al., 2009). Approximately 65% of Central NPO storms formed between 140°W and 160°W, to the south and southeast of the Hawaiian Islands.

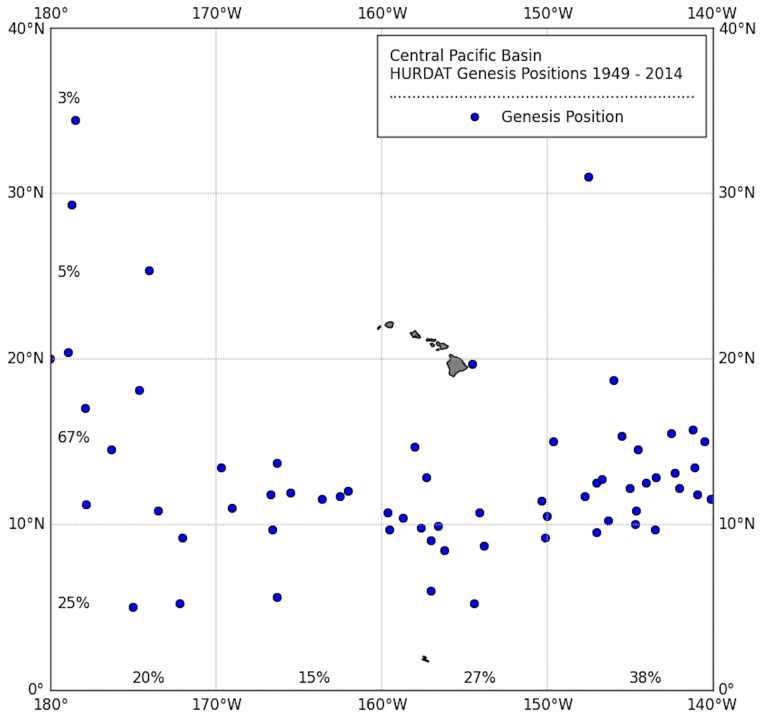

Figure 2.2: Genesis locations (dots) of Central NPO TCs from 1949 to 2014. Numbers indicate percentage for genesis within 10° latitude and longitude regions.

A long-term annual average of 1.02 TC forms each season, however several years experienced more than one TC[3], as well as several years with none. It is noted that the overall number of storms originating in this basin, and thus the mean, is most likely underestimated due to limited observations prior to the satellite era (1970s). August is the most frequent month for TC development, with 43% of all TC formations. September follows closely as the second most frequent month, with 30% of all formations. Most Central NPO storms remained below hurricane status (54%), while approximately one fifth (23%) attained major hurricane status (Category-3 and greater). The Central NPO has generated three Category-5 hurricanes. Hurricane Dot[4] (1959) and Hurricane Iwa[5] (1982) are the only Central NPO originating hurricanes to have made landfall in Hawaii.

2.6 El Niño Southern Oscillation

Until recently, there was a gap in the literature that statistically evaluates the connection between NPO storms and the El Niño Southern Oscillation (ENSO; Jien et al. (2015)). Associated with ENSO events are large-scale anomalies of warm SST, low sea level pressure, low outgoing longwave radiation (OLR), and westerly zonal wind, indicating weakened easterly trade winds (Wang and Fiedler, 2006). During El Niño events, cyclogenesis locations in the NPO were found to shift westward (Whitney and Hobgood, 1997; Camargo et al., 2008; Jien et al., 2015). Due to this shift, some TCs may reach the Central and Western NPO, and even impact the Hawaiian Islands (Boucheral et al., 2016). ENSO-induced subsurface heat redistribution strongly controls annual variations in extreme TC activity in the NPO (Jin et al., 2014). Thus, El Niño SST signals observed in boreal winter are highly indicative of TC activity during subsequent summers, capturing 40 – 70% predictability in extreme TC variability (Jin et al., 2014).

[3]The unprecedented eight Central NPO TCs of 2015 are not included in this estimate, but genesis locations align reasonably well within the percentages of Figure 2.2.

[4]Hurricane Dot: http://www.prh.noaa.gov/cphc/summaries/1959.php

[5]Hurricane Iwa: http://www.prh.noaa.gov/cphc/summaries/1982.php

Recently in the literature, there has been a recommendation for more detailed classification of El Niño events as either East or Central NPO El Niño events (Jien et al., 2015; Caron et al., 2015; Boucheral et al., 2016). East and Central NPO El Niño events are named for the region of influence in their respective basins. Several studies have shown that basin-wide ENSO could not explain variations in TC activity in both regions (Caron et al., 2015; Boucheral et al., 2016). Central NPO TCs were found to be more responsive to ENSO-induced environmental influences (Jien et al., 2015), whereas ENSO-related oceanic anomalies exhibit stronger control on East NPO TCs (Boucheral et al., 2016). Thus, the different varieties of El Niño can be identified through onset time, propagation features, and the location of maximum SST anomalies (Boucheral et al., 2016). ENSO-induced changes in SSTA and subsurface heat anomalies are known to alter influential factors for cyclogenesis, such as atmospheric stability, vertical wind shear, and environmental relative humidity (Jin et al., 2014). It is now apparent that the 2014 NPO season was influenced by the onset of a major East NPO El Niño event. While the significance of other global teleconnections are frequently discussed in the literature (*e.g.* Caron et al. (2015)), only ENSO will be discussed in detail in this work.

Chapter 3
Data and Methods

3.1 Data

3.1.1 Sea Surface Temperature Data

For gridded SST observations, the Microwave Optimally Interpolated SST v4 data were obtained from Remote Sensing Systems[1]. This dataset blends observations from the Advanced Microwave Sounding Radiometer 2 (AMSR-2), the WindSat microwave radiometer, and the Tropical Rainfall Measuring Mission/Microwave Imager (TRMM/TMI) (Gentemann et al., 2010). SST values were diurnally corrected to represent a 12-noon temperature. The spatial and temporal resolutions are 0.25° and daily, respectively, with SST measurement accuracy of approximately 0.5°C (Wentz et al., 2000). SST animations were constructed from daily SSTs for 2012 and 2014 in order to detect pre- and post- hurricane season trends, as well as hurricane cool wakes. While data for January 1 – December 31 for both 2012 and 2014 were acquired, the files specific to the official NPO hurricane season dates (May 15 – November 30) were given additional scrutiny.

One major benefit of using microwave-retrieved SST is the ability to effectively view the sea surface unimpeded by clouds. SST retrieval is only prevented in regions with rain or close to land (approximately 75 km to the coast). While data close to land are masked, rain contamination presented a challenge to this hurricane study. To overcome both rain and cool wake contamination in the SST data, as well as the primary intent to study the hurricane intensification phase, values were extracted along-track several days prior to the actual date of hurricane passage. SST validation tests were run on all major hurricanes at the following time intervals: day of (no change in extraction), and one through five days prior to storm passage. 'Day of' and 'one-day prior' data demonstrated strong cool wake

[1]Data available at: remss.com

signatures in several storms, thus invalidating usage in analyses. Data for 'two-days prior' through 'five-days prior' revealed the average trend of SSTs prior to passage, and were felt to best represent the oceanic condition. In some circumstances, 'five-days prior' data exhibited temperatures warmer than the trend seen in the previous three days data and were also deemed inappropriate. 'Four-days prior' SST data are used throughout all analyses in this study. See Appendix A for further information on the SST validation scheme.

3.1.2 Upper Ocean Heat Content Data

The UOHC data used in this study were obtained from Dr. Iam-Fei Pun at the National Taiwan University. UOHC is a derived quantity calculated from *in-situ* microwave SST measurements, and contemporaneous satellite altimetry observations, specifically sea surface height anomaly measurements (SSHA). Pun et al. (2014) developed a regression-based method to derive ocean thermal structure (OTS) for the Western NPO, where thousands of *in-situ* Argo floats are stationed. Typically, OTS concerns the uppermost 200 – 300 m of the ocean and is critical in TC intensification as this layer is where air-sea-hurricane interactions take place. The regression method for the Western North Pacific (REGWNP) was developed to increase the vertical resolution of the Two-Layer Reduced Gravity Model (TLM) used in many North Atlantic and NPO OTS studies (Shay et al., 2000; Goni and Trinanes, 2003; Goni et al., 2009; Shay and Brewster, 2010; Pun et al., 2016). The TLM calculates upper ocean layer thickness based on the depth of the 20°C isotherm, *in-situ* temperature profiles, and SST (Goni et al., 1996). Fig 3.1 illustrates the improvement of REGWNP over the less accurate TLM method, as well as calculated UOHC values between the two methods.

In the REGWNP method, a temperature divergence was calculated between Argo surface and subsurface temperature profiles, satellite-retrieved microwave SST, and the World Ocean Atlas 2001 climatological temperature profile. The isotherm displacement was then

linearly regressed onto the corresponding SSHA by least squares fit, and varies from location, isotherm, and month. This process was repeated for the depths of the 4 – 29°C isotherms. Provided with daily microwave SST, SSHA, and the monthly climatological mixed layer depth from the U.S. Naval Research Laboratory, daily OTS was then derived. UOHC can then be derived from the OTS profile for D26. The resulting gridded dataset has a spatial resolution of 0.25° and a daily temporal resolution. While the UOHC and OTS derivation was completed for use in the Western NPO, the same methods were utilized for an East and Central NPO application. For further details, see Pun et al. (2014).

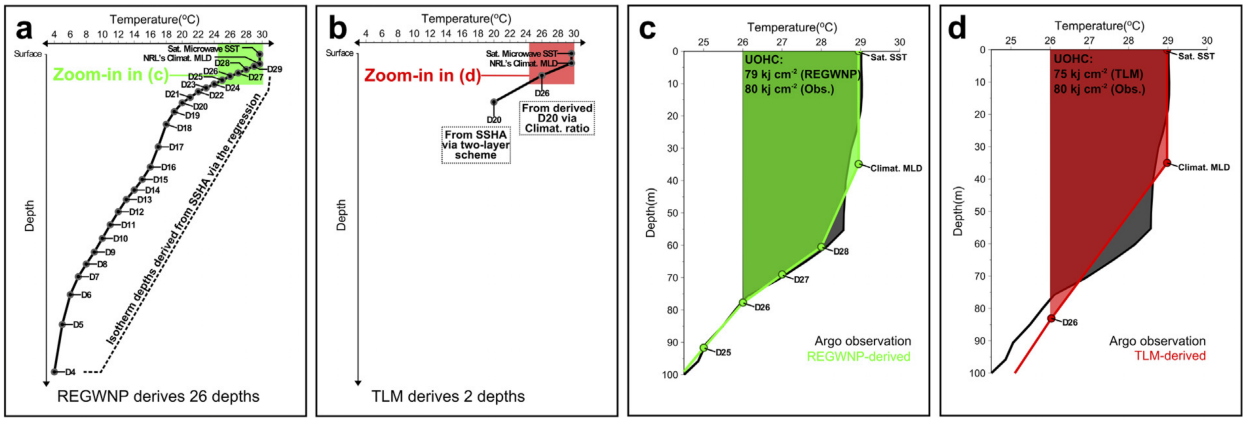

Figure 3.1: Schematic of (a) REGWNP-derived profile, (b) TLM-derived profile with (c) comparison between REGWNP (green) and Argo (black), and (d) comparison between TLM (red) and Argo (black). Shaded areas in (c) and (d) indicate UOHC. From Pun et al. (2014).

3.1.3 Hurricane Observation Data

TC research routinely makes use of the National Hurricane Center's HURricane DATabase 2 (HURDAT2), a best-track post-storm quality controlled observational record database for the North Atlantic and NPO. The HURDAT2 includes 6-hourly observations for TC position in latitude and longitude, minimum sea-level pressure (mb), 1-min sustained maximum wind speed at 10 m (U_z; kn), categorical information based on the Saffir-Simpson scale, as well as 34-, 50-, and 64- knot wind radii (nm). This study employed information from all TCs that obtained major hurricane ($> 50\ ms^{-1}$) status in 2012 and 2014 from

the Northeast/North Central (NE/NC) version of HURDAT2[2]. Uncertainty estimates for North Atlantic best track parameters are available, and may be applicable to Northeast Pacific best track data as well (Landsea and Franklin, 2013).

To ensure that the observational record for all major hurricanes throughout their lifecycle contained at least 30 values, spline interpolation of several parameters was implemented for selected data in this study. The interpolation process for the NPO was adapted from the North Atlantic interpolation scheme found in Elsner and Jagger (2012). Latitude, longitude, and maximum wind speed from the HURDAT2, SST, and UOHC were interpolated, effectively creating hourly observations for each major hurricane. It is noted that the hourly-interpolated data is derived, and not best-track quality controlled, and thus conclusions should be treated with caution.

3.1.4 Enthalpy Flux Data

In this study, enthalpy flux estimates for Hurricane Iselle (2014) were calculated using two different datasets: atmospheric model fields and real-time dropsonde data. For the model method, 4-times daily surface air temperature (T_a) and relative humidity (RH) data were obtained from the National Center for Environmental Prediction/National Center for Atmospheric Research Reanalysis-1 model[3] (Kalnay et al., 1996). Reanalysis variables are considered instantaneous at the reference time. Spatial and temporal resolutions for the Reanalysis products are 2.5° and daily, respectively. Values from the SST, UOHC, air temperature, and relative humidity datasets were extracted as nearest-pixel to the along-track location of Hurricane Iselle at that particular time.

[2]Downloaded 1 March 2016

[3]Data available at: http://www.esrl.noaa.gov/psd/data/gridded/data.ncep.reanalysis.surface.html

In comparison to the atmospheric model data, data from real-time GPS-dropsonde deployments during Hurricane Iselle were provided courtesy of the Hurricane Research Division of the Atlantic Oceanographic and Meteorological Laboratory. The full resolution data dropsonde data were chosen for in-flight or post-flight quality control processing. Each file contains processing parameters, bias corrections, and launch information, including location, pressure, and geopotential altitude at the aircraft at time of launch. During descent, sensors within the dropsonde measure latitude, longitude, atmospheric pressure (mb), air temperature (°C), relative humidity, geopotential height (m), wind direction, wind speed (ms^{-1}), U- and V- components of wind speed (ms^{-1}), and vertical velocity (ms^{-1}). The expected time increment between observations is one-half second. All available dropsonde full resolution data were obtained for Hurricane Iselle (5 August – 7 August 2014)[4].

3.2 Methods

3.2.1 Determination of a Neutral Year for Comparison

In order to understand the uniqueness of the 2014 NPO season, it was prudent to compare results against a 'normal' or neutral condition year. As it became apparent that the 2014 season was at the onset of an El Niño phase, the normal year was selected based on several criteria by using records from two atmospheric indices, the Southern Oscillation Index (SOI) and the Outgoing Longwave Radiation index (OLR[5]), and one oceanic index, the Oceanic Niño Index (ONI[6]). All three indices are available online through the Climate Prediction Center. Using the entire historical record for both the SOI and OLR, the mean and standard deviation were calculated during the hurricane season months, May through November. The ONI was used to determine whether the hurricane season months for each year were in positive El Niño, negative La Niña, or neutral phase. See Table 3.1 for SOI and OLR values and ONI designation for the 2010 – 2014 seasons. The 2012 hurricane

[4]Data available at: http://www.aoml.noaa.gov/hrd/Storm_pages/iselle2014/sonde.html
[5]SOI and OLR downloaded 08 June 2015
[6]ONI downloaded 01 April 2016

season was chosen as the neutral comparison year due to minimal anomaly values for both the SOI and OLR indices, as well as neutral ONI conditions. Both the 2012 and 2014 hurricane seasons lasted for 173 days each, providing further justification to the selection of the neutral year. This statistical analysis was performed in the R programming language.

Table 3.1: Calculated means and standard deviations of SOI and OLR in hurricane season months. Bold values indicate chosen 'neutral' year.

Year	SOI	OLR	ONI
2010	2.40 ± 1.60	1.17 ± 0.38	La Niña
2011	1.14 ± 0.58	0.41 ± 0.46	Onset of La Niña
2012	**0.93 ± 0.44**	**-0.14 ± 0.33**	**Neutral**
2013	0.93 ± 0.72	0.57 ± 0.25	Neutral
2014	0.57 ± 0.90	0.00 ± 0.38	Onset of El Niño

3.2.2 Storm Selection

An important consideration is the selection of only major hurricanes within this thesis. Ideally, all 22 named storms of the 2014 season and the 17 named storms of the 2012 season would be investigated. This would have expanded the scope of analyses to include Tropical Depressions, Tropical Storms, Category-1, and Category-2 hurricanes. Instead, it was felt that the major hurricanes (Category-3 and above) would best reveal the processes vital to intensification, while providing a long enough duration to study different stages within the hurricane's lifespan. While the major hurricanes were the most severe TCs, there were several minor TCs in each season that broke basin-wide records in themselves. Those storms, worthy of independent study, are not included in this thesis.

3.2.3 Along Track Analysis

To understand the relationship between UOHC in the formative and intensification stages within a major hurricane life cycle, along-track data were graphed for all major hurricanes. Parameters considered include SST, UOHC, maximum wind speed, and translation speed (U_H; ms^{-1}). Translation speed for each storm was calculated from each observation,

at an hourly interval, following a similar approach to that of Mei et al. (2012). The distance a storm covered in the hour prior and hour after the current position was divided by the total time interval (2-hours). For the starting and ending positions of each storm, forward and backward differencing was used with a 1-hour time interval. The importance of translation speed on the intensification of Category-5 typhoons is discussed in Lin et al. (2009). These graphs were used to identify correlations and lags between parameters as well as to ascertain dependence upon extant mesoscale features in the data. Along-track analysis was performed in the Python programming language.

3.2.4 Regression Analysis

A statistical analysis of the significance and correlation of parameters conducive for intensification was performed using several regression models. A total of 22 regression models were run on the major hurricanes (labeled **1** – **22**), for the intensification stage of the hurricane lifecycle only. An additional 25 supplementary storm-specific models were run and are discussed in Appendix C (labeled **23** – **47**). Individual regression models were not performed on Hurricanes Bud (2012), Cristina (2014), Daniel (2012), Genevieve (2014), Julio (2014), Miriam (2012), Norbert (2014), Paul (2012), and Simon (2014) due to fewer than 30 observations at major hurricane status. In order to perform regression analysis, parameters were tested using the method of least squares and several assumptions were tested for validity. To produce reliable results, model residuals should be normally distributed, which was tested with histograms, Q-Q plots, and the Shapiro-Wilks normality test, and parameters should not exhibit strong auto-correlation (multicollinearity). If model residuals only slightly deviate from normal, the model was treated with caution, but still considered valuable. See Table 3.2 for the regression model scheme.

Table 3.2: Summary of Statistical Regression Models

Name	Type	Explanatory Variable(s)	Response Variable
1 – 2012 Majors	Simple	SST	U_z
2 – 2012 Majors	Simple	UOHC	U_z
3 – 2014 Majors	Simple	SST	U_z
4 – 2014 Majors	Simple	UOHC	U_z
5 – All Majors	Simple	SST	U_z
6 – All Majors	Simple	UOHC	U_z
7 – 2012 Majors	Multiple	SST, Latitude, Longitude, U_H	U_z
8 – 2012 Majors	Multiple	UOHC, Latitude, Longitude, U_H	U_z
9 – 2014 Majors	Multiple	SST, Latitude, Longitude, U_H	U_z
10 – 2014 Majors	Multiple	UOHC, Latitude, Longitude, U_H	U_z
11 – All Majors	Multiple	SST, Latitude, Longitude, U_H	U_z
12 – All Majors	Multiple	UOHC, Latitude, Longitude, U_H	U_z
13 – Amanda	Multiple	SST, Latitude, Longitude, U_H	U_z
14 – Amanda	Multiple	UOHC, Latitude, Longitude, U_H	U_z
15 – Emilia	Multiple	SST, Latitude, Longitude, U_H	U_z
16 – Emilia	Multiple	UOHC, Latitude, Longitude, U_H	U_z
17 – Iselle	Multiple	SST, Latitude, Longitude, U_H	U_z
18 – Iselle	Multiple	UOHC, Latitude, Longitude, U_H	U_z
19 – Marie	Multiple	SST, Latitude, Longitude, U_H	U_z
20 – Marie	Multiple	UOHC, Latitude, Longitude, U_H	U_z
21 – Odile	Multiple	SST, Latitude, Longitude, U_H	U_z
22 – Odile	Multiple	UOHC, Latitude, Longitude, U_H	U_z

The regression models are as follows. Models **1** and **2** are simple linear regressions between SST or UOHC and along-track maximum wind speed (U_z) for all of the 2012 major hurricanes. Similarly, Models **3** and **4** are simple linear regressions for the 2014 major hurricanes. Models **5** and **6** are simple linear regressions for all major hurricanes considered from both seasons. These six simple models were run for the intensification stage of the storm to determine any linear relationship between an oceanic parameter and maximum wind speed up to peak intensity. Models **7** through **12** are multiple linear regression models that incorporate SST (or UOHC), storm latitude and longitude, and translation speed. There is some evidence that the addition of environmental predictors into multiple linear regressions improves the accuracy of intensification forecasts (Petty and Hobgood, 2000). In fact, Hobgood (1998) argued that latitude is the most significant predictor for intensity

variations, which are also often strongly correlated with SSTs. Translation speed is included in the multiple linear regressions, but Hobgood (1998) indicated that relatively consistent storm motion would explain less of the variability in intensification. Models **13** through **22** are storm-specific regression models, rather than season-specific regressions. All models attempt to clarify along-track intensification variations in maximum wind speed (U_z). It is noted that some statistical models exhibit some difficulty in producing good forecasts throughout the entire lifetime of a TC, suggesting that when a model performs well during one stage, its skill decreases during the opposite stage, thus separating the two phases is ideal in regression work (Petty and Hobgood, 2000). Statistical analyses of linear regression models were completed with the R programming language.

3.2.5 Enthalpy Flux Analysis

The bulk aerodynamic equations (Equations 3.1, 3.2, 3.3) provide a practical method for estimating air-sea fluxes with average measurements of temperature, wind speed, and water vapor density (DeCosmo et al., 1996; Cione and Uhlhorn, 2003). With a positive latent heat flux, heat is lost by the ocean and gained by the atmosphere, and vice versa. The aerodynamic method for calculating oceanic enthalpy is dependent upon two flux exchange coefficients: the Stanton number, C_E, and the Dalton number, C_H. These exchange coefficients are functions of stability and height, and are commonly evaluated for the equivalent neutral case at 10 m height (Large and Pond, 1982). In this study, the coefficients were based on high wind speed drag measurements in Powell et al. (2003) and Black et al. (2007). Enthalpy flux (Equation 3.1) is the combination of sensible heat flux (Q_H, Equation 3.2) and latent heat flux (Q_E, Equation 3.3),

$$Enthalpy = Q_H + Q_E \tag{3.1}$$

$$Q_H = C_p \rho_a U_z C_H (SST - T_a) \tag{3.2}$$

$$Q_E = L_v \rho_a U_z C_E (q_s - q_a) \tag{3.3}$$

where C_p is specific heat of air at constant pressure, ρ_a is the density of air, U_z is the maximum sustained wind speed, SST is along-track sea surface temperature, T_a is along-track air temperature, L_v is the latent heat of vaporization, q_s is specific humidity at the air-sea surface boundary, q_a is specific humidity for air at 10 m, and C_E and C_H are the drag coefficients at high wind speeds. A full discussion on the bulk aerodynamic method derivation is available in Appendix B.

Enthalpy flux was calculated with the bulk aerodynamic formulas with two separate datasets (Section 3.1.4) in order to address the role of enthalpy fluxes upon intensification and the advantages/disadvantages of particular data sources. While providing along-track enthalpy flux observations, a major shortcoming of the atmospheric model method is that the air temperature and relative humidity datasets have a spatial resolution that theoretically encompass the entire spatial extent of the hurricane itself, rather than extracting finer resolution values under the center of the storm. Air temperature and relative humidity values obtained by this method are therefore highly suspect, potentially not accurately simulating inner-eyewall conditions. In the reverse situation, dropsondes were able to measure and report in real-time the unique conditions of the entire vertical profile of Iselle at the time of deployment. Literature have shown that under the influence of a hurricane, the sea surface is dominated by sea spray and foam due to breaking waves (Holthuijsen et al., 2012). Thus, dropsonde humidity sensors may be contaminated by sea spray and result in inaccurate moisture estimates. Because wave height may reach 10 m and above, dropsonde observations at 30 m were considered appropriate for use after validating wave height observations from nearest-track buoys to the storm track[7]. However, a disadvantage to using the dropsonde data was the inability to produce along-track enthalpy flux mea-

[7]Buoys analyzed were those surrounding the Hawaiian Islands. Buoy data are available from the National Data Buoy Center at http://www.ndbc.noaa.gov

surements, as observations were not taken along-track of the hurricane. See Appendix B for further detail on the enthalpy flux derivation. Enthalpy flux calculations were executed in the Python programming language.

Chapter 4
Results

4.1 Along-Track Analyses

In order to assess the influence of anomalously high SSTs and related UOHC, an along-track analysis was performed for each major hurricane in the 2012 and 2014 NPO seasons. The following subsections are storm-specific, include a brief synoptic storm history, and discuss along-track wind speeds (U_z), SST, and UOHC. This analysis was included to expand upon the existing storm reports and to identify a positive relationship between SSTs and hurricane intensity, and whether that relationship was immediately influential upon the maximum wind speed or was temporally lagged. In this analysis, the 26°C isotherm was critical in the potential for hurricane development and maintenance, as well as the reference threshold from which UOHC was calculated (Leipper and Volgenau, 1972).

While this thesis does not discuss atmospheric parameters in detail, they are important to mention here, as a hurricane is a powerful interaction of the air and sea. Meteorological information for each storm was provided by the NHC post-storm and end-of-season summary reports (Pasch, 2014; Berg, 2015). Storm track figures were developed using the hourly-interpolated data, the NE/NC HURDAT2 database, and the SST and UOHC datasets. An hourly time series of maximum wind speeds, SST, and UOHC was presented for each storm, with important oceanic mesoscale features, such as warm core eddies (WCEs) and cold core eddies (CCEs) identified. In this research, WCEs were identified as pools of considerably deeper UOHC of at least 20 kJ cm^{-2} compared to the surrounding UOHC spatial field. Additionally, daily UOHC subplots were produced to further understand hurricane intensification, mesoscale features, and unusual track directions during the intensification phase of each storm. Following the NHC definition, any storm discussed here that underwent 'rapid' intensification deepened by at least 1 mb per hour for 24-hours.

4.1.1 2012 Major Hurricanes

- **Hurricane Bud (20 – 26 May 2012)**

Hurricane Bud was the first major hurricane of the 2012 season, which originated from a low-latitude tropical wave (Blake, 2012). A low-pressure system developed from this tropical wave south of Acapulco, Mexico, where it slowly organized into a Tropical Depression on 20 May (Figure 4.1). Easterly wind shear initially prevented intensification, which once abated, allowed Bud to quickly develop into a hurricane on 23 May. At this time, Bud diverted from a northwestward to northeastward track as a developing mid-latitude trough steered atmospheric flow aloft (Blake, 2012). Bud weakened rapidly with increased wind shear upon approaching Cabo Corrientes, and was downgraded to a Tropical Storm 80 km southwest of the coast on 25 May before dissipation the next day. Due to close proximity to the coastline, minor structural damage was reported near Manzanillo, Mexico (Blake, 2012).

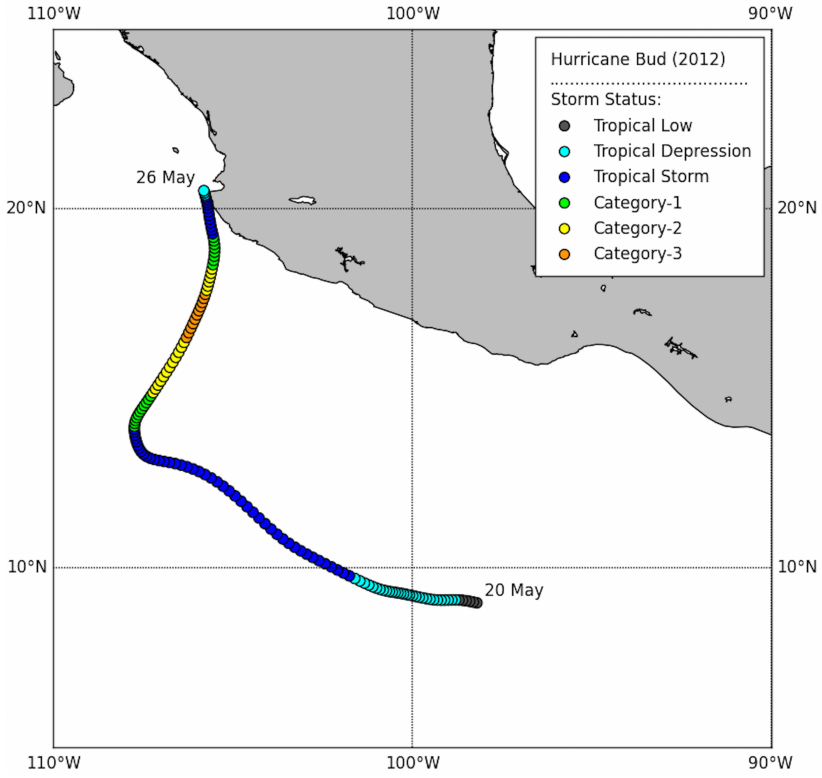

Figure 4.1: Hurricane Bud (2012) track.

Along-track analysis revealed that despite high SSTs consistent around 29.5°C, Bud only slowly intensified to major hurricane status. Beginning at 1800 UTC 23 May, SSTs began a slow 24-hour decline to 26.5°C underneath Bud's path (Figure 4.2). The storm formed in 51 kJ cm^{-2} of UOHC, which steadily increased to a high of 87 kJ cm^{-2} close to a well-developed WCE. Upon exiting this WCE, UOHC values along-track declined quickly to a minimum of 8 kJ cm^{-2}, where SST values hovered around 27°C. At the moment of maximum intensity, Bud exhibited wind speeds of 51.44 ms^{-1}, over high 27.45°C SSTs and 12.16 kJ cm^{-2} of UOHC. A clear correlation between wind speeds and SST/UOHC is not clear throughout the intensification phase of Bud. This may resulted from unfavorable atmospheric conditions present at the time, as well as the early season genesis date. A 45-hour delay was noted between the peak UOHC value and when Bud expressed maximum wind speeds. SST and UOHC values closer than 75 km to the coastline were not reported, as they were considered contaminated from proximity to land.

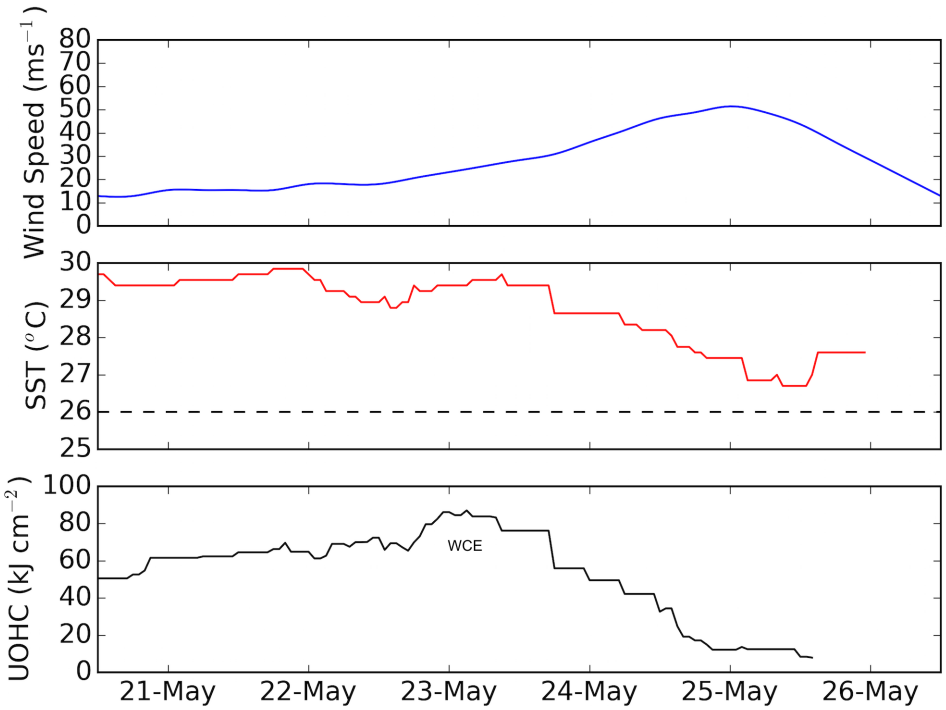

Figure 4.2: Hurricane Bud (2012) time series of along-track U_z (Top), SST (Center) and UOHC (Bottom). The 26°C isotherm is designated by a black dashed line.

It was noted that the WCE observed in the UOHC time series was essentially undetectable in the SST data. The spatial extent of the WCE is depicted in Figure 4.3. Upon formation in 51 kJ cm^{-2} of UOHC, Bud tracked to the south of the WCE where UOHC values were recorded at approximately 80 kJ cm^{-2} (Figure 4.3a). At that time, and for the following 24-hours, Bud maintained Tropical Storm status while slowly tracking to the north around a western extension of the WCE (Figure 4.3b). Bud underwent rapid intensification to a major hurricane on 24 May, while UOHC values ranged fairly constantly between 10 – 20 kJ cm^{-2} (Figure 4.3c). However, Bud's time as a major hurricane was a short lived 10-hours. After this intensification period, Bud quickly decayed over UOHC of approximately 15 kJ cm^{-2} near the Cabo Corrientes coastline (Figure 4.3d).

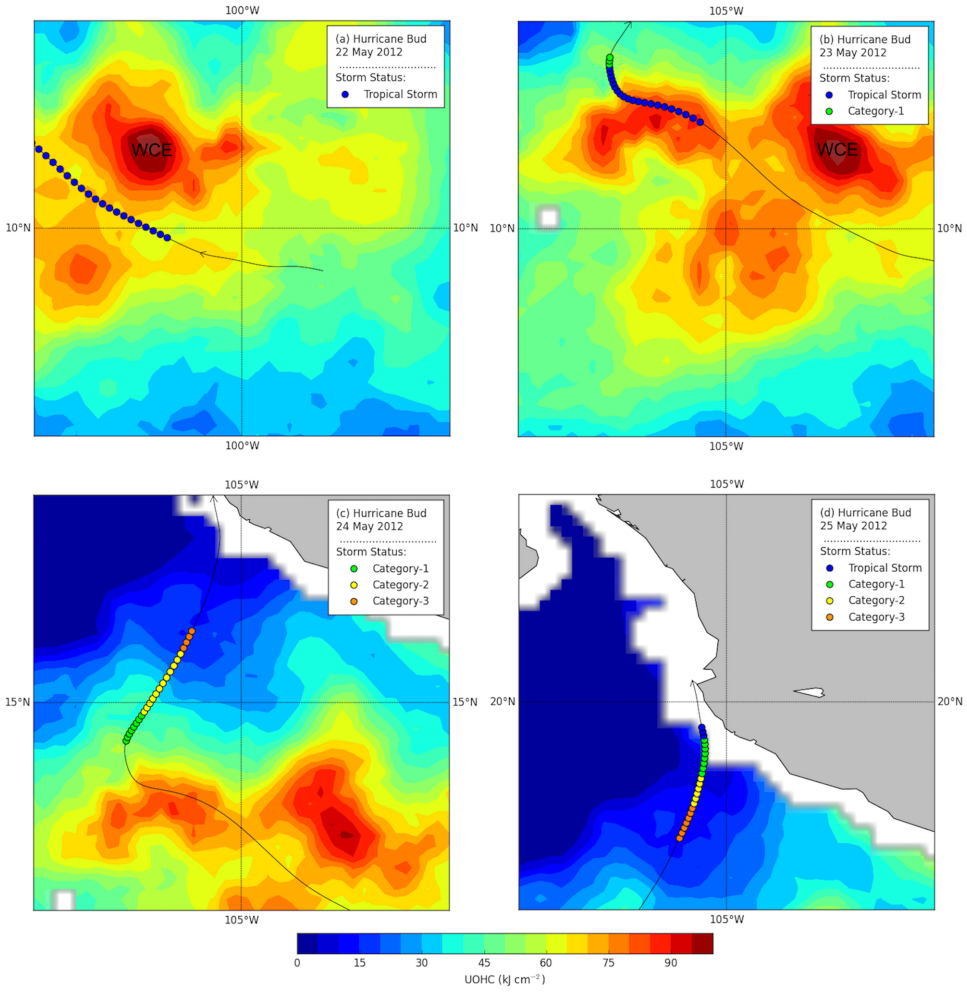

Figure 4.3: Daily UOHC with Hurricane Bud (2012) track overlain.

- **Hurricane Daniel (4 – 14 July)**

Hurricane Daniel originated from a tropical wave that developed into a low-pressure system south of the Gulf of Tehuantepec on 1 July (Avila and Hogsett, 2012). This system was classified a Tropical Depression by 0600 UTC 4 July, and a Tropical Storm 24-hours later. Daniel tracked primarily on a westward path embedded in easterly flow south of a stationary subtropical ridge that prevailed throughout Daniel's entire lifecycle (Avila and Hogsett, 2012). At 0000 UTC 7 July, easterly wind shear relaxed, enabling steady intensification to major hurricane status the following day. A few hours later, Daniel weakened as the storm system tracked over cooler waters and into a stable atmospheric environment. Storm circulation dissipated on 12 July. See Figure 4.4 for Daniel's track.

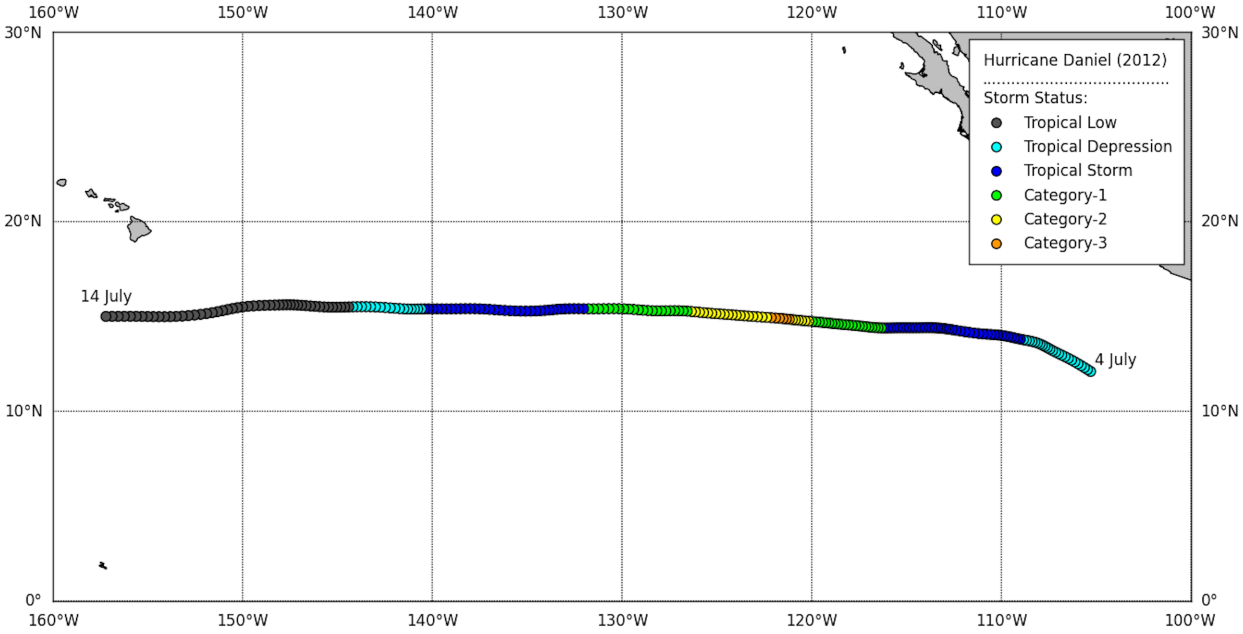

Figure 4.4: Hurricane Daniel (2012) track.

Daniel was a relatively short-lived major hurricane, maintaining wind speeds above 50 ms^{-1} for only 6-hours. SST values along-track revealed that the system formed in relatively high 28.2°C waters, which remained constant up until to the attainment of major hurricane status (Figure 4.5). Daniel weakened as the storm reached cool, less than 26°C waters. SST plummeted as low as 24°C, and Daniel weakened from a Category-1 status to a Tropical

Storm and lower. Analysis of UOHC revealed that Daniel formed around the periphery of a WCE with values peaking at 61 kJ cm^{-2}. Movement away from this mesoscale feature led to declining UOHC values which hovered around 20 kJ cm^{-2}, until an abrupt decline over waters less than 26°C, and thus 0 kJ cm^{-2} of excess heat. These cooler conditions persisted for the remainder of Daniel's duration. A clear correlation between the intensification phase and the underlying favorable oceanic conditions was evident, which curtailed immediately after peak intensity as SSTs fell below the 26°C isotherm threshold.

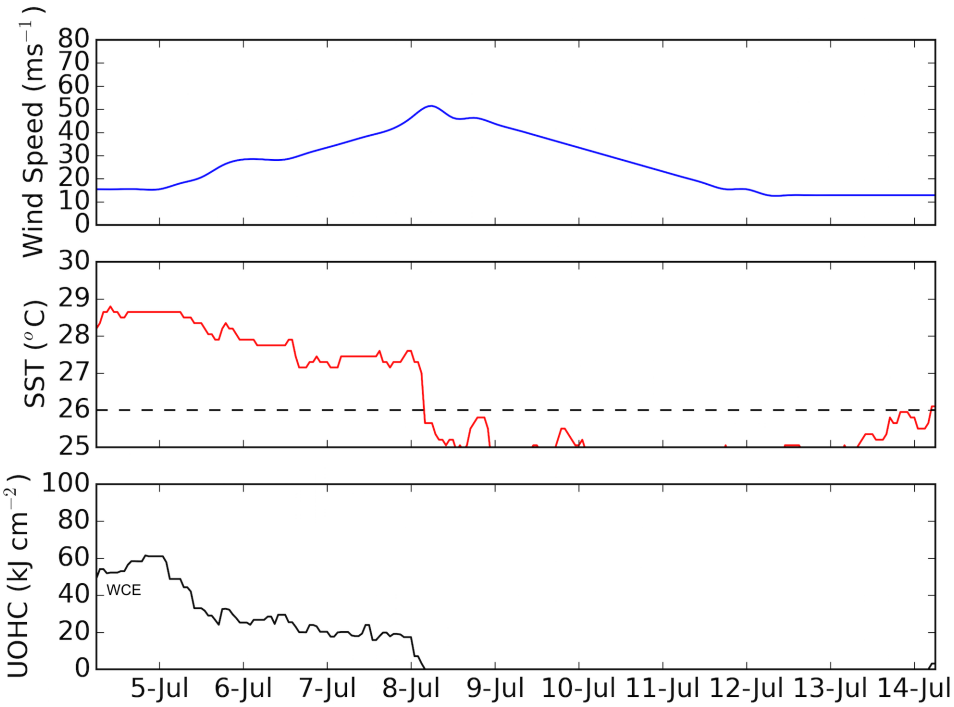

Figure 4.5: Hurricane Daniel (2012) time series of along-track U_z (Top), SST (Center) and UOHC (Bottom). The 26°C isotherm is designated by a black dashed line.

Upon analysis of the UOHC region at the time of genesis, Daniel formed in the outer bands of a large WCE, with UOHC of approximately 85 kJ cm^{-2} (Figure 4.6a). By the following day, Daniel attained Tropical Storm strength to the northwest of the WCE where waters exhibited lower UOHC values of 30 – 35 kJ cm^{-2} (Figure 4.6b). On 6 July, Daniel tracked on a direct westward path, and passed between two northern extensions of 30 kJ cm^{-2} of UOHC each, and as low as 20 kJ cm^{-2} between these two features (Figure 4.6c). At this time, Daniel reached hurricane force wind speeds that continually strengthened, de-

spite the low UOHC present near 15°N (Figure 4.6d). Daniel maintained major hurricane status for 6-hours on 8 July while immediately over very low UOHC of 10 – 20 kJ cm^{-2} (Figure 4.6e).

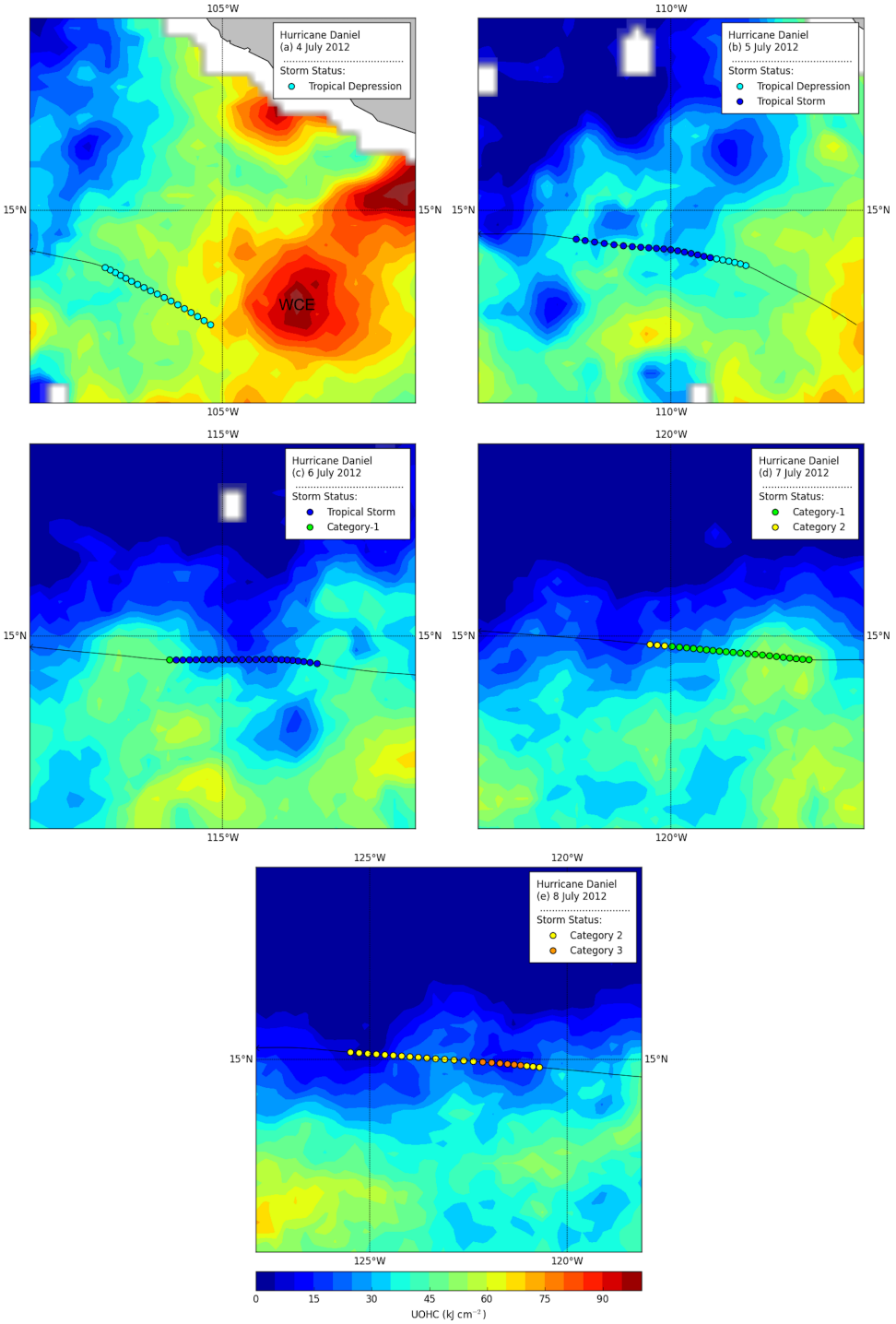

Figure 4.6: Daily UOHC with Hurricane Daniel (2012) track overlain.

- **Hurricane Emilia (7 – 18 July)**

Hurricane Emilia developed from a tropical wave merging with an Intertropical Convergence Zone disturbance around 0600 UTC 7 July (Cangialosi, 2012). The storm system rapidly intensified to hurricane status by 0600 UTC 9 July in favorable atmospheric and oceanic conditions. A day later, Emilia attained peak intensity as a Category-4 major hurricane (Figure 4.7). Cangialosi (2012) reported that Emilia underwent an eyewall replacement cycle, during which the hurricane weakened to a Category-2 storm, before re-intensifying to Category-3 status. After the second intensity peak, Emilia slowly weakened over cooler water, before dissipating at 1800 UTC on 15 July east-southeast of Hawaiian Islands.

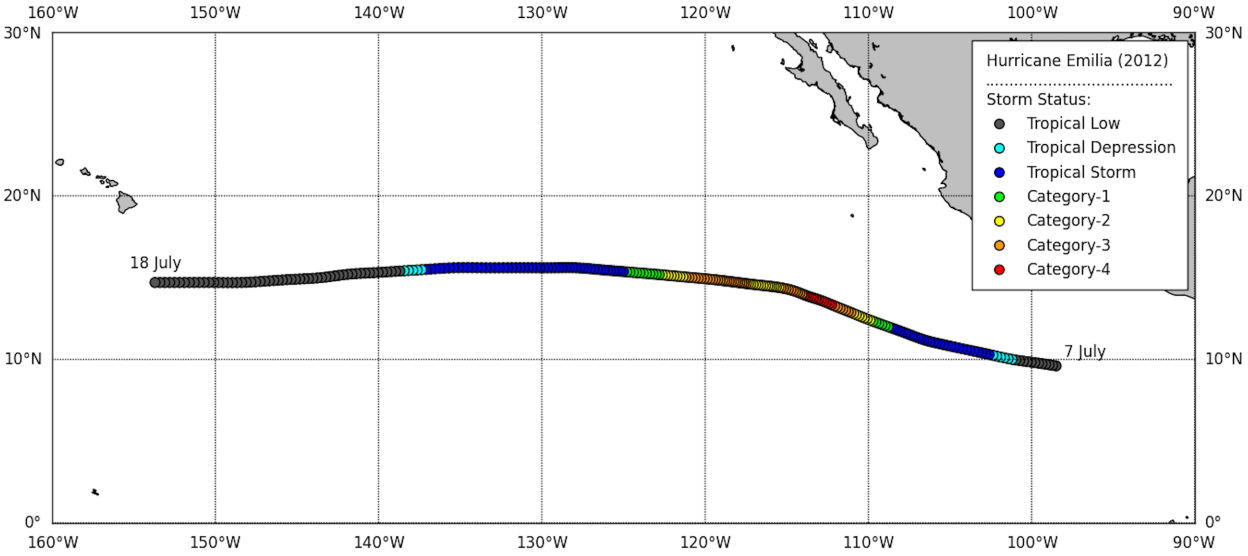

Figure 4.7: Hurricane Emilia (2012) track.

Along-track analysis revealed that Emilia formed in high 28.9°C waters, which fluctuated throughout the formative stages of the storm complex before decreasing below the critical 26°C isotherm late on 11 July (Figure 4.8). SSTs dropped as low as 23.7°C along-track on 15 July, while Emilia was a weakening Tropical Storm. At maximum storm intensity of 61.7 ms^{-1} wind speeds, SSTs were 26.8°C, and 25.9°C during the second re-intensification stage. Storm genesis occurred in 30 kJ cm^{-2} of UOHC, which fluctuated between 60 kJ

cm^{-2} before declining quickly to no excess oceanic heat as SSTs dropped below 26°C. At the moment of maximum intensity, Emilia was situated over minimal UOHC values of 1.5 kJ cm^{-2}. Emilia weakened to a Category-2 storm on 11 July, where UOHC values ranged between 0 – 25 kJ cm^{-2}. Six hours before Emilia reached its second intensity maximum, the storm tracked over small UOHC values of less than 10 kJ cm^{-2}.

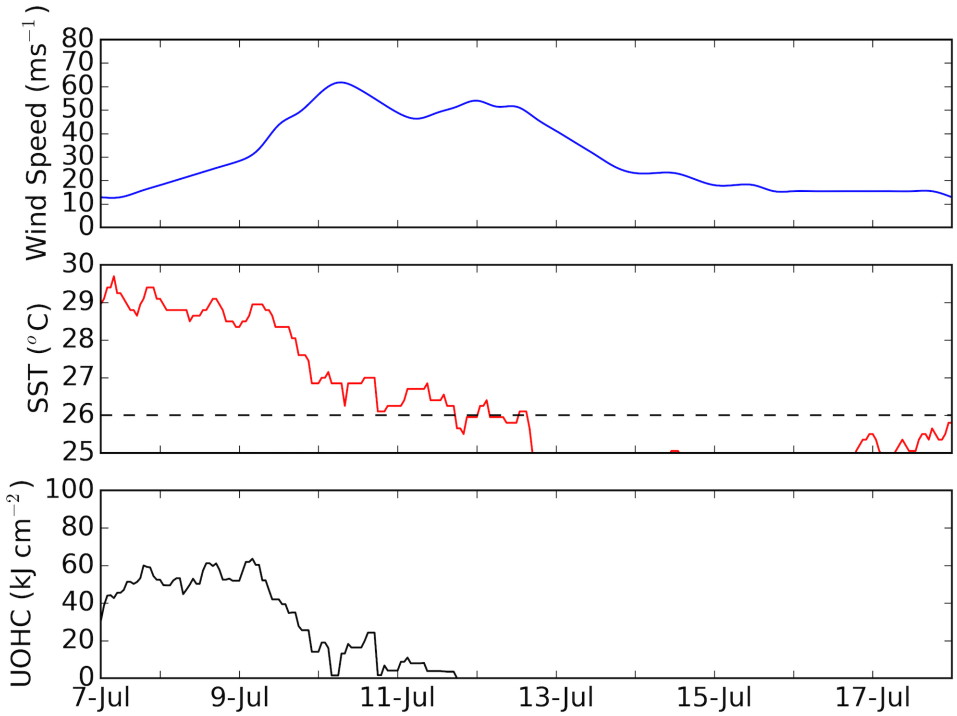

Figure 4.8: Hurricane Daniel (2012) time series of along-track U_z (Top), SST (Center) and UOHC (Bottom). The 26°C isotherm is designated by a black dashed line.

Upon analysis of the gridded UOHC fields, it is evident that Emilia formed on the western edge of a low UOHC region that transitioned to values nearing 60 kJ cm^{-2} of UOHC along-track (Figure 4.9a). The following day, the storm continued to pass over UOHC consistent in the 50 – 60 kJ cm^{-2} range (Figure 4.9b). During the rapid intensification stage (Figure 4.9c), Emilia tracked over declining UOHC, as low as 20 kJ cm^{-2}. Despite further storm intensification, Emilia tracked further over minimal UOHC values between 0 – 20 kJ cm^{-2} (Figure 4.9d). The second intensification phase of Emilia is not shown here, as it is evident from Figure 4.9 that this occurred over negligible UOHC.

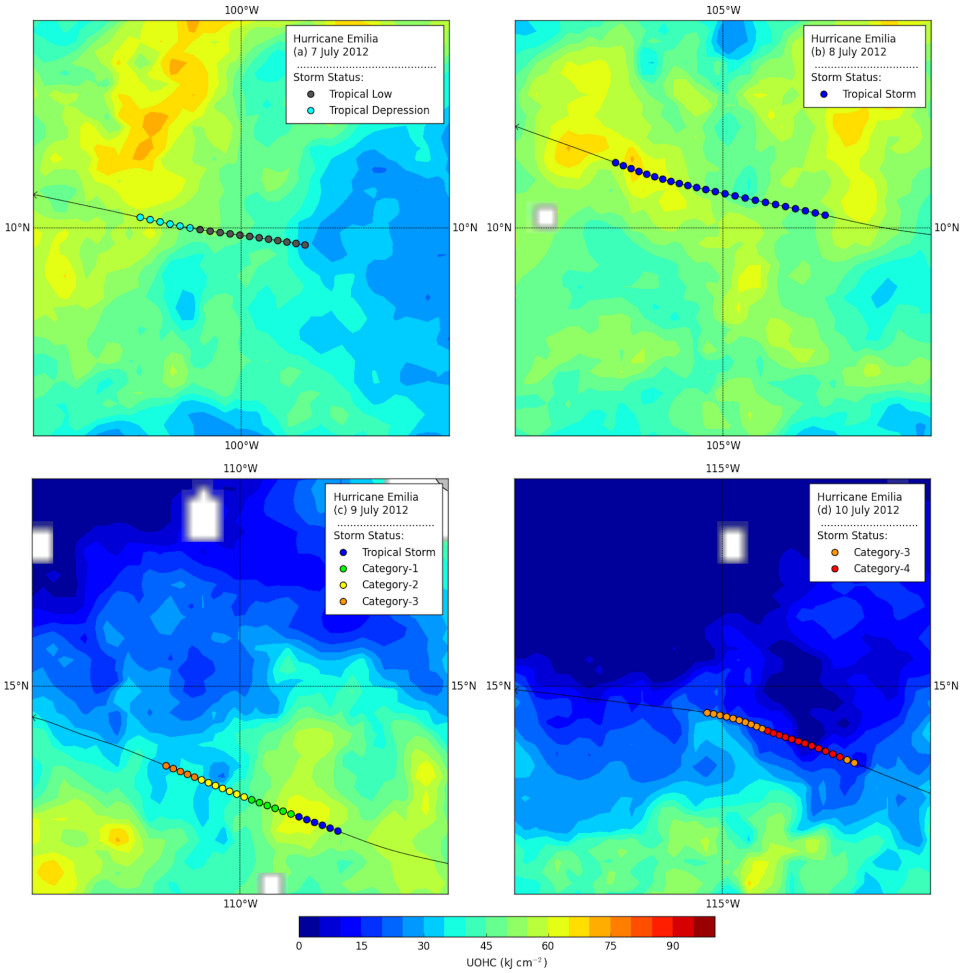

Figure 4.9: Daily UOHC with Hurricane Emilia (2012) track overlain.

- **Hurricane Miriam (22 September – 2 October)**

Hurricane Miriam originated from a very active tropical wave that also generated long-lived Hurricane Nadine 10 days earlier in the North Atlantic basin (Avila, 2013). Miriam was named at 0000 UTC on 22 September south of Cabo Corrientes, where a low wind shear environment and high ocean temperatures favored a steady intensification to hurricane status by 24 September. The system then rapidly intensified into a Category-3 hurricane, but convection quickly declined as the hurricane crossed into much cooler SSTs. Miriam became a remnant low at 1800 UTC 27 September, from which it meandered southward with the low-level atmospheric flow until dissipation (Avila, 2013). See Figure 4.10 for Miriam's track.

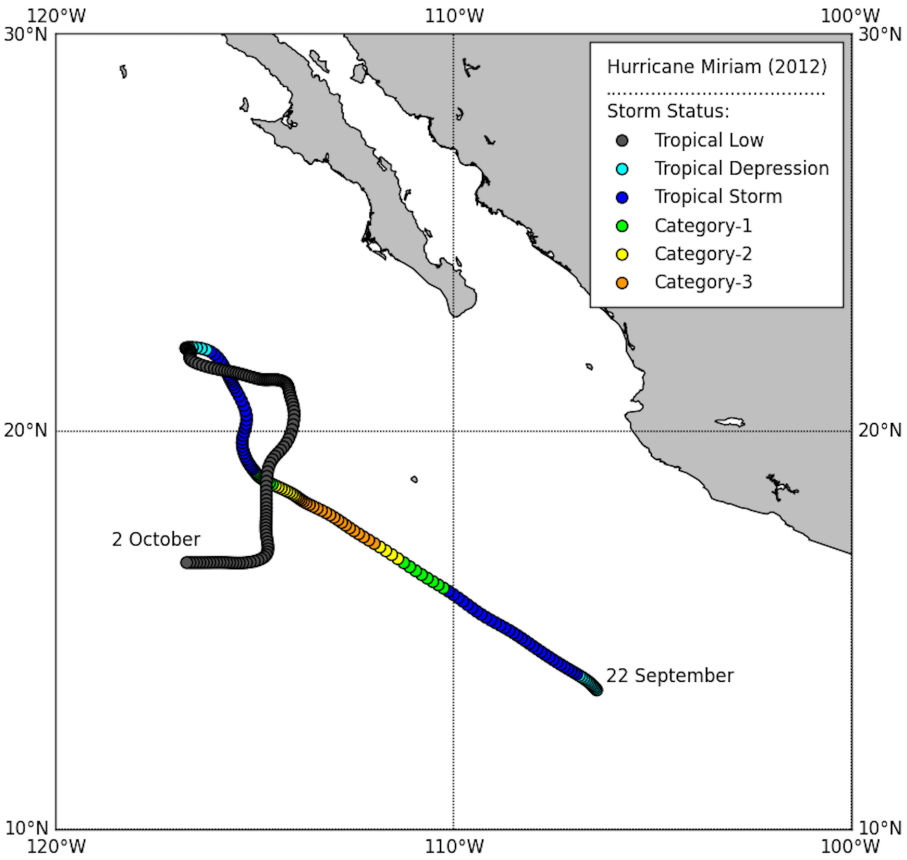

Figure 4.10: Hurricane Miriam (2012) track.

Time series analysis of Miriam's track indicated that Miriam formed in very high SSTs of 29.9°C and approximately 70 kJ cm^{-2} of UOHC. SST declined steadily as Miriam tracked northwards, with 28.7°C waters present when the storm rapidly intensified from a Tropical Storm to a major hurricane (Figure 4.11). At peak intensity, wind speeds reached 54 ms^{-1} where UOHC values hovered around 30 kJ cm^{-2}. Soon after peak intensification, SST values steeply declined to less than 26°C and excess UOHC diminished. Reported SST values were unavailable while Miriam tracked within 75 km of Clarion Island, Mexico. Wind speeds at this time declined slowly, before leveling off as a low-pressure system for the remainder of the storm duration. At 1200 UTC on 1 October, Miriam once again tracked over SSTs of 26.3°C as the storm turned south. Miriam dissipated while situated over 30 kJ cm^{-2} of UOHC.

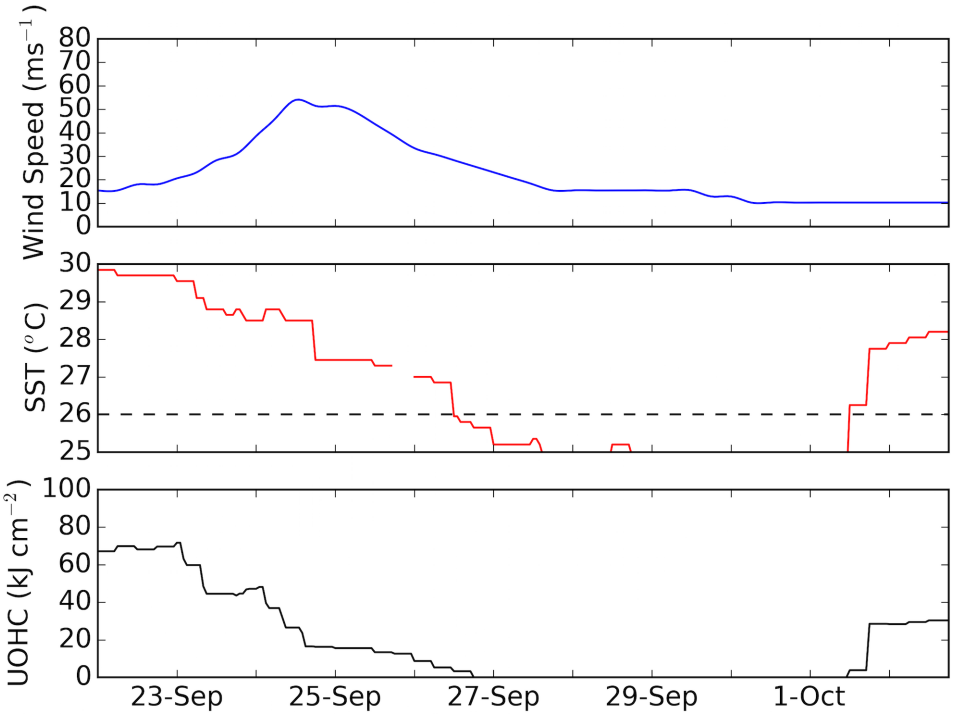

Figure 4.11: Hurricane Miriam (2012) time series of along-track U_z (Top), SST (Center) and UOHC (Bottom). The 26°C isotherm is designated by a black dashed line.

Analysis of UOHC surrounding the hurricane region revealed that Miriam formed within the south-southwestern edge of a WCE centered near 15°N 105°W, and near a second, deeper UOHC WCE (Figure 4.12a) to the east. After slowly passing along the western front of the western WCE, Miriam strengthened into a Category-1 hurricane while over approximately 50 kJ cm^{-2} of UOHC (Figure 4.12b). The following day, Miriam tracked away from the WCEs and over a substantial UOHC decline of approximately 20 kJ cm^{-2}, while storm intensity reached peak intensity status as a Category-3 hurricane during the descent into minimal UOHC waters (Figure 4.12c). However, Miriam's time as a major hurricane was short lived, as the storm weakened to a Category-1 storm to the northeast of Clarion Island the following day (Figure 4.12d).

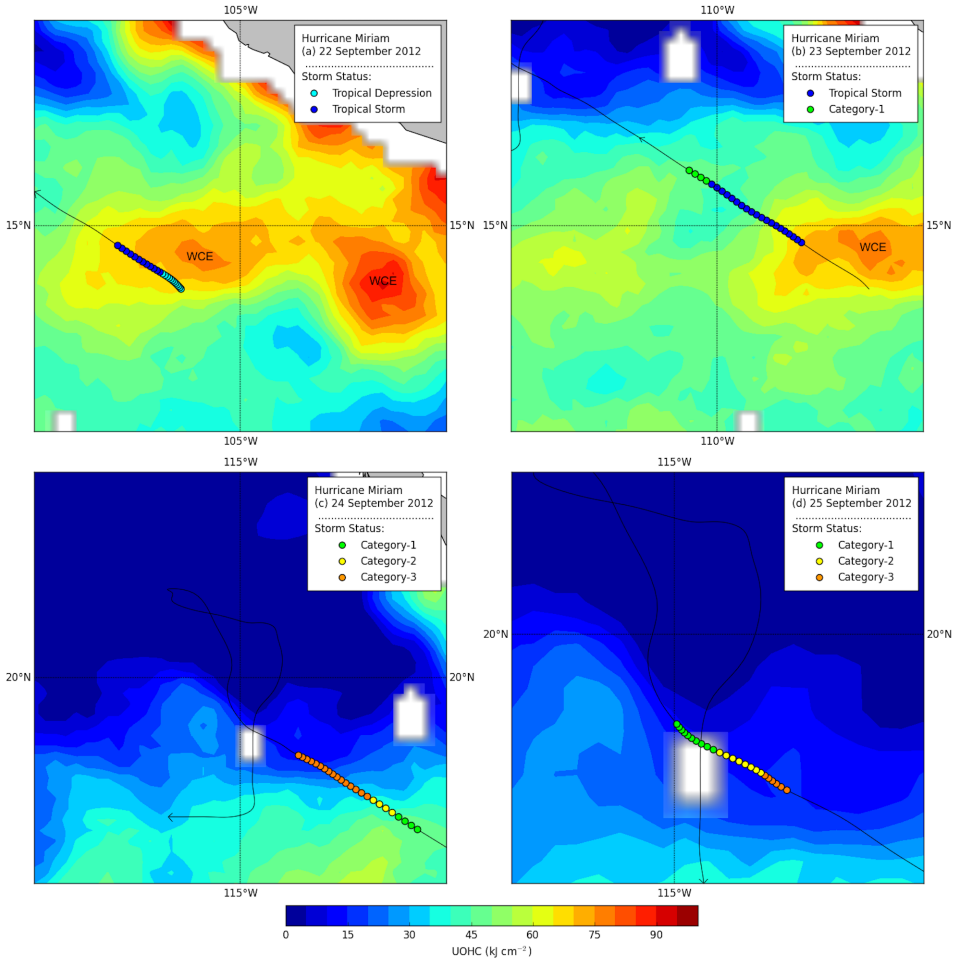

Figure 4.12: Daily UOHC with Hurricane Miriam (2012) track overlain.

- **Hurricane Paul (13 – 18 October)**

In early October, a tropical wave organized into a Tropical Depression that would steadily intensify into Hurricane Paul (Berg, 2013). The system moved westward around the southern periphery of a subtropical ridge and then turned northwards with mid- to upper-level steering flow. At this time, Paul rapidly intensified and embedded within the southwesterly flow between a mid- to upper-level low west of the Baja California peninsula and a ridge centered over northern Mexico. Paul passed within 50 km of Clarion Island, Mexico and reached peak intensity at 1800 UTC on 15 October. Upon reaching the peninsula, Paul encountered south-southwesterly wind shear that induced rapid weakening to Tropical Storm status. Caught in the mid- to upper-level steering flow, Paul turned paral-

lel to the peninsula's western coastline, making landfall at Baha Asunción, and dissipating shortly afterwards. Paul produced heavy flooding in Baja California Sur, affecting more than 16,000 people, with damages estimated at approximately USD $15.5 million (Berg, 2013). See Figure 4.13 for Paul's track.

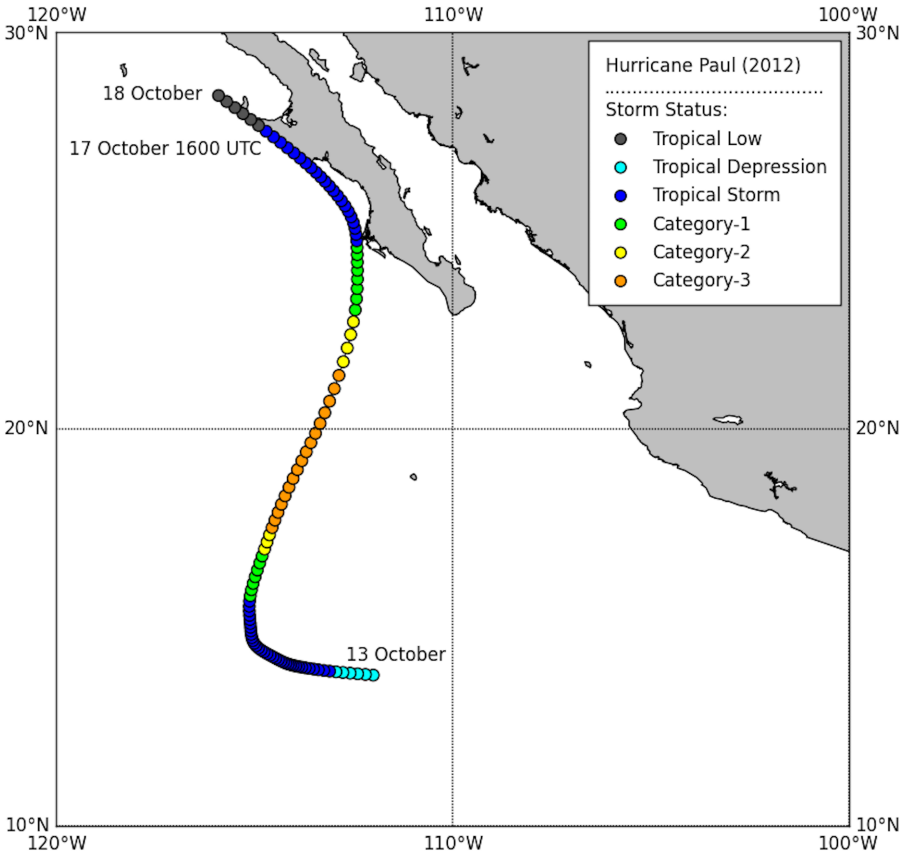

Figure 4.13: Hurricane Paul (2012) track. Date and time at landfall are provided.

Along-track analysis revealed that Paul continually intensified over 29 – 30°C SSTs that gradually declined to 27°C (Figure 4.14). In the 12-hours prior to attaining 54 ms^{-1} winds, SSTs swiftly dropped an additional 2°C. SSTs dipped below 26°C as Paul weakened to a Category-2 hurricane. During Paul's decline, SSTs increased to approximately 28.5°C. Afterwards, SST information about the storm track parallel to the peninsula was not known. Storm genesis occurred over 52 kJ cm^{-2} of UOHC that increased to 66 kJ cm^{-2} as Paul intensified to a Tropical Storm. Oceanic heat content then gradually declined as SSTs dropped. In the 6-hours before peak intensity, UOHC plummeted 30 kJ cm^{-2}. As

Paul weakened to a Category-2 hurricane, UOHC rose to 30 kJ cm^{-2} before observations ceased. Throughout the intensification phase, SSTs were 1 – 3°C above the favorable 26°C threshold, which quickly fell immediately after peak intensity.

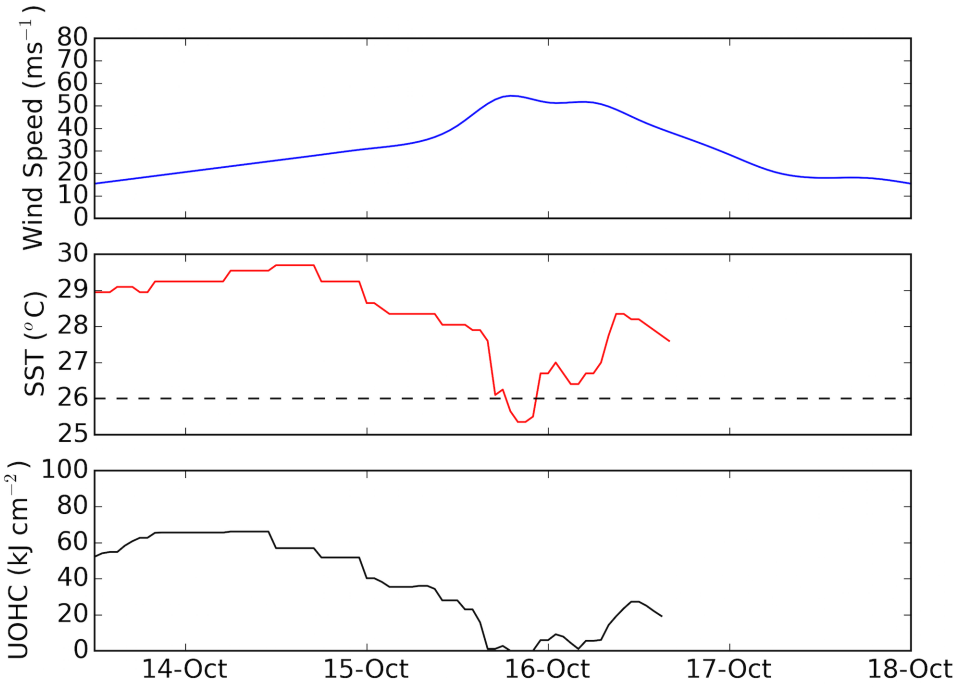

Figure 4.14: Hurricane Paul (2012) time series of along-track U_z (Top), SST (Center) and UOHC (Bottom). The 26°C isotherm is designated by a black dashed line.

Upon analysis of the UOHC field near genesis, it is evident that Paul formed to the northeast of a small WCE (Figure 4.15a). The storm's forward motion then slowed along the northern edge of the WCE. By 14 October, Paul exited the immediate region of the WCE as a Tropical Storm, and began to track northwards (Figure 4.15b). Paul's translation speed then rapidly increased and the storm strengthened to major hurricane status while over 30 – 45 kJ cm^{-2} of UOHC (Figure 4.15c). After passing to the east of Clarion Island, Paul crossed over UOHC that ranged between 0 – 20 kJ cm^{-2} on direct approach to the Baja Peninsula before slightly turning to track parallel to the coastline (Figure 4.15d).

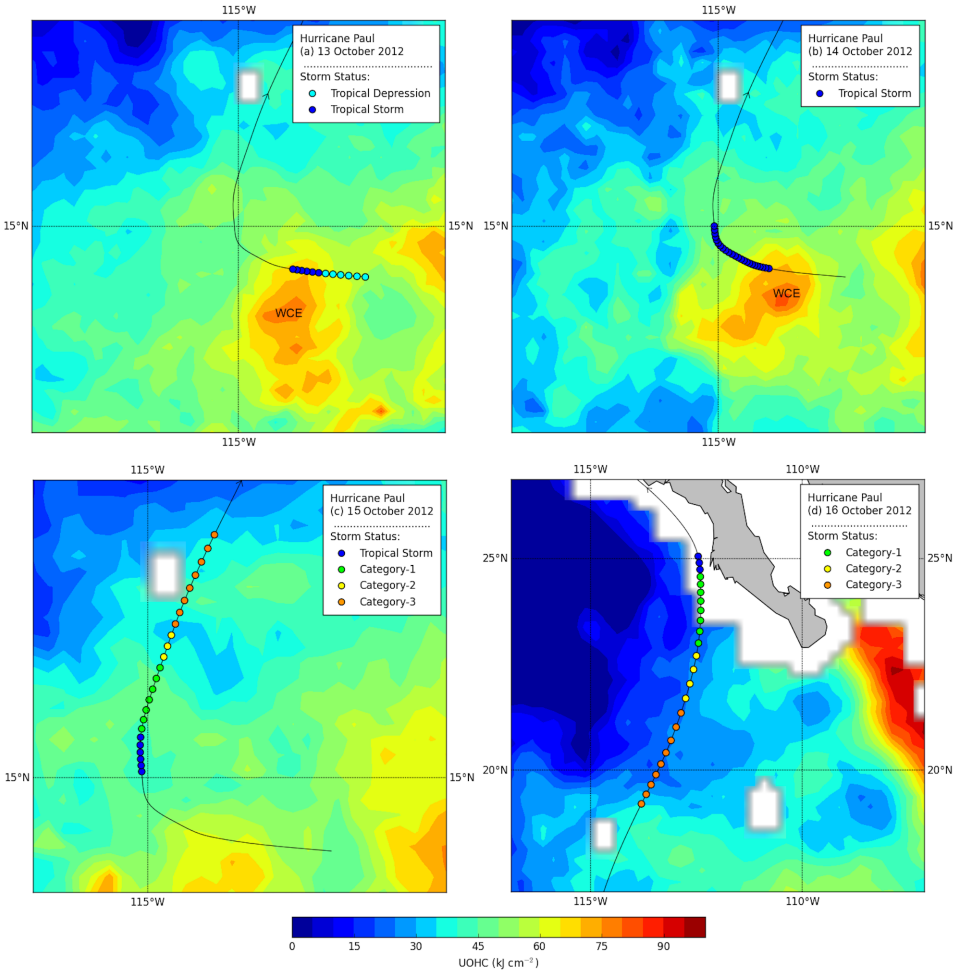

Figure 4.15: Daily UOHC with Hurricane Paul (2012) track overlain.

4.1.2 2014 Major Hurricanes

- **Hurricane Amanda (22 – 29 May)**

Hurricane Amanda, the first TC of the 2014 NPO hurricane season, originated from a tropical wave south of Acapulco, Mexico (Stewart, 2014a). Convection was slow to organize, and a Tropical Depression was named at 1800 UTC 22 May (Figure 4.16). On 23 – 25 May, Amanda underwent rapid intensification as weak wind shear, high atmospheric moisture content, and very high SSTs provided very favorable conditions for development. Due to an intense inner-core wind field and a very slow translation speed of 1.5 ms^{-1}, Amanda induced a 6°C cool wake from strong upwelling beneath the storm (Stewart, 2014a). Increased southerly wind shear and SSTs less than 24°C forced Amanda to quickly

weaken by almost 21 ms^{-1} in 24-hours. At Tropical Storm status, Amanda moved slowly northeastward around the periphery of a subtropical ridge, and the introduction of dry, stable air led to storm dissipation. At peak intensity, Amanda surpassed Hurricane Adolph (2001) as the strongest hurricane ever in the month of May during the satellite era (Stewart, 2014a).

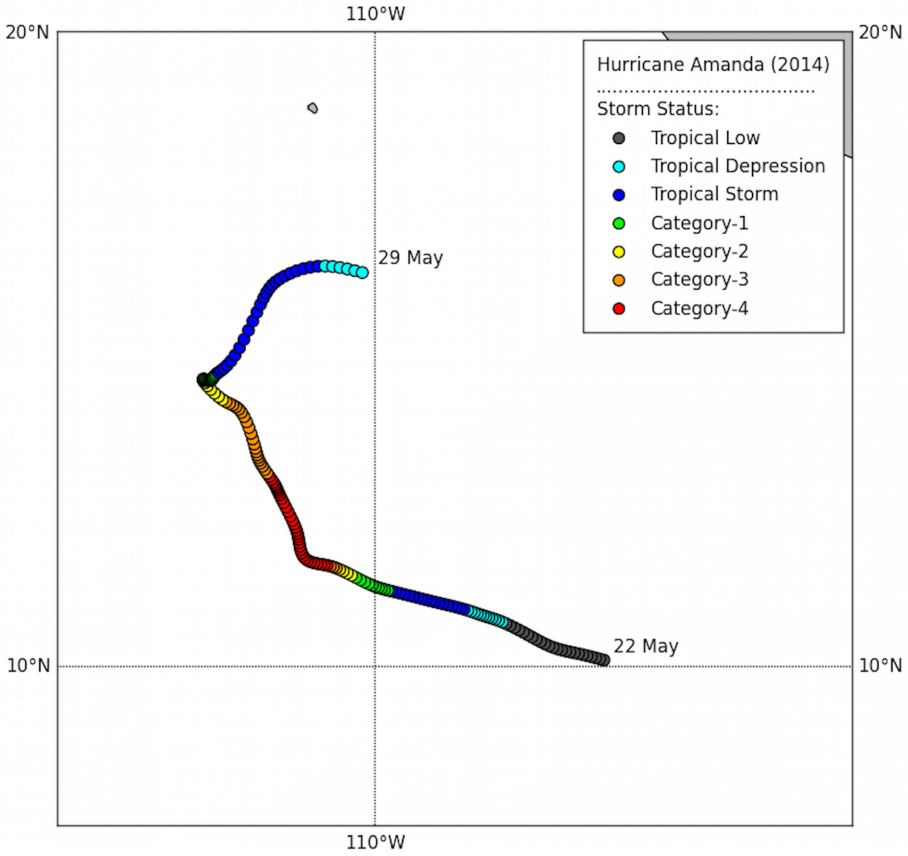

Figure 4.16: Hurricane Amanda (2014) track.

An analysis of along-track conditions revealed that for the entire storm duration, SSTs were very steady and did not range beyond 28 – 29.5°C (Figure 4.17). Thus, no clear correlation between intensification stage wind speeds and high SSTs and/or UOHC was determined. Interestingly, as Stewart (2014a) mentioned, Amanda induced a significant cooling of surface waters immediately behind the storm's track that was not detectable in the along-track SST data, but was noticeable in animations of season-wide and annual SST. Oceanic heat values were slightly more variable along-track, with genesis in 66 kJ cm^{-2}

and peak intensity over 80 kJ cm^{-2} of UOHC. Throughout the decaying stage, along-track UOHC values also slowly declined to 28 kJ cm^{-2} at time of dissipation. Amanda was a long-lived major hurricane, sustaining above 50 ms^{-1} winds for 57 hours.

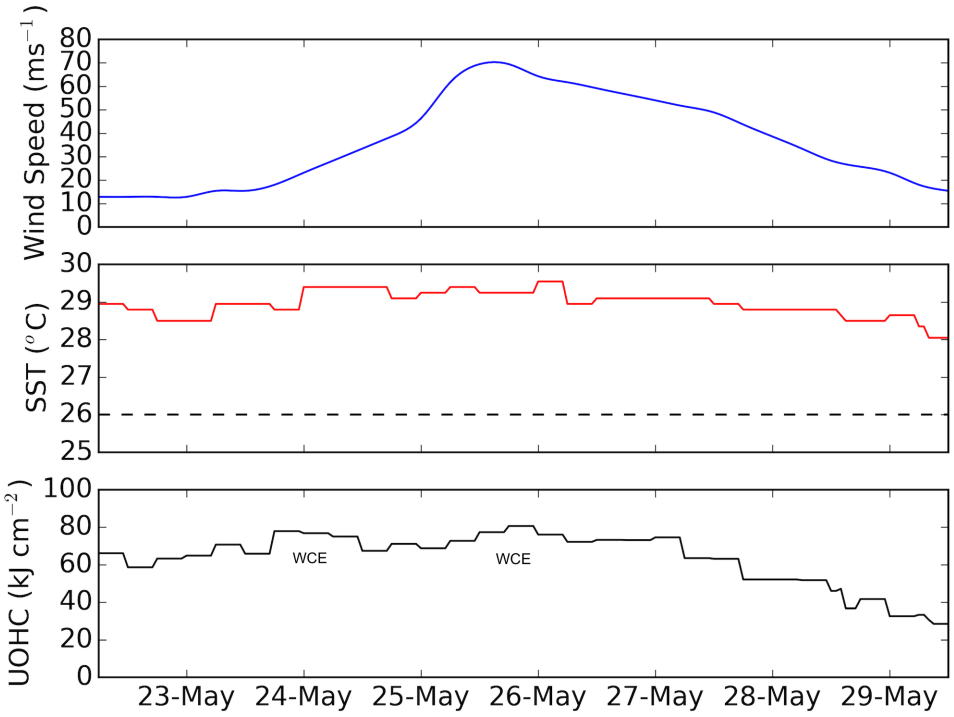

Figure 4.17: Hurricane Amanda (2014) time series of along-track U_z (Top), SST (Center) and UOHC (Bottom). The 26°C isotherm is designated by a black dashed line.

While there was some variability in the along-track UOHC, a spatial visualization of UOHC surrounding the track during the intensification phase revealed a substantial WCE was present as Amanda strengthened to a high-end Category-4 hurricane (Figure 4.18). On 24 May (Figure 4.18a), the storm tracked over a deep UOHC values that promoted intensification from Tropical Storm to Category-2 status. Ahead of this warm pool was an extensive WCE with UOHC values exceeding 90 kJ cm^{-2}. Amanda promptly intensified to a Category-3 major hurricane upon nearing the periphery of the deep WCE (Figure 4.18b) and to a Category-4 hurricane 6-hours later. Due to a very slow forward translation speed, Amanda tracked to the east around the center of the WCE, which provided a considerable amount of heat available for intensification to a very strong Category-4 storm. By

26 May (Figure 4.18c), evidence of strong upwelling beneath the track was evident in the northeastern quadrant of the WCE, where UOHC values were approximately 15 kJ cm^{-2} less than the previous day. As Amanda began to track north of the WCE, wind speeds dropped to high Category-3 status. By the end of 27 May, Amanda had passed out of the densest pocket of deep, warm waters of the WCE, leading to a rapid decline in intensity (Figure 4.18d). At this time, further evidence of significant along-track cooling was seen at the eastern and northeastern edges of the WCE.

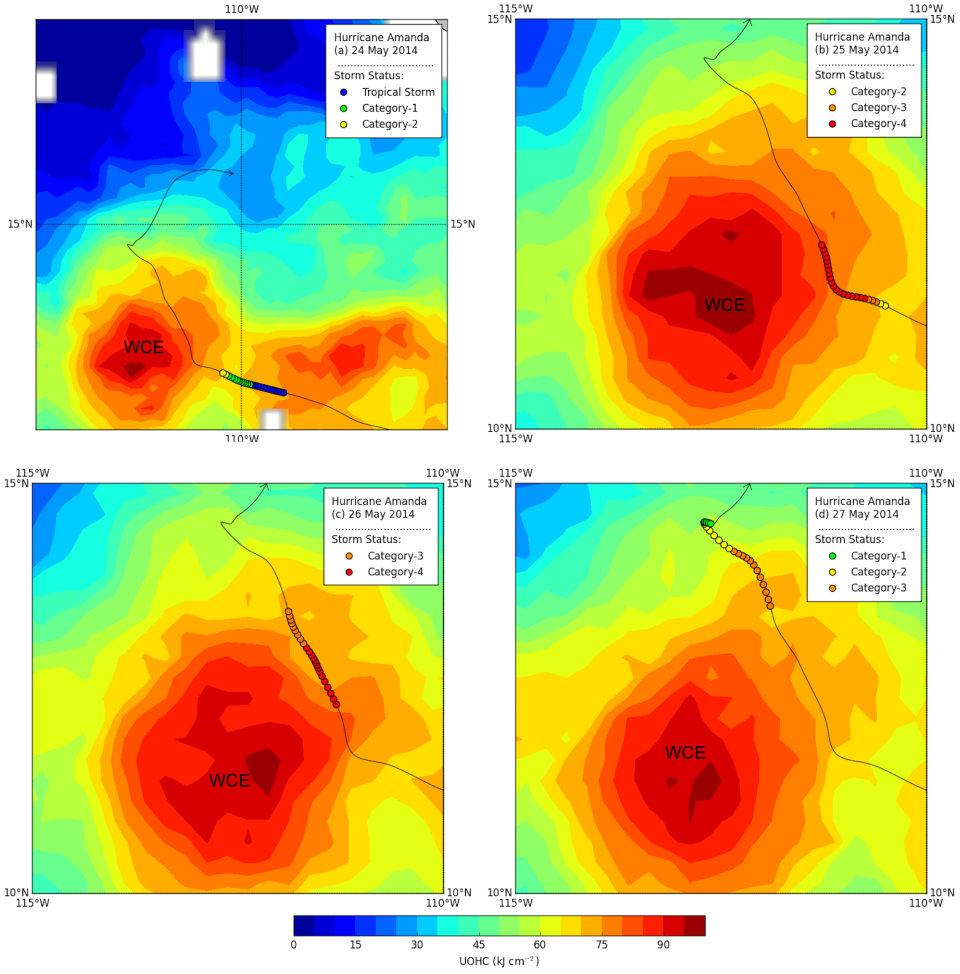

Figure 4.18: Daily UOHC with Hurricane Amanda (2014) track overlain.

- **Hurricane Cristina (9 – 19 June)**

Hurricane Cristina formed from the complex interaction between an Intertropical Convergence Zone disturbance, a tropical wave, and a Kelvin wave (Blake, 2014). The low-

pressure system slowly drifted northwestward and organized into a Tropical Depression by 1200 UTC 9 June, 250 km southwest of Acapulco, Mexico. Initially, the low- and mid-level circulations were not vertically aligned, likely due to northerly wind shear, slowing intensification. As wind shear abated, Cristina's circulation became more vertically aligned and led to rapid intensification to hurricane status by 11 June and major hurricane status the following day. However soon after, Cristina underwent an eyewall replacement cycle, prompting a brief decrease in intensity. By the time Cristina completed the replacement cycle, the storm had tracked into much cooler waters. Cristina slowly decreased in intensity until the storm lost all deep convection on 15 June. Embedded in low-level flow, the remnant low-pressure system turned eastward and then southeastward and dissipated at 0000 19 June (Blake, 2014). Hurricane Cristina became the earliest second major hurricane of any season, breaking the previous record set by Hurricane Darby (2010). Figure 4.19 illustrates Cristina's track.

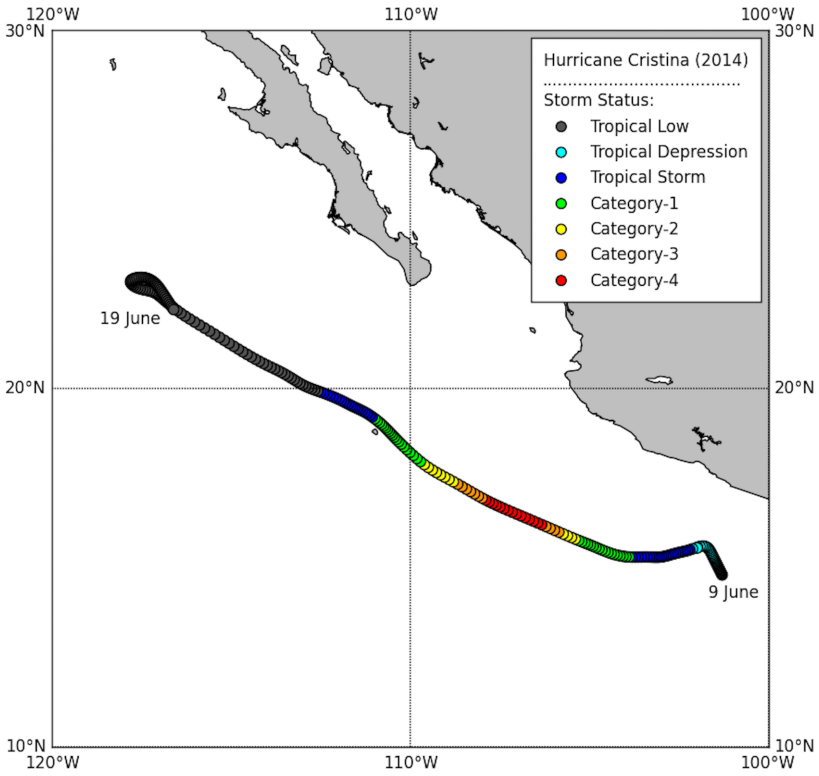

Figure 4.19: Hurricane Cristina (2014) track.

Time-series analysis indicated that while Cristina's circulation was misaligned, SSTs were very high at 30.5°C (Figure 4.20). By 11 June, Cristina aligned and wind speeds increased while over warm waters of 29.5°C. As Cristina attained Category-4 status, SSTs beneath the track increased from 29.5°C to 30.1°C. During the entirety of the intensification phase, SSTs and UOHC were consistently above the 26°C isotherm threshold for hurricane maintenance. SST values then declined to 28°C, briefly cutting out south of Isla Socorro. SSTs north of the island ranged 1°C lower, before a sharp drop to 25°C, throughout which Cristina maintained Tropical Storm status. As the storm tracked further north, SSTs were below 22.5°C. Due to a deep WCE, UOHC values at storm genesis were a very high 85 kJ cm^{-2}. As Cristina's circulation aligned and rapid intensification began, UOHC dipped below 60 kJ cm^{-2}. When Cristina peaked with 67 ms^{-1} winds, UOHC values hovered around 48 kJ cm^{-2} and steadily declined with lower SSTs. Excess heat content quickly dropped north of Isla Socorro with SSTs less than 26°C.

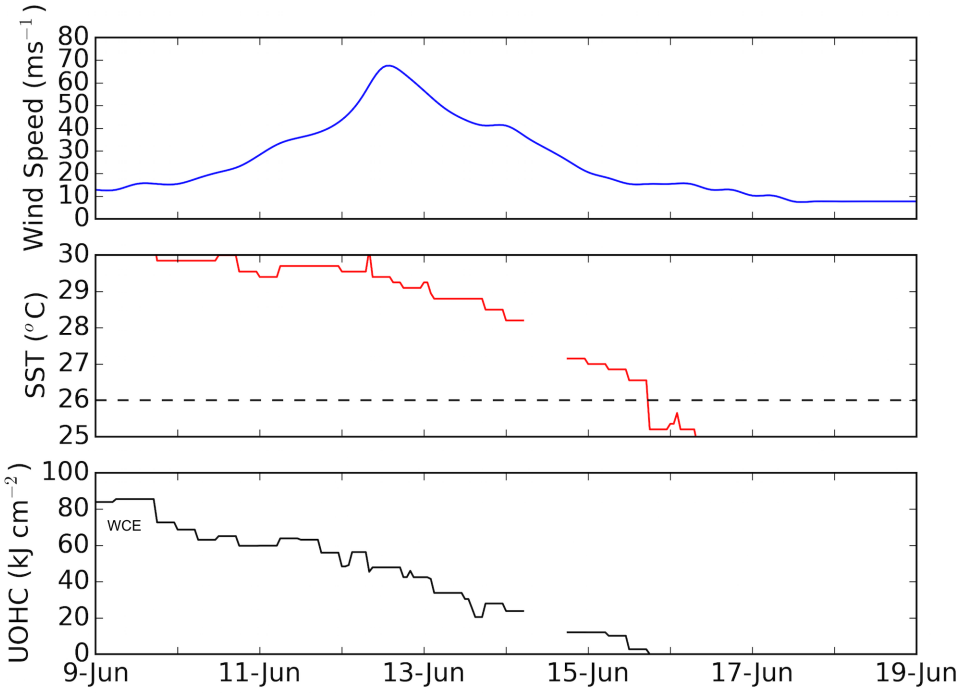

Figure 4.20: Hurricane Cristina (2014) time series of along-track U_z (Top), SST (Center) and UOHC (Bottom). The 26°C isotherm is designated by a black dashed line.

Cristina formed in the northern front of an extensive WCE (Figure 4.21a). UOHC at the center of this WCE exceeded 90 kJ cm^{-2}. Cristina took a sharp westward turn, avoiding a very weak CCE of low UOHC values (Figure 4.21b) and intensified to Tropical Storm status. Following this feature, UOHC values progressively declined along the northwestward track. Cristina intensified to a Category-1 hurricane while situated over 60 – 70 kJ cm^{-2} of UOHC (Figure 4.21c). The storm then passed out of the influence of the overall warmer coastal waters and into a UOHC region of approximately 50 kJ cm^{-2}. At this time, Cristina attained major hurricane status and developed into a Category-4 hurricane (Figure 4.21d). Late on 12 June, Cristina weakened to a Category-3 hurricane, ending the intensification phase of the storm's lifecycle.

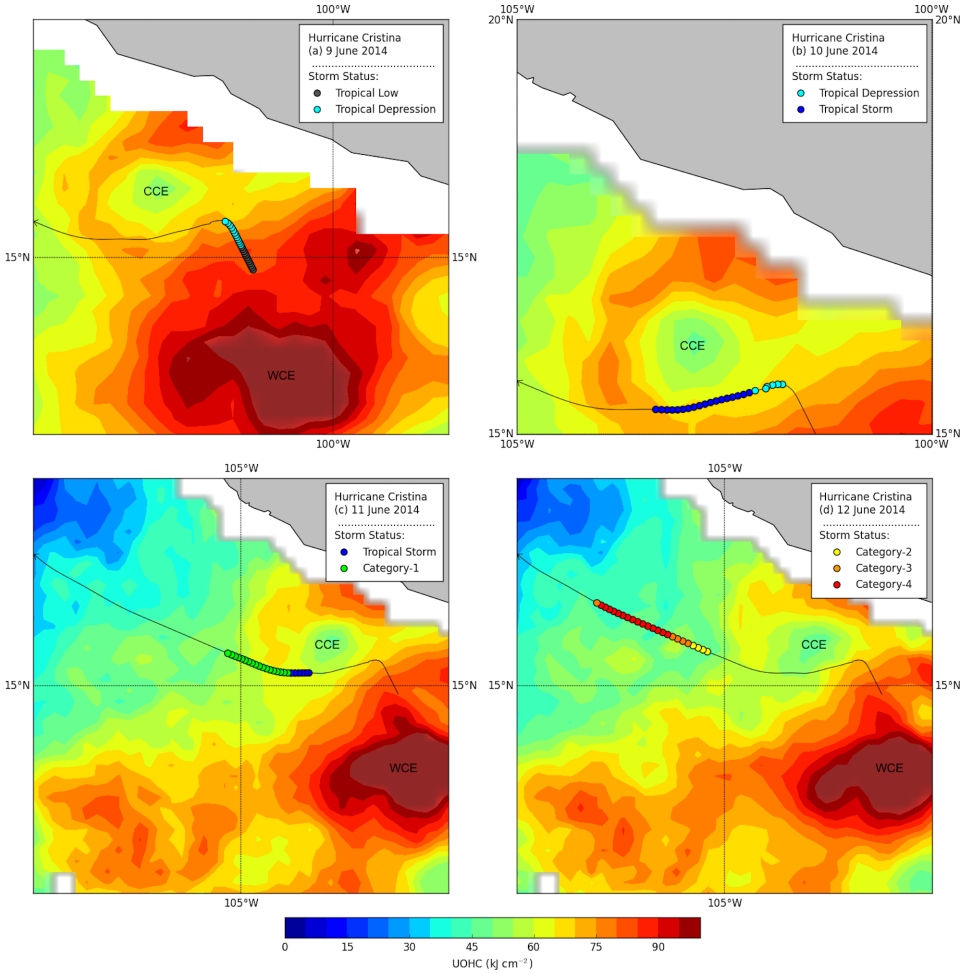

Figure 4.21: Daily UOHC with Hurricane Cristina (2014) track overlain.

- **Hurricane Genevieve (22 July – 7 August)**

Hurricane Genevieve was the first in a sequence of four TCs that formed in the NPO over an 11-day period in late July and early August (Beven, 2015). Storm genesis was triggered by an Intertropical Convergence Zone disturbance south of Panama. After 3 days as a weak low-pressure system, a Tropical Depression formed early on 25 July, and strengthened to Tropical Storm status later that day. Storm intensity then weakened to Tropical Depression status on 26 July as westerly wind shear increased and Genevieve slowly crossed into the Central Pacific. Genevieve then experienced two cycles of decay to a Tropical Disturbance and intensification to Tropical Depression status (Figure 4.22). As Genevieve tracked west-southwest of the Hawaiian Islands, rapid intensification began on 5 August, attaining hurricane status on 6 August, and major hurricane status on 7 August. While still in the NPO, Genevieve was a major hurricane for 6 hours with 67 ms^{-1} wind speeds minutes before crossing the International Date Line (180°) into the Western NPO basin. Records from the Japanese Meteorological Agency indicated that Genevieve reached 72 ms^{-1} winds quickly (Beven, 2015). An extremely rare occurrence, Genevieve existed in all three Pacific Ocean basins at some instance throughout its entire lifecycle.

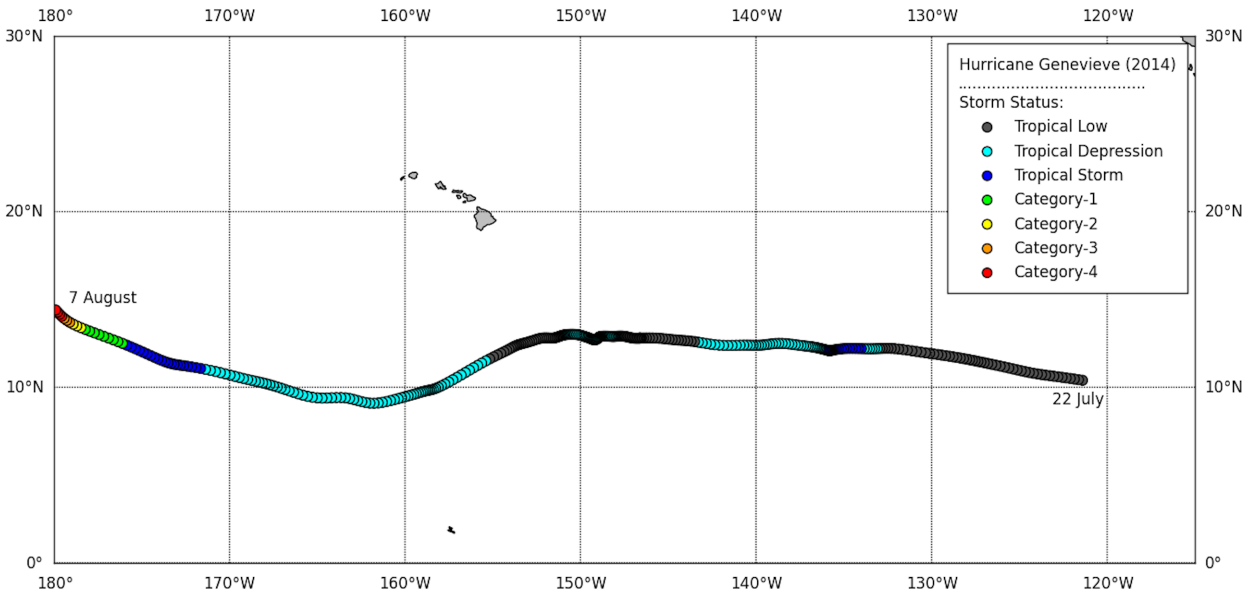

Figure 4.22: Hurricane Genevieve (2014) track.

The along-track analysis for Genevieve indicated that despite several intensification and weakening periods, SSTs remained above the favorable 26°C isotherm for the entire track duration in the East and Central NPO basins (Figure 4.23). For fourteen days, Genevieve slowly oscillated between 13 ms^{-1} and 21 ms^{-1} wind speeds. Around 1800 UTC on 5 August, the storm rapidly intensified to a Category-4 hurricane with 67 ms^{-1} wind speeds before Genevieve crossed into the Western NPO. SSTs along-track indicated that genesis occurred in very high 29°C waters, which slowly waned to approximately 26.2°C on 29 July while Genevieve was a weak Tropical Depression. As Genevieve approached the International Date Line (180°), SSTs increased upwards of 27 – 28°C. Genevieve generated in approximately 46 kJ cm^{-2} of UOHC, which briefly peaked around 55 kJ cm^{-2} while as a Tropical Low pressure system. The mean UOHC experienced throughout the entire storm duration was 38 kJ cm^{-2}. UOHC values of 40 kJ cm^{-2} and greater were consistently observed after 1200 UTC on 3 August, as Genevieve entered a region of very deep, warm waters and UOHC. At the moment of intensification to a Category-1 hurricane, UOHC values were greater than 90 kJ cm^{-2}, with a peak of 96 kJ cm^{-2}. Storm conditions, SST, and UOHC data concerning Genevieve's duration in the Western NPO were not investigated in this study.

Rather than the full fourteen day intensification phase, for the daily UOHC subplots during Genevieve, the 6-days prior to maximum intensity is shown in Figure 4.24. It is important to note here that the Genevieve UOHC subplots are on a modified scale (1 – 130 kJ cm^{-2}) compared to the previous storms (on a 1 – 100 kJ cm^{-2} scale) in order to further resolve oceanic mesoscale features within the very deep UOHC pool near the International Date Line. On 2 August, Genevieve maintained Tropical Low status, which then intensified into a Tropical Depression after tracking southwestward over patchy UOHC regions of 45 – 50 kJ cm^{-2} (Figure 4.24a). Genevieve returned back onto a westward trajectory into very stable 50 – 60 kJ cm^{-2} waters near 9°N. Evidence of the very deep UOHC pool

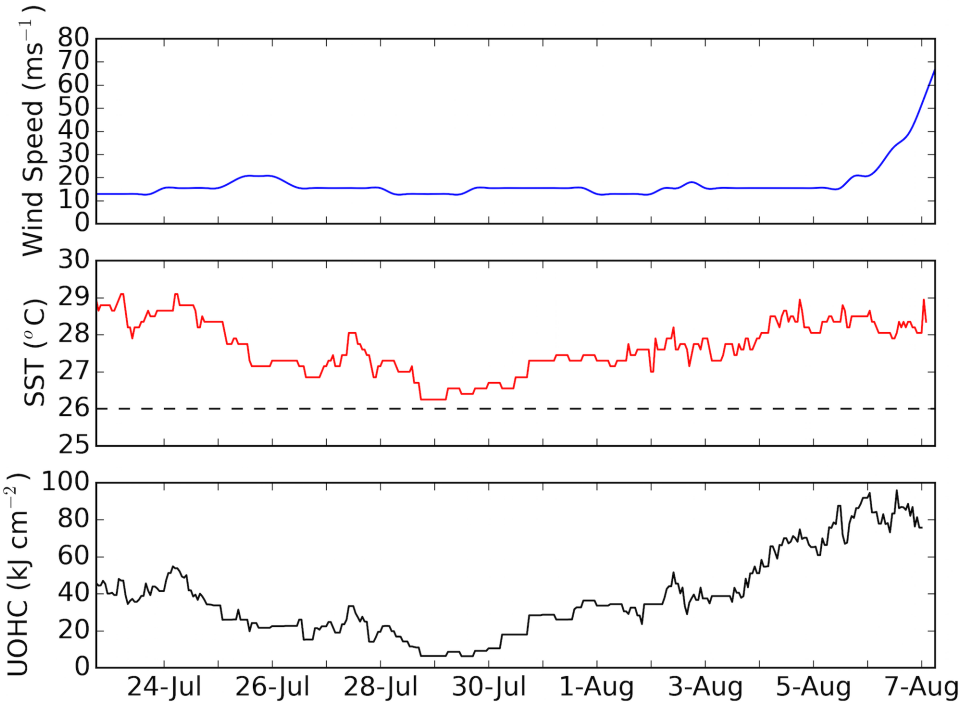

Figure 4.23: Hurricane Genevieve (2014) time series of along-track U_z (Top), SST (Center) and UOHC (Bottom). The 26°C isotherm is designated by a black dashed line.

near the central equatorial tropics was apparent below 7°N, where values exceeded 130 kJ cm^{-2} (Figure 4.24b). As Genevieve tracked further westward (Figure 4.24c), UOHC values increased to approximately 80 – 85 kJ cm^{-2}, over which Genevieve again strengthened into a Tropical Storm (Figure 4.24d). Further intensification occurred as the storm tracked over a deep WCE of 90 – 110 kJ cm^{-2}, eventually attaining Category-2 status late on 6 August (Figure 4.24e). The following day Genevieve quickly attained Category-4 status before passing into the Western NPO basin and out of this thesis' study region. Reports from the Japanese Meteorological Agency confirmed that Genevieve further deepened and was classified a Super-Typhoon, the equivalent of a Category-5 hurricane, after crossing the International Date Line (Beven, 2015).

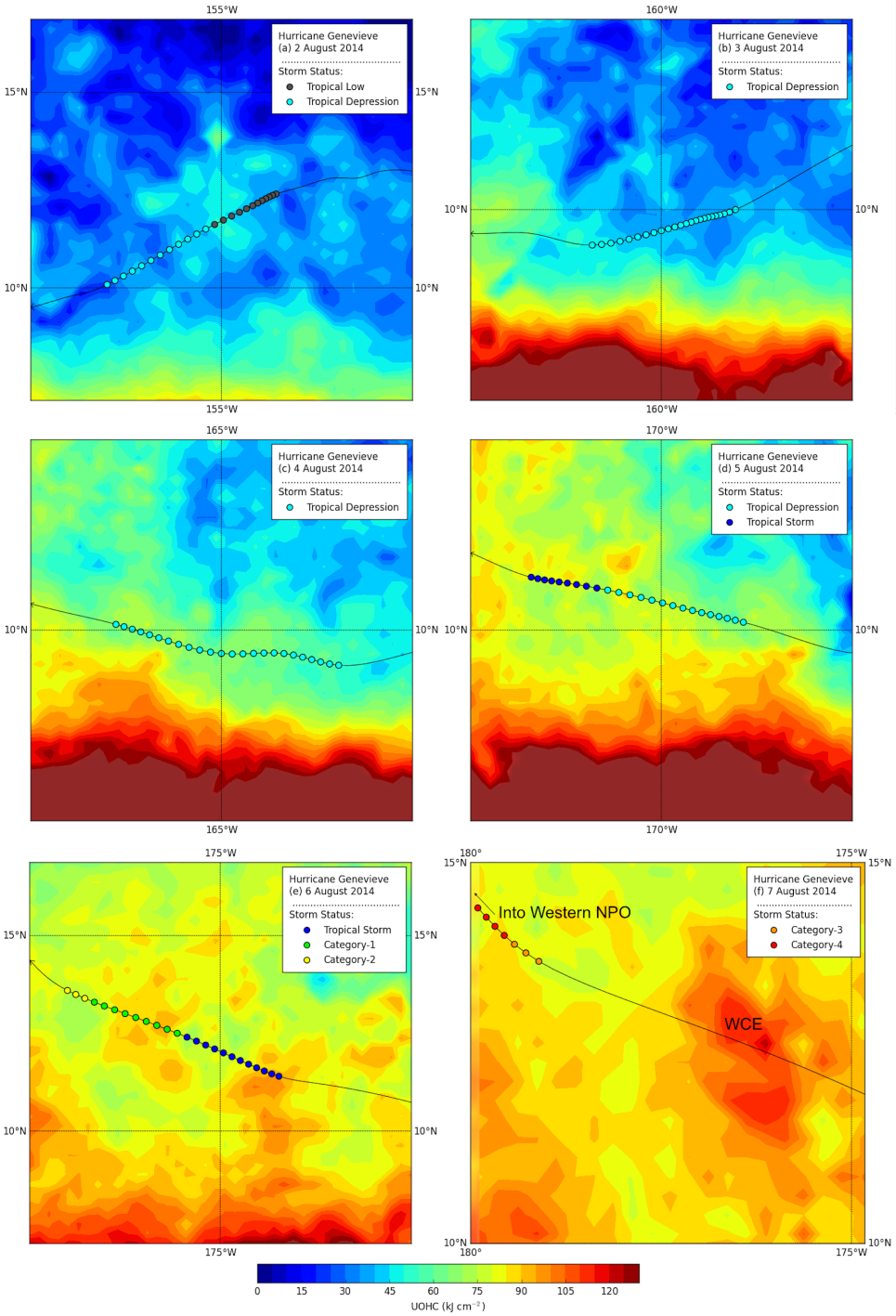

Figure 4.24: Daily UOHC with Hurricane Genevieve (2014) track overlain.

- **Hurricane Iselle (30 July – 9 August)**

Iselle stemmed from an easterly wave that became convectively active upon entering the NPO. Due to subsident upper-level outflow from Hurricane Hernan to the northwest, the wave was slow to organize (Kimberlain, 2016). The passage of an atmospheric Kelvin wave resulted in favorable conditions for storm genesis on 30 July, with weakened easterly wind shear and increased atmospheric moisture. Iselle reached hurricane strength 36-hours after genesis, and rapidly intensified over the following 24-hours to major hurricane status under moderate north-northeastern wind shear. By 4 August, Iselle tracked parallel to the 26°C isotherm and wind shear over the storm complex abated. Due to these factors, Iselle evolved into an annular structure (Knaff et al., 2003), with a large eye, an axisymmetric ring of deep convection, and lack of convective rain bands (Kimberlain, 2016). Challenges with forecasting annular hurricane intensity are discussed in Section 4.3.

Iselle attained peak intensity at 1800 UTC on 4 August with wind speeds of 61.7 ms^{-1} just east of the 140°W meridian. Translation speed slowed when less favorable thermodynamic conditions and increased southwesterly wind shear disrupted the annular structure, promoting decay. Iselle accelerated on a west-northwestward path towards the Hawaiian Islands as a northern subtropical ridge strengthened and wind shear weakened (Birchard and Ballard, 2014). Abundant dry air entrainment combined with adverse wind shear conditions resulted in rapid weakening (Houston, 2014) before Iselle made landfall as an intense Tropical Storm on the Big Island, with the island terrain disrupting the main circulation (Birchard, 2014a,b; Ballard, 2014a,b). Iselle dissipated at 0900 UTC on 9 August to the north-northwest of the Big Island (Donanldson, 2014)[1]. Iselle's rare landfall on the Hawaiian Islands was only the fourth TC to ever do so, and the first to directly hit the Big Island (Jarrell et al., 2001)[2]. See Figure 4.25 for Iselle's track.

[1]At the time of writing, the NHC report for Iselle had not yet been updated for summarized storm conditions and damage totals in the CPHC domain. Instead, real-time forecast advisories were used here.

[2]Hurricane Dot (1959), Hurricane Iwa (1982), and Hurricane Iniki (1992) made landfall on Kauai.

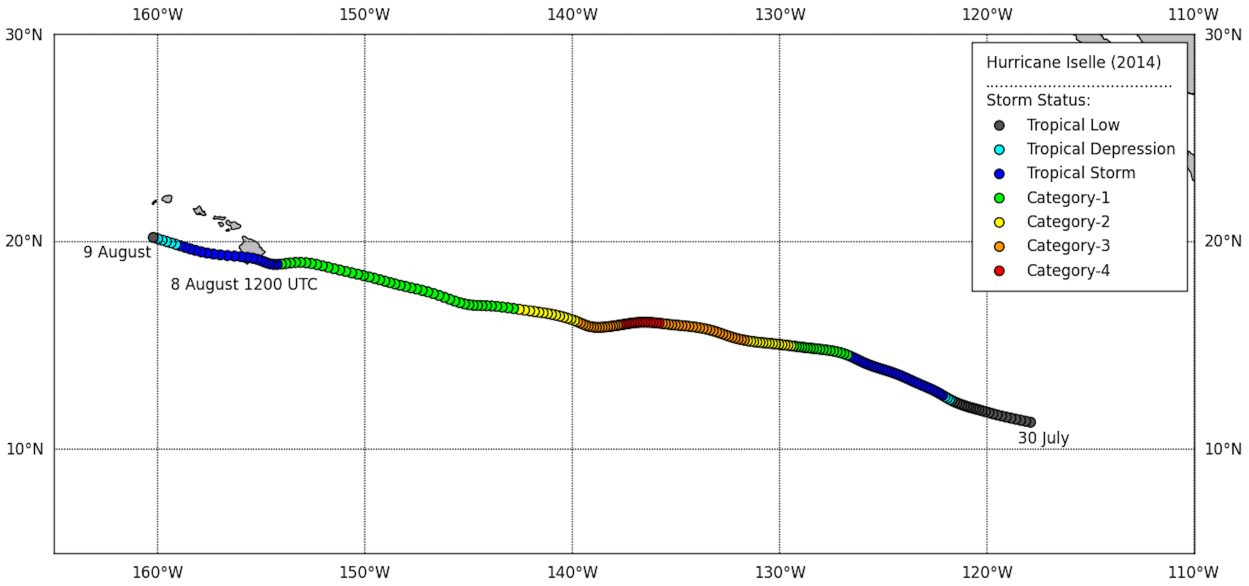

Figure 4.25: Hurricane Iselle (2014) track. Date and time at landfall are provided.

Along-track conditions implied that Iselle formed over consistently high SSTs of 28.7°C for the 36-hours after storm genesis (Figure 4.26). While Iselle attained 33 ms^{-1} wind speeds as a Category-1 at 0000 UTC on 2 August, along-track SSTs had dipped to 27°C, but increased above 28°C as wind speeds reached 41 ms^{-1}. SSTs then gradually declined to approximately 26.5°C as Iselle reached Category-4 status, and ranged from 25.5°C to 27°C as the storm tracked to the west-northwest along the 26°C isotherm. At landfall, SSTs surrounding the Hawaiian Islands were approximately 26.5°C. Oceanic heat content peaked during genesis, forming over 61 kJ cm^{-2}. UOHC values fell as the storm tracked northwards, falling to approximately 30 – 35 kJ cm^{-2}. At attainment of Category-1 status, UOHC beneath the storm track was 15 kJ cm^{-2}, which climbed to 27 kJ cm^{-2} as the storm intensified to a Category-3. UOHC fell quickly afterwards as SST dropped to 26°C, but again rose to 10 – 15 kJ cm^{-2} as the storm developed 59.2 ms^{-1} wind speeds. During Iselle's slow de-intensification phase, UOHC values averaged a low 7 kJ cm^{-2}. At landfall, UOHC beneath the storm was 10 kJ cm^{-2}. UOHC post-landfall rose with increased SSTs, despite a quick drop to 2 kJ ms^{-1}.

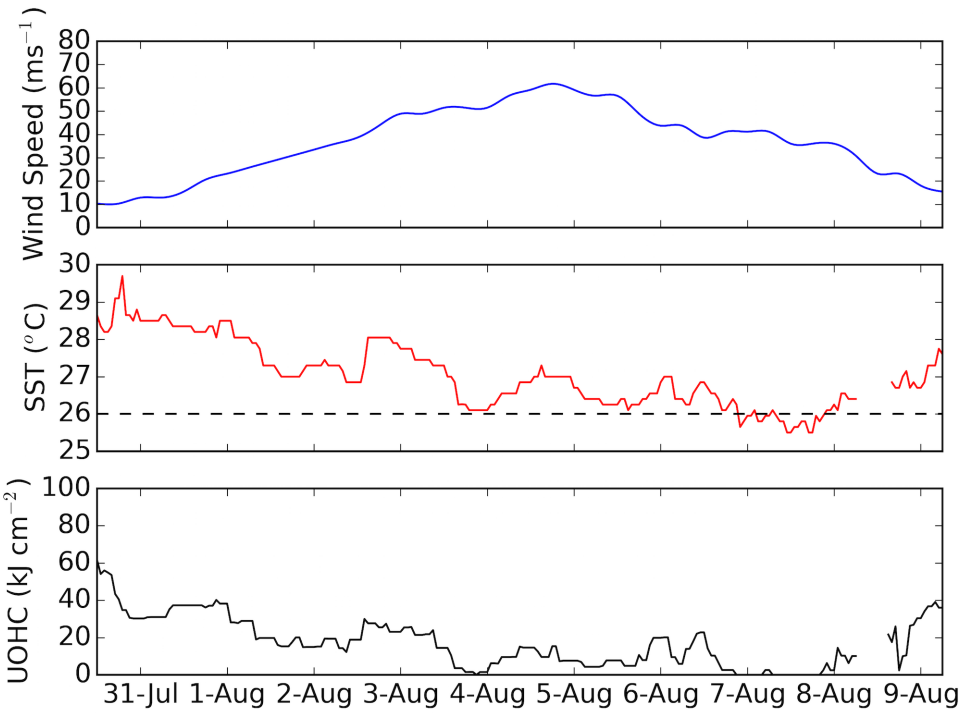

Figure 4.26: Hurricane Iselle (2014) time series of along-track U_z (Top), SST (Center) and UOHC (Bottom). The 26°C isotherm is designated by a black dashed line.

Analysis of UOHC revealed that Iselle formed in a high UOHC region of approximately 55 – 60 kJ cm^{-2} before dropping approximately 25 kJ cm^{-2} (Figure 4.27a). After Iselle passed out of this lower UOHC region and into 35 – 40 kJ cm^{-2}, the storm quickly strengthened to Tropical Storm status (Figure 4.27b). The following day, the storm tracked out of the main deep UOHC region and approached the 26°C isotherm. Despite declining UOHC values, Iselle attained Category-1 status late on 1 August (Figure 4.27c). At this time, Iselle rotated onto a more westward track and further intensified as UOHC values increased by 5 – 10 kJ cm^{-2} (Figure 4.27d). It is evident that Iselle obtained a significant amount of heat from this northern UOHC region, as UOHC values at approximately 15°N, 131°W dropped by 5 – 10 kJ cm^{-2} after storm passage. Shortly after this, Iselle attained major hurricane status and tracked above the 26°C and into no excess UOHC (Figure 4.27e). On 4 August, Iselle moved over very low UOHC values of 0 – 15 kJ cm^{-2}, during which storm intensity obtained peak Category-4 hurricane force wind speeds (Figure 4.27f). After reaching peak intensity, Iselle tracked along the 26°C boundary.

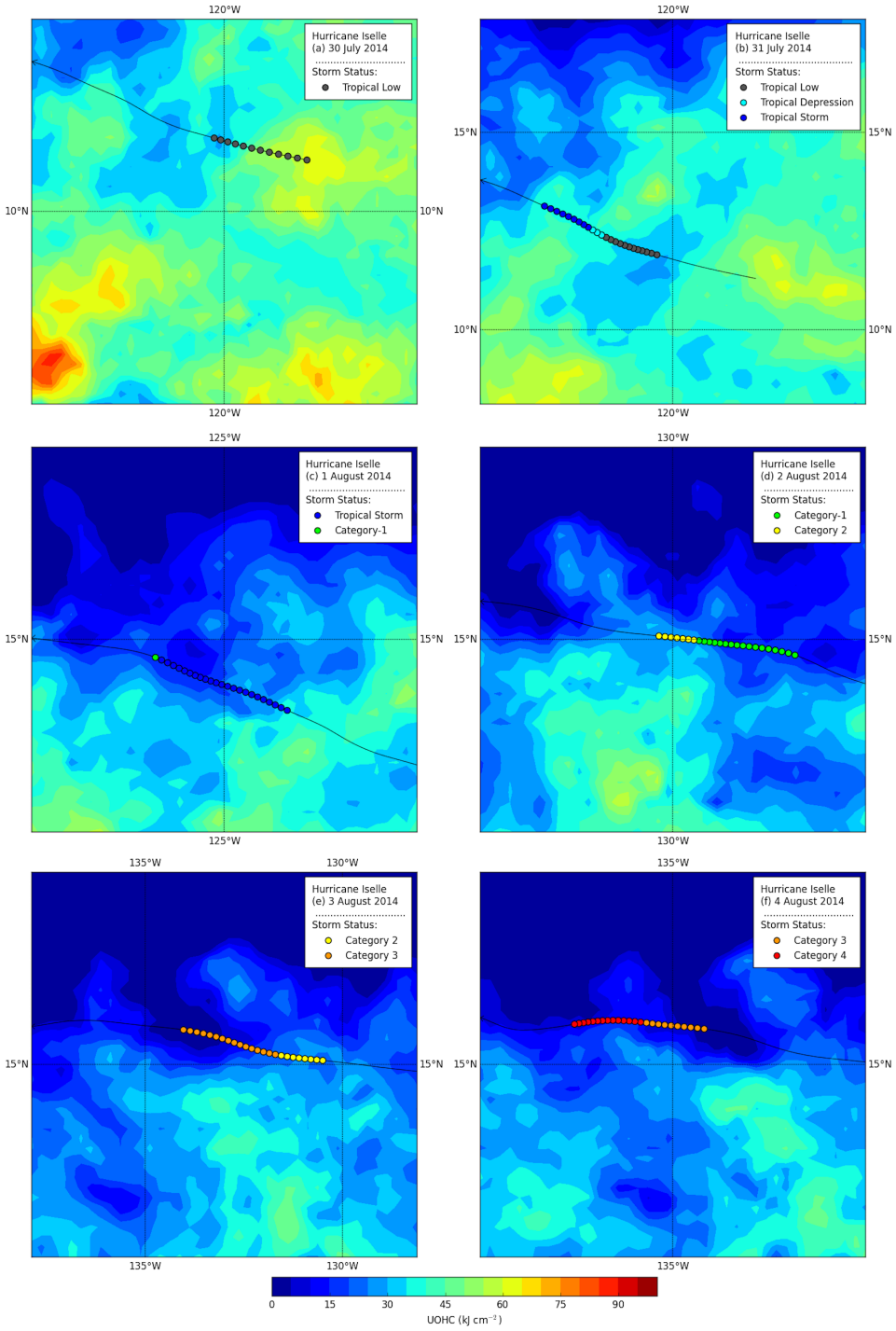

Figure 4.27: Daily UOHC with Hurricane Iselle (2014) track overlain.

- **Hurricane Julio**

Hurricane Julio formed from a tropical wave that steadily organized into a low-pressure system at 0000 UTC 2 August (Stewart and Jacobson, 2016) (Figure 4.28). Two days later, the system was designated a Tropical Depression, quickly followed by Tropical Storm status. Julio intensified in a weak wind shear and high SST environment as it moved west-northwest around the southern edge of a subtropical high in the NPO. By 0600 UTC 6 August, Julio reached Category-1 status, and peak intensity two days later with 54.0 ms^{-1} wind speeds. Despite negligible wind shear, Julio weakened after crossing into the Central NPO, likely due to a 3°C decline from cool wake upwelling. On 10 August, southwesterly wind shear increased sharply, turning the weakening storm towards the northwest. While north of the Hawaiian Islands, Julio regained Category-1 status briefly under abnormally higher SSTs for that region and diminished wind shear. Almost immediately after the second peak, southwesterly wind shear increased and dry mid-level air forced Julio to rapidly weaken into a remnant low while on a northward path. Julio dissipated by 1200 UTC 18 August more than 1,800 km north of the Hawaiian Islands (Stewart and Jacobson, 2016).

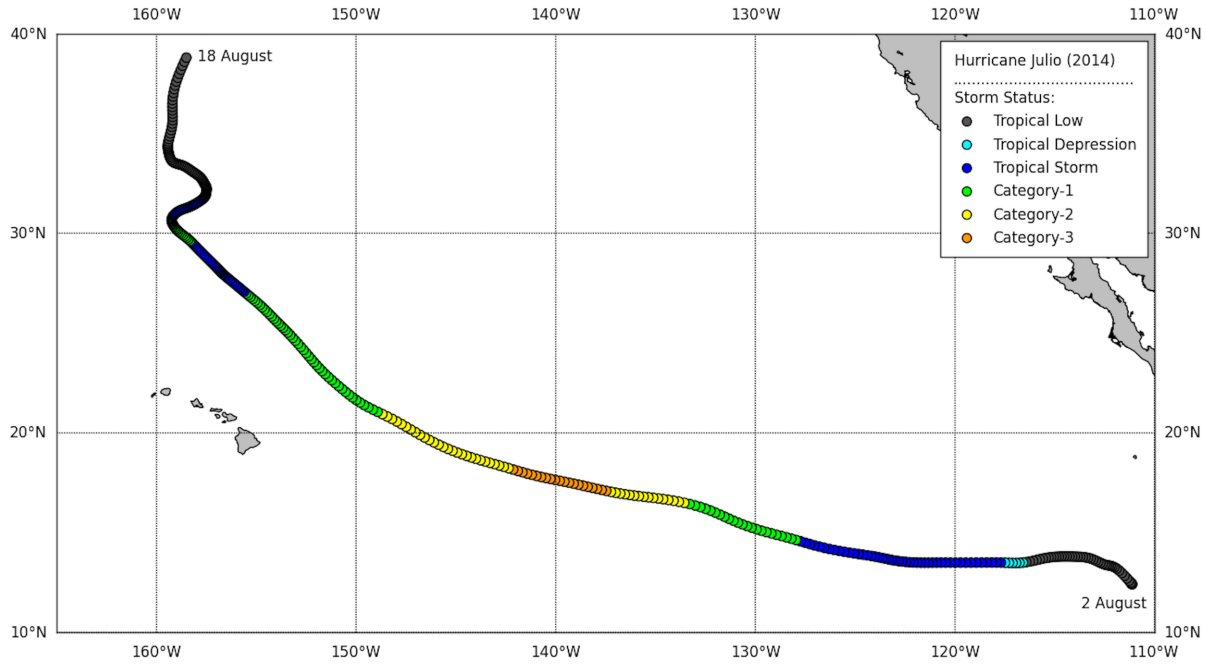

Figure 4.28: Hurricane Julio (2014) track.

Time series analysis indicated that Julio formed in 28.4°C SSTs, which increased to 29.6°C, as the storm remained a well-organized Tropical Low (Figure 4.29). Shortly before 4 August, SSTs along-track fell to 28.2°C as the storm deepened into a Tropical Storm. Two days later while over 27°C waters, Julio attained 33.0 ms^{-1} wind speeds. SSTs continued to drop, cooling to 25.5°C and lower, not more than 12 hours after achieving hurricane status. Despite very cool SSTs, Julio peaked with 54.0 ms^{-1} wind speeds at 0600 UTC 8 August. SSTs remained below 26°C for the next three days as Julio weakened, until the storm moved into relatively higher SSTs, north of the Hawaiian Islands. SSTs increased to 27°C, which allowed Julio to re-intensify to 36.0 ms^{-1} wind speeds. However, SSTs quickly fell to 21°C, forcing Julio to weaken and dissipate on 18 August. Along-track UOHC values revealed that Julio formed in low UOHC of 32 kJ cm^{-2}, peaking at 60 kJ cm^{-2} where SSTs exceeded 29.5°C. As Julio passed over 55 kJ cm^{-2} of UOHC, Julio transitioned from a Tropical Depression to a Tropical Storm. Afterwards, UOHC along-track fell with declining SSTs, with a brief peak of 25 kJ cm^{-2} before falling to 0 kJ cm^{-2} as Julio strengthened to a Category-1 hurricane. Not more than 24-hours later, UOHC beneath Julio reached 20 kJ cm^{-2} as SSTs climbed to 27°C, prompting Julio to attain 50 ms^{-1} winds speeds as a Category-3 hurricane. At maximum intensity and for the following intensity decline, there was no excess oceanic heat above 26°C. Early on 11 August, UOHC climbed to a peak of 21 kJ cm^{-2}, allowing Julio to quickly increase to 36.0 ms^{-1} wind speeds before UOHC values decreased as Julio tracked out of this northern warm pool.

Daily UOHC fields revealed that Julio attained Tropical Depression status while situated in a large region of 45 – 55 kJ cm^{-2} before quickly passing into gradually declining UOHC (Figure 4.30a). The following day, a large region to the south of Julio developed into a large CCE where UOHC dropped as low as 5 kJ cm^{-2} (Figure 4.30b). On 6 August, Julio moved on a northwesterly trajectory, and attained Category-1 hurricane status over waters of 20 – 35 kJ cm^{-2}, while deeper UOHC was located to the south of the storm track

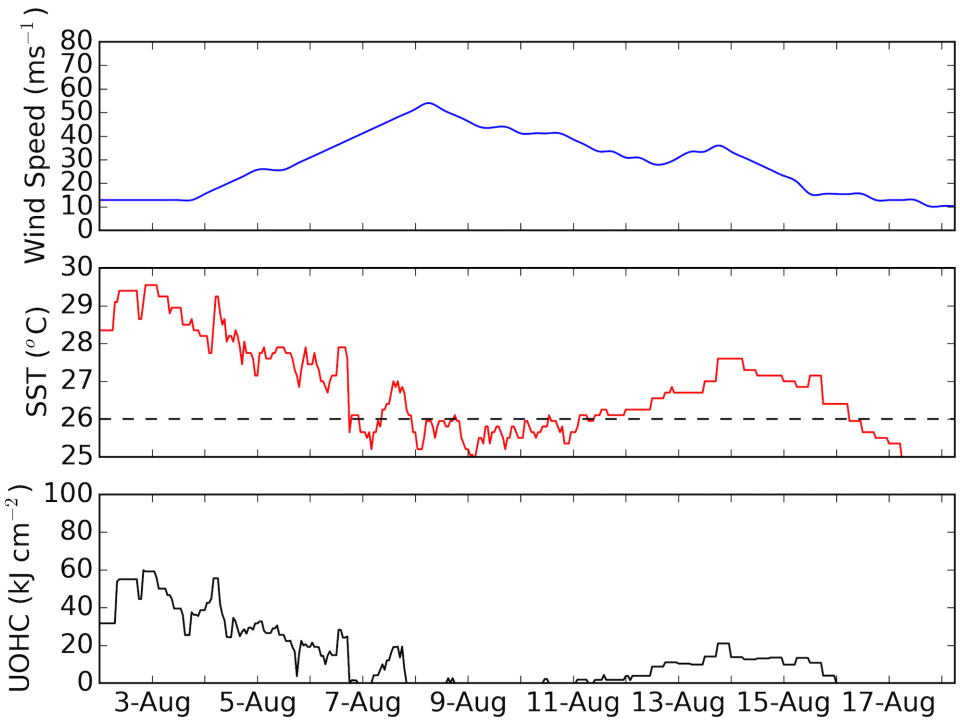

Figure 4.29: Hurricane Julio (2014) time series of along-track U_z (Top), SST (Center) and UOHC (Bottom). The 26°C isotherm is designated by a black dashed line.

(Figure 4.30c). Quickly moving out of this region, Julio tracked directly into 0 kJ cm^{-2} of UOHC. Upon comparison to the location of transition from Category-1 status the previous day to Category-2 on 7 August, it is evident that approximately 15 kJ cm^{-2} of UOHC was removed immediately beneath Julio's track, providing energy for intensification at this time. Julio then tracked over a northern extension of UOHC where values increased by 20 kJ cm^{-2}, allowing for further strengthening to major hurricane status (Figure 4.30d). At the time of peak intensity, Julio was situated over waters with no excess heat content, promoting a steady weakening. However, 5-days later as Julio tracked well above the Hawaiian Islands, the storm entered into a large region of 0 – 20 kJ cm^{-2} (Figure 4.30e). At this time, Julio tracked directly into the center of this deep UOHC region, and briefly re-intensified to Category-1 hurricane status (Figure 4.30f). At 0000 UTC 14 August Julio weakened to Tropical Storm status and dissipated several days later.

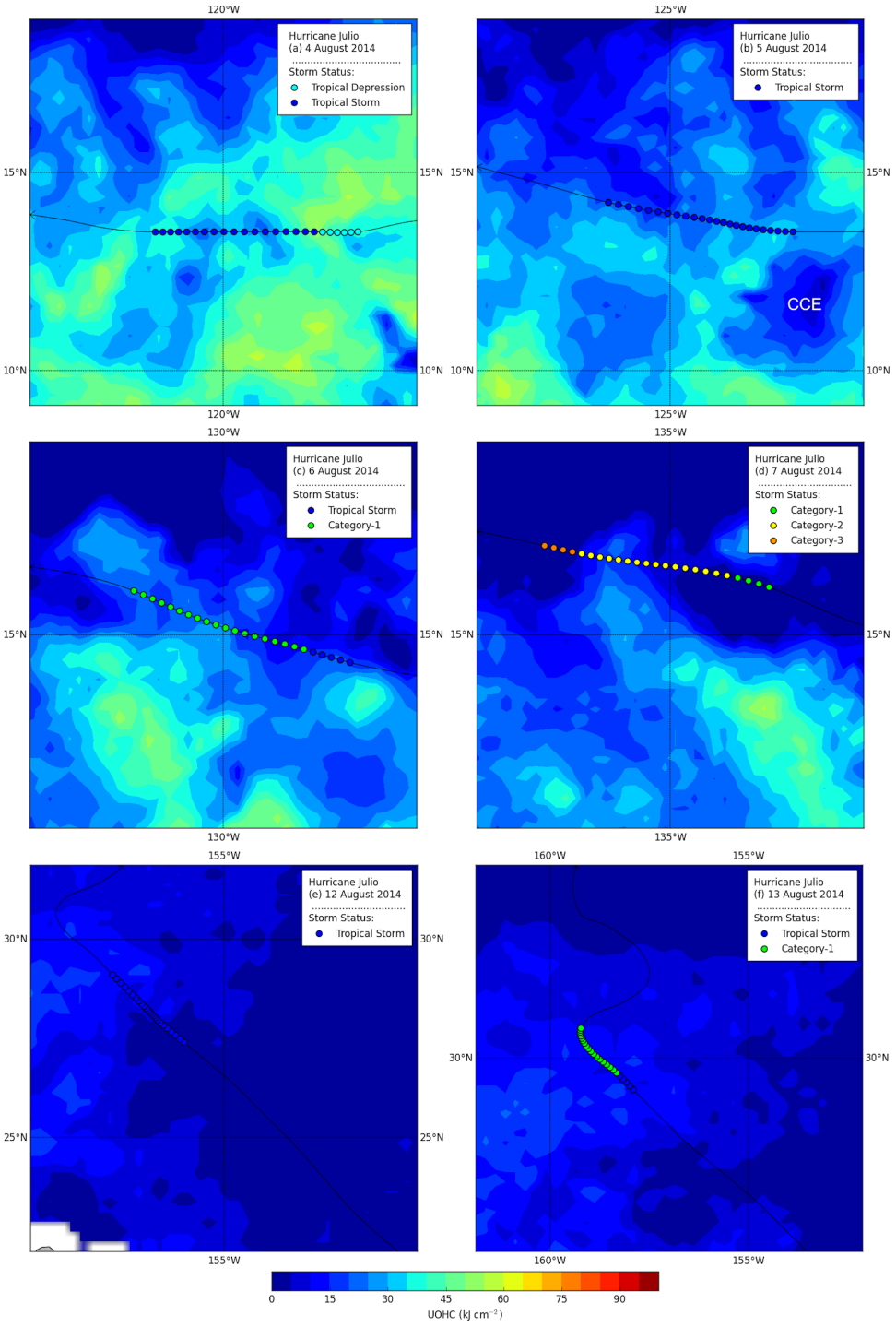

Figure 4.30: Daily UOHC with Hurricane Julio (2014) track overlain.

- **Hurricane Marie (22 August – 2 September)**

Marie originated when a tropical wave organized into a Tropical Depression on 22 August south-southeast of Acapulco, Mexico (Zelinsky and Pasch (2015); Figure 4.31). Embedded in a favorable environment of low wind shear, high atmospheric moisture, and SSTs near 30°C, Marie underwent a rapid 66-hour intensification, resulting in 72.0 ms^{-1} wind speeds. Intensification ended as an eyewall replacement cycle began, inducing a steady weakening trend. Late on 26 August, Marie tracked over a large SST gradient, resulting in rapidly decreasing SSTs, thus weakening into a Tropical Storm 18-hours later. By 29 August, Marie was a remnant-low that traveled with low-level easterly flow before dissipation on 2 September (Zelinsky and Pasch, 2015). In addition to being the first Category-5 hurricane in the NPO basin since Hurricane Celia in 2010, Marie was also a very large hurricane, spanning nearly 950 km in diameter. There were 4 casualties associated with Marie, as well as USD $16 million in wave damages (Zelinsky and Pasch, 2015).

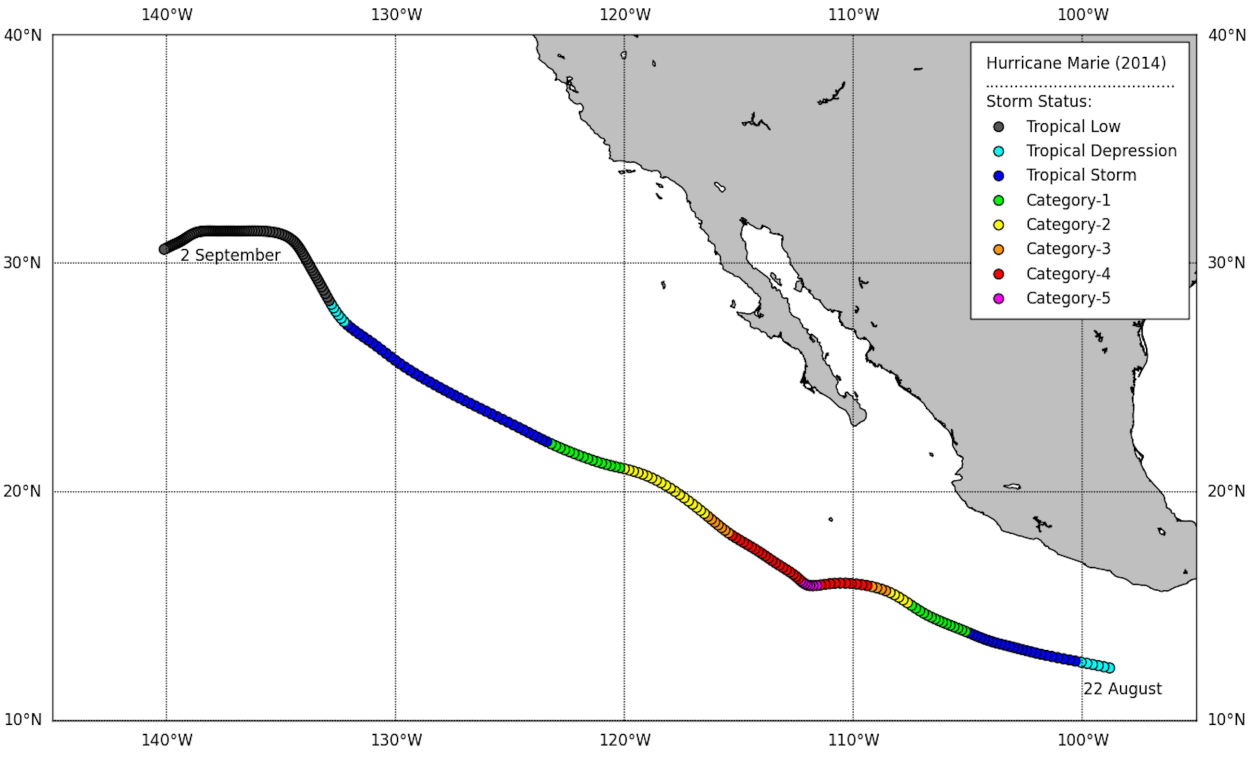

Figure 4.31: Hurricane Marie (2014) track.

Along-track analysis demonstrated that Marie formed in SSTs of 29.2°C that dropped by 0.5°C before increasing to 30.2°C as the storm attained Category-1 status wind speeds of 33.0 ms^{-1} (Figure 4.32). Marie's explosive intensification period consisted of two stages: an increase of 25 ms^{-1} within the first 42- hours, and then a further strengthening of 30.1 ms^{-1} during the next 24-hours. Average SSTs during the entire strengthening process were 29.4°C. At the moment Marie sped up during the second intensification stage, SSTs increased by over 0.5°C. At maximum intensity of 72.0 ms^{-1} winds at 1800 UTC 24 August, SSTs remained above 29.1°C. Immediately afterwards, SSTs declined incrementally, with a brief return to 29.3°C, which slowed Marie's weakening from 64 ms^{-1} wind speeds to 55 ms^{-1}. Over the next 14-hours, Marie subsequently tracked over a large SST gradient of a 2°C decline to 25.7°C, furthering de-intensification. 12-hours before downgrading to a Tropical Storm, SSTs along-track were as low as 23.7°C. SSTs dropped further to 20.7°C 3-hours prior to becoming a Tropical Depression.

During Marie's long decline at 12.86 ms^{-1} wind speeds, SSTs did not rise above 23.5°C. UOHC at the time of formation hovered around 60 kJ cm^{-2}, before quickly rising to a maximum of 96.8 kJ cm^{-2} in a deep WCE directly off the coast of Mexico. Marie attained Category-1 status less than 12-hours after passing through this very warm pool of water. Marie encountered a second, localized maximum of 74 kJ cm^{-2} at the time of transition between intensification stages. At peak intensity of 72.0 ms^{-1} wind speeds, UOHC beneath the track was still very high with consistent values of 52 kJ cm^{-2}. UOHC declined with cooling SSTs, with a momentary rise of approximately 15 kJ cm^{-2} as Marie's weakening slowed on 26 August. At this time Marie crossed the strong SST gradient, and UOHC values plummeted by 50 kJ cm^{-2} in 20 hours. Along-track UOHC remained at 0 kJ cm^{-2} for the duration of Marie's slow decline.

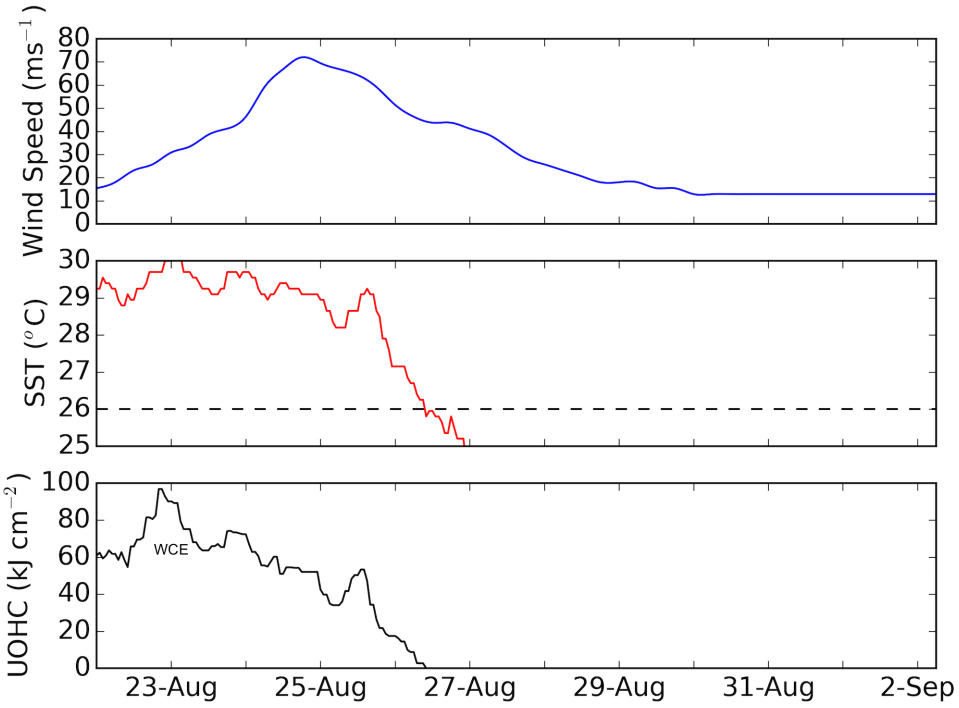

Figure 4.32: Hurricane Marie (2014) time series of along-track U_z (Top), SST (Center) and UOHC (Bottom). The 26°C isotherm is designated by a black dashed line.

Spatially visualized UOHC revealed that at genesis, Marie was situated to the southeast of an extensive WCE, in which UOHC exceeded 95 kJ cm^{-2} (Figure 4.33a). Marie subsequently tracked towards the southern edge of this WCE, and crossed the southernmost periphery of the deepest warm waters and quickly strengthened to a Category-2 hurricane the same day (Figure 4.33b). The immense size of the storm complex likely had a two-fold effect at this time: as Marie tracked northwards out of the WCE, heat was still extracted from the deep WCE to the east-southeast, allowing for rapid intensification to Category-5 status. However, the north and northeastern quadrants were already situated over quickly declining SSTs and UOHC, shortly curtailing any further intensification (Figure 4.33c). On 25 August, Marie's eye crossed the sharpest portion of the UOHC gradient, immediately weakening to a Category-3 hurricane before tracking to the west-northwest over 0 kJ cm^{-2} UOHC (Figure 4.33d).

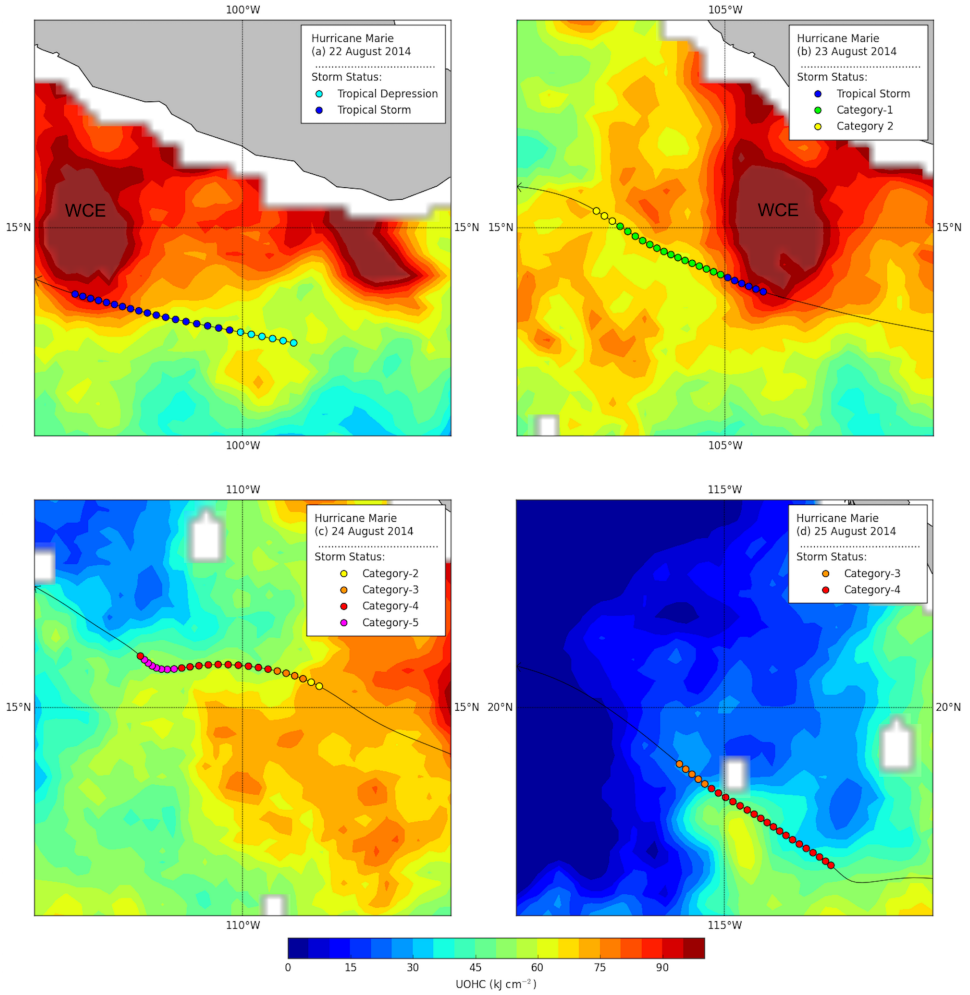

Figure 4.33: Daily UOHC with Hurricane Marie (2014) track overlain.

- **Hurricane Norbert (2 – 11 September)**

Hurricane Norbert originated from a West African tropical wave that organized in the Intertropical Convergence Zone on 1 September (Avila (2014); Figure 4.34). A broad low-pressure system developed several hundred kilometers south of Manzanillo, Mexico, with most of the associated thunderstorm activity located to the southwest, due to strong northeasterly wind shear. Despite strong wind shear, the system moved towards the north-northeast and a Tropical Storm formed on 2 September. As Norbert moved northward, the storm encountered a mid-level high-pressure system centered over northern Mexico, inducing a westward turn. Very warm SSTs along with weakened wind shear resulted in storm intensification to Category-1 status while on a northwest path parallel to the Baja Califor-

nia peninsula. Shortly after Norbert reached peak intensity of 56.6 ms^{-1} at 0600 UTC on 6 September, the storm became deeply embedded within a dry, stable atmosphere, which forced an abrupt decay over cool SSTs. By 0000 UTC 8 September, Norbert downgraded to a remnant low-pressure system and meandered southeastward within light steering flow before dissipating 3 days later. There were three direct casualties associated from heavy rainfalls in the Baja California peninsula, and damage to over 1,000 homes and seawall infrastructure were reported (Avila, 2014).

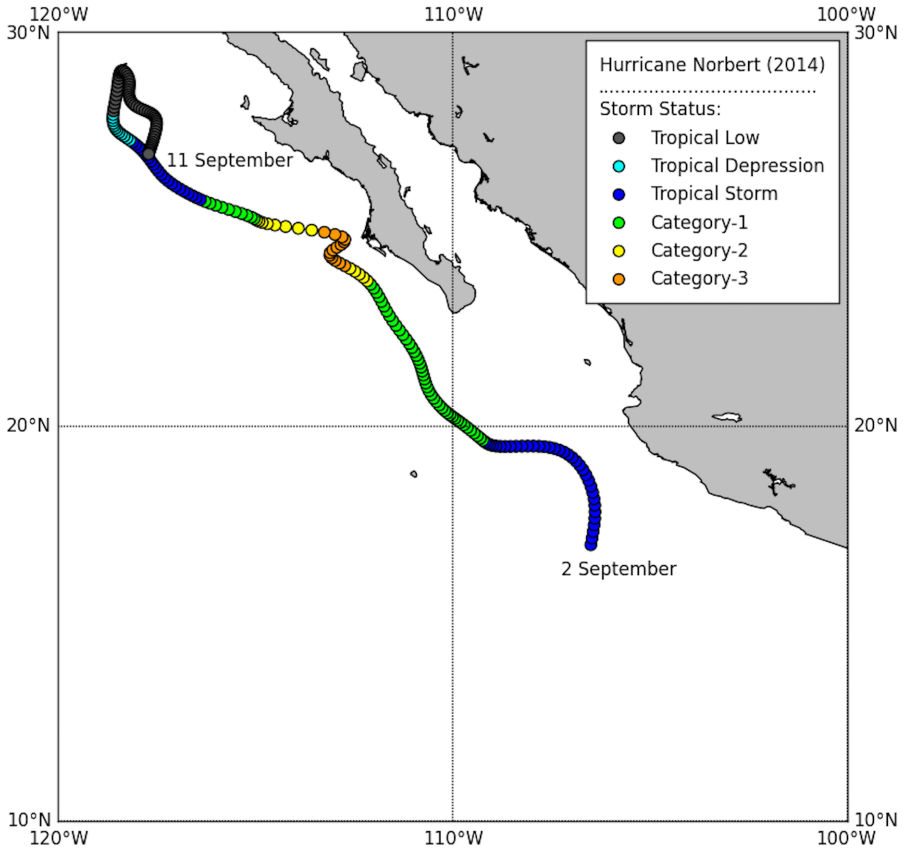

Figure 4.34: Hurricane Norbert (2014) track.

An along-track time series analysis for Norbert indicated that the storm originated in very high 30°C SSTs with Tropical Storm wind speeds of 18.0 ms^{-1} (Figure 4.35). SSTs dropped 1°C as Norbert tracked to the northwest before rising again to 31.1°C, during which Norbert's wind speeds increased to 33 ms^{-1} twelve hours later. Norbert remained over high SSTs of 30.1°C up to maximum intensity at 56.6 ms^{-1} on 6 September. A strong

correlation is highlighted between the intensification stage and high SSTs. However, SSTs immediately fell by 2°C as atmospheric moisture also declined (Avila, 2014) and Norbert quickly weakened to a Category-1 hurricane with 41.1 ms^{-1} wind speeds. By 0900 UTC 7 September, Norbert slowed to 30.1 ms^{-1} wind speeds as SSTs dropped below 26°C. Two days later, Norbert weakened to 10.5 ms^{-1} wind speeds over low SSTs of 23.4°C. UOHC at genesis was very high, with approximate values of 76 kJ cm^{-2}. As Norbert moved away from this WCE and into another smaller WCE, along-track UOHC increased to 85.8 kJ cm^{-2}. Afterwards, UOHC values fell quickly as deep, low temperature water rose to the sea surface. After 0300 UTC on 7 September, no excess of UOHC was seen along-track.

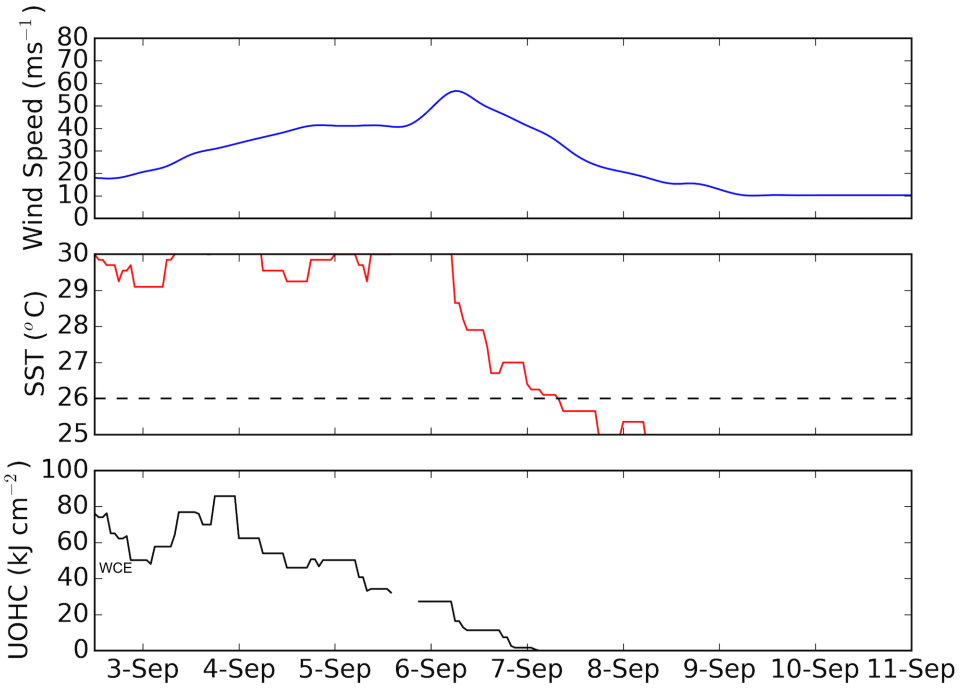

Figure 4.35: Hurricane Norbert (2014) time series of along-track U_z (Top), SST (Center) and UOHC (Bottom). The 26°C isotherm is designated by a black dashed line.

Coincidentally, Norbert formed around the northern periphery of the extensive WCE that promoted Marie's intensification a week earlier (Figure 4.36a). While not directly associated with Norbert, shallow UOHC values were seen to the immediate southwest of Norbert. This location marked the southernmost tip of Hurricane Marie's widespread cool wake, a feature first detected at 6 September in Norbert's along-track time series. Instead

of following a more west-northwesterly path out into the open ocean, Norbert shifted onto a north-northwest heading, intensifying to a Category-1 storm around a minor WCE, and away from Marie's rapidly deepening cool wake (Figure 4.36b). The proximity of this deep cool wake signature to the prominent WCE provided further evidence that Marie extracted large amounts of heat while located over much lower UOHC to the northwest. After passing to the west of the smaller WCE, Norbert tracked into stable UOHC waters of approximately 50 kJ cm^{-2} (Figure 4.36c) before intensifying to Category-2 status within 75-km of the Baja Peninsula where UOHC data were unfortunately unavailable (Figure 4.36d). The following day, Norbert briefly strengthened to a major hurricane before moving into very cool waters where UOHC fell below the 26°C isotherm threshold (Figure 4.36e). The unusual switchback within Norbert's track was not discussed within the NHC report and may be an anomaly within the hourly-interpolated data for Norbert.

- **Hurricane Odile (9 – 18 September)**

Hurricane Odile originated as a West African tropical wave that slowly organized, forming a low-pressure system at 0000 UTC on 9 September south-southwest of the Gulf of Tehuantepec (Cangialosi and Kimberlain, 2015). The next day, a Tropical Depression formed and quickly strengthened to a Tropical Storm (Figure 4.37). Odile generally moved northwestward between two mid-level ridges while moderate northeasterly to northerly wind shear limited the rate of intensification. By 0600 UTC 13 September, Odile reached Category-1 status and became embedded in the flow between a Gulf of Mexico mid-level ridge and a southward drifting upper-level low to the northwest. Odile accelerated and rapidly intensified between these two features, reaching peak intensity of 61.7 ms^{-1} on 14 September. At this time, Odile developed concentric eyewalls and maximum wind speeds decreased to 56.6 ms^{-1}. Four hours later, Odile made landfall at 0445 UTC 15 September east of Cabo San Lucas as a strong Category-3 hurricane. Weakening over the mountainous terrain, Odile moved northwest up the Peninsula before turning northeast in response to

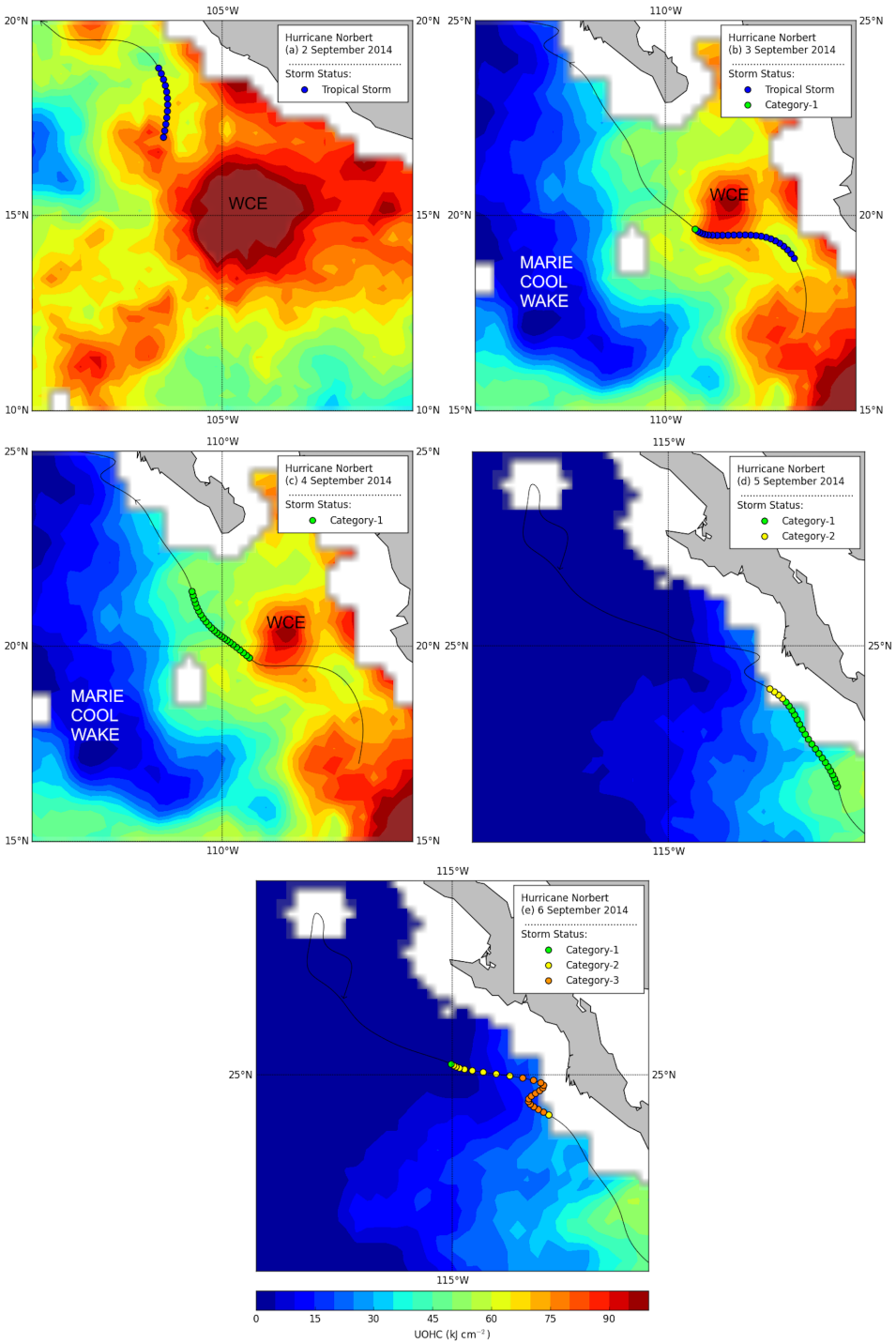

Figure 4.36: Daily UOHC with Hurricane Norbert (2014) track overlain.

an approaching mid-latitude trough. Quickly crossing the Gulf of California, Odile made a second landfall as a Tropical Storm near Alvaro Obregón. Odile dissipated 12-hours later over the northern Sierra Madre mountains (Cangialosi and Kimberlain, 2015).

Odile broke several long-held records. It was the third major hurricane to make landfall on Baja California during the satellite era, tied Hurricane Olivia (1967) as the strongest TC to affect the peninsula, was the strongest landfalling TC on the peninsula since Hurricane John (2006), and the first Tropical Storm to make landfall north of 30°N in Mexico since Hurricane Nora (1997). Odile was also the most destructive TC on record for Baja California Sur. Over 90% of the population was left without electricity and the Cabo San Lucas International Airport was badly damaged, effectively stranding over 4,000 tourists. Thousands of residents were left homeless, with unavailable drinking water and inoperative communications. There were 14 fatalities attributed to flooding and lightning strikes from Odile. Damage estimates totaled over USD $1 billion (Cangialosi and Kimberlain, 2015).

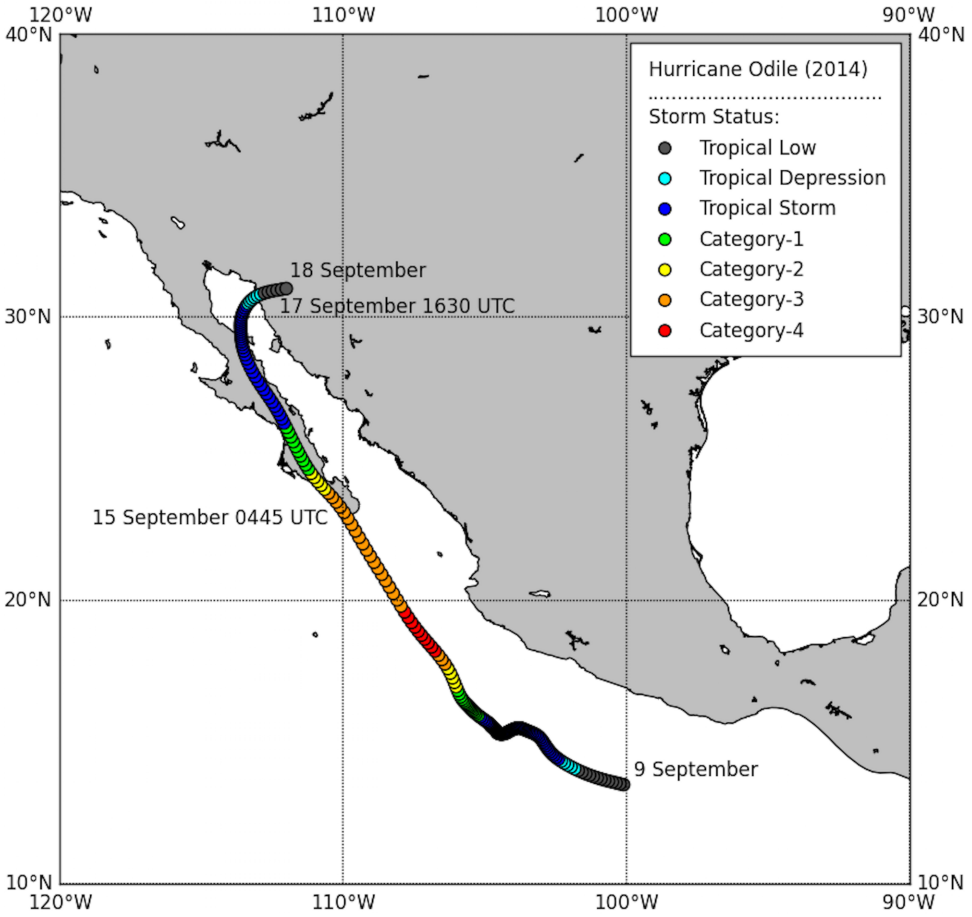

Figure 4.37: Hurricane Odile (2014) track. Date and time at landfall are provided.

The along-track time series indicated that Odile formed in very high SSTs of 29.6 – 30.2°C (Figure 4.38). As Odile moved parallel to the coastline, the storm tracked into the northeast quadrant of the WCE that had previously influenced Marie and Norbert. Despite very high SSTs for the majority of storm duration and a translation speed of 0.5 – 2.0 ms^{-1} near the WCE, Odile slowly strengthened. However, by 13 September, Odile's translation speed accelerated to 8 ms^{-1} and obtained 61.7 ms^{-1} wind speeds as a Category-4 hurricane. At this time, SSTs were 29.3°C. 6-hours before landfall, Odile encountered a 2°C SST drop. Prior to landfall, the oceanic conditions were highly conducive for intensification. UOHC values for the first 110-hours of Odile's lifecycle were fairly consistent, averaging 82 kJ cm^{-2} as the storm slowly moved around the WCE. On 11 September, UOHC peaked at 100 kJ cm^{-2} as Odile tracked over the northern edge of the WCE center. After exiting the WCE's region of influence, UOHC values dropped 20 kJ cm^{-2}, before a sharp decline to 17 kJ cm^{-2} UOHC. Odile quickly passed over a small coastal extension of high 71 kJ cm^{-2} UOHC before values fell to 17 kJ cm^{-2} surrounding the tip of the peninsula.

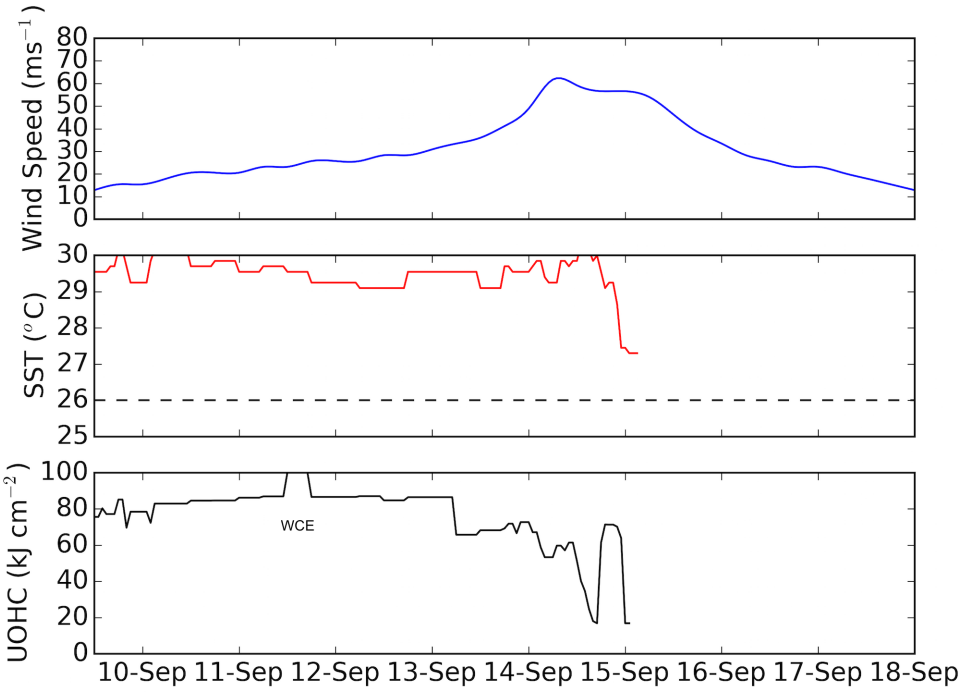

Figure 4.38: Hurricane Odile (2014) time series of along-track U_z (Top), SST (Center) and UOHC (Bottom). The 26°C isotherm is designated by a black dashed line.

Like Hurricanes Marie and Norbert, Odile formed in close proximity to the deep WCE centered approximately at 15°N, 105°W (Figure 4.39a). Slow to intensify, Odile moved around the northern edge of the WCE, briefly diverting into the center (Figure 4.39b), and rapidly strengthened while the storm tracked to the north-northwest (Figure 4.39c). To the west of Odile, the remnants of Marie's intense cool wake and a smaller upwelling signature associated with Norbert lingered as Odile tracked directly towards the Baja California peninsula (Figure 4.39d). As Odile intensified to a major hurricane, the storm tracked over a very small pool of comparatively low UOHC before tracking over a warm deep pool of UOHC. Odile maintained Category-3 status upon striking the Baja California peninsula.

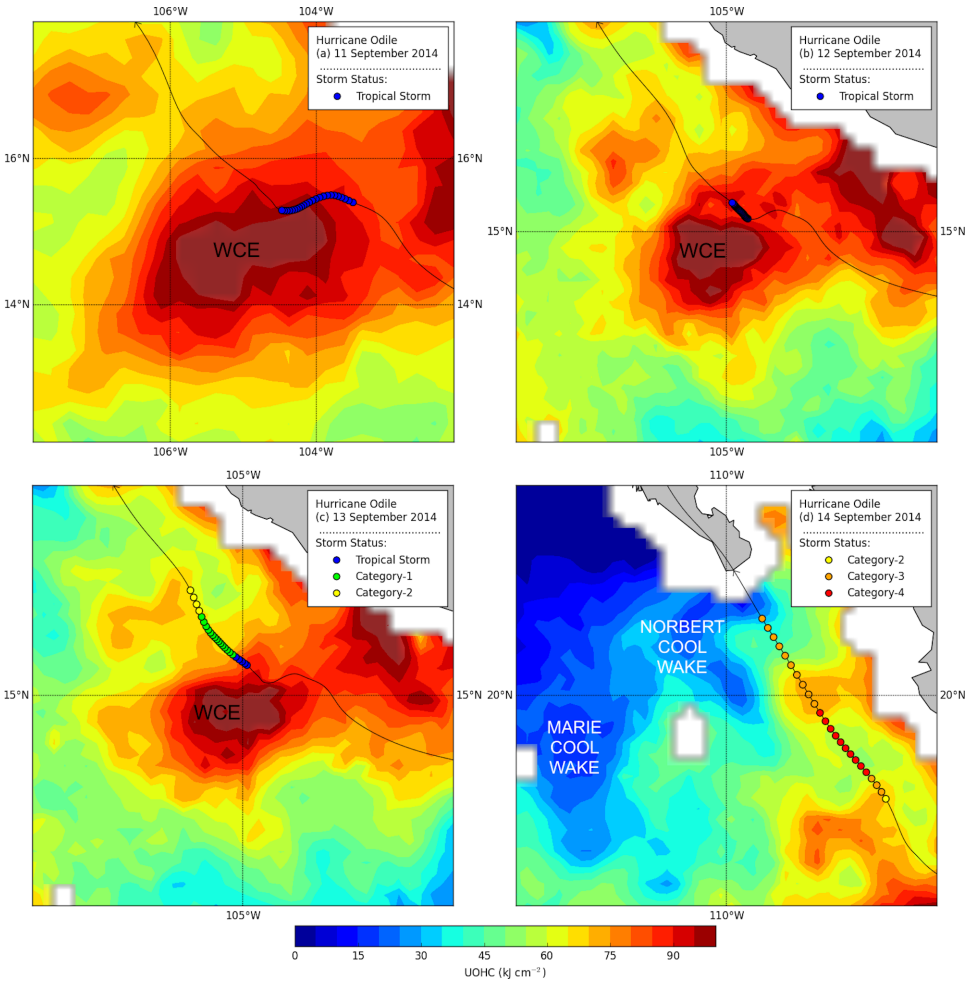

Figure 4.39: Daily UOHC with Hurricane Odile (2014) track overlain.

- **Hurricane Simon (30 September – 9 October)**

Hurricane Simon was the ninth major hurricane of the 2014 NPO hurricane season, and developed from a tropical wave interaction with the Intertropical Convergence Zone (Stewart, 2014b). On 30 September, deep convection within the low-pressure system formed 230 km south of Acapulco, Mexico, moving offshore into SSTs of approximately 30°C and a light to moderate wind shear environment. As favorable conditions continued, a Tropical Storm formed by 0600 UTC 2 October. After a period of slow intensification, low wind shear, high mid-level atmospheric moisture, and warm SSTs proved very conducive for strengthening, and Simon became a hurricane by 4 October. On the same day, Simon's eye passed within 15 km of Socorro Island. Simon peaked at 0000 UTC on 5 October with 59.1 ms^{-1} wind speeds while west-southwest of the southern tip of the Baja California peninsula. Rapid weakening ensued almost immediately after peak wind speeds, as Simon turned northwestward around a deep-layer subtropical ridge and over 26°C waters. Strong inner-core winds induced strong cold upwelling beneath the hurricane, resulting in SSTs less than 22°C. After weakening to a Tropical Storm by 6 October, cooler SSTs and dry air entrainment led Simon to turn northeastward and further weakened to a remnant low-pressure system. The remnant circulation of Simon made landfall north of Guerrero Negro at 1700 UTC on 8 October, and dissipated hours later. Due to the rapid storm erosion prior to landfall, rainfall was less than 2 inches, with no reports of damage (Stewart, 2014b). Hurricane Simon's track is illustrated in Figure 4.40.

As Simon moved away from the high SSTs bordering the Mexican coastline during the intensification phase, SSTs along-track dropped from 30°C at genesis to 28.5°C 24-hours later (Figure 4.41). SSTs then increased up to 29°C while Simon strengthened to Tropical Storm status early on 2 October. Temperatures subsequently dropped to 27.5°C while slowly gaining strength as a Tropical Storm. After passing near Socorro Island, Simon rapidly intensified over declining SSTs approaching 26.5°C. Maximum intensity of 59.1

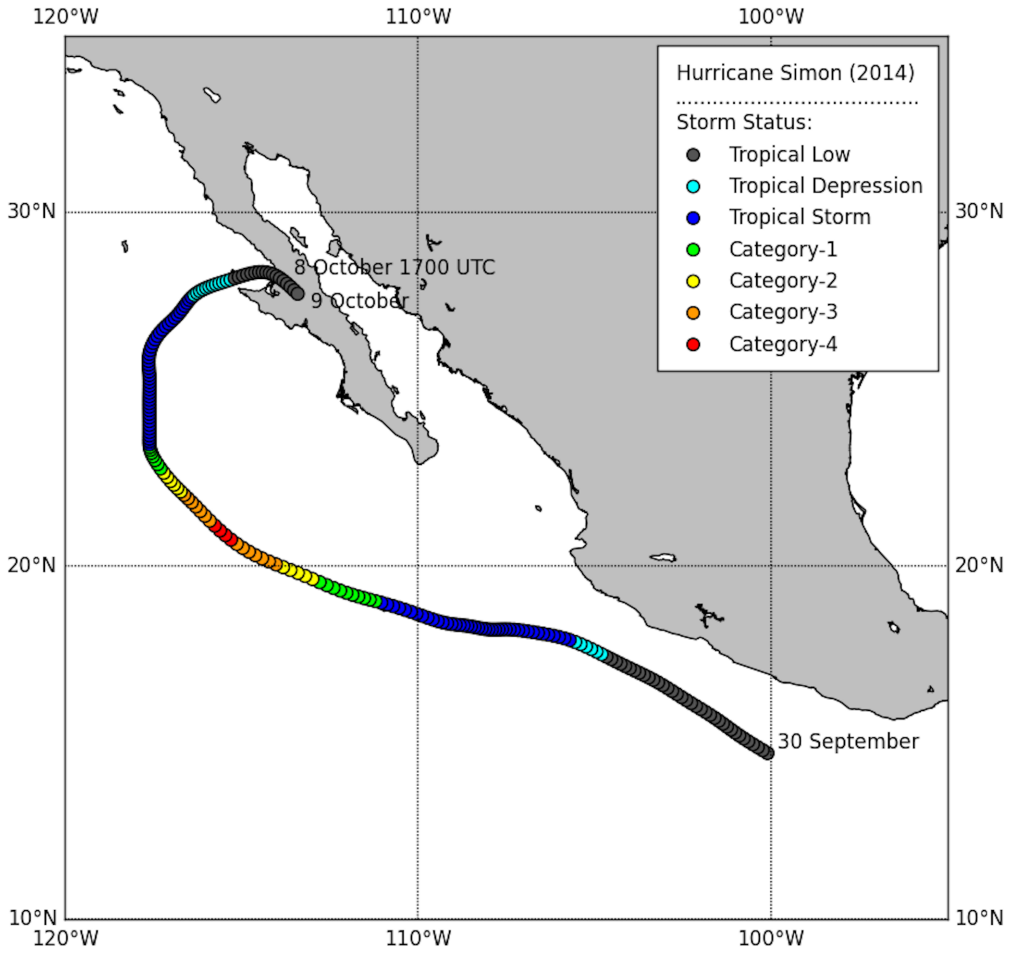

Figure 4.40: Hurricane Simon (2014) track. Date and time at landfall are provided.

ms^{-1} wind speeds occurred on 3 October while Simon was situated over 26.5°C waters, which dropped greater than 1°C less than 6-hours later. Wind speeds quickly fell as Simon tracked over very cool waters, as low as 24.1°C. SST observations stopped upon proximity to Baja California Sur. UOHC values along-track began very high, with genesis at 75 kJ cm^{-2}. The along-track time series clearly indicated that reduced intensity was related to lower SST and UOHC throughout Simon's duration. As Simon tracked away from the coastline, UOHC fell as low as 50 kJ cm^{-2}, before a brief rise to 61 kJ cm^{-2} with a 0.3°C temperature increase late on 1 October. UOHC values then steeply declined to 23 kJ cm^{-2} in 15-hours, but slightly rose to 36 kJ cm^{-2} in the region surrounding Socorro Island. As Simon tracked north of the island and into drastically cooler waters, UOHC fell to 0 kJ cm^{-2} of excess heat content that persisted for the remainder of the storm duration.

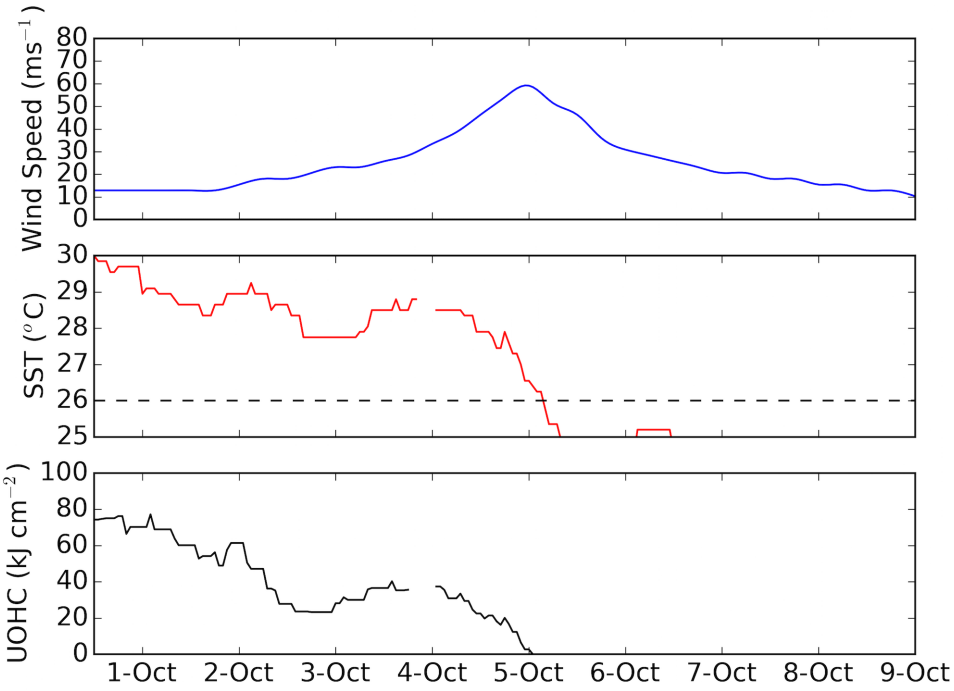

Figure 4.41: Hurricane Simon (2014) time series of along-track U_z (Top), SST (Center) and UOHC (Bottom). The 26°C isotherm is designated by a black dashed line.

Almost undetectable within the along-track data, Simon passed between two small CCEs shortly after genesis, in which UOHC values dropped as much as 20 kJ cm^{-2} compared to the surrounding waters (Figure 4.42). These CCEs correspond to a long-lasting upwelling cool wake signature from Hurricane Odile, three weeks earlier (Figure 4.39). Despite observation dropout near land, a steep UOHC gradient was visible, and estimated at 90 kJ cm^{-2} over 150 km. Simon successfully avoided the southern CCE and passed along the southern edge of the northern CCE, where UOHC values along-track were as low as 23 kJ cm^{-2}. On 3 October, Simon tracked westward away from Odile's cool wake and to the south of Clarion Island as a Tropical Storm (Figure 4.42b). Although SST and UOHC information were unavailable within the coastal waters of the island, Simon rapidly strengthened at this time to a Category-1 hurricane, becoming a Category-4 hours later (Figure 4.42c). Simon maintained peak Category-4 wind speeds for 4-hours, before tracking across the 26°C isotherm and into waters with no excess heat content (Figure 4.42d). Storm intensity weakened over these very cool waters.

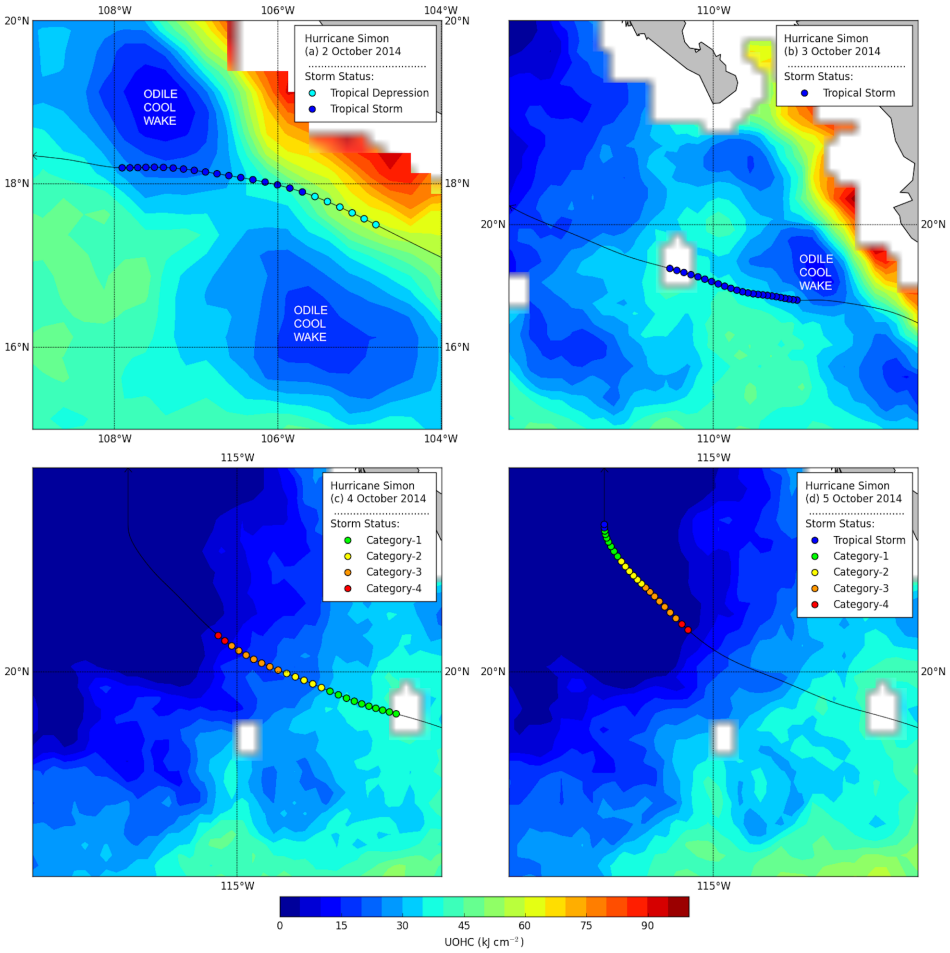

Figure 4.42: Daily UOHC with Hurricane Simon (2014) track overlain.

4.2 Regression Analysis

A series of regression models were developed using various combinations of the oceanic data. A summary of the primary regression models employed and their respective results are presented in Table C.1. Specifically, six simple linear regression models (labeled **1** – **6**) were run in order to assess the relationships between the potential oceanic forcing factors of SST and UOHC, relative to along-track maximum wind speeds (U_z) for the major hurricanes. An additional eight multiple linear regression models (**7** – **12**) were developed using storm latitude, longitude, translation speed, and SST (or UOHC) as explanatory variables for season-specific along-track variations in U_z. SST and UOHC were not used as explanatory parameters in the same model due to potential correlation and dependence between the two

variables. Storm latitude and longitude were specifically selected as explanatory parameters based on their usefulness in the Hobgood (1998) and Petty and Hobgood (2000) NPO intensify forecast regression models. All parameters were analyzed for auto-correlation to prevent biased results. Finally, storm-specific multiple regression models (labeled **13** – **22**) were analyzed for five of the major hurricanes, one from 2012 and four from 2014. Petty and Hobgood (2000) utilized multiple linear regression to improve NPO TC intensity forecasts and suggested that when a model performed well for one phase (intensification or decay), its skill decreased during the opposite phase. Thus, all regressions were designed to analyze only the intensification phase, defined as genesis to maximum intensity. Regression models **23** – **47** were supplementary model runs to regression models **13** – **22** and are discussed in Appendix C. In all regression models, the hourly-interpolated data were used for both the response and explanatory variables to increase the number of observations per storm and ensure a proper ordinary least-squares regression analysis. All storm-specific regression models analyzed contained at least 100 observations. All regression models were checked to ensure that key regression assumptions were not violated, specifically, the normality of residuals and multicollinearity. In addition to a histogram of model residuals, the Shapiro-Wilks test[3] was performed to further assess normality.

4.2.1 Regressions 1 and 2 – 2012 Major Hurricanes

Regression **1** was a simple linear regression model that included all data for the five 2012 major hurricanes with SST as the explanatory variable for variations in U_z. The model indicated that SST was a very significant parameter with a p-value of <0.001. This model performed sufficiently well in explaining along-track variation in U_z. An adjusted R-squared value of 0.5248 suggested that SST as the sole explanatory predictor could explain approximately 52% of variation in U_z. Residuals indicated a somewhat non-normal

[3]The level of significance for the Shapiro-Wilks test was set to be 0.05. P-values below this threshold rejected the null hypothesis of normality, and vice versa

distribution, violating the regression model assumptions. The Shapiro-Wilks normality test resulted in a W-value of 0.969 and p-value of <0.001. Based on these results, there was evidence against a normal distribution of residuals.

Regression **2** was a simple linear regression model similar to Regression **1**, but one that utilized UOHC as the explanatory predictor rather than SST. UOHC was found to be a highly significant parameter for the five 2012 hurricanes, with a p-value of <0.001. This model performed quite similar to the SST model with an adjusted R-squared value of 0.5392, indicating that approximately 54% of variability in U_z could be explained by UOHC. Residuals were distributed non-normally, violating model regression assumptions. The Shapiro-Wilks normality test resulted in a W-value of 0.973 and a p-value of <0.001, indicating statistical evidence against a normal distribution. Compared to Regression **1**, this model was slightly more useful, revealing that both SST and UOHC as oceanic predictors can provide insight on the controls of U_z variability. Scatter plots of Regressions **1** and **2** (Figure 4.43) illustrated an inverse relationship between U_z and SST (or UOHC), revealing that as wind speeds increased, SST (and UOHC) were decreasing but still remained above the minimum threshold.

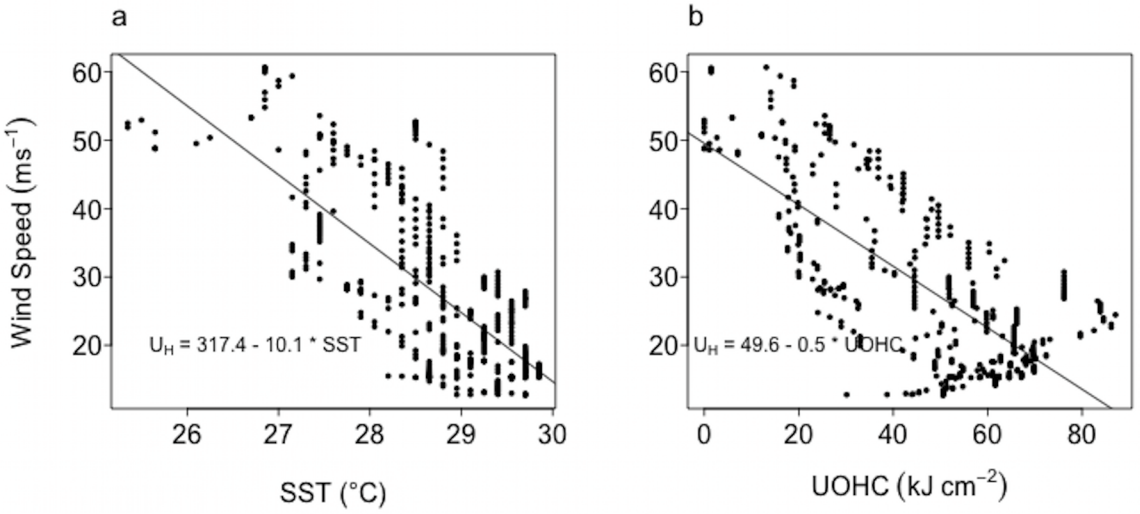

Figure 4.43: Scatterplot of regression variables for (a) Regression 1 and (b) Regression 2. Model fit indicated by solid black line, with regression equation provided.

4.2.2 Regressions 3 and 4 – 2014 Major Hurricanes

Regression **3** was a simple linear regression model similar to the first two regressions, but now all data for the nine 2014 major hurricanes were considered, with SST as the explanatory variable. The model revealed that SST was a highly significant parameter with a p-value of <0.001. This model presented poor results compared to Regression **1**, with an adjusted R-squared value of 0.0355, explaining approximately 3% of along-track variation in U_z. Model residuals were non-normally distributed and skewed towards the left tail of the data, violating model assumptions. Results from the Shapiro-Wilks normality test indicated a W-value of 0.922 and corresponding p-value of <0.001. The output from this test confirmed a non-normally distributed model.

Regression **4** was a simple linear regression model that used UOHC as an explanatory predictor in the nine 2014 major hurricanes. UOHC was found to be a significant parameter for the nine 2014 major hurricanes, with a p-value of <0.001. This model performed poorly, with a low adjusted R-squared value of 0.0974. As this accounted for less than 10% of variability, this regression model was a poor indicator for estimating variability in along-track U_z. Residuals were non-normally distributed and skewed towards the left tail, violating model assumptions. A normality test confirmed non-normality with a W-value of 0.941 and p-value of <0.001. Compared to its SST counterpart, this regression model added some usefulness of UOHC as an explanatory model predictor. A model scatter plot of Regressions **3** and **4** was provided (Figure 4.44). The same declining trend between SST/UOHC and wind speeds was evident in the season-wide regressions for 2014 as well. The rates of decline in Figure 4.44 were more gradual than those seen in Figure 4.43.

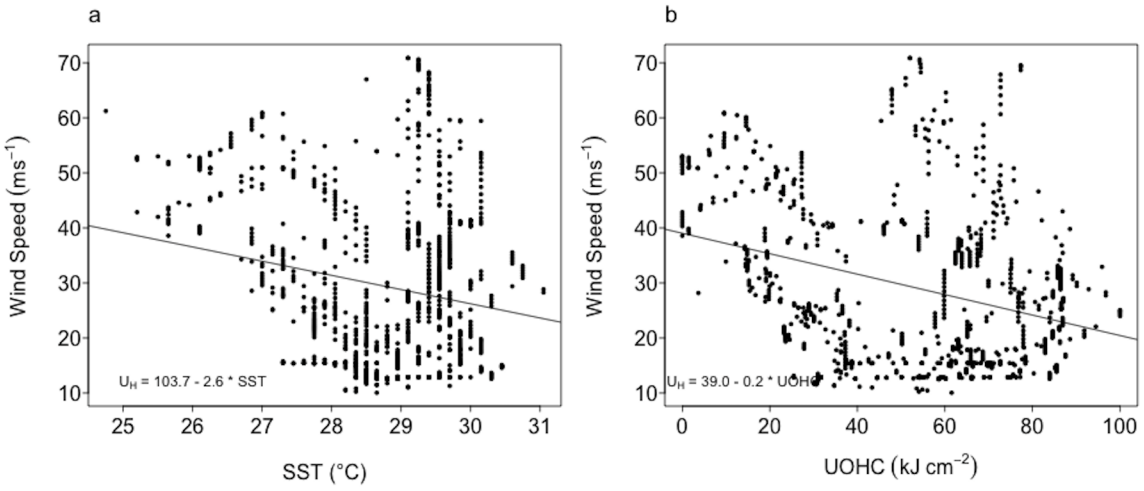

Figure 4.44: Scatterplot of regression variables for (a) Regression 3 and (b) Regression 4. Model fit indicated by solid black line, with regression equation provided.

4.2.3 Regressions 5 and 6 – All Major Hurricanes

Regression **5** was a simple linear regression model that included all fourteen major hurricanes from both seasons, with SST as the explanatory predictor. The simple model indicated that SST was a highly significant parameter for all hurricanes considered with a p-value of <0.001. This model demonstrated somewhat similar results to Regression **4**, with an adjusted R-squared value of 0.0975. These results signified that when considering the 2012 and 2014 hurricane seasons together, SST may have explained approximately 10% of the variability in along-track U_z. However, the results of Regressions **1** and **2** indicate that hurricanes in 2012 contributed much more to the relationship than those in 2014. This model demonstrated non-normally distributed residuals, skewed towards the left tail, violating model assumptions.

Regression **6** was a simple linear regression model for all major hurricanes in this study with UOHC as the explanatory variable for along-track U_z variability. UOHC was found to be a significantly useful parameter in the all hurricanes model, with a p-value of <0.001. This model resulted in adjusted R-squared value of 0.1656. According to these results, this model explained approximately 16% of variation in U_z. Like the previous five models,

this model also demonstrated non-normally distributed residuals with a skewed left tail. The Shapiro-Wilks test provided evidence against a normal distribution with a W-value of 0.949 and p-value of <0.001. Regression models **1** – **6** should be interpreted with extreme caution as model assumptions failed in all instances. While models that incorporated all major hurricanes from both 2012 and 2014 demonstrated poor results, the season-specific models for 2012 performed better, indicating a possible shift in environmental influences season-to-season. Evidence from these six simple linear regression models revealed that a single explanatory oceanic predictor could not explain U_z variability in NPO major hurricanes. In all instances, UOHC performed better than SST as an explanatory predictor. A model scatter plot for Regressions **5** and **6** was provided (Figure 4.45). Like the two previous season-wide models, the all-inclusive regressions also demonstrated a negative trend between SST (or UOHC) and wind speeds, with similar rates of weakening.

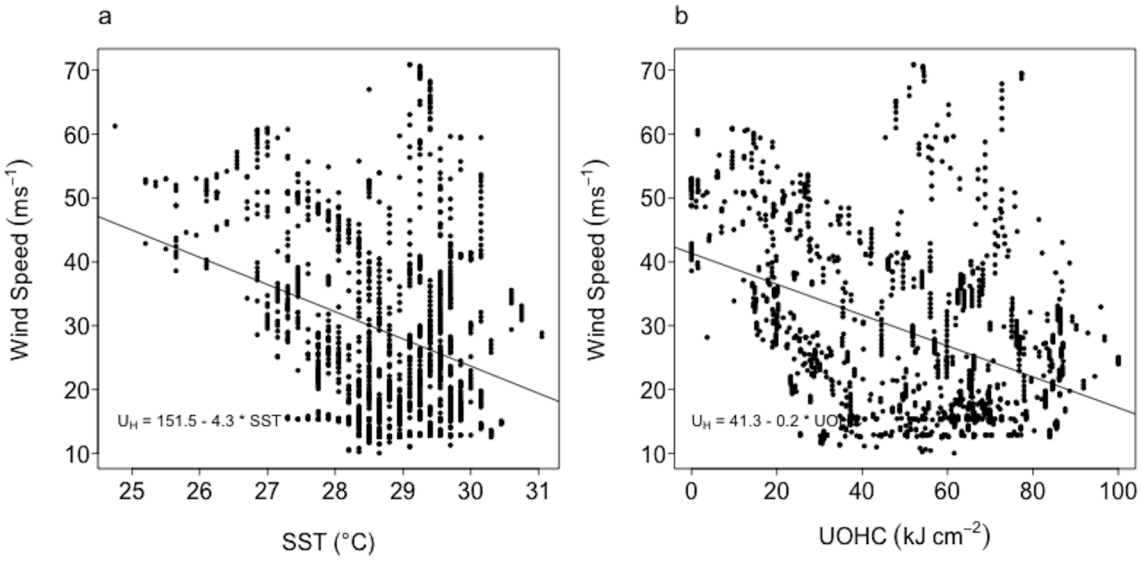

Figure 4.45: Scatterplot of regression variables for (a) Regression 5 and (b) Regression 6. Model fit indicated by solid black line, with regression equation provided.

4.2.4 Regressions 7 and 8 – 2012 Major Hurricanes

Regression **7** was a multiple linear regression model that incorporated storm position and translation speed in addition to SST as explanatory predictors for the five 2012

major hurricanes. In this multiple regression model, SST and latitude were found to be statistically significant parameters with a p-value of <0.001, while storm longitude and translation speed proved to be less significant, with p-values of 0.07 and 0.02 respectively. This model performed considerably better than the single explanatory variable models (**1** – **6**), with an adjusted R-squared value 0.6453, indicating the combination of storm latitude and longitude, translation speed, and SST explained approximately 65% of along-track U_z variability. These results should be treated cautiously however, as plotted residuals demonstrated non-normality, skewed towards the right tail. The Shapiro-Wilks test also indicated non-normality with a W-value of 0.978 and p-value of <0.001.

Regression **8** was a multiple linear regression model for the five major hurricanes of 2012 that employed storm latitude and longitude, translation speed, and UOHC as explanatory predictors. Two parameters in this model proved to be very significant: UOHC and latitude resulted in p-values of <0.001 each, while longitude and translation speed were considered not significant with p-values of 0.83 and 0.80 respectively. This model performed well, with an adjusted R-squared value of 0.6410. These results signified that the explanatory predictors could explain approximately 64% of along-track variability in 2012. Plotted residuals demonstrated non-normality, with a long right tails. The Shapiro-Wilks test confirmed this, with a W-value of 0.975 and p-value of <0.001. Thus, regression results should be interpreted with caution as model assumptions were violated.

4.2.5 Regressions 9 and 10 – 2014 Major Hurricanes

Regression **9** was also a multiple linear regression model similar to that of Regression **7** in which storm position, translation speed, and SST were used as explanatory predictors for the nine major hurricanes of 2014. In this model, all parameters except translation speed were considered highly significant with p-values of <0.001. Translation speed was considered not significant, with a p-value of 0.41. For this storm subset, this model per-

formed poorly with an adjusted R-squared value of 0.2664. Such results indicated that the explanatory predictors could account for 26% of along-track U_z variation. Plotted residuals again displayed a non-normal distribution strongly skewed towards the right. The Shapiro-Wilks test confirmed non-normality, with a W-value of 0.903 and p-value of <0.001. Like all of the previous models, these regression results should be interpreted carefully.

Regression **10** was a similar multiple linear regression model to Regression **8**, but for the major hurricanes of 2014. Explanatory predictors were UOHC, storm latitude and longitude, and translation speed. The model indicated that UOHC, latitude, and longitude were the most significant parameters with p-values of <0.001 each. Translation speed was considered not significant with p-value of 0.67. This model yielded a low adjusted R-squared value of 0.2527. Unlike the major hurricanes of 2012 studied in Regression **18**, Regression **10** could only account for approximately 26% of variability. As expected, model residuals were distributed non-normally. The model residuals exhibited a long skewed right tail. Normality tests confirmed these results, with a W-value of 0.914 and p-value of <0.001. Much like the simple linear Regressions **3** and **4**, the regressions for the 2014 season did not perform as well as their 2012 counterparts.

4.2.6 Regressions 11 and 12 – All Major Hurricanes

Regression **11** was a multiple linear regression model that incorporated all major hurricanes from both seasons. Storm latitude and longitude, translation speed, and SST were utilized as explanatory predictors for along-track variability in U_z. SST and latitude were highly significant with p-values each of <0.001. Longitude was somewhat significant with a p-value of 0.08, while translation speed was highly not significant, with a p-value of 0.99. Model performance resulted in an adjusted R-squared value of 0.3321, indicating approximately 33% of variability could be explained with the given predictors. Model residuals revealed a somewhat normal distribution with a long right-skewed tail, and decent model fit

of the left tail. The Shapiro-Wilks test confirmed a non-normal distribution with a W-value of 0.930 and p-value of <0.001. These results were expected given the model performance of Regressions **7** and **9**.

Regression **12** was a multiple linear regression model that included all major hurricanes in 2012 and 2014. To attempt to quantify along-track U_z variability, storm position, translation speed, and UOHC were utilized. The model revealed that UOHC, latitude, and longitude were highly significant parameters with p-values of <0.001 each, while translation speed was considered a not useful parameter with p-values of 0.73. Given the decent performance of Regression **11**, adjusted R-squared results for this model were similar with a value of 0.3913. Plotted residuals displayed a similar somewhat normality with a dominantly skewed right tail with fair model fit of the left tail. The Shapiro-Wilks test revealed a non-normal distribution with a W-value of 0.939 and p-value of <0.001. As should be expected from similar regression models, results should be interpreted with extreme caution, but are still considered useful in the identification of beneficial predictors.

4.2.7 Regressions 13 and 14 – Hurricane Amanda (2014)

Regression **13** was a multiple linear regression model run for Hurricane Amanda, the first TC and major hurricane of the 2014 season. Regression **13** used storm storm latitude, longitude, translation speed, and SST as explanatory predictors for along-track U_z variability. Storm longitude proved to be a significant parameter with a p-value of 0.002. SST, latitude, and translation speed were fount to be not significant, with p-values of 0.31, 0.12, and 0.10, respectively. This model performed very well with an adjusted R-squared value of 0.8425. However, plotted model residuals exhibited non-normality with a long right tail. The Shapiro-Wilks normality test confirmed non-normality with a W-value of 0.909 and p-value of <0.001. Model coefficients for latitude, longitude, translation speed, and SST were considered appropriate values with small standard deviations respectively.

The regression model equation was the following:

$$U_z = -1995.5 - 4.29(SST) - 32.33(Latitude) - 23.10(Longitude) - 5.57(U_H) \quad (4.1)$$

where -4.29, -32.33, -23.10, and -5.57 were the coefficients for SST, latitude, longitude, and translation speed, respectively, with corresponding units. It is noted that all explanatory predictors exerted a negative effect on U_z. A scatter plot of all predictors utilized in Regression **13** was provided in Figure 4.46. To understand the following storm-specific scatter plots, it is first important to note that the variable labels and axes are aligned along the plot diagonal. The figure is read as column by row, and each plot is the relationship between the chosen variables for that column and row. For example, the scatter plot for longitude compared with wind speed is in column 1, row 3, and so on. For these figures, the third row (or third column) represent each predictor's relationship to wind speed. Plots are flipped along the diagonal, *i.e.*, longitude compared with wind speed is also plotted in column 3, row 1. It was immediately evident from Figure 4.46 that latitude and longitude both exhibited a near-linear relationship with wind speeds, while SST and translation speed had widely variable slopes, demonstrating a strong non-linear relationship with wind speed during Amanda. It is noted that whilst SST revealed a varying, non-linear relationship to wind speed, values were clustered together, whereas translation speed was considerably more scattered in values.

Regression **14** was a multiple linear regression model also run with UOHC as an explanatory predictor instead of SST. This regression model was run to compare the advantages and disadvantages of the inclusion of either UOHC or SST in a storm-specific intensification model. The model revealed that UOHC was somewhat significant with a p-value of 0.02, while longitude was suggestive with a p-value of 0.06. Latitude and translation speed were found to be not significant, with p-values of 0.95 and 0.50, respectively.

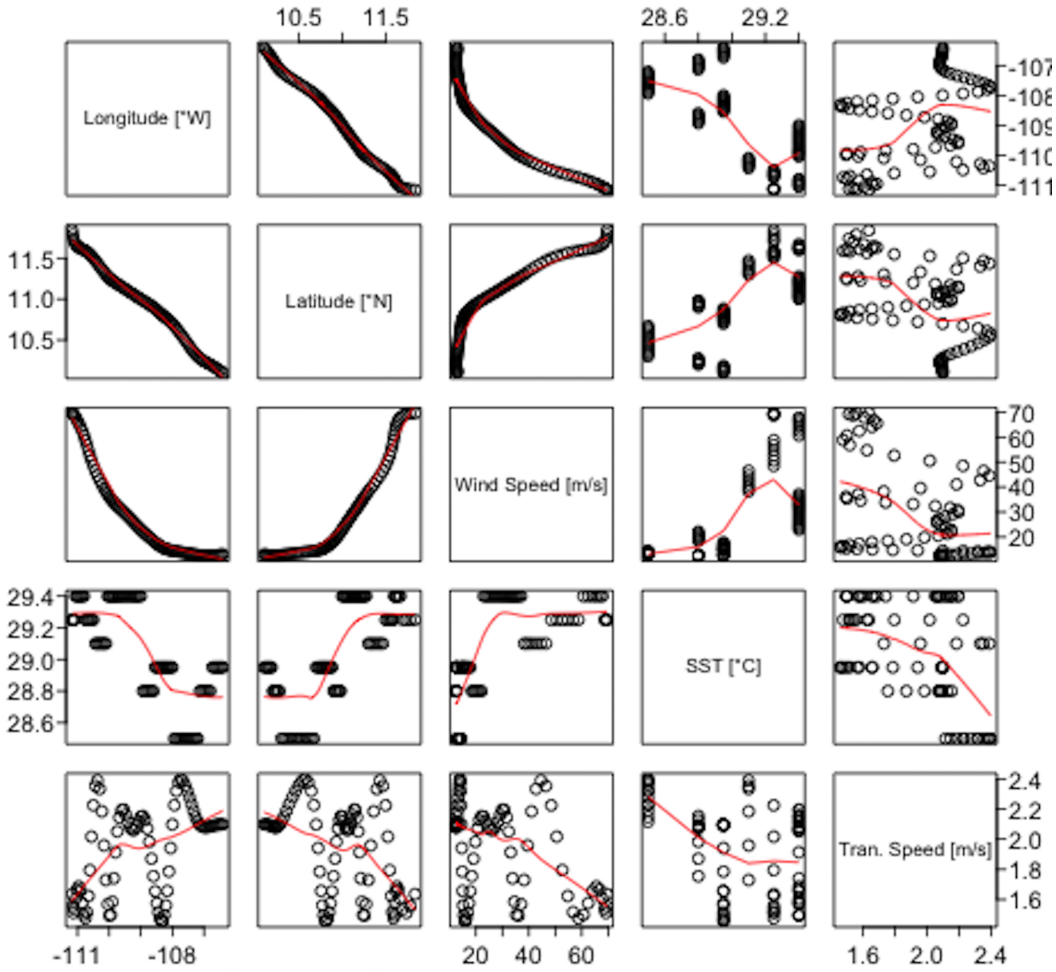

Figure 4.46: Scatterplot of regression variables for Regression 13. Model fit indicated by solid red line. Axis labels are along the figure diagonal. The third row is most useful for analysis.

This regression model performed very well, with an adjusted R-squared value of 0.8514. Compared to Regression **13**, the inclusion of UOHC instead of SST as a predictor resulted in a 0.009 increase in the model explanatory power. This equated to an approximate 1% better regression model fit using UOHC. Model residuals demonstrated a non-normal distribution with a long right tail. The Shapiro-Wilks test confirmed non-normality with a W-value of 0.903 and p-value of <0.001. With the poor model fit, the Regression was considered with caution for use here. The regression model equation was as follows:

$$U_z = -1366.7 - 0.49(UOHC) - 1.25(Latitude) - 13.30(Longitude) - 2.42(U_H) \quad (4.2)$$

where -0.49, -1.25, -13.30, and -2.42 were the coefficients for UOHC, latitude, longitude, and translation speed, respectively, with their corresponding units. It is noted that the model coefficients for each predictor demonstrated the same negative influence over U_z and were smaller values than that of Regression **13**. A scatter plot of all predictors in utilized in Regression **14** was provided in Figure 4.47. Like the multiple scatter plot for SST, the same trends were evident for UOHC in Regression **14**. Latitude and longitude demonstrated near-linear relationships with wind speed, while UOHC and translation speed revealed highly non-linear trends. Figures 4.46 and 4.47 should be interpreted with caution, as model assumptions failed to verify.

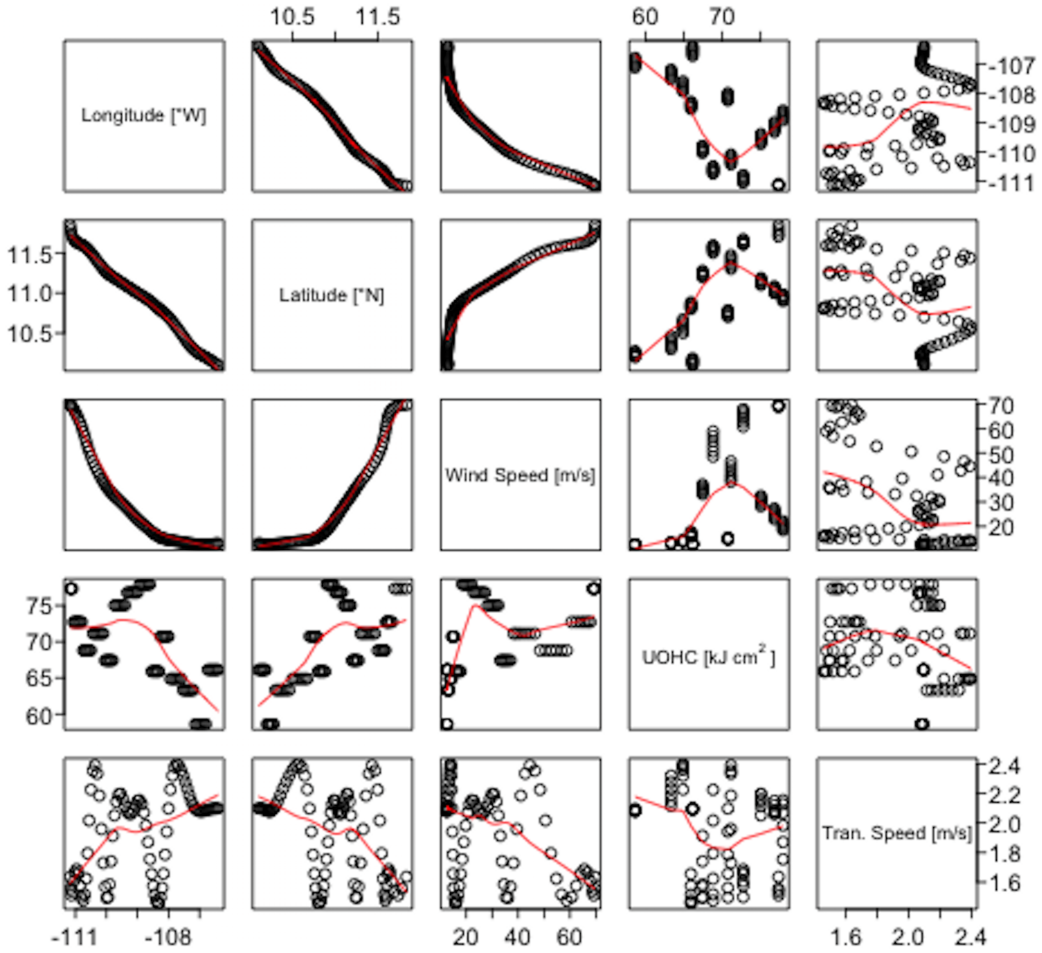

Figure 4.47: Scatterplot of regression variables for Regression 14. Model fit indicated by solid red line. Axis labels are along the figure diagonal. The third row is most useful for analysis.

4.2.8 Regressions 15 and 16 – Hurricane Emilia (2012)

Regression **15** was a multiple linear regression model run for Hurricane Emilia, the only major hurricane in 2012 that sustained major hurricane status ($> 50\ ms^{-1}$) for longer than 30 observations. In this model, latitude, longitude, and translation speed were highly significant parameters with p-values of <0.001 each. SST was also strongly significant, with a p-value of 0.03. This regression performed extremely well, with an adjusted R- squared value of 0.9955. Plotted residuals indicated a somewhat normal distribution with a slight left tail. The Shapiro-Wilks test indicated a W-value of 0.977 and p-value 0.194, confirming the likely normal distribution of the data. The equation for the regression model was:

$$U_z = 123.0 - 1.19(SST) + 23.93(Latitude) + 3.23(Longitude) + 1.93(U_H) \tag{4.3}$$

where -1.19, 23.93, 3.23, and 1.93 were the coefficients for the explanatory predictors respectively with corresponding units. Unlike the Amanda models, all model parameters except SST trended positively, with latitude as the most dominant predictor. Unlike the Amanda models, all model parameters except SST trended positively, with latitude as the most dominant predictor. A scatter plot of all predictors in utilized in Regression **15** was provided in Figure 4.48. For Regression **15** similar trends between latitude and longitude were revealed, but surprisingly, a better near-linear fit was seen between SST and wind speeds for Hurricane Emilia. Translation speed exhibited a less variable relationship as well. As Regression **15** performed extremely well, with model assumptions met, the trends seen in Figure 4.48 may reveal an ideal regression scheme between the selected parameters.

Regression **16** was a multiple linear regression model run for Hurricane Emilia with UOHC as an explanatory predictor for variation in along-track U_z. All model parameters were highly significant, with p-values of <0.001. This regression performed slightly better than the SST regression, with an adjusted R-squared value was 0.996. Plotted residuals

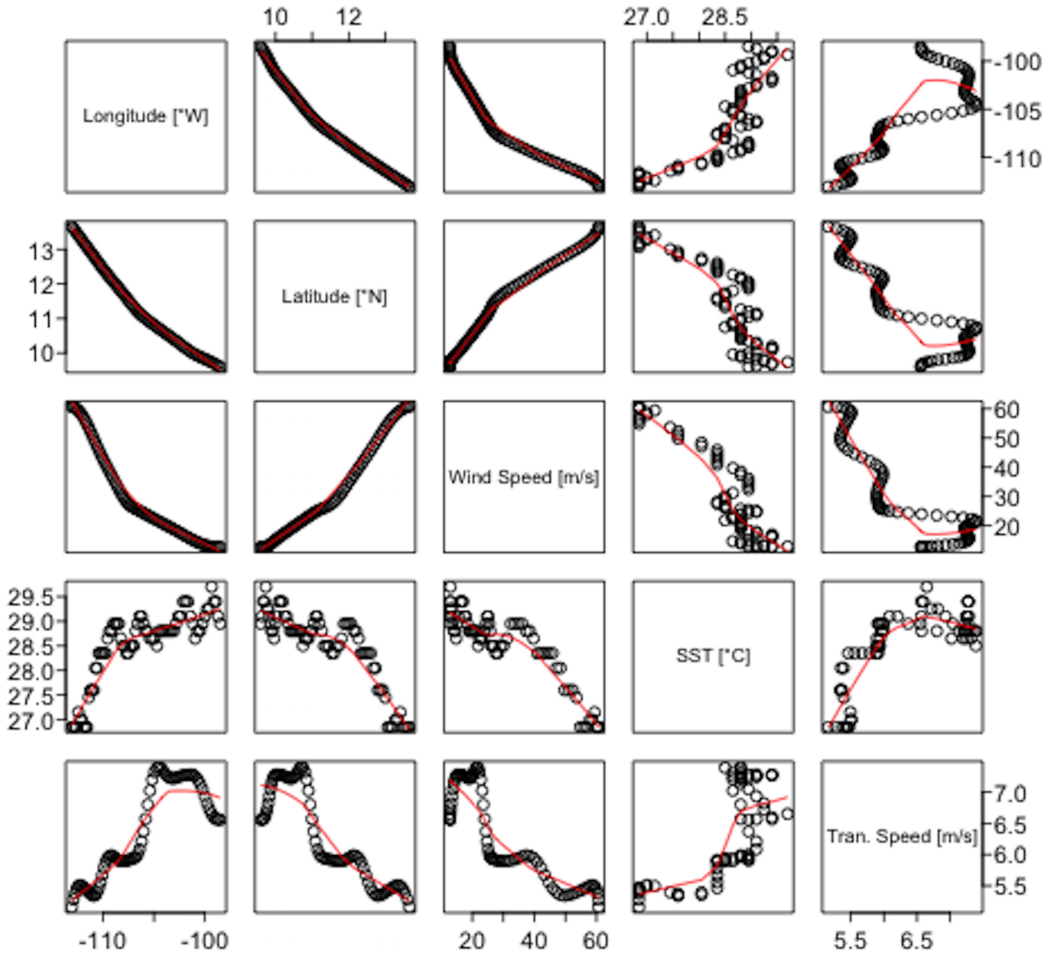

Figure 4.48: Scatterplot of regression variables for Regression 15. Model fit indicated by solid red line. Axis labels are along the figure diagonal. The third row is most useful for analysis.

demonstrated a mostly normal distribution with slight skewness in the right tail and few outliers. Normality was confirmed with the Shapiro-Wilks test with a W-value of 0.977 and p-value of 0.192. The regression model equation was as follows:

$$U_z = 38.4 - 0.08(UOHC) + 20.87(Latitude) + 2.38(Longitude) + 1.79(U_H) \qquad (4.4)$$

where -0.08, 20.87, 2.38, and1.79 were the coefficients for UOHC, latitude, longitude, and translation speed, respectively, with their corresponding units. Coefficient values in this model were smaller than the previous model, with positive influence of all explanatory predictors except the oceanic parameter. Like the Amanda regression models, UOHC per-

formed slightly better than SST in predicting along-track U_z variability. A scatter plot of all predictors in utilized in Regression **16** was provided in Figure 4.49. The trends for Regression **16** did not perform as well as those for Regression **15**. Non-linear trends were present for both UOHC and translation speed during Emilia, while a near-perfect linear relationship was shown for latitude and longitude.

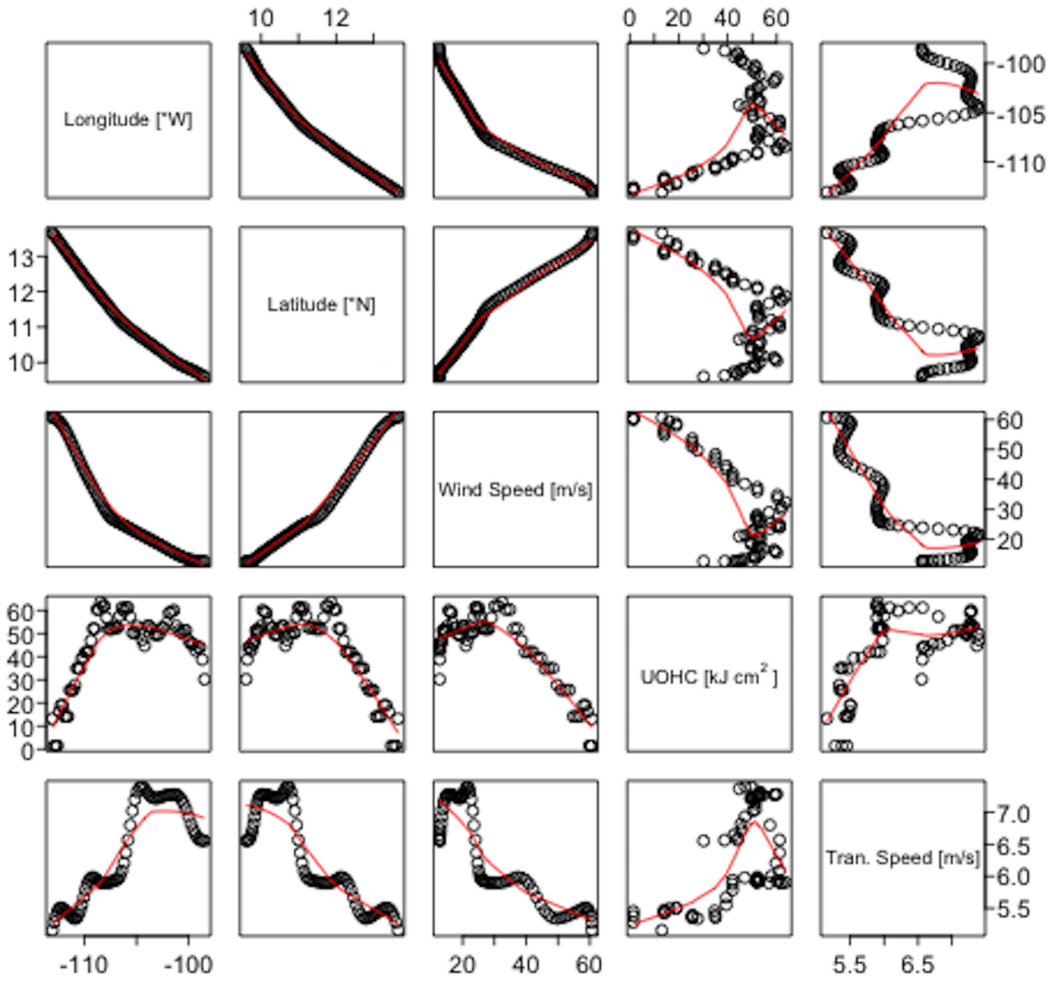

Figure 4.49: Scatterplot of regression variables for Regression 16. Model fit indicated by solid red line. Axis labels are along the figure diagonal. The third row is most useful for analysis.

4.2.9 Regressions 17 and 18 – Hurricane Iselle (2014)

Regression **17** was a multiple linear regression model for Hurricane Iselle with SST, storm latitude, longitude, and translation speed as explanatory predictors. As Iselle made

a rare landfall on the Big Island of Hawaii, it was especially prudent to analyze the relative importance of the variables considered in this model. This model revealed all explanatory predictors to be very significant, with p-values each of <0.001. Like the regressions for Emilia, this model performed extremely well, with an adjusted R-squared value of 0.9937. Model residuals indicated a near-normal distribution, with few outliers. Normality was rejected with a W-value of 0.970 and p-value of 0.007. In spite of the outliers, the model for Iselle is considered useful for variability explanation. The regression equation was the following:

$$U_z = -390.0 + 2.47(SST) + 3.53(Latitude) - 2.37(Longitude) + 0.96(U_H) \tag{4.5}$$

where 2.47, 3.53, -2.37, and 0.96 were the coefficients for SST, latitude, longitude, and translation speed, respectively, with their corresponding units. In the reverse scenario of the previous storm-specific regressions, here SST exhibited a positive influence on U_z, while storm longitude revealed a negative trend. Latitude was found to be the most influential predictor, followed closely by both SST and longitude. A scatter plot of all predictors in utilized in Regression **17** was provided in Figure 4.50. Surprisingly, latitude and longitude exhibited less linearity in Regression **17**, while SST revealed a slight overall negative trend and translation speed demonstrated a highly variable relationship to wind speed.

Regression **18** was a multiple linear regression for Iselle that utilized UOHC, instead of SST, as one of the explanatory predictors. Much like Regression **17**, this model revealed very high significance with model parameters. All explanatory predictors had p-values <0.001. The model performed extremely well with an adjusted R-squared value of 0.9946. This result was an indiscernible increase of 0.0009 in explanatory power over the model with SST for Iselle. Both regression models indicated that nearly all of variability in along-track U_z could be explained with storm position, translation speed, and either SST or UOHC.

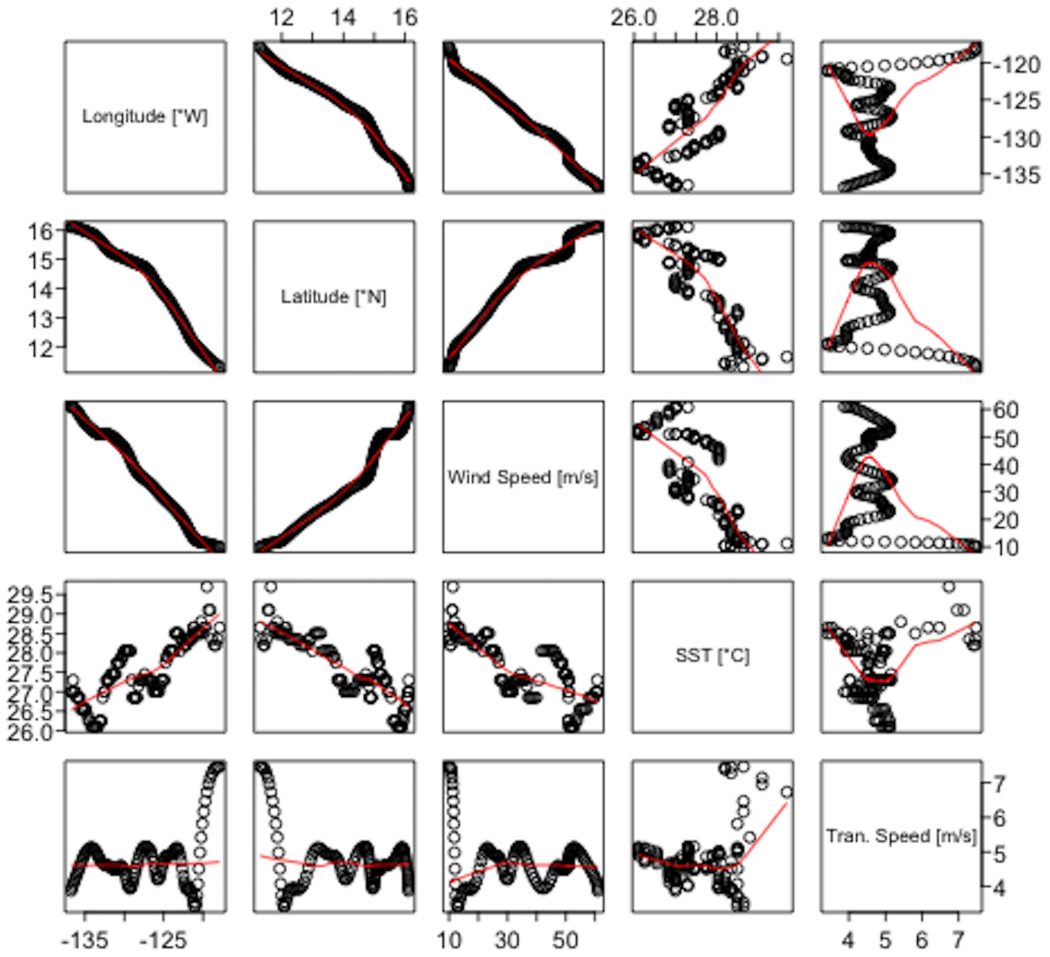

Figure 4.50: Scatterplot of regression variables for Regression 17. Model fit indicated by solid red line. Axis labels are along the figure diagonal. The third row is most useful for analysis.

Model residuals demonstrated a similar near-normal distribution, with several outliers and a slightly skewed right tail. The Shapiro-Wilks test revealed non-normality with a W-value of 0.971 and p-value of 0.009. Regression results were considered to still be useful in this regard. The regression model equation was:

$$U_z = -326.5 + 0.17(UOHC) + 3.50(Latitude) - 2.40(Longitude) + 0.53(U_H) \qquad (4.6)$$

where 0.17, 3.50, -2.40, and 0.53 were the coefficients for the explanatory predictors, respectively, with their corresponding units. Once again, the oceanic predictor UOHC exhibited a slight, but positive influence on U_z. Latitude indicated the most positive influence, while

longitude demonstrated an almost equal, but negative effect on U_z. Compared to the SST model for Iselle, UOHC demonstrated greater influence over U_z variability than SST. A scatter plot of all predictors in utilized in Regression **18** was provided in Figure 4.51. Like those for Regression **17**, that for **18** illustrated similar, more variable relationships to wind speed. Translation speed appeared to be the weakest predictor of wind speed variability during Iselle. As the SST and UOHC regressions failed to meet model assumptions, Figures 4.50 and 4.51 should be interpreted with caution.

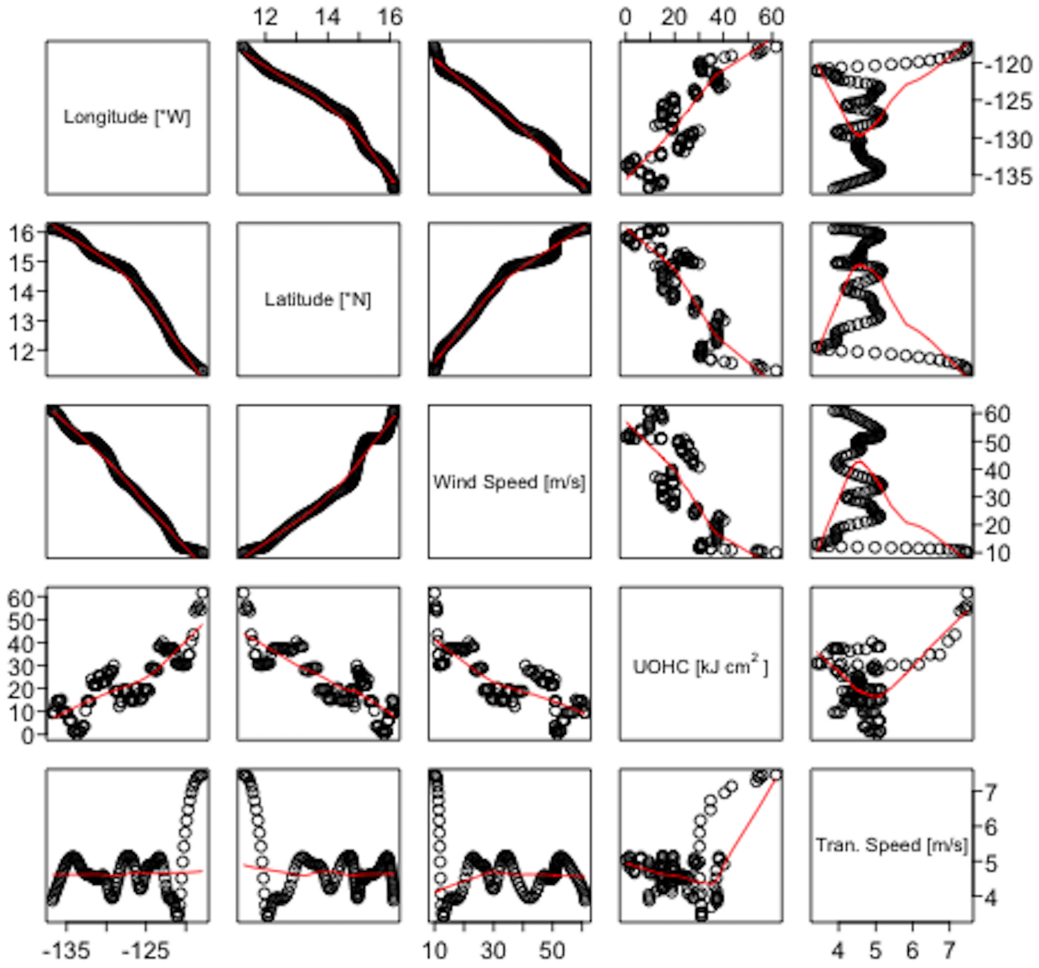

Figure 4.51: Scatterplot of regression variables for Regression 18. Model fit indicated by solid red line. Axis labels are along the figure diagonal. The third row is most useful for analysis.

4.2.10 Regressions 19 and 20 – Hurricane Marie (2014)

Regression **19** was a multiple linear regression model for Hurricane Marie, the only Category-5 storm in this study, and one that made a powerful landfall on Mexico. SST, storm latitude, longitude, and translation speed were highly significant with p-values of <0.001 each. Latitude was somewhat significant, with a p-value of 0.002. SST proved to be not significant in this model with a p-value of 0.12. This model performed very well, with an adjusted R-squared of 0.9781. Model residuals indicated a weak normal distribution, with a few outliers and a strongly skewed right tail in the data. The Shapiro-Wilks test rejected the null hypothesis, with a W-value of 0.956 and p-value of 0.02. With this fit, the model is cautiously considered for determining predictor usefulness. The explanatory predictor coefficients were of a size that was deemed suitable. The model equation was:

$$U_z = -569.9 - 1.69(SST) - 5.76(Latitude) - 6.77(Longitude) + 3.26(U_H) \tag{4.7}$$

where -1.69, -5.76, -6.77, and 3.26 were the coefficients for SST, latitude, longitude, and translation speed, respectively, with their corresponding units. Surprisingly, translation speed exerted the greatest positive influence, while latitude and longitude appeared to have equally negative controls on U_z. A scatter plot of all predictors in utilized in Regression **19** was provided in Figure 4.52. For Regression **19**, very weak relationships were revealed between SST, translation speed, and wind speeds. Latitude and longitude appeared to have slight curved tails within the data, but overall exhibited a near-linear trend.

Regression **20** was a multiple linear regression model for Marie, which used UOHC as an explanatory predictor instead of SST. Storm latitude, longitude, and translation speed were also used. In Regression **20**, all model parameters proved to be highly significant, with p-values <0.001. The model performed very well, with an adjusted R-squared value of 0.9822. Compared to Regression **19**, the usage of UOHC in the place of SST resulted in a 0.004

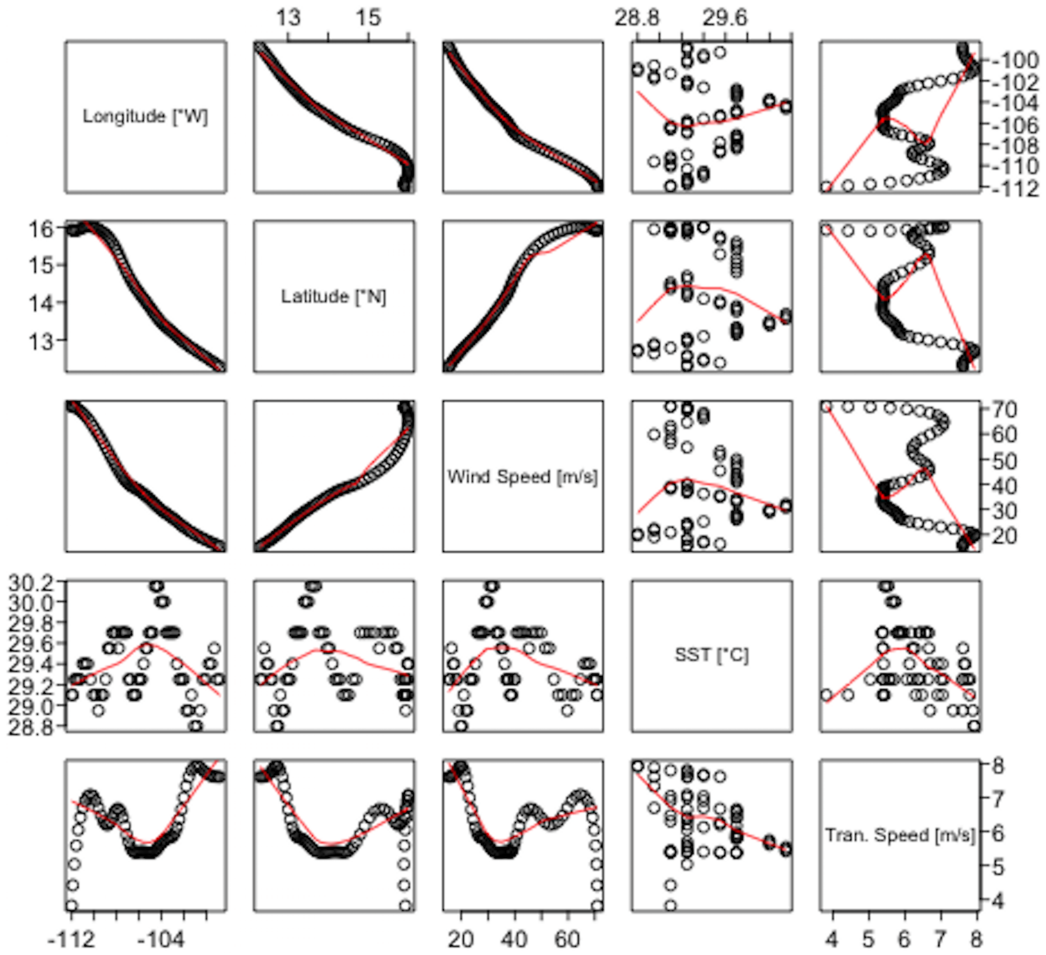

Figure 4.52: Scatterplot of regression variables for Regression 19. Model fit indicated by solid red line. Axis labels are along the figure diagonal. The third row is most useful for analysis.

increase in model explanatory power. Like Regression **19**, model residuals demonstrated a weak normal distribution with several outliers. The W-value for Regression **20** was 0.960 with a p-value of 0.03, rejecting normality. The results were treated with caution, but still considered useful, given its SST regression model counterpart. The regression model equation was as follows:

$$U_z = -574.6 - 0.13(UOHC) - 5.61(Latitude) - 6.50(Longitude) + 2.54(U_H) \qquad (4.8)$$

where -0.13, -5.61, -6.50, and 2.54 were the coefficients for the explanatory variables, respectively, with their corresponding units. Compared to Regression **19**, the oceanic UOHC

exhibited the most difference in influence, trending towards a slightly negative effect. Translation speed again appeared to be the most positive influence in the UOHC-version of the Marie regression models. Latitude and longitude both exhibited approximately equal negative controls on U_z. A scatter plot of all predictors in utilized in Regression **20** was provided in Figure 4.53. Much of the same trends and slopes between parameters discussed for Regression **19** were present in that for Regression **20**, which incorporated UOHC in SSTs place. Figures 4.52 and 4.53 should be interpreted with extreme caution, as the model assumptions failed to verify.

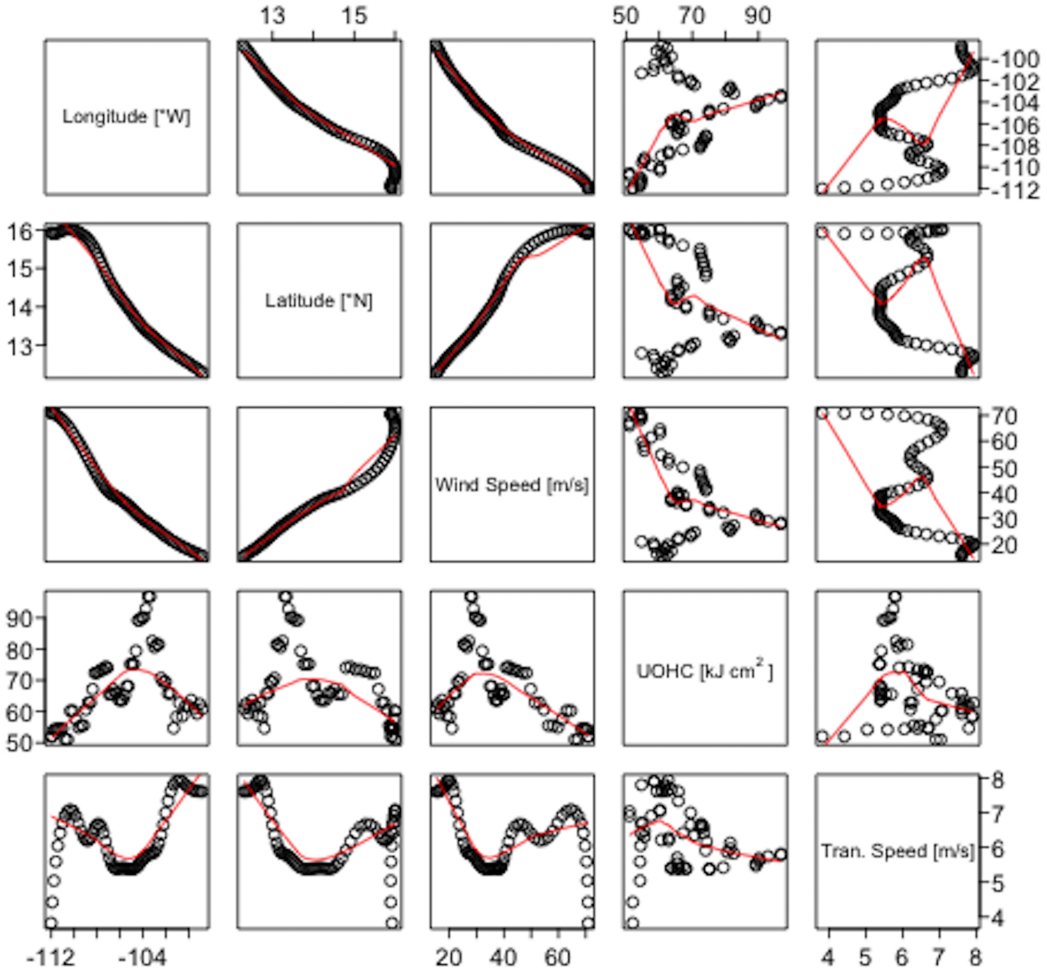

Figure 4.53: Scatterplot of regression variables for Regression 20. Model fit indicated by solid red line. Axis labels are along the figure diagonal. The third row is most useful for analysis.

4.2.11 Regressions 21 and 22 – Hurricane Odile (2014)

Regression **21** was a multiple linear regression model for Hurricane Odile, with SST as an explanatory predictor. A regression model scheme for Odile was considered very prudent, as the storm made several landfalls on Mexico, one of which devastated Baja California. Like the other storm-specific regressions, this model revealed high parameter significance. All explanatory predictors resulted in p-values of <0.001. This model also performed very well, with a high adjusted R-squared value of 0.9829. This value theoretically explained almost 98% of all variability in along-track U_z in Odile. A plot of model residuals indicated a somewhat normal distribution, with a strongly skewed right tail in the data. The Shapiro-Wilks normality test revealed a W-value of 0.953 and p-value of <0.001, thus rejecting normality. The regression equation was the following:

$$U_z = -369.8 - 2.67(SST) + 3.24(Latitude) - 4.04(Longitude) + 2.48(U_H) \tag{4.9}$$

where -2.67, 3.24, -4.04, and 2.48 represented the coefficients for the explanatory predictors, respectively, and their corresponding units. Latitude and translation speed exhibited positive influences on U_z, while the SST and longitude predictors trended negatively. In this model, storm position predictors exhibited nearly equal but opposite controls of U_z. A scatter plot of all predictors in utilized in Regression **21** was provided in Figure 4.54. The trends in Regression **21** were slightly more unusual than those previous seen in the other storm-specific regressions. While latitude revealed a similar near-linear relationship, longitude did not with a slight bowing in values. SST and translation speed demonstrated highly variable non-linear relationships to wind speed. It may be that the decay stage of Hurricane Odile may reveal stronger, linear trends than the intensification phase.

Lastly, Regression **22** was a multiple linear regression model for Odile with UOHC, latitude, longitude, and translation speed as explanatory predictors for along-track variation

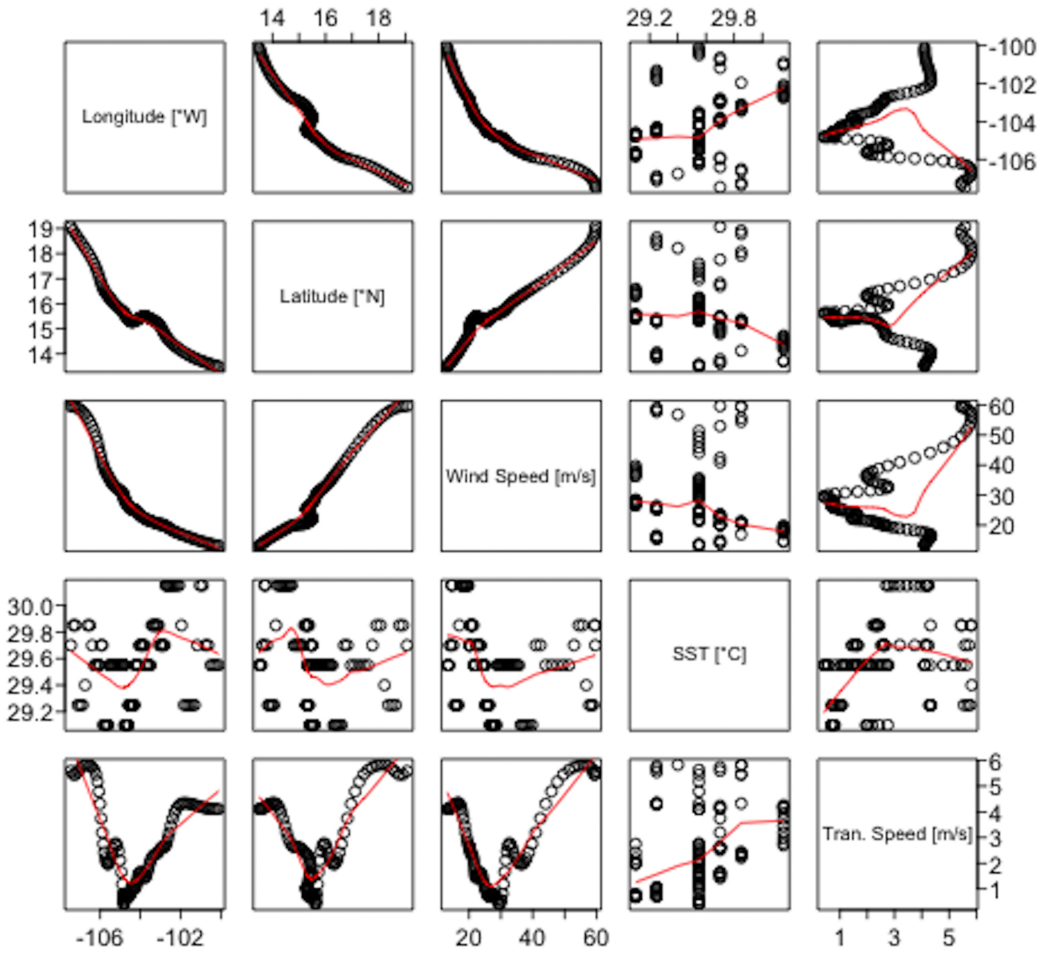

Figure 4.54: Scatterplot of regression variables for Regression 21. Model fit indicated by solid red line. Axis labels are along the figure diagonal. The third row is most useful for analysis.

in U_z. Model parameters demonstrated high significance. Storm latitude, longitude, and translation speed resulted in p-values of <0.001, while UOHC was considered significant with a p-value of 0.002. This regression model demonstrated a high adjusted R-squared value of 0.9812. Model residuals indicated some normality, but with a long left tail and a few outliers. The Shapiro-Wilks test indicated a non-normal distribution with a W-value of 0.976 and p-value of 0.03. The regression model equation was as follows:

$$U_z = -461.0 - 0.08(UOHC) + 2.78(Latitude) - 4.29(Longitude) + 2.03(U_H) \qquad (4.10)$$

where -0.08, -2.78, -4.29, and 2.03 were the coefficients for UOHC, latitude, longitude,

and translation speed, respectively, with their corresponding units. UOHC exerted an almost insignificant negative control over U_z in this regression model. Storm latitude and longitude predictors displayed opposite controls, where longitude revealed to be the most dominant factor in U_z variation. A scatter plot of all predictors in utilized in Regression **22** was provided in Figure 4.55. Like the previous model, a slight curved, bowing effect was seen between longitude and wind speed. The relationships between latitude, UOHC, and translation speed followed similar to that of Regression **21**.

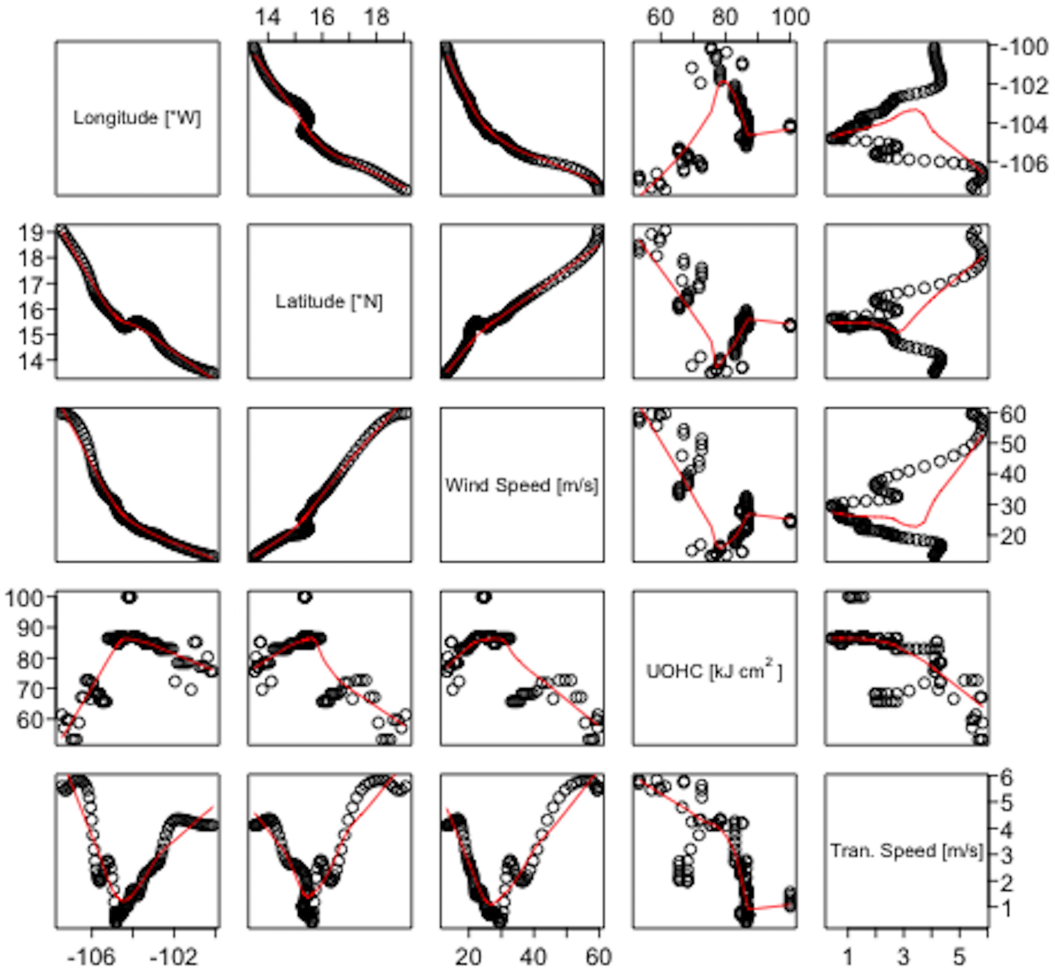

Figure 4.55: Scatterplot of regression variables for Regression 22. Model fit indicated by solid red line. Axis labels are along the figure diagonal. The third row is most useful for analysis.

Table 4.1: Summary of Regression Results. Bold values are considered extremely useful.

Name	Explanatory Variable(s)	Response Variable	# of Obs.	Adjusted R^2 Value
1 – 2012 Majors	SST	U_z	1013	0.5248
2 – 2012 Majors	UOHC	U_z	1013	0.5392
3 – 2014 Majors	SST	U_z	2301	0.0355
4 – 2014 Majors	UOHC	U_z	2301	0.0974
5 – All Majors	SST	U_z	3314	0.0975
6 – All Majors	UOHC	U_z	3314	0.1656
7 – 2012 Majors	SST, Latitude, Longitude, U_H	U_z	1013	0.6453
8 – 2012 Majors	UOHC, Latitude, Longitude, U_H	U_z	1013	0.6410
9 – 2014 Majors	SST, Latitude, Longitude, U_H	U_z	2301	0.2664
10 – 2014 Majors	UOHC, Latitude, Longitude, U_H	U_z	2301	0.2577
11 – All Majors	SST, Latitude, Longitude, U_H	U_z	3314	0.3321
12 – All Majors	UOHC, Latitude, Longitude, U_H	U_z	3314	0.3193
13 – Amanda	SST, Latitude, Longitude, U_H	U_z	81	0.8425
14 – Amanda	UOHC, Latitude, Longitude, U_H	U_z	81	0.8514
15 – Emilia	SST, Latitude, Longitude, U_H	U_z	73	**0.9955**
16 – Emilia	UOHC, Latitude, Longitude, U_H	U_z	73	**0.9960**
17 – Iselle	SST, Latitude, Longitude, U_H	U_z	125	0.9937
18 – Iselle	UOHC, Latitude, Longitude, U_H	U_z	125	0.9946
19 – Marie	SST, Latitude, Longitude, U_H	U_z	67	0.9781
20 – Marie	UOHC, Latitude, Longitude, U_H	U_z	67	0.9822
21 – Odile	SST, Latitude, Longitude, U_H	U_z	118	0.9829
22 – Odile	UOHC, Latitude, Longitude, U_H	U_z	118	0.9812

4.3 Enthalpy Flux Analysis

Fisher (1958) was one of the first to hypothesize that energy flux between the ocean and atmosphere may be a primary mechanism by which the behavior of a hurricane is influenced. Since then, energy exchange at the air-sea boundary has been identified as one of the major physical processes governing hurricane intensity (Wroe and Barnes, 2003; Bell et al., 2012; Pun et al., 2016). Fluxes of momentum, moisture, and heat provide the necessary energy to establish and maintain deep convection over the ocean (Large and Pond, 1982; Cione and Uhlhorn, 2003; Pun et al., 2014). In this research, heat and moisture fluxes were computed via two separate methods for Hurricane Iselle (2014). Enthalpy derivation during Iselle was chosen for several reasons, of which the primary motivation was to understand the prevailing factors that led to a rare and powerful landfall on the

Hawaiian Islands. Additionally, Iselle also exhibited an annular structure that is estimated to occur in only 3% of all NPO TCs (Knaff et al., 2003). Annular hurricanes experience a long period of intensity steadiness following maximum intensity, leading to larger forecast errors and negative biases (Knaff et al., 2003). Iselle maintained an annular structure 4 – 5 August (Kimberlain, 2016) before a prolonged intensity decline.

The first method computed enthalpy flux using average atmospheric model data for the NPO using NCEP Reanalysis-1 products, while the second method utilized *in-situ* dropsonde observations. It is crucial to note here that while the atmospheric model method calculated enthalpy flux along-track for the duration of Iselle's lifecycle, the dropsonde method did not, as those observations were spatially and temporally limited. For more information on the calculation of enthalpy, see Section 3.2.5 and Appendix B.

4.3.1 Enthalpy Flux via Model

Sensible heat flux values slowly increased to 186 W m^{-2} while as a Tropical Storm and into a Category-1 hurricane, and rapidly peaked at 339 W m^{-2} upon attaining Category-2 intensity (Figure 4.56). Values then declined to a local minimum of 167 W m^{-2} as the storm maintained Category-3 status. At maximum intensity, values of sensible heat flux were 259 W m^{-2}, after which values declined as the storm decayed. Sensible heat flux reached a secondary peak value of 294 W m^{-2}, as the storm tracked over a region of higher SSTs and T_a surrounding the Hawaiian Islands, with a temperature gradient of 3.35°C and declining wind speeds of 36.0 ms^{-1} (Figure 4.57). Throughout the entire track, sensible heat flux values exhibited a positive flux whilst the temperature gradient between SST and T_a was at its smallest, and vice versa (Figure 4.57). However, this observation is likely obscured by wind speeds of less than 20 ms^{-1} at those times. In fact, Jaimes et al. (2015) found that bulk enthalpy fluxes in a major hurricane were controlled by the thermodynamic gradient between the sea surface and the near-surface air, independent of wind speed.

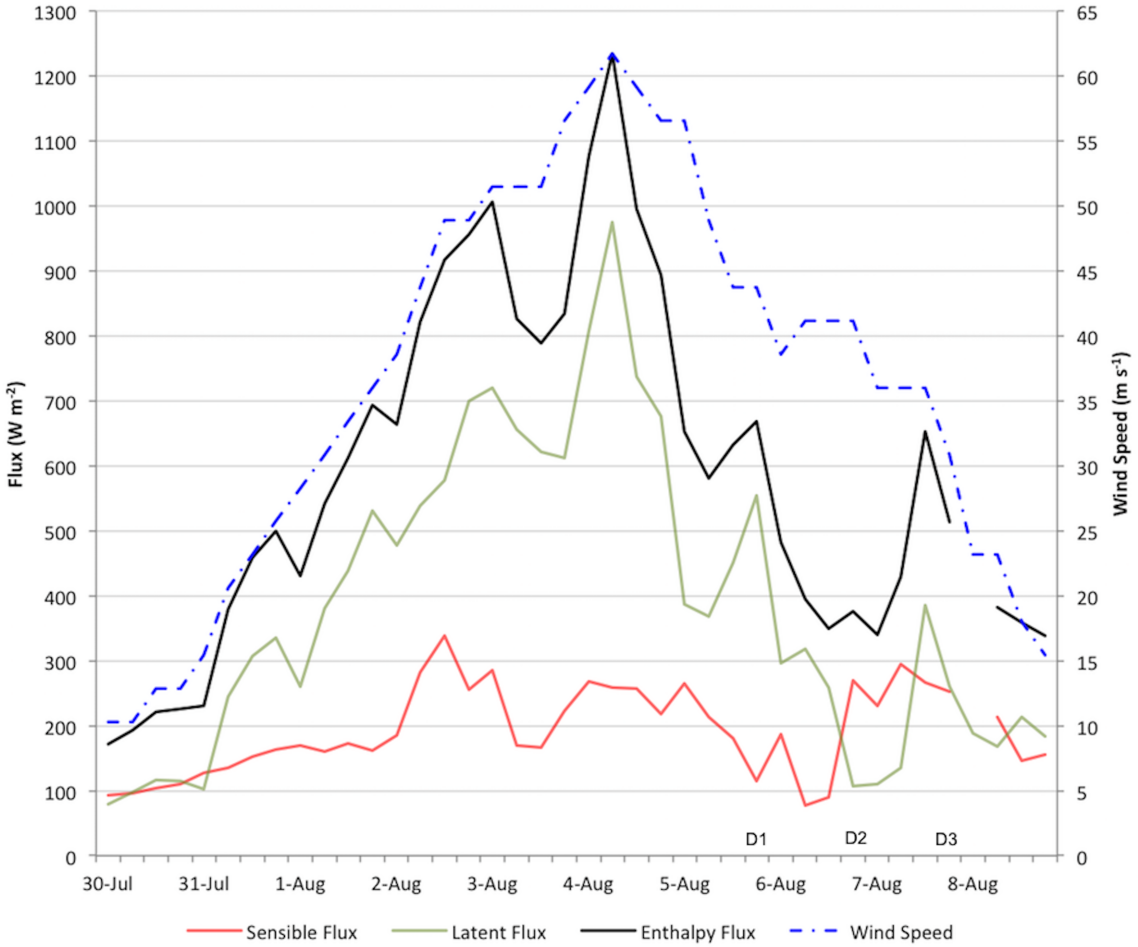

Figure 4.56: Along-track heat and moisture fluxes and maximum wind speeds throughout Hurricane Iselle (2014). D1, D2, and D3 mark corresponding times of dropsonde deployment.

Unlike sensible heat flux, latent heat flux values were larger in magnitude during storm evaluation. Latent heat values steadily climbed with increased wind speeds, but fluctuated with changes in atmospheric moisture content. At the moment of maximum intensity as a Category-4 hurricane, latent heat values peaked at 975 W m^{-2}. Latent heat then rapidly declined to approximately 368 W m^{-2} as wind speeds decreased to 48.9 ms^{-1} and the moisture gradient weakened. Values rose to 554 W m^{-2}, likely as the moisture gradient sharply increased near the Hawaiian Islands, before a decline to 107 W m^{-2} (Figure 4.57). Twelve hours before landfall, latent heat values increased to 385 W m^{-2}, which may resulted from an increased moisture gradient as SSTs rose while T_a declined with the entrainment of dry

air aloft (Figure 4.57). These results indicate a direct relationship between variations in latent heat flux, wind speed, and the moisture gradient.

As the combination of sensible and latent heat fluxes, enthalpy flux throughout Iselle demonstrated similar trends to those discussed above. Most notably, enthalpy flux values peaked at 1234 W m^{-2} as wind speeds also reached their maximum of 61.7 m s^{-1}. A later peak of 650 W m^{-2} in enthalpy flux experienced prior to landfall as both the temperature and moisture gradients increased with rising SSTs (Figure 4.57).

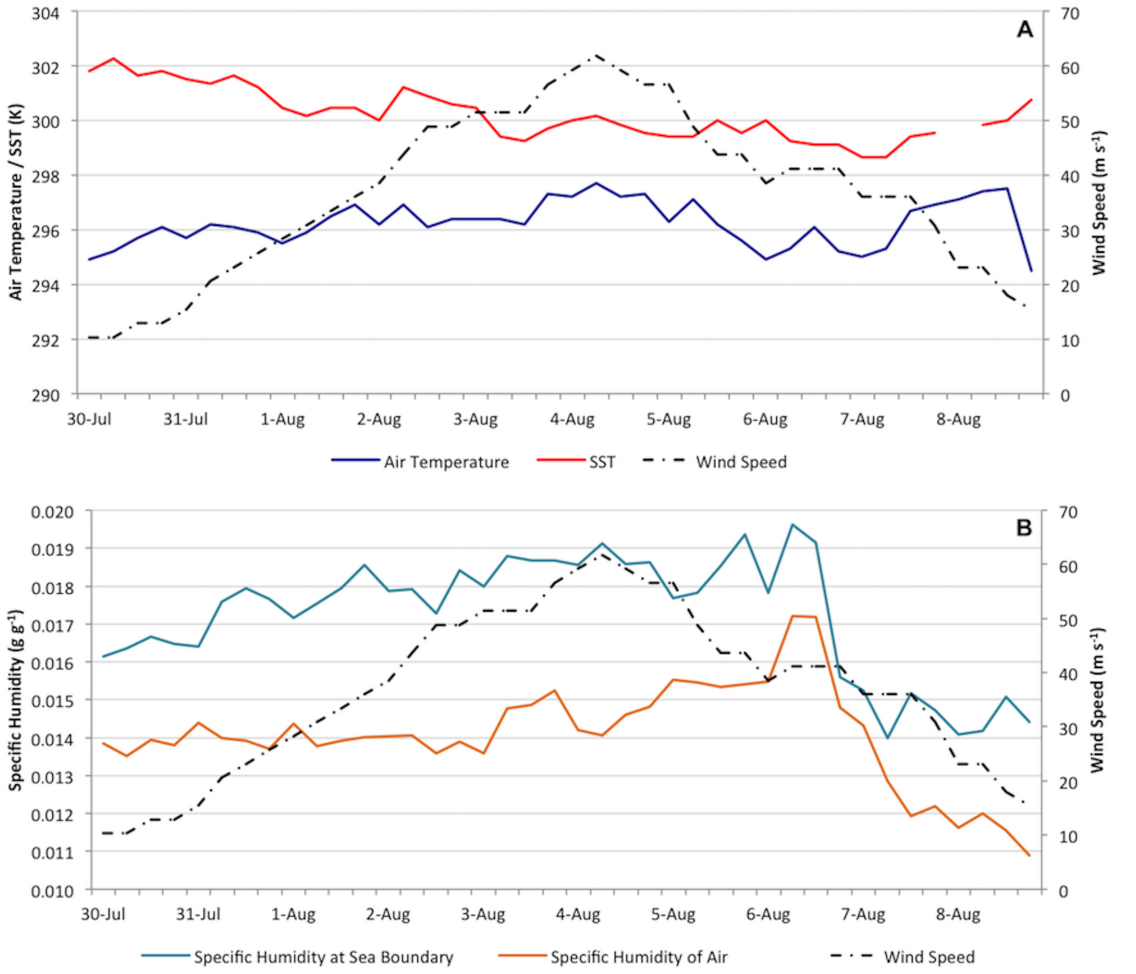

Figure 4.57: Model enthalpy method input parameters for sensible heat flux (A) and latent heat flux (B) during Hurricane Iselle (2014).

4.3.2 Enthalpy Flux via Dropsonde Observations

Sensible, latent, and enthalpy fluxes were also calculated using *in-situ* dropsonde observations. Unlike the atmospheric model derivation for enthalpy, the dropsonde enthalpy calculations were not determined along-track for the entirety of Hurricane Iselle's lifecycle. Dropsondes were deployed three days prior to landfall as Iselle weakened, beginning at approximately 1800 UTC on August 5 – 7 2014. Air temperature, relative humidity, and wind speed observations from each dropsonde were averaged between 25 and 35 m in order to compensate for any measurements not directly observed at 30 m. While enthalpy flux values are discussed at each dropsonde location, flux values observed closest to Iselle's eye at the time of deployment were considered as most representative of inner eye storm conditions at that time.

On the first day of dropsonde deployment, Iselle was a strong Category-2 hurricane with 48.9 ms^{-1} wind speeds. Sensible, latent, and enthalpy flux values are shown in Figure 4.58, and the parameters essential to those fluxes are graphed in Figure 4.59. For reference, the 19th dropsonde deployed on 5 August was the closest to Iselle's eye. Dropsonde measurements began in the north and northeastern quadrants ahead of the storm to assess the near-storm environment (Birchard and Ballard, 2014). Sensible heat flux remained below 40 W m^{-2} for all 5 August dropsonde measurements. The maximum sensible heat flux value of 36 W m^{-2} was observed during the 8th dropsonde, as air temperature at this location dropped and thus increased the temperature gradient to 2.1K (Figure 4.59). Sensible heat flux at the dropsonde closest to the storm eye was 32 W m^{-2}, likely resulting from a 1.8K temperature gradient between the ocean and the atmosphere. Dropsondes 20 – 28 were deployed to the northwest and north of the storm, in order to ascertain environmental conditions in the direct path of the storm. Sensible heat flux values in those quadrants exhibited a weak flux, with values close to 10 W m^{-2} or less. The temperature gradient at those dropsonde locations was less than 1K (Figure 4.59).

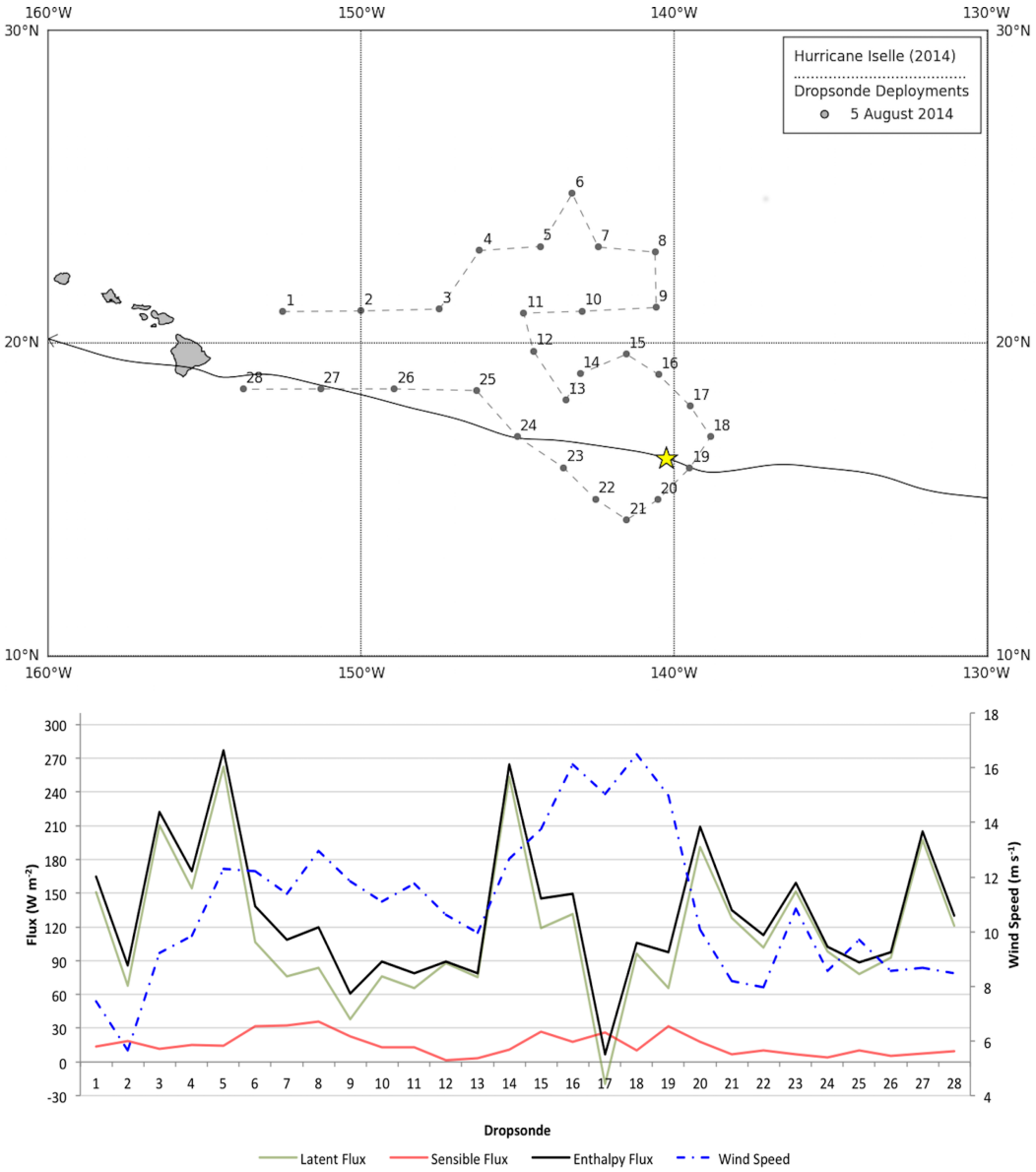

Figure 4.58: Sensible, latent, and enthalpy fluxes observed via dropsonde at 30 m on 5 August 2014 along the flight path for locations 1 – 28. Yellow star denotes approximate storm position at time of dropsonde deployment.

Latent heat flux values were observed to be an order of magnitude greater than the sensible heat flux experienced on 5 August. Moisture flux peaked at the 5th dropsonde location, with a value of 262 W m^{-2}. Latent heat flux had a secondary peak of 254 W m^{-2} at the 14th dropsonde location. Both of these latent heat flux peaks were likely due to increased wind speeds in tandem with an increased moisture gradient at those locations (Figure 4.59). At Iselle's eye location, latent heat flux was 66 W m^{-2}, where relatively

high wind speeds of 15 ms^{-1} were observed. Surprisingly, latent heat flux was negative at the 17th dropsonde where specific humidity of the air exceeded that of the sea-surface boundary (Figure 4.59); most likely this observation was taken within a precipitating rain band of the storm where wind speeds had momentarily decreased by 1.5 ms^{-1}. In the north and northwest quadrant deployments, latent heat flux values ranged between 80 and 190 W m^{-2}, where a large moisture gradient persisted.

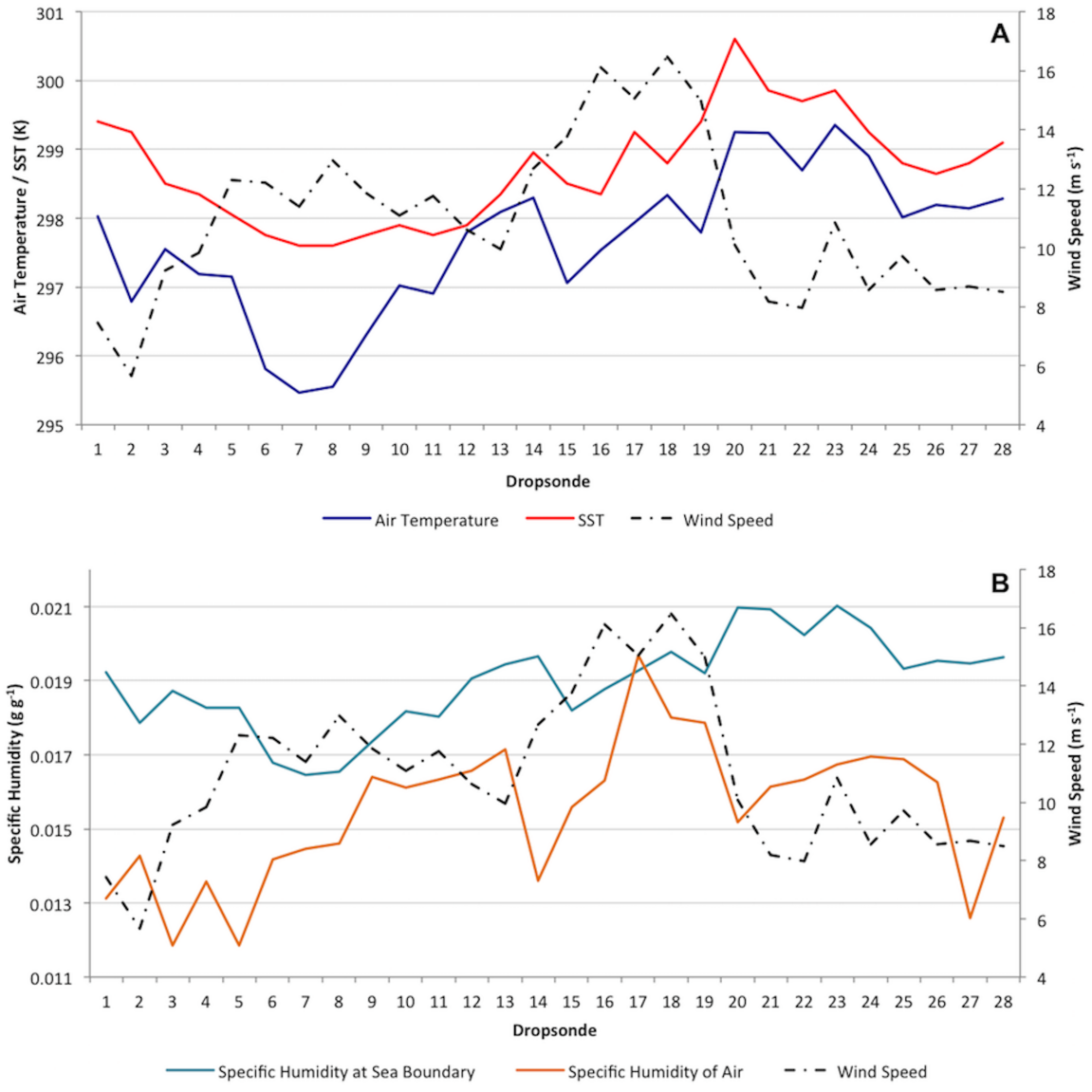

Figure 4.59: Dropsonde observation enthalpy method input parameters for sensible heat flux (A) and latent heat flux (B) on 5 August 2014 along the flight path for locations 1 – 28.

Enthalpy flux values followed a very similar trend to the latent heat flux observed throughout this dropsonde deployment, as sensible heat flux values were minimal throughout. Maximum enthalpy flux was observed at the 5th dropsonde location with a value of 277 W m^{-2} while observed wind speeds were 12.3 ms^{-1}. A minimum in enthalpy flux was detected at the location where latent heat values were also negative. It is noted that flux values from this dropsonde derivation are diminished in comparison to the model derivation of the same fluxes. It is believed this disparity resulted from the wind speed observations utilized by each method. The atmospheric model method was designed with the NHC HURDAT2 maximum 10 m wind speeds observed for Iselle, while the dropsonde enthalpy derivation incorporated the wind speeds observed by the instrument at that location in space and time. It was noted that the NHC maximum wind speeds were based on satellite classifications by the Tropical Analysis and Forecast and Satellite Analysis Branches, and not dropsonde measurements (Kimberlain, 2016). To roughly compare between the two methods, the 19th dropsonde resulted in an enthalpy flux value of 97 W m^{-2}, whereas the model derived enthalpy value at that location and time resulted in a value of 632 W m^{-2}. This is an 85% difference between the model derived enthalpy flux and the *in-situ* observed enthalpy flux on 5 August.

A second dropsonde deployment was performed on 6 August and latent, sensible, and enthalpy flux values are provided in Figure 4.60, and the parameters essential to those fluxes are graphed in Figure 4.61. Like the previous day's measurements, dropsondes were positioned primarily in the northeast quadrant of Iselle's projected trajectory. For reference, the 15th dropsonde was the closest dropsonde to Iselle's eye on 6 August. Sensible heat flux measurements throughout this deployment remained within 0 – 30 W m^{-2}, and with a single value which reached approximately 54 W m^{-2} where the temperature gradient exceeded 2K and wind speeds rapidly increased by 4 ms^{-1} (Figure 4.61). At the 20th dropsonde, sensible heat flux values dropped to 0 W m^{-2} as both air temperature and SST were

approximately 298.7K, thus eliminating any temperature gradient at that location. Latent heat flux values on 6 August were observed to be slightly smaller than those experienced the day prior. At this time, Iselle had begun declining in intensity from a Category-3 hurricane to a Category-1. A maximum value of latent heat flux of 189 W m^{-2} was observed at the 13th dropsonde location, northeast of Iselle's position at that time (Figure 4.60). At that location, wind speeds had increased to 15.9 ms^{-1} and a large moisture gradient existed (Figure 4.61). Latent heat flux values closest to Iselle's eye were a low 39 W m^{-2} despite 19.3 ms^{-1} wind speeds, due to a reduced moisture gradient. A large 15 ms^{-1} wind speed decline is seen between locations 16 – 19, strongly impacting the resulting fluxes at those locations despite a large moisture gradient. At that time, the flight path crossed the track of Iselle, and entered the left-hand side of the storm, where wind speed intensity was expected to be not as prominent as in the right-hand side of the hurricane (Figure 4.60).

Enthalpy flux values followed extremely similar trends to that of the latent heat flux observed. Maximum enthalpy flux was 220 W m^{-2}, calculated at the 13th dropsonde on 6 August. At this time, wind speeds were 15.9 ms^{-1} with a large moisture gradient. At the dropsonde closest to Iselle's eye, enthalpy flux was observed to be 56 W m^{-2}, indicating that a decline in enthalpy from 97 W m^{-2} at Iselle's eye location the previous day may have prompted intensity decay. For comparison, model derived enthalpy flux at this location in time was 350 W m^{-2}, an 84% difference between the climatological data and in-situ observations.

Lastly, dropsondes were deployed the day prior to Iselle's landfall on the Big Island. For reference, the 4th, 29th, and 30th dropsondes were closest to Iselle's eye (Figure 4.62). In this deployment, dropsondes were released well behind the main storm complex. This may have been done for several reasons: to determine the cause for Iselle's decay or due to another rapidly approaching major hurricane, Julio, which was forecasted to directly follow

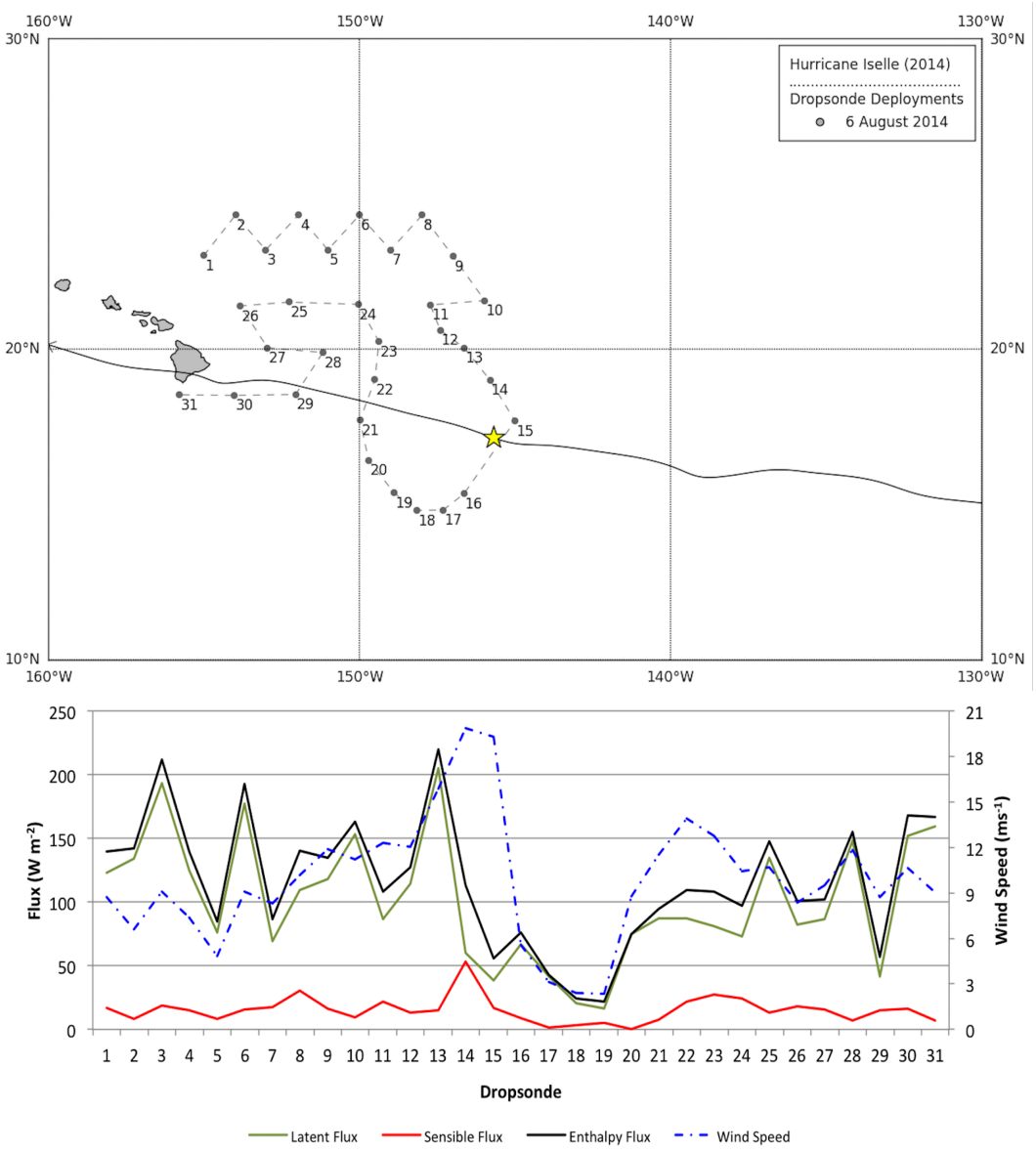

Figure 4.60: Sensible, latent, and enthalpy fluxes observed via dropsonde at 30 m on 6 August 2014 along the flight path for locations 1 – 31. Yellow star denotes approximate storm position at time of dropsonde deployment.

Iselle's path and also strike the Hawaiian Islands. Corresponding to Iselle, sensible heat flux observed at the 4th dropsonde peaked at 25.5 W m^{-2} where wind speeds were a high 18.4 ms^{-1} with a large temperature gradient (Figure 4.63). Sensible heat flux peaked at the 17th dropsonde with a value of 46 W m^{-2}, the highest sensible heat flux value observed in any dropsonde calculation. At this location, wind speeds were 15.3 ms^{-1} and a 2.3K temperature gradient was present (Figure 4.63). Most sensible heat flux values remained

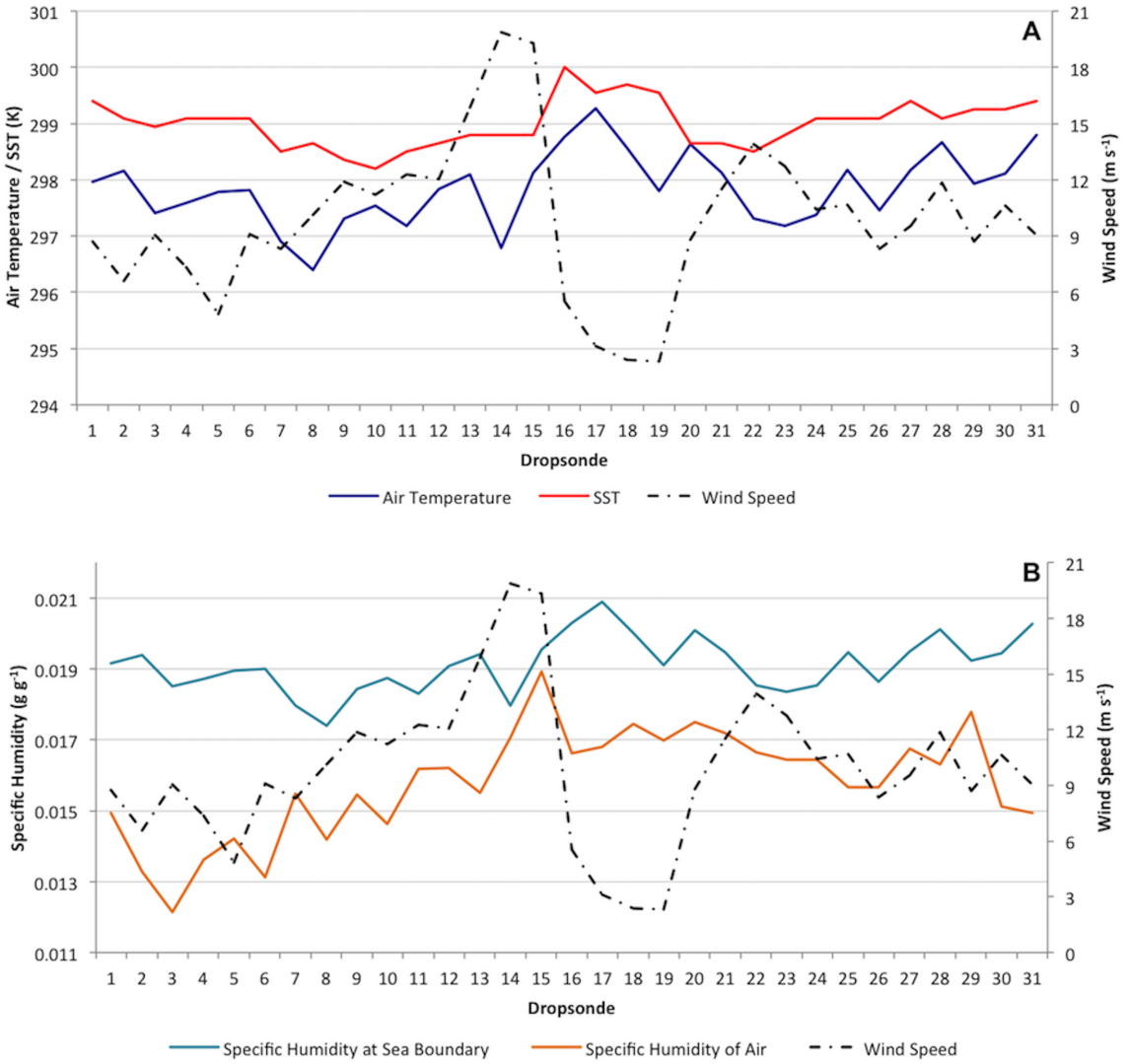

Figure 4.61: Dropsonde observation enthalpy method input parameters for sensible heat flux (A) and latent heat flux (B) on 6 August 2014 along the flight path for locations 1 – 31.

within 0 – 30 W m^{-2}, however, with a few notable exceptions. Negative sensible heat flux values were observed at all instances when T_a exceeded SST, indicating energy transfer from the atmosphere to the ocean (Figure 4.63).

Surprisingly, the most negative sensible heat flux coincided with the highest latent heat flux value at the 16th dropsonde, with values of -20 W m^{-2} and 232 W m^{-2}, respectively. At that location, there existed a large 0.004 g g^{-1} moisture gradient. As this dropsonde location is well behind the storm complex for Iselle, it is proposed that the 16th drop-

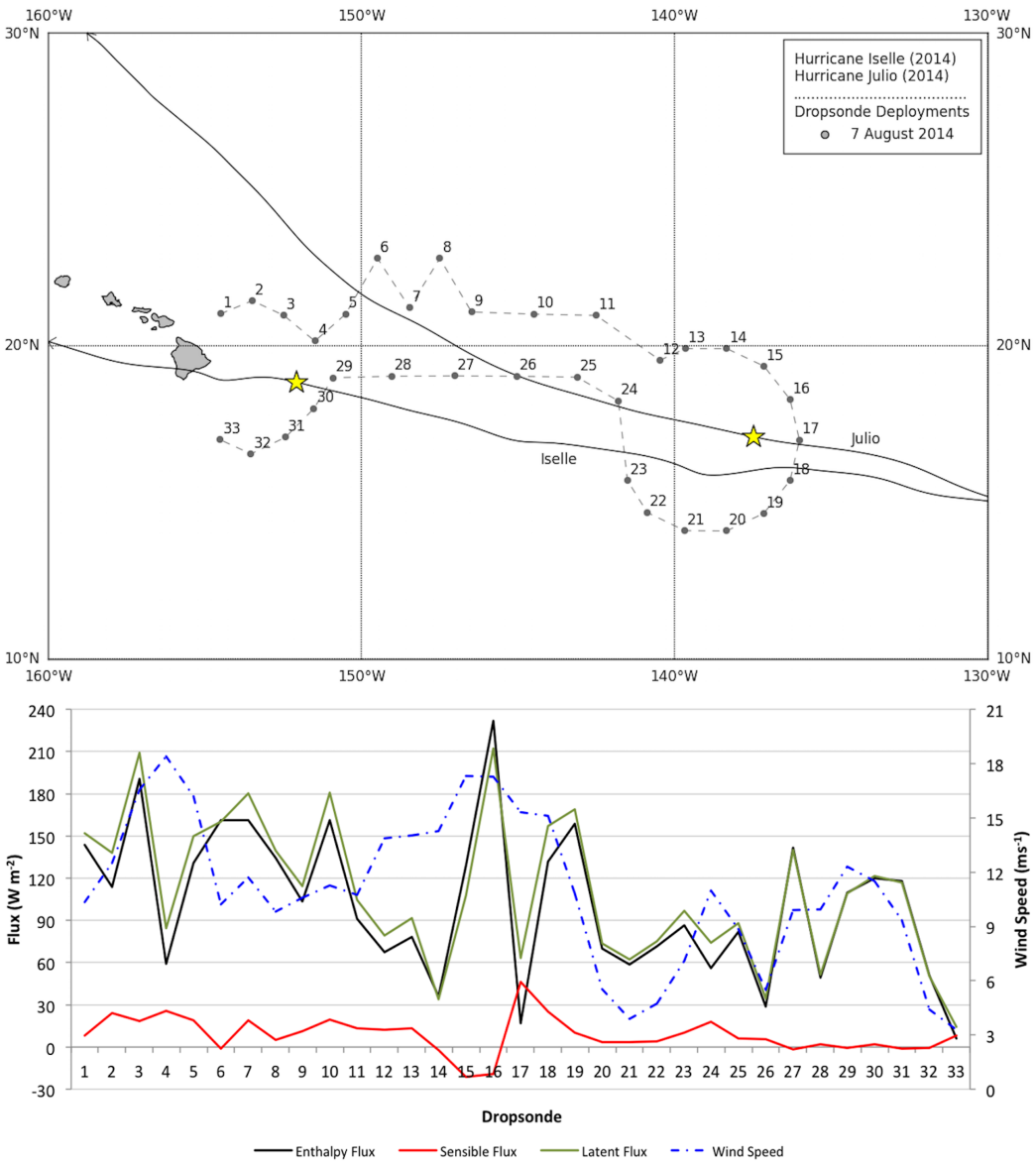

Figure 4.62: Sensible, latent, and enthalpy fluxes observed via dropsonde at 30 m on 7 August 2014 along the flight path for locations 1 – 33. Yellow star denotes approximate storm position at time of dropsonde deployment. Fluxes associated with Hurricane Iselle and Julio are labeled.

sonde was actually intended to measure Hurricane Julio (Figure 4.62). In fact, the 16th dropsonde fell almost directly onto Julio's track, revealing that the flux peaks observed were from Julio and not Iselle. This lends further evidence to the reasoning behind the dropsonde deployments well behind Iselle's position at that moment in time.

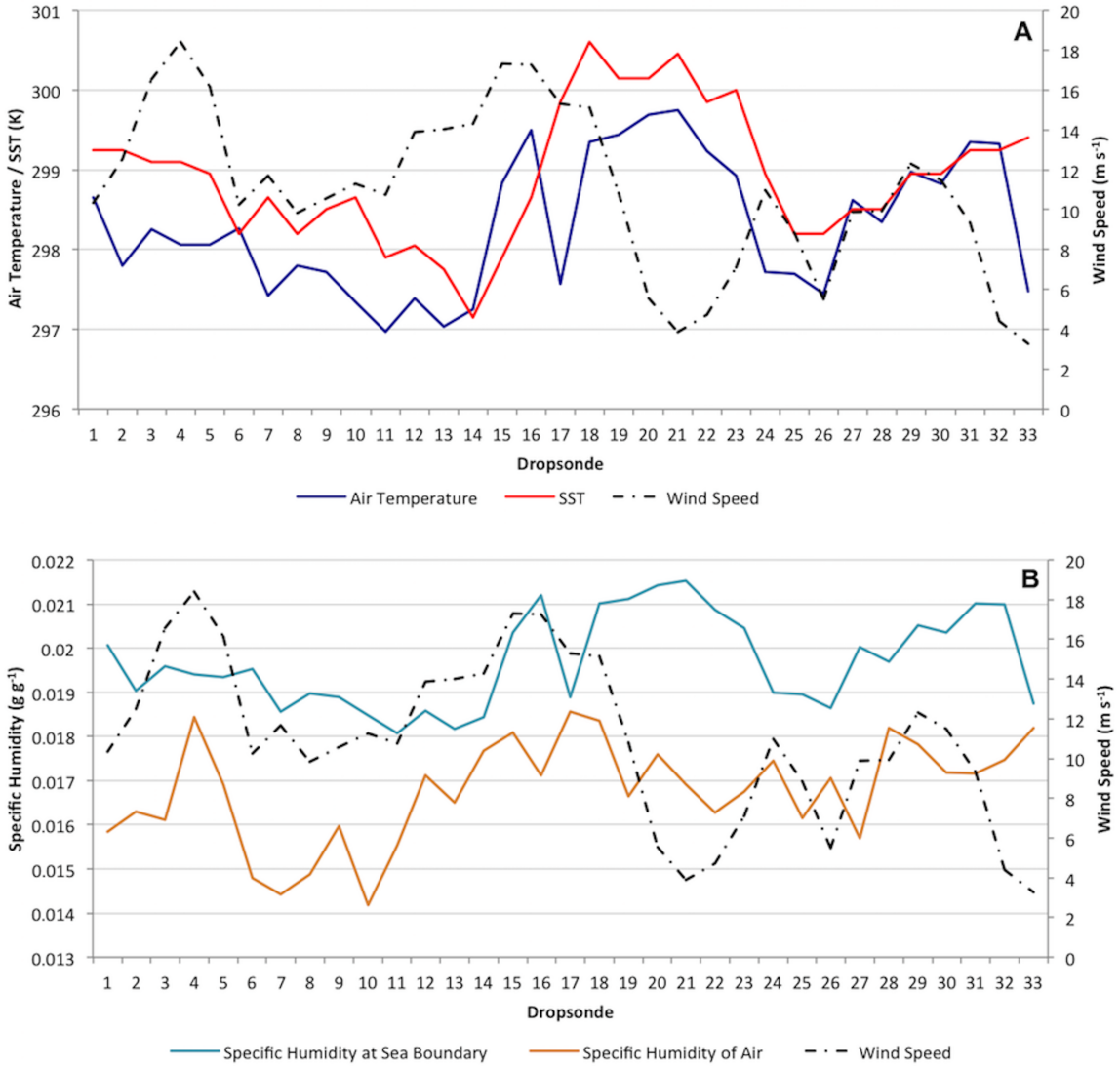

Figure 4.63: Dropsonde observation enthalpy method input parameters for sensible heat flux (A) and latent heat flux (B) on 7 August 2014 along the flight path for locations 1 – 33.

Latent heat flux were variable at those locations closest to Iselle's eye, dependent upon which quadrant was analyzed. To the immediate east of the eye, the 4th dropsonde observed a latent flux of 59 W m^{-2}, while wind speeds were high at 18.4 ms^{-1} and the moisture gradient diminished (Figure 4.63). South and southwest of the eye experienced latent fluxes between 109 and 120 W m^{-2}, respectively. At the 30th dropsonde location, a large 0.026 g g^{-1} moisture gradient existed. For Iselle, enthalpy fluxes ranged were 85 W m^{-2} at the 4th dropsonde and 122 W m^{-2} at the 30th dropsonde location. Variability in

enthalpy between 5th – 12th dropsondes and the 24th – 28th dropsondes may resulted from complex interactions between Iselle and Julio at that time, and are difficult to relate to an individual storm. For comparison to the model derived data, at 0000 UTC on 8 August, enthalpy flux values were 652 W m^{-2}, an 81% difference between the model data and the *in-situ* observations.

Lastly, a spatial visualization of dropsonde-derived enthalpy is illustrated in Figure 4.64, where locations are color shaded according to the corresponding enthalpy flux. In 4.64a, the highest enthalpy flux is located to the north and northeast of Iselle's position at that time. Interestingly, the lowest value of enthalpy flux is seen closer to the eye than the maximum flux values. To the north and northwest, enthalpy flux primarily remained below 150 W m^{-2} except for two locations with approximately 205 – 210 W m^{-2}. On 6 August, enthalpy fluxes diminished in intensity, with a maximum value of 220 W m^{-2} to the northeast of Iselle. Values to the west-northwest are considerably lower than the previous day, no higher than 75 W m^{-2}. At this time, Iselle no longer exhibited an annular structure, and the disparity between the left- and right-hand sides of the eye was detected in the enthalpy fluxes. Values on the left-hand side of the eye averaged 49 W m^{-2}, while on the stronger, right-hand side, average fluxes more than doubled to 117 W m^{-2} (Figure 4.64b). On the last day of deployments, two hurricanes were sampled. For Iselle, the highest enthalpy flux remained within the northeast quadrant, with 209 W m^{-2}. To the north-northwest, enthalpy fluxes averaged 82 W m^{-2}. Iselle made landfall on the Big Island of Hawaii the next day. For Julio, maximum enthalpy flux was also located within the northeast quadrant, with 212 W m^{-2}. However, Julio also exhibited relatively high enthalpy flux in locations immediately to the west-southwest, averaging 163 W m^{-2} (Figure 4.64c). Unlike Julio exhibited low enthalpy to the northeast and northwest ahead of the storm path, averaging 72 W m^{-2}. Enthalpy fluxes between these two powerful hurricanes may resulted from their interactions, and are difficult to relate to a particular storm.

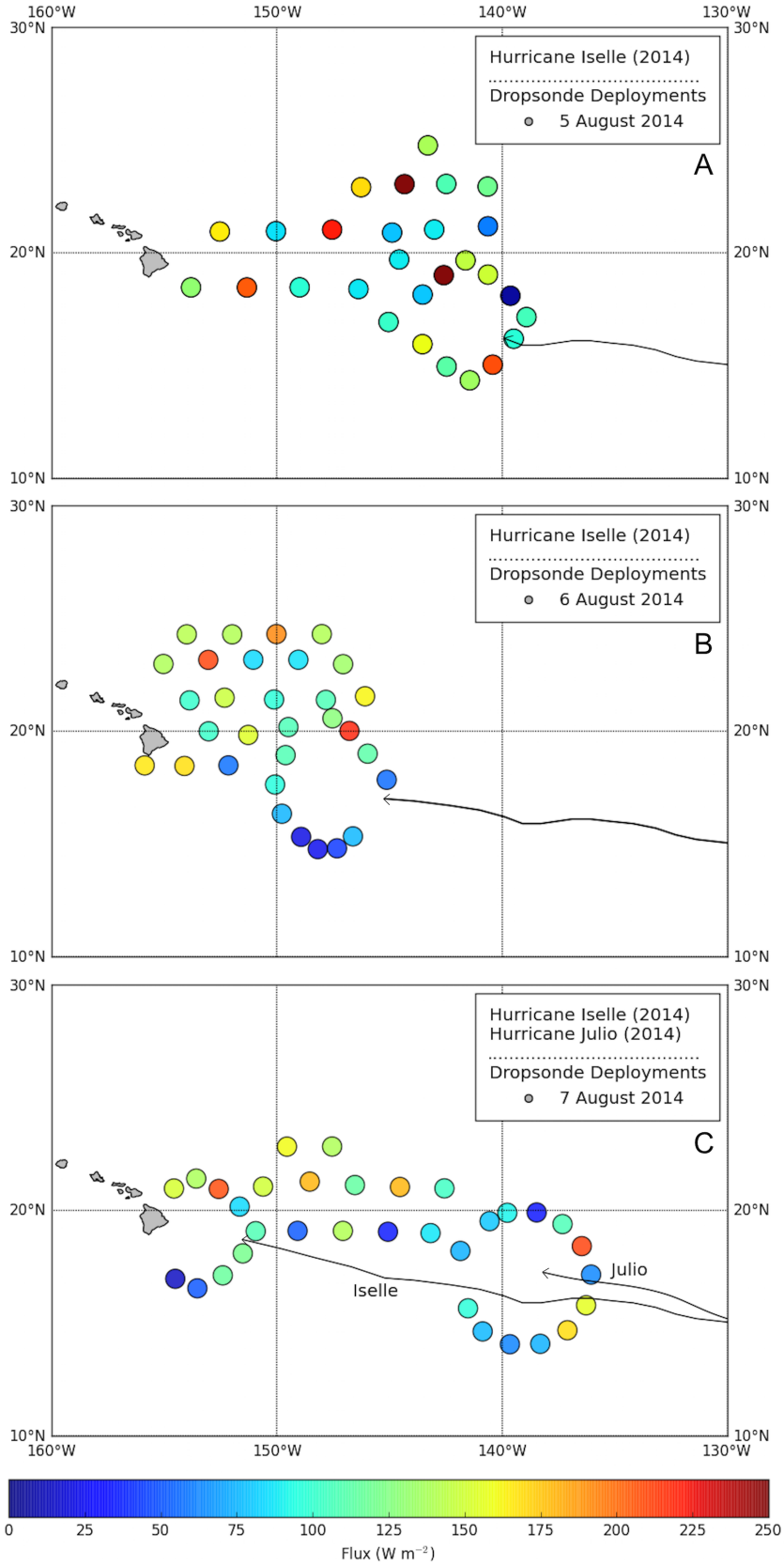

Figure 4.64: Dropsonde-derived enthalpy for 5 August (A), 6 August (B), and 7 August (C).

Chapter 5
Discussion

5.1 Along-Track Analyses

The aim of the along-track analyses were to assess the influence of anomalously high SSTs and corresponding UOHC upon the maximum wind speed and overall intensity of each major hurricane in the 2012 and 2014 NPO hurricane seasons. While atmospheric influences were not extensively utilized in the overall scope of this research, the synoptic history and atmospheric environment involved in the genesis, duration, intensification, and decay of each major hurricane was briefly discussed.

A few key observations were made from the along-track analyses. The first inference drawn from this analysis was the importance of UOHC throughout the TC lifecycle. The majority of the hurricanes studied experienced their highest UOHC at genesis, or shortly afterwards. While there appears to be no exact correlation between UOHC at genesis and the delay to attain maximum intensity, the inclusion of additional TCs may illuminate the relationship between the two factors. More likely, the delay to attain maximum intensity was a function of UOHC at genesis and sustained favorable SSTs and UOHC along-track, as well as translation speed and atmospheric factors. Based on the oceanic conditions summarized in Table 5.1, 30.2 kJ cm^{-2} was the lowest observed UOHC at genesis for a major hurricane in either season. Similarly, 28.2°C was the lowest observed SST at genesis, well above the favorable 26°C isotherm threshold, cited extensively in the literature. Thus, it is proposed that a 30 kJ cm^{-2} minimum UOHC requirement existed in the generation of NPO major hurricanes in 2012 and 2014. It was apparent that all of the major hurricanes formed in very high SSTs as well as UOHC. Throughout the along-track time series for each storm, a relationship was typically observed between declining SST/UOHC and subsequent intensity changes; however, the opposite positive trend was not. This may be due

to the fact that the highest UOHC values along-track was present at genesis and decreased along-track to the north and west. This tendency overwhelmed the regression analyses, which will be discussed later in this Chapter.

Second, there were several oceanic mesoscale features that appeared to be critical for either the formation or rapid intensification of TCs and were essentially undetectable in the along-track time series of SST and UOHC for those storms. This was especially evident for the quasi-stationary, deep WCE located in the vicinity of 14°N, 104°W for which UOHC ranged between 90 – 105 kJ cm^{-2} at its center. This specific WCE was detected to have in some way influenced Hurricanes Bud (2012), Daniel (2012), Cristina (2014), Marie (2014), Norbert (2014), and Odile (2014). The persistence of this WCE in both the 2012 and 2014 seasons indicated that this feature might be present year-round or annually recurring during the hurricane season. Whether this WCE is consistent on an annual basis or a unique feature of these seasons requires further analysis of UOHC data.

Table 5.1: Summary of Oceanic Conditions at Genesis.

Name	Genesis SST	Genesis UOHC	Delay to Max Intensity
Bud (20 – 26 May 2012)	29.7°C	50.5 kJ cm^{-2}	45 hr
Daniel (4 – 14 July 2012)	28.2°C	49.2 kJ cm^{-2}	82 hr
Emilia (7 – 18 July 2012)	28.9°C	30.2 kJ cm^{-2}	26 hr
Miriam (22 September – 2 October 2012)	29.9°C	67.1 kJ cm^{-2}	20 hr
Paul (13 – 18 October 2012)	28.9°C	52.2 kJ cm^{-2}	36 hr
Amanda (22 – 29 May 2014)	28.9°C	66.1 kJ cm^{-2}	-6 hr
Cristina (9 – 19 June 2014)	30.3°C	83.9 kJ cm^{-2}	78 hr
Genevieve (23 July – 7 August 2014)	28.9°C	45.8 kJ cm^{-2}	29 hr
Iselle (30 July – 9 August 2014)	28.7°C	61.5 kJ cm^{-2}	126 hr
Julio (2 – 18 July 2014)	28.4°C	31.7 kJ cm^{-2}	130 hr
Marie (22 August – 2 September 2014)	29.3°C	60.9 kJ cm^{-2}	46 hr
Norbert (2 – 11 September 2014)	30°C	76.0 kJ cm^{-2}	60 hr
Odile (9 – 18 September 2014)	29.6°C	75.6 kJ cm^{-2}	78 hr
Simon (30 September – 9 October 2014)	30°C	74.3 kJ cm^{-2}	94 hr

On the opposite spectrum from WCEs, cool wake CCEs were also present and observed to be potential influential factors in the trajectories of subsequent TCs. Like the WCEs, cool wake upwelling was not easily detectable within the along-track time series for that storm. However, this was not surprising as the original sampling procedure mandated a 4-day prior extraction of data, in order to prevent cool wake signature contamination. More often, if a second TC followed near or tracked across a SST gradient, the cool wake signature would be detectable within the subsequent TC along-track time series. It is recommended that a larger SST and UOHC area be sampled in addition to along-track data extraction for a more detailed assessment of the spatial extent of important oceanic mesoscale features. The inclusion of the radius of maximum winds, the radius of the outermost closed isobar, and/or the 30-, 50-, and 64-knot wind radii as a metric of hurricane size in the sampling technique may prove especially valuable.

As the along-track analyses failed to resolve large-scale oceanic mesoscale features it was decided to examine difference maps which compare 2014 to 2012 monthly UOHC values. For the purposes of future TC forecasting and analysis, the utilization of a UOHC anomaly map (derived from a climatological UOHC average product) and monitoring of UOHC anomalies may be more applicable. A UOHC anomaly dataset was not available during this research.

Figures 5.1 – 5.7 are the basin-wide averaged monthly differences of UOHC in 2014 compared with 2012 (2014 - 2012) for the NPO. For reference, the East NPO is defined as the region extending from the western coastline of North America to 140°W. The Central NPO ranges from 140°W to 180°, and the Western NPO encompasses the area west of 180°. The genesis position and tracks of the 2014 major hurricanes were overlain in their applicable months. Overall, the largest differences were observed west of 140°W. In May, a positive difference extended as far north as 20°N in the western portion of the Central

NPO (160°W – 180°; Figure 5.1). This positive UOHC difference was confirmed by a positive SST anomaly of 1 – 2°C in that region (Appendix Figure D.1). In subsequent months, positive UOHC differences moved northwards to encompass the Hawaiian Islands. By July, large positive differences extended to 30°N (Figure 5.3) and by August/September, as far north as 35°N (Figures 5.4 – 5.5). Interestingly, the SST anomaly maps for August through November (Appendix Figures D.4 – D.7) revealed a positive 1 – 2°C increase across the NPO at latitudes between 15 – 35°N, and not widespread below. This observation confirmed that while SSTs were consistently high below 15°N, temperatures at higher latitudes were regionally anomalous. The abnormally high UOHC in the Central NPO region likely led to the unusual tracks of Hurricanes Genevieve, Iselle, and Julio. Whilst TCs weaker than major hurricane status were not analyzed, atypical northern tracks were also observed for two minor TCs near Hawaii, Tropical Storm Wali and Hurricane Ana, both of which formed in the Central NPO. There was no unusual TC activity or trajectories in the Central NPO in 2012. In the East NPO in May, several pockets of weak <-15 kJ cm^{-2} UOHC were observed near 10°N, 90 – 120°W, indicating that these locations may have resulted from CCEs in the TC genesis region. Hurricane Amanda was an early start-of-season TC that remained within a fairly limited pool of positive UOHC difference (Figure 5.1).

In June, the region of very deep UOHC difference (20°N, 150°W – 180°) traveled 2 – 5° northwards, reaching the western boundary of the Hawaiian Islands (Figure 5.2). In the East NPO, positive UOHC differences continued to increase northwards by 1 – 2°, especially near the Baja California peninsula. A SST anomaly map for June (Appendix Figure D.2) confirmed a positive 1 – 2.5°C anomaly centered on the southern half of the peninsula. The sparse CCE pools seen in May (Figure 5.1) near the Gulf of Tehuantepec and TC genesis area diminished in quantity throughout June. Hurricane Cristina developed in mid-June, tracking over a positive UOHC difference of approximately 10 – 20 kJ cm^{-2} within the Baja California positive SST anomaly (Appendix Figure D.2) near 15°N, 100 –

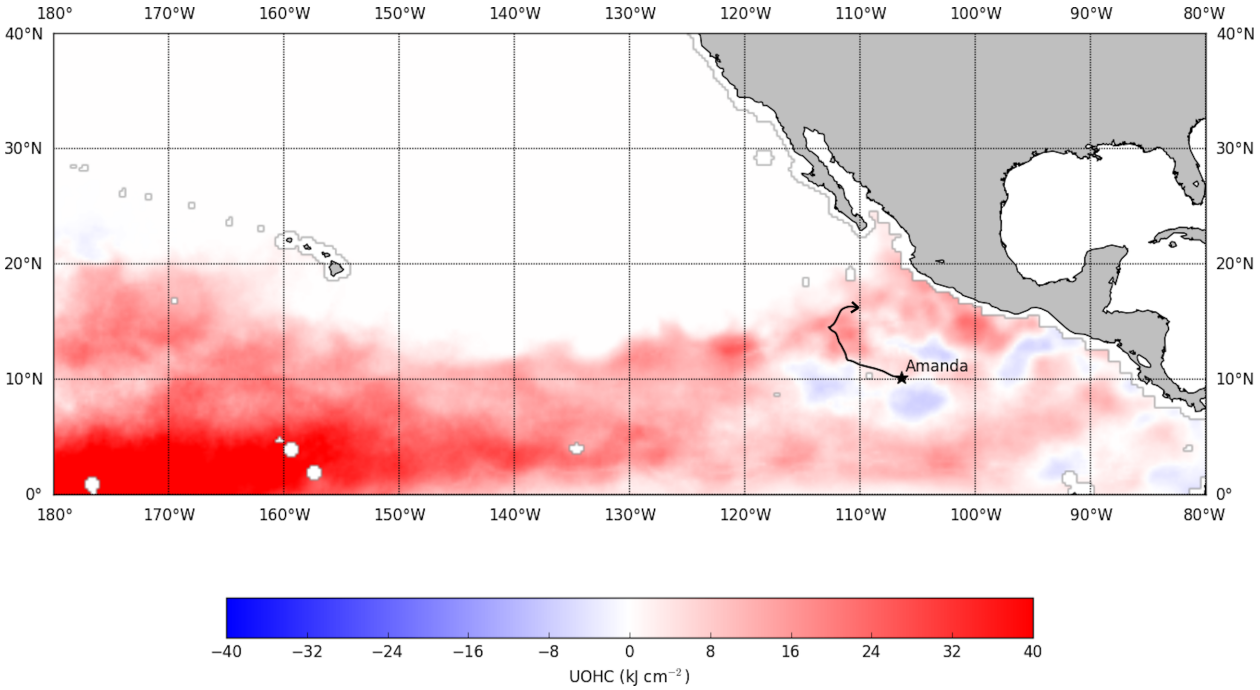

Figure 5.1: Monthly averaged UOHC difference between May 2014 – 2012. Genesis position (black star) and track of the May 2014 major hurricanes are overlain.

120°W before crossing into waters of neutral difference (Figure 5.2). While storm intensity is not depicted in Figure 5.2, once within the neutral difference UOHC region, Cristina weakened from a Category-1 hurricane to a remnant-low pressure system (see Figure 4.19).

By July, positive UOHC differences west of 155°W in the Central NPO extended as far north as 28 – 30°N, as well as along the windward (east) side of the Hawaiian Islands (Figure 5.3). Positive UOHC differences in the western portion of the East NPO (120 – 140°W) were observed to be as far north as 18 – 19°N. Pervasive throughout the eastern portion of the East NPO (90 – 120°W) was a dominant 1 – 3°C SST anomaly, with values exceeding a 3°C positive anomaly around the tip of the Baja California peninsula (Appendix Figure D.3). Long lived Hurricane Genevieve formed in late July near 120°W, and tracked westward across the large positive UOHC difference present from 120°W to 180°, dipping briefly near the large pool of very deep UOHC difference near 5°N, 155°W – 180° (>40 kJ cm^{-2}; Figure 5.3). Surprisingly, no positive SST anomaly consistently covered

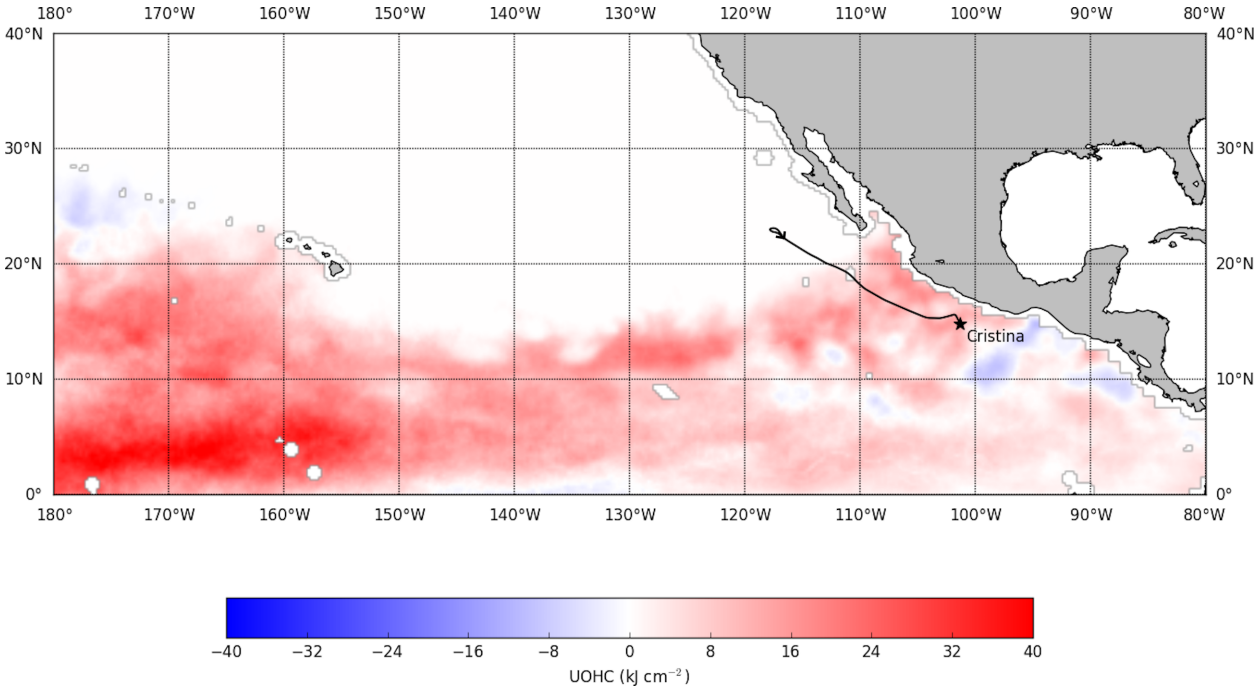

Figure 5.2: Monthly averaged UOHC difference between June 2014 – 2012. Genesis position (black star) and track of the June 2014 major hurricanes are overlain.

the area from 120°W to 180°, over which Genevieve tracked (Appendix Figure D.3). It would be interesting to visualize UOHC in the West NPO as well for Genevieve, as the TC further intensified after leaving the NPO. Hurricane Iselle also formed in late July near 11°N, 118°W, and tracked towards the boundary between positive UOHC difference and the neutral waters observed near 18°N (Figure 5.3).

By August, positive UOHC differences of 5 – 20 kJ cm^{-2} dominated near the Hawaiian Islands, and it is proposed that Iselle tracked as far north, and made landfall, due to the abnormal northern extent of high UOHC near 19°N, 155°W (Figure 5.4). Positive UOHC differences reached as far north as 35°N, 160 – 170°W in the Central NPO. A SST anomaly map for August revealed a positive 1 – 2°C anomaly for latitudes above 20°N and west of 150°W, confirming the unusual nature of the northern extent of high UOHC (Appendix Figure D.4). Hurricane Julio formed near 12°N, 111°W, but followed much the same trajectory as Iselle, before turning to the north-northwest. It was apparent that Julio also

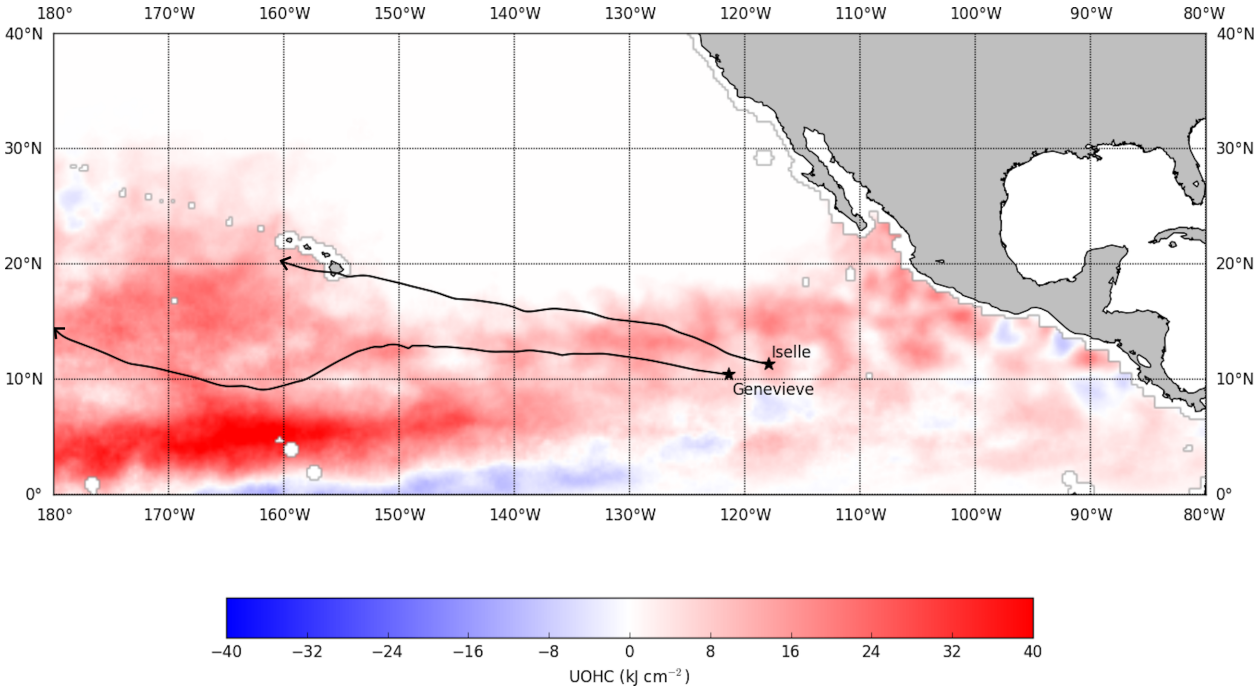

Figure 5.3: Monthly averaged UOHC difference between July 2014 – 2012. Genesis position (black star) and track of the July major hurricanes are overlain.

weakly followed the boundary between the positive UOHC differences and neutral waters near 20°N, 140 – 160°W (Figure 5.4). Also noted were several small weak CCEs directly beneath Genevieve's track. Although storm intensity was not included in Figure 5.4, the CCEs corresponded well to the frequent intensity oscillations that Genevieve experienced (see Figure 4.22). In the East NPO, positive UOHC difference of approximately 10 – 20 kJ cm^{-2} extended near 20°N and greater, surrounding the Baja California Peninsula. SST anomalies remained consistent around 1 – 2.5°C east of 120°W (Appendix Figure D.4). In late August, Hurricane Marie formed near 13°N 100°W and the beginning of the storm's extensive cool wake was evident with the development of a -10 kJ cm^{-2} CCE near the genesis position (Figure 5.4).

During September, high latitude positive UOHC differences in the Central NPO were seen to extend eastward towards 145°W, having thus completely encompassed the Hawaiian Islands (Figure 5.5). In the SST anomaly map for September, a positive 0.5 – 2°C anomaly

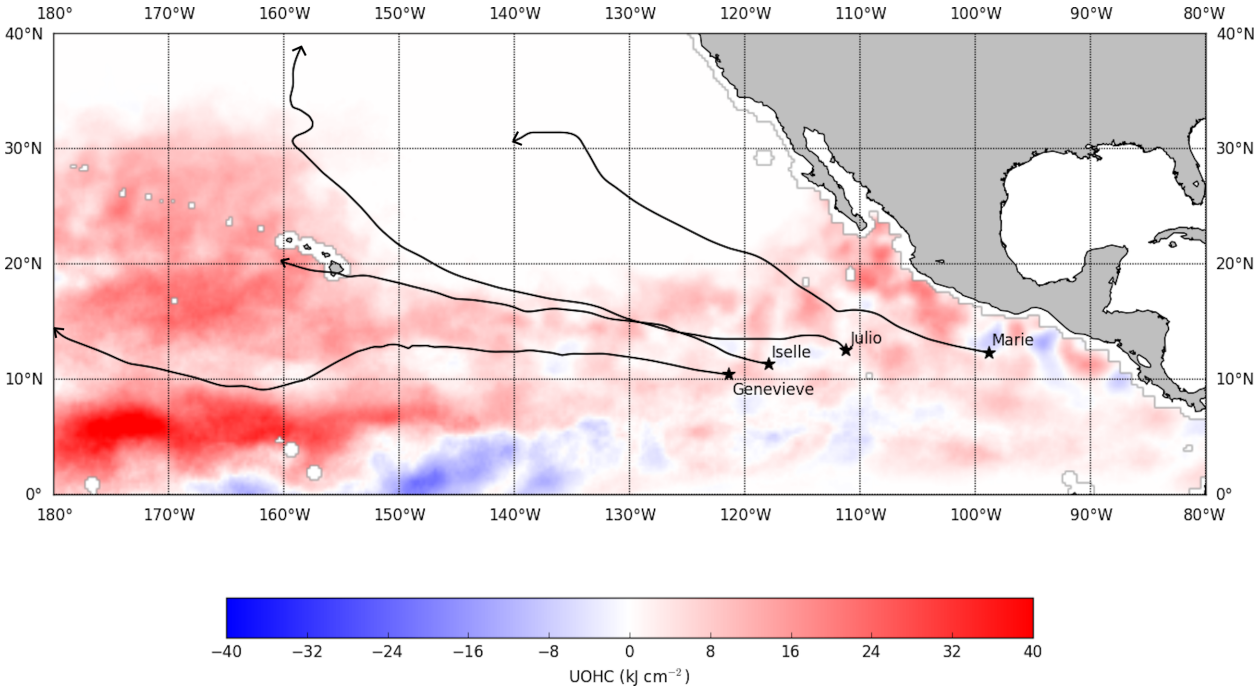

Figure 5.4: Monthly averaged UOHC difference between August 2014 – 2012. Genesis position (black star) and track of the August 2014 major hurricanes are overlain.

is revealed across the entire East and Central NPO at high latitudes above 20°N (Appendix Figure D.5). Of more interesting note, is the significant CCE cool wake signature of -5 – 20 kJ cm^{-2} observed along the Mexico coastline throughout the month. With the large spatial extent of Marie's cool wake near 15°N, 100 – 120°W, subsequent Hurricanes Norbert, Odile, and Simon were forced along north-northwest paths that aligned with the Baja California coastline (Figure 5.5). In the SST anomaly map, much of the positive SST anomaly observed in previous months (Appendix Figures D.3 – D.4) no longer remained, and even a slight -0.5°C anomaly was evident near 15°N, 110°W (Appendix Figure D.5). This weak negative anomaly corresponded very well with the location of Marie's cool wake CCE. The CCEs parallel to the Mexico mainland also corresponded extremely well with Odile's passage in September (Figure 5.5).

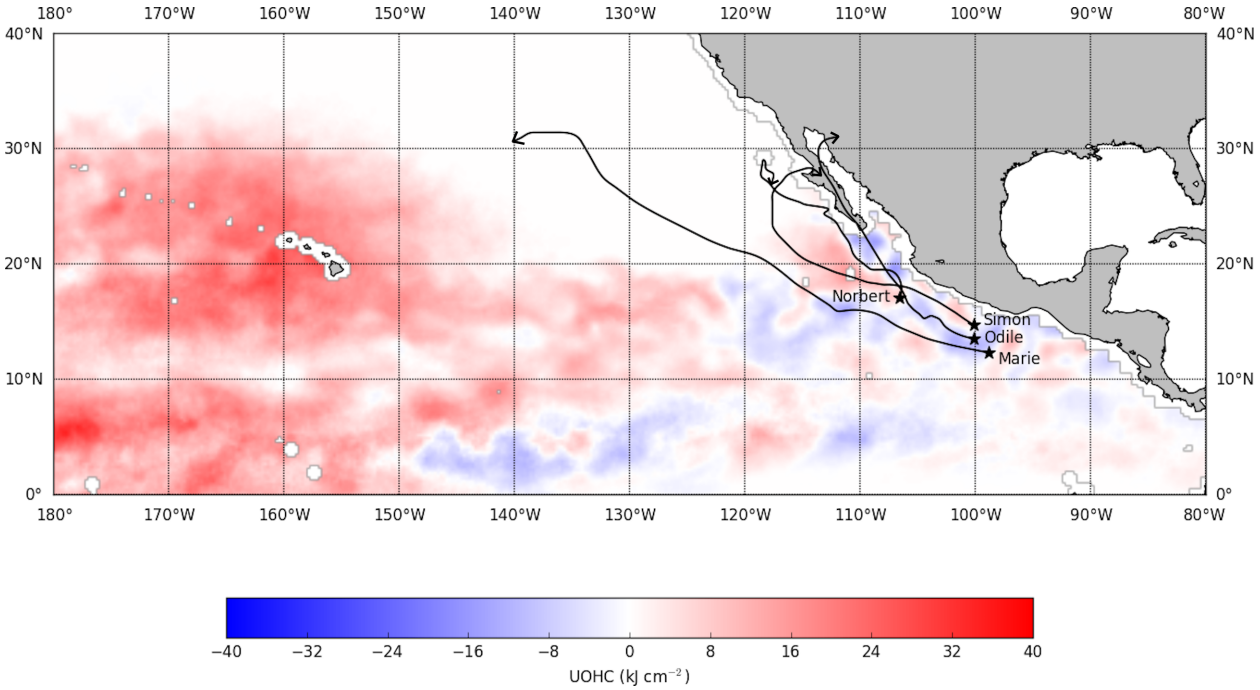

Figure 5.5: Monthly averaged UOHC difference between September 2014 – 2012. Genesis position (black star) and the track of the September 2014 major hurricanes are overlain.

By October, the positive UOHC differences in the Central NPO had retreated below 30°N, but continued to surround the Hawaiian Islands (Figure 5.6). SST anomalies in October revealed a 0.5 – 2°C anomaly extending southwards from high latitudes to ∼15°N (Appendix Figure D.6), indicating that the northern extent of high UOHC differences continued to be abnormal for this time of year. In the East NPO, positive UOHC differences still extended as far north as 19°N from 115°W to approximately 145°W. The CCEs along the Mexican coastline observed in September (Figure 5.5) had mostly diminished by October (Figure 5.6), except for a negative UOHC difference of -15 to -25 kJ cm^{-2} near the tip of the Baja California peninsula, a remnant feature of Hurricane Odile. Apparent in the SST anomaly maps for September and October (Appendix Figures D.5 – D.6) was a neutral SST anomaly near 20°N, 105°W that may correspond to the cool wake CCEs observed there in Figure 5.6.

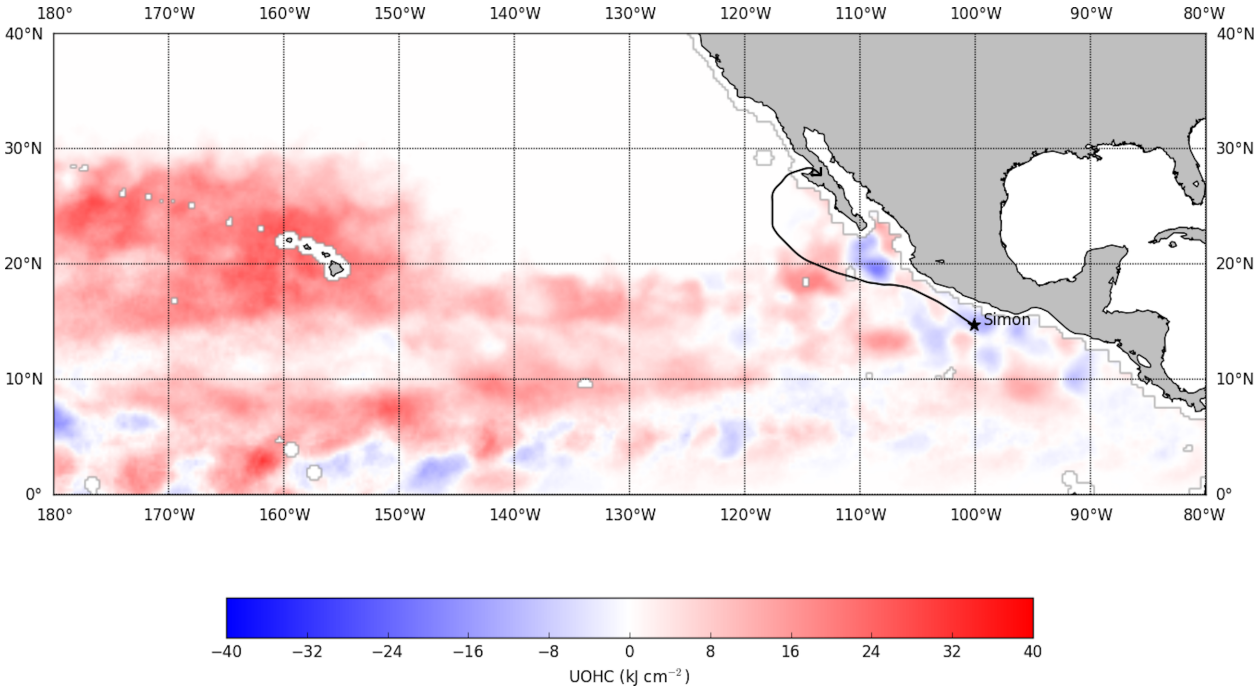

Figure 5.6: Monthly averaged UOHC difference between October 2014 and October 2012. Genesis position (black star) and track of the October 2014 major hurricanes are overlain.

By November, positive UOHC differences in the Central NPO had retreated to around 25°N, from 150°W – 180° (Figure 5.7). At the close of the official hurricane season, the Hawaiian Islands continued to be surrounded by abnormally high UOHC. A SST anomaly map for November revealed that much of the mid- to high-latitudes across the East and Central NPO remained within a positive 0.5 – 2°C anomaly (Appendix Figure D.7). Small pools of -5 to -15 kJ cm^{-2} UOHC differences persisted near the Mexican coastline (Figure 5.7). Odile's CCE cool wake signature was still observed near the tip of the Baja California peninsula. It is noted that throughout the hurricane season (Figures 5.1 – 5.7, Appendix Figures D.1 – D.7), no detectably high positive UOHC difference or SST anomaly was routinely observed near 14°N, 104°W, the presumed location of the very influential WCE in 2014. This observation lends evidence to the presence of an annually recurring quasi-stationary WCE at that location that may fuel intensification in both average and active seasons.

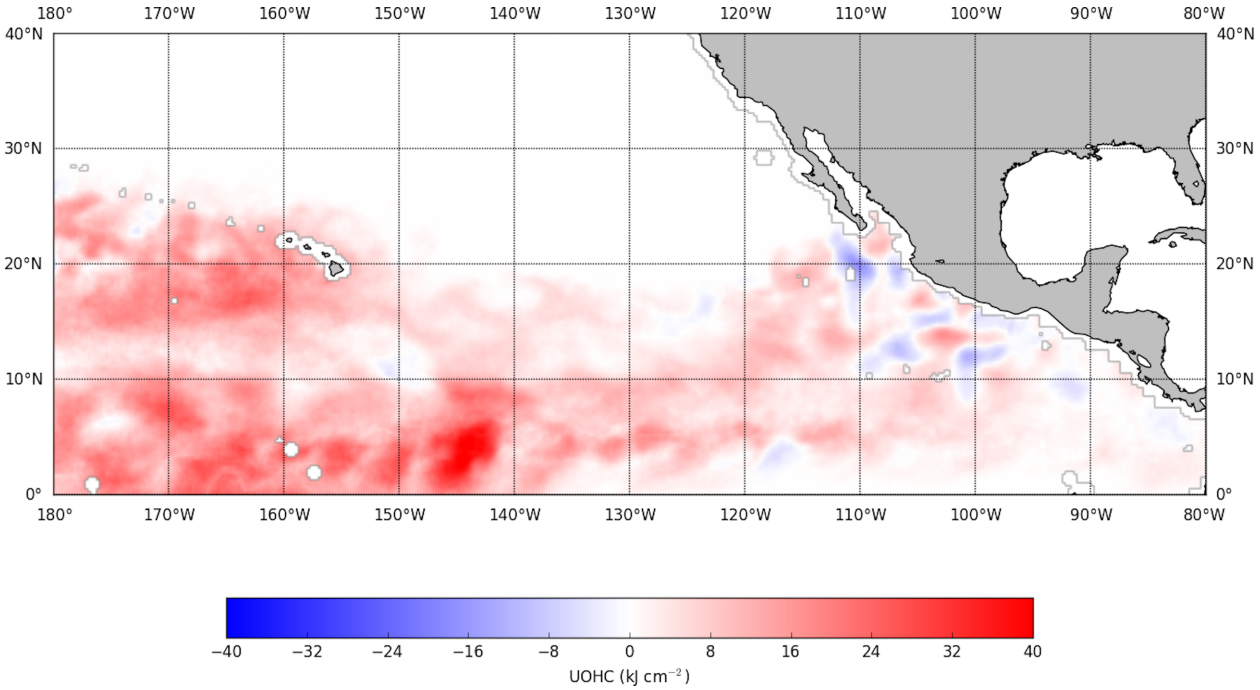

Figure 5.7: Monthly averaged UOHC difference between November 2014 – 2012.

Lastly, it is also interesting to note that many of the major hurricanes were generated from West African tropical waves that became convectively active in the NPO basin. Whether this was a normal triggering process for TC genesis in this basin or another unusual feature of the 2014 hurricane season is beyond the scope of this research.

5.2 Regression Analysis

Statistical regression models were employed to ascertain the explanatory power of various combinations of oceanic and environmental data upon variations in along-track wind speeds. SST and UOHC were separately analyzed for the major hurricanes season-wide and for 'combined' seasons, and were found to have somewhat variable explanatory power over along-track U_z variability. The utilization of an oceanic predictor (either SST or UOHC) in the season-wide models for 2012 revealed a dominant influence in estimating the explanatory power of along-track U_z variability. However, the season-wide models for 2014 performed very poorly and did not clarify a dominant oceanic influence. In addition to providing poor results, all season-wide regression models violated model assumptions, indi-

cating that a simple relationship between hurricane wind speeds and an oceanic predictor for the selected tracks were not revealed by the statistical tests used. In the multiple linear regression models, storm latitude and longitude (DeMaria and Kaplan, 1994; Hobgood, 1998; Petty and Hobgood, 2000), and translation speed were chosen for inclusion in the full oceanic models. The combination of multiple variables demonstrated more promising results than the previous simple linear models. However, these season-wide models also failed model assumptions, and little further use can be gained from these specific models. Storm-specific models were run on five major hurricanes that maintained wind speeds above 50 ms^{-1} for more than 30 observations. These models were designed to study the intensification phase of the storm duration (Hobgood, 1998). Several storm-specific models revealed adjusted R-squared values in excess of 0.8 and are described in more detail below. Latitude especially, has been shown to be a highly significant predictor for East NPO intensity variation (DeMaria and Kaplan, 1994; Hobgood, 1998). The results of several of the regression models supported this finding. Future work is recommended to investigate the weakening phase in the storm-specific models to ascertain model skill in comparison to the intensification regressions.

In many of the storm-specific models, either SST or UOHC influenced along-track wind speed variation far more dominantly than the other parameter, providing statistical evidence for the inclusion of both predictors in regression work. For Hurricane Amanda (2014), Regressions **13**, **14**, and supplemental models **23** – **27** were run. The full model runs performed very well, with adjusted R-squared values of 0.8425 (**13**) and 0.8514 (**14**). However, model residuals failed to meet the regression assumptions for all 6 models, and thus the statistical results for Amanda are considered fairly unreliable, despite relatively high adjusted R-squared values. Along-track SST for Amanda did not fluctuate beyond a 2°C range and UOHC demonstrated a stronger variability in values, but still failed to improve the model's explanatory power. In fact, despite limited variation, SST proved to

be more influential than UOHC in the full model runs. As Amanda did not travel very far in any direction, the reliability of along-track changes in latitude and longitude were poor. Both latitude and longitude resulted in high adjusted R-squared values above 0.8, but deemed unreliable due to non-normality. Translation speed was deemed a poor environmental predictor for Amanda, as along-track forward speed of the storm was fairly consistent at $1 - 3$ ms^{-1} for the majority of storm duration. The supplemental regression models illustrated the same trends mentioned in their separate models. In this manner, too little variability occurred in the explanatory predictors themselves to account for variation intensity.

For Hurricane Emilia (2012), Regressions **15**, **16**, and supplemental models **28** – **32** were run. The full model runs performed extremely well, with adjusted R-squared values of 0.9955 (**15**) and 0.996 (**16**). Q-Q plots of model residuals demonstrated mostly normal distributions, validating the model assumptions and providing credibility to results. Given the declining relationship observed between SST/UOHC and intensity in the along-track analyses, it was unsurprising that the oceanic predictors demonstrated negative influences over U_z. Whilst resulting in very high adjusted R-squared values, model residuals failed assumptions in the latitude-longitude supplemental models. Emilia did not track very far north-south, thus potentially skewing the reliability of these predictors.

For Hurricane Iselle, Regressions **17**, **18**, and supplemental models **33** – **37** were run. The full version models performed extremely well with adjusted R-squared values of 0.9937 (**17**) and 0.9946 (**18**). However, model residuals demonstrated non-normal distributions, rejecting regression assumptions. All of the supplemental models for Iselle failed to demonstrate normal distributions, violating regression assumptions and thus the reliability of results. SST and UOHC revealed nearly identical outputs, in which the amount of time Iselle tracked over <26°C SSTs likely skewed the UOHC significance. Despite a variable

3 – 9 ms^{-1} forward speed throughout storm duration, translation speed failed to capture along-track intensity variability. Thus, it is proposed that the full regression model parameters could best explain along-track U_z variability throughout Iselle. There may be other beneficial atmospheric predictors that would better resolve model accuracy. As wind shear was critical throughout both Iselle's intensification and decay stages, the inclusion of wind shear calculated from 200 – 850 mb may prove insightful.

For Hurricane Marie, regressions **19**, **20**, and supplemental models **38** – **42** were run. Like the Emilia and Iselle models, the Marie regressions also performed extremely well, with adjusted R- squared values of 0.9781 (**19**) and 0.9822 (**20**). However, the results for both models demonstrated strong non-normal distributions, violating model assumptions. The supplementary models for Marie all revealed non-normal distributions, thus invalidating their usefulness as separate regressions. Storm location parameters performed the best, which is unsurprising with Marie's long northwestward track, covering large distances both latitudinally and longitudinally. Translation speed throughout Marie oscillated between 3 – 7 ms^{-1} for the majority of the storm duration, before dropping to 1 – 2 ms^{-1} in the last 48-hours. It may be that translation speed was not consistent in variation, as in large changes between a moderate speed and a slow forward speed did not match well with U_z variability at those times. SST also did not vary with respect to changes in intensity (Figure 4.32), likely skewing the regression results as well. From these observations, it may be that the weakening stage in Marie would be better modeled and resolved than in the intensification stage, as Marie induced strong widespread upwelling along-track as seen in the daily UOHC subplots (Figure 4.33).

Lastly, for Hurricane Odile, regressions **21**, **22**, and supplemental models **43** – **47** were run. The full version regressions performed extremely well, with adjusted R-squared values of 0.9829 (**21**) and 0.9812 (**22**). Despite the high adjusted R-squared values, model resid-

uals were non-normally distributed, failing the model assumptions. In both models, the oceanic predictor demonstrated a negative influence over U_z variability, SST more so than UOHC. In the supplementary model runs, less trustworthiness was awarded to the explanatory predictors except UOHC. Surprisingly, Regression **44** for UOHC revealed a normal distribution that could explain nearly 46% of all variability in along-track U_z. Based on this information, it is believed that the full regression model that employed UOHC as the oceanic explanatory predictor was most beneficial to questions concerning Odile intensity variability.

The along-track analyses for individual storm cases revealed that the regression analyses did not reflect the true influence of oceanic SST and UOHC on TC intensity changes. Previous regression studies in the NPO have shown that SSTs (and thus, UOHC) decline the further north and west a TC travels (Hobgood, 1998; DeMaria and Kaplan, 1999; Petty and Hobgood, 2000). The along-track analysis clearly demonstrated that the highest SST and UOHC occurred in areas of TC genesis in the NPO, and the results of both analyses decreased with storm duration and motion away from genesis regions. The negative relationships between SST/UOHC and TC intensity were observed in the season-wide regressions and most of the storm-specific models. Because SSTs cool to the north and west in the NPO, the influence of latitude and longitude on wind speed intensity thus also decreased to the north and west. However, several regression models illustrated the opposite trend. The abnormal northern and western extent of high SSTs in 2014 may offer some explanation for this curiosity, as well as possible anomalous atmospheric conditions. More probable is unfavorable multi-collinearity between paired regression parameters as a culprit. A trend between storm translation speed and hurricane wind speeds was more difficult to identify. Research has shown that trajectories over shallow UOHC require a faster forward motion in order to maintain high intensity. In regions of deep UOHC, TCs need not travel as quickly to maintain strength (Lin et al., 2009; Mei et al., 2012). As translation speed did

not significantly contribute to the regression schemes, results may benefit from its removal from the multiple linear regression models.

The violation of normality was a major issue within the entire statistical regression scheme. Such issues may arise from non-normal distributions, as was clearly evident in all but 3 regressions, as well as from a violation of the linearity assumption. A log-linear transform of the most sensitive parameters and/or normalization of coefficients may resolve this particular issue. Additional testing for multicollinearity of paired variables may also address the mismatched coefficient and scatter plot slopes. The NPO regressions in Hobgood (1998) and Petty and Hobgood (2000) utilized intensity change over a 12-hour interval instead of actual hourly wind speed. The use of the rate of intensity change as a predictor can indicate a strengthening or weakening period, which may produce more reliable results for intensification phase regression work.

5.3 Enthalpy Analysis

In order to quantify heat and moisture transfer during a major hurricane, enthalpy fluxes were computed with two separate methods; an atmospheric model-derived enthalpy flux along-track for the entire duration of the storm, and an *in-situ* dropsonde observation-derived enthalpy flux during a specific temporal window prior to landfall. Hurricane Iselle was specifically chosen for analysis due to the availability of *in-situ* dropsonde deployments, an unusual intensity structure that allowed for a slow decay, and a rare landfall event.

The calculation of sensible, latent, and enthalpy fluxes during Iselle revealed some differences in the overall magnitude of those fluxes between the two methods employed. While based on atmospheric model data, the fluxes analyzed along-track corresponded well with previous enthalpy studies in the hurricane environment. The latent heat and enthalpy flux values calculated along-track were lower than those expected for a Category-4 hurricane,

but still remained within the reasonable range for maximum moisture exchange described by Cione and Uhlhorn (2003), Walker et al. (2014), and Pun et al. (2014). Values of sensible heat flux were deemed of the appropriate magnitude for a tropical cyclone (Cione and Uhlhorn, 2003). In fact, the model-derived enthalpy fluxes at wind speeds above 50 ms^{-1} aligned very well with the *in-situ* fluxes measured as a part of the CBLAST campaign (Bell et al., 2012). As the CBLAST experiments were the first to accurately quantify air-sea enthalpy at major hurricane wind speeds (Zhang et al., 2008; Bell et al., 2012), the along-track model derivation of enthalpy proved to be reasonably accurate and very valuable.

Unlike the model-derivation, the dropsonde enthalpy method provided less than clear results. Sensible, latent, and enthalpy fluxes via the dropsonde method captured a broad region of heat and moisture conditions not only close to the hurricane eye, but also in the near hurricane environment, especially in the northeastern and northern quadrants ahead of the storm path (Figure 4.64). During Iselle, the highest dropsonde-derived enthalpy fluxes were observed to the right of the track where the strongest winds were expected. In the weaker, left of the track quadrants, enthalpy fluxes were approximately an order of magnitude smaller (See Figures 4.58 – 4.63). There was one curiosity discovered during the dropsonde-derived enthalpy analysis; the matter of reduced hurricane wind speeds. Dropsonde observations of wind speeds at 10 and 30 m did not agree well with the maximum wind speeds reported by the NHC. In fact, dropsonde wind speeds at those heights were nearly half of the HURDAT2 reported maximum sustained wind speeds. This is likely because dropsondes measure instantaneous wind speeds as the instrument falls throughout the vertical atmospheric column, and not the 1-min sustained wind speeds that the NHC issues (Murnane, 2004). Previous GPS dropsonde studies have found that surface winds range between 63 – 73% of flight level winds, although the authors report that this is an underestimate, as observations were taken at some distance away from the location of max-

imum winds. More appropriately, the operational practice of the NHC is to scale the flight level winds to the surface (approximately 10 m), of which the maximum sustained winds are assumed to be 90% of flight level winds (Murnane, 2004). Cursory results of a dropsonde wind speed correction to the NHC reported maximum sustained wind speeds revealed far better agreement between the two methods, as much as an 18 – 38% improvement in the calculation of enthalpy fluxes for Iselle.

One major drawback to this particular method was the inability to calculate enthalpy flux along-track. Instead, enthalpy flux was computed along the flight path in which the dropsondes were released. It is critical to note that dropsondes were only deployed during the decay stage of Iselle's lifecycle, and not during the intensification phase or maximum intensity period. Thus, the two methods can not be reliably compared to one another, as only a single observation - if it was in close proximity to the track - can be compared at any one time.

Chapter 6
Summary and Conclusions

6.1 Summary and Conclusions

This research reported on a thorough quantitative approach to understanding the intensity of NPO major hurricanes during a normal, average activity season and an abnormal, above average activity season. Analyses throughout this work addressed several research objectives regarding the influence of anomalous sea surface temperatures (SSTs) and upper ocean heat content (UOHC), defined as the excess of heat above the 26°C isotherm. Through the use of basin-wide difference maps, SSTs and UOHC were found to be highly anomalous during the 2014 hurricane season (May – November). This was especially prudent for the Hawaiian Islands and the Central NPO, where an unprecedented 10 – 15° northern displacement of the 26°C isotherm was revealed. While smaller, a 1 – 5° northern displacement of the 26°C isotherm was also experienced in the East NPO.

SST anomaly maps throughout the 2014 hurricane season confirmed dominant positive anomalies of 0.5 – 3°C throughout the East and Central NPO. Early season SST anomalies were detected primarily in the Central NPO, west of Hawaii, and subsequently extended eastward across the NPO to Baja California at 20°N (Figures D.1 – D.7). May exhibited the highest UOHC in the East NPO near the Mexico coastline. In the Central NPO, the month of September demonstrated an abnormal northern extent of high UOHC north of the Hawaiian Islands and also north of 30°N. It is proposed that the unusual northern extent of SST and UOHC throughout the entire NPO basin promoted at least six unusual major hurricanes in 2014. Hurricanes Genevieve, Iselle, and Julio – which occurred concurrently – all experienced extended storm durations, tracking far west and north into the Central NPO. Genevieve crossed into the Western NPO, while Iselle and Julio endangered the Hawaiian Islands. Due to the long lasting deep cool wake upwelling signature of Hurricane

Marie, subsequent Hurricanes Norbert, Odile, and Simon each displayed active trajectories away from the coldest SST center of the cool wake, forcing close encounters and landfalls with the Baja California peninsula and Mexico mainland.

Through along-track time series analyses, it was found that many of the fourteen major hurricanes of the 2012 and 2014 seasons formed in regions of high values of UOHC. The data analyzed suggested a minimum UOHC threshold of 30 kJ cm^{-2} and 28.2°C SSTs at genesis. In addition to forming in high SST and UOHC environments, several storms were largely influenced by oceanic mesoscale features such as warm-core eddies (WCEs) and cool wake upwelling from previous hurricane passage. Specifically, Hurricanes Amanda (2014), Bud (2012), Cristina (2014), Daniel (2012), Marie (2014), Norbert (2014), and Odile (2014) interacted with significant WCEs that fueled rapid intensification periods. Several hurricanes produced significant upwelling along-track, leading to large-scale SST cooling and intensified cold-core eddies that appeared to have influenced the trajectory of subsequent tropical cyclones. Hurricane Marie, a strong Category-5 hurricane, produced a widespread ˜6°C cool wake that was visible in UOHC gridded fields for subsequent Hurricanes Norbert and Odile. Their tracks revealed that the large cool wake area was likely avoided as both hurricanes tracked to the east of this feature.

A complex scheme of simple and multiple linear regression models was developed that employed SST or UOHC, storm latitude, longitude, and translation speed as the explanatory variables of along-track maximum wind speeds (U_z), and thus hurricane intensity. The regression models indicated largely variable results, in which season-wide and 'combined' season simple and multiple linear regressions demonstrated inconsistent explanatory power for intensity variation. More promising results were found in several storm-specific intensification stage regressions. All ten storm-specific regression models demonstrated adjusted R-squared values above 0.8, indicating a very high explanatory power of the model param-

eters utilized. The full regression models for Hurricanes Emilia (2012) and Odile (2014) demonstrated the highest overall adjusted R-squared regression results, indicating that a combination of along-track SST or UOHC, storm latitude, longitude, and translation speed likely influenced the intensity response of the hurricane. Of the additional supplementary regression models, eleven exhibited adjusted R-squared values above 0.8, ten of which were the individual latitude and longitude regressions for each storm. Undeniably, the use of latitude and longitude within a storm-centric model in regression work for the NPO is essential (Hobgood, 1998; Petty and Hobgood, 2000). A negative correlation between SST (or UOHC) and hurricane wind speeds was established in the NPO, as tropical cyclones repeatedly formed in the highest SST and UOHC values, which declined with storm movement and cool wake upwelling. The remaining storm-specific regression models demonstrated less reliable results, and may benefit from additional atmospheric predictors or the removal of translation speed from the regression models.

The regulation of hurricane intensification from enthalpy fluxes, via sensible and latent heat, was calculated via two methods, along the TC track and along the Air Force Reserve reconnaissance dropsonde flight path. Along-track atmospheric model-derived computations revealed that a 1234 W m^{-2} maximum enthalpy flux occurred at the moment Hurricane Iselle (2014) attained Category-4 wind speeds. Values of enthalpy flux from this method corresponded very well to recent *in-situ* measurements of enthalpy flux for major hurricane wind speeds above 50 ms^{-1}. The dropsonde-derived along-flight path enthalpy flux indicated overall weaker fluxes of heat and moisture, but created a more comprehensive view of enthalpy fluxes throughout the broad scale hurricane environment, rather than just along-track of the hurricane eye. Fluxes derived from the dropsonde method were significantly underestimated due to the influence of low measurements of instantaneous wind speeds. The dropsonde-derived enthalpy flux values revealed more accurate results after a correction to the reported National Hurricane Center maximum 1-min sustained wind

speeds. While overall fluxes were lower than that expected for a Category-4 hurricane, values remained within the reasonable range for maximum thermodynamic exchange between the ocean and atmosphere during Iselle.

6.2 A Note on the 2015 Northeast Pacific Season

It is important to note that during the course of this research, the 2015 NPO hurricane season surpassed many of the records set by several of the 2014 major hurricanes. For example, the Central NPO generated an unprecedented number of tropical cyclones during the 2015 hurricane season. A total of eight tropical cyclones formed in the Central NPO region of influence, at least two of which strengthened to hurricane status. Hurricane Patricia (2015) rapidly intensified into the strongest Category-5 hurricane on record for the Western Hemisphere and made the strongest landfall in the history of Mexico. A quick glance at Patricia's track revealed that Patricia's location immediately prior to attaining maximum intensity was in close proximity to a substantial WCE whose location matched that of the quasi-stationary WCE that influenced Hurricanes Marie, Odile, and Norbert. However, without further analysis, this is just speculation. The number of total depressions, hurricanes, and major hurricanes in the very active 2015 season broke records set by the previous 2014 hurricane season.

6.3 Limitations and Future Research

While provided with a wealth of data, this research was limited by several factors. The most critical consideration was the inclusion of only one average and one very active hurricane season, of which, only the tropical cyclones that attained major hurricane status were studied. While the 2012 NPO hurricane season was considered an 'average' year for this research's purposes, another year may be considered a more ideal normal year by methods and indices not analyzed here. In other words, the 2012 NPO season may be slightly above average, and thus not a perfect comparison. For a full spectrum analysis, a below average

NPO hurricane season, or inactive year, could further illuminate the intricacies between SST, UOHC, and major hurricane intensity variability. The data in this study were analyzed with the highest spatial and temporal resolution currently available. The inclusion of more accurate atmospheric products than those provided by the Reanalysis-1 project would be highly beneficial, but are currently unavailable on the basin-wide scope that this research required. While briefly discussed in Chapter 2, this research did not fully explore the intricacies of a strong East NPO El Niño event that influenced the expansive extent of abnormally high SSTs, UOHC, and tropical cyclone quantity.

There are countless avenues for future research on the topic of hurricane intensity variability. Several hurricanes discussed in this research induced impressive cool wake upwelling signatures, which were shown to influence the trajectory of subsequent tropical cyclones. In the style of Walker et al. (2005), chlorophyll-a blooms may have occurred near these features. The use of non-parametric regressions and modeling to aid the development of improved hurricane forecasts could be fruitful, as well as the inclusion of additional atmospheric data to the analyses performed in this research. To name one, the implementation of radius of maximum winds within the regression analyses may result in additional insight in regards to hurricane intensity. For example, due to the large size of Hurricane Marie (2014), radius of maximum winds could potentially account for the spatial extent of post-storm cool wake upwelling. While infrequent, NPO tropical cyclones can and will continue to make devastating landfalls in populated regions along Central America. In addition to forecasters, researchers, meteorologists, and oceanographers, the natural hazards and emergency management community can also benefit from further investigations into these powerful storms. As one of the most isolated populations on the planet, the Hawaiian Islands present an entirely unique environment for the implementation of a weather ready nation.

References

Allard, R., 1984: *A Climatology of the Characteristics of Tropical Cyclones in the Northeast Pacific During the Period 1966-1980*. Master's thesis, Texas Tech University.

Amador, J., E. Alfaro, O. Lizano, and V. Magaña, 2006: Atmospheric forcing of the eastern tropical Pacific: A review. *Progress in Oceanography*, **69**, 101–142.

Avila, L., 2013: Hurricane Miriam (EP132012). Technical report, National Hurricane Center Tropical Cyclone Report.

— 2014: Hurricane Norbert (EP142014). Technical report, National Hurricane Center Tropical Cyclone Report.

Avila, L. and W. Hogsett, 2012: Hurricane Daniel (EP042012). Technical report, National Hurricane Center Tropical Cyclone Report.

Ballard, R., 2014a: Hurricane Iselle Discussion Number 31. Technical report, Central Pacific Hurricane Center, United States National Oceanic and Atmospheric Administration's National Weather Service.

— 2014b: Tropical Storm Iselle Discussion Number 35. Technical report, Central Pacific Hurricane Center, United States National Oceanic and Atmospheric Administration's National Weather Service.

Bell, M., M. Montgomery, and K. Emmanuel, 2012: Air-Sea Enthalpy and Momentum Exchange at Major Hurricane Wind Speeds Observed during CBLAST. *Journal of Atmospheric Science*, **69**, 3197–3222.

Berg, R., 2013: Hurricane Paul (EP162012). Technical report, National Hurricane Center Tropical Cyclone Report.

— 2015: 2014 Eastern Pacific Hurricane Season. Technical report, National Hurricane Center Annual Summary.

Beven, J., 2015: Hurricane Genevieve (EP072014). Technical report, National Hurricane Center Tropical Cyclone Report.

Birchard, T., 2014a: Tropical Storm Iselle Discussion Number 32. Technical report, Central Pacific Hurricane Center, United States National Oceanic and Atmospheric Administration's National Weather Service.

— 2014b: Tropical storm iselle discussion number 34. Technical report, Central Pacific Hurricane Center, United States National Oceanic and Atmospheric Administration's National Weather Service.

Birchard, T. and R. Ballard, 2014: Hurricane Iselle Discussion Number 22. Technical report, Central Pacific Hurricane Center, United States National Oceanic and Atmospheric Administration's National Weather Service.

Black, P., E. D'Asaro, W. Drennan, J. French, P. Niiler, T. Sanford, E. Terrill, E. Walsh, and J. Zhang, 2007: Air-sea exchange in hurricanes: Synthesis of Observations from the Coupled Boundary Layer Air-Sea Transfer Experiment. *Bulletin of the American Meteorological Society*, **88**, 357–374.

Blake, E., 2012: Hurricane Bud (EP022012). Technical report, National Hurricane Center Tropical Cyclone Report.

— 2014: Hurricane Cristina (EP032014). Technical report, National Hurricane Center Tropical Cyclone Report.

Boucheral, J., F.-F. Jin, I.-I. Lin, H.-C. Huang, and M. England, 2016: Different controls of tropical cyclone activity in the Eastern Pacific for two types of El Niño. *Geophysical Research Letters*, **43**, 1679–1686.

Camargo, S., A. Robertson, A. Barnston, and M. Ghil, 2008: Clustering of eastern North Pacific tropical cyclone tracks: ENSO and MJO effects. *Geochemistry, Geophysics, Geosystems*, **9**.

Cangialosi, J., 2012: Hurricane Emilia (EP052012). Technical report, National Hurricane Center Tropical Cyclone Report.

Cangialosi, J. and T. Kimberlain, 2015: Hurricane Odile (EP152014). Technical report, National Hurricane Center Tropical Cyclone Report.

Caron, L.-P., M. Boudreault, and S. Camargo, 2015: On the Variability and Predictability of Eastern Pacific Tropical Cyclone Activity. *Journal of Climate*, **28**, 9678–9696.

Chu, P.-S., 2004: *Hurricanes and Typhoons: Past, Present, and Future*, New York: Columbia University Press, chapter ENSO and tropical cyclone activity. 297–332.

Cione, J., 2015: The Relative Roles of the Ocean and Atmosphere as Revealed by Buoy Air-Sea Observations in Hurricanes. *Monthly Weather Review*, **143**, 904–913.

Cione, J., P. Black, and S. Houston, 2000: Surface Observations in the Hurricane Environment. *Monthly Weather Review*, 1550–1561.

Cione, J. and E. Uhlhorn, 2003: Sea surface temperature variability in hurricanes: Implications with respect to intensity change. *Monthly Weather Review*, **131**, 1783–1796.

Dare, R. and J. McBride, 2011: The Threshold Sea Surface Temperature Condition for Tropical Cyclogenesis. *Journal of Climate*, **24**, 4570–4576.

DeCosmo, J., K. Katsaros, S. Smith, R. Anderson, W. Oost, K. Bumke, and H. Chadwick, 1996: Air-sea exchange of water vapor and sensible heat: The Humidity Exchange Over the Sea (HEXOS) results. *Journal of Geophsyical Research*, **101**, 12001–12016.

DeMaria, M. and J. Kaplan, 1994: Sea surface temperature and the maximum intensity of Atlantic tropical cyclones. *Journal of Climate*, **7**, 1325–1334.

— 1999: An Updated Statistical Hurricane Intensity Prediction Scheme (SHIPS) for the Atlantic and Eastern North Pacific Basins. *Weather and Forecasting*, **14**, 326–337.

Donanldson, P., 2014: Post-Tropical Cyclone Iselle Advisory Number 37. Technical report, Central Pacific Hurricane Center, United States National Oceanic and Atmospheric Administration's National Weather Service.

Elsner, J. and T. Jagger, 2012: *Hurricane Climatology, A Modern Statistical Guide Using R*. Oxford University Press.

Emmanuel, K., 1988: The maximum intensity of hurricanes. *Journal of Atmospheric Science*, **45**, 1143–1155.

Farfán, L., 2012: *Experimental and Theoretical Advances in Fluid Dynamics*, Springer Berlin Heidelberg, chapter Eastern Pacific Tropical Cyclones and Their Impact Over Western Mexico. 135–148.

Fisher, E., 1958: Hurricanes and the Sea-Surface Temperature Field. *Journal of Meteorology*, **15**, 328–333.

Gentemann, C., T. Meissner, and F. Wentz, 2010: Accuracy of Satellite Sea Surface Temperatures at 7 and 11 GHz. *IEEE Transactions on Geoscience and Remote Sensing*, **48**, 1009–1018.

Goni, G., P. Black, J. Cione, J. Trinanes, L. Shay, M. Mainelli, and R. Cheney, 2002: Use of Satellite Altimetry to Identify Regions of Hurricane Intensification. *Seventh International Conference on Remote Sensing for Marine and Coastal Environments*.

Goni, G., M. DeMaria, J. Knaff, C. Sampson, I. Ginis, F. Bringas, A. Mavume, C. Lauer, I.-I. Lin, M. Ali, P. Sandery, S. Ramos-Puaraque, K. Kang, A. Mehra, E. Chasssignet, and G. Halliwell, 2009: Applications of satellite-derived ocean measurements to tropical cyclone intensity forecasting. *Oceanography*, 190–197.

Goni, G., J. Kamholz, S. Garzoli, and D. Olson, 1996: Dynamics of the Brazil-Malvinas Confluence based on inverted echo sounders and altimetry. *Journal of Geophysical Reseach: Oceans*, **101**, 16273–16289.

Goni, G. and J. Trinanes, 2003: Ocean thermal structure monitoring could aid in the intensity forecast of tropical cyclones. *EOS Transactions American Geophysical Union*, **83**, 573–578.

Gray, W., 1968: Global View of the Origin of Tropical Disturbances and Storms. *Monthly Weather Review*, **96**, 669–700.

Hobgood, J., 1998: The Effects of Climatological and Persistence Variables on the Intensities of Tropical Cyclones over the Eastern North Pacific Ocean. *Weather and Forecasting*, **13**, 632–639.

Holthuijsen, L., M. Powell, and J. Pietrzak, 2012: Wind and waves in extreme hurricanes. *Journal of Geophsyical Research*, **117**, 1–15.

Houston, S., 2014: Hurricane Iselle Forecasts/Advisory Number 25. Technical report, Central Pacific Hurricane Center, United States National Oceanic and Atmospheric Administration's National Weather Service.

Hsu, S., 1988: *Coastal Meteorology*. Associated Press.

Jaimes, B. and L. Shay, 2009: Mixed layer cooling in mesoscale oceanic eddies during Hurricanes Katrina and Rita. *Monthly Weather Review*, **137**, 4188–4207.

Jaimes, B., L. Shay, and E. Uhlhorn, 2015: Enthalpy and Momentum Fluxes during Hurricane Earl Relative to Underlying Ocean Features. *Monthly Weather Review*.

Jarrell, J., M. Mayfield, E. Rappaport, and C. Landsea, 2001: The Deadliest, Costliest, and Most Intense United States Hurricanes from 1900 to 2000 (and other frequently requested hurricane facts). Technical report, NOAA Technical Memorandum NWS TPC-3.

Jien, J., W. Gough, and K. Butler, 2015: The Influence of El Niño-Southern Oscillation on Tropical Cyclone Activity in the Eastern North Pacific Basin. *Journal of Climate*, **28**, 2459–2474.

Jin, F.-F., J. Boucheral, and I.-I. Lin, 2014: Eastern Pacific tropical cyclones intensified by El Niño delivery of subsurface ocean heat. *Nature*, **516**, 82–85.

Kalnay, E., M. Kanamitsu, R. Kistler, W. Collins, D. Deaven, L. Gandin, M. Iredell, S. Saha, G. White, J. Woollen, Y. Zhu, M. Chelliah, W. Ebisuzaki, W. Higigns, J. Janowiak, K. Mo, C. Ropelewski, J. Wang, A. Leetmaa, R. Reynolds, R. Jenne, and D. Joseph, 1996: The NCEP/NCAR 40-year reanalysis project. *Bulletin of the American Meteorological Society*, **77**, 437–470.

Kimberlain, T., 2016: Hurricane Iselle (EP092014). Technical report, National Hurricane Center Tropical Cyclone Report.

Knaff, J., J. Kossin, and M. DeMaria, 2003: Annular Hurricanes. *Weather and Forecasting*, **18**, 204–223.

Landsea, C. and J. Franklin, 2013: Atlantic Hurricane Database Uncertainty and Presentation of a New Database Format. *Monthly Weather Review*, **141**, 3576–3592.

Large, W. and S. Pond, 1982: Sensible and Latent Heat Flux Measurements over the Ocean. *Journal of Physical Oceanography*, **12**, 464–482.

Leipper, D. and D. Volgenau, 1972: Hurricane Heat Potential of the Gulf of Mexico. *Journal of Physical Oceanography*, **2**, 218–224.

Lin, I.-I., I.-F. Pun, and C.-C. Wu, 2009: Upper-Ocean Thermal Structure and the Western North Pacific Category 5 Typhoons. part II: Dependence on Translation Speed. *Monthly Weather Review*, **137**, 3744–3757.

Mainelli, M., M. DeMaria, L. Shay, and G. Goni, 2008: Application of oceanic heat content estimation to operational forecasting of recent Atlantic category 5 hurricanes. *Weather and Forecasting*, **23**, 3–16.

Mei, W., C. Pasquero, and F. Primeau, 2012: The effect of translation speed upon the intensity of tropical cyclones over the tropical ocean. *Geophysical Research Letters*, 1–6.

Molinari, J., D. Vollaro, S. Skubis, and M. Dickinson, 2000: Origins and mechanisms of eastern Pacific tropical cyclogenesis: A case study. *Monthly Weather Review*, **128**, 125–139.

Murnane, R., 2004: *The Importance of Best-Track Data for Understanding the Past, Present, and Future of Hurricanes and Typhoons*, Columbia University Press, chapter 9. 249–266.

Palmén, E., 1948: On the formation and structure of tropical cyclones. *Geophysica*, **3**, 26–38.

Pasch, R., 2014: 2012 Eastern North Pacific Hurricane Season. Technical report, National Hurricane Center Annual Summary.

Perlroth, I., 1967: Hurricane behavior as related to oceanographic environmental conditions. *Tellus*, **19**, 258–268.

Petty, K. and J. Hobgood, 2000: Improving Tropical Cyclone Intensity Guidance in the Eastern North Pacific. *Weather and Forecasting*, **15**, 233–244.

Powell, M., P. Vickery, and T. Reinhold, 2003: Reduced drag coefficients for high wind speeds in tropical cyclones. *Nature*, **422**, 279–283.

Price, J., 1981: Upper Ocean Response to a Hurricane. *Journal of Physical Oceanography*, **11**, 153–174.

Pun, I.-F., Y. Chang, I.-I. Lin, T. Tan, and R.-C. Lien, 2011: Typhoon-Ocean Interaction in the Western North Pacific Part 2. *Oceanography*, **24**, 32–41.

Pun, I.-F., I.-I. Lin, and D. Ko, 2014: New generation of satellite-derived ocean thermal structure for the western North Pacific typhoon intensity forecasting. *Oceanography*, **121**, 109–124.

Pun, I.-F., J. Price, and S. Jayne, 2016: Satellite-Derived Ocean Thermal Structure for the North Atlantic Hurricane Season. *Monthly Weather Review*, **144**, 877–896.

Shay, L. and J. Brewster, 2010: Oceanic Heat Content Variability in the Eastern Pacific Ocean for Hurricane Intensity Forecasting. *Monthly Weather Review*, **138**, 2110–2131.

Shay, L., G. Goni, and P. Black, 2000: Effects of a warm oceanic feature on Hurricane Opal. *Monthly Weather Review*, **128**, 1366–1383.

Stewart, S., 2014a: Hurricane Amanda (EP012014). Technical report, National Hurricane Center Tropical Cyclone Report.

— 2014b: Hurricane Simon (EP192014). Technical report, National Hurricane Center Tropical Cyclone Report.

Stewart, S. and C. Jacobson, 2016: Hurricane Julio (EP102014). Technical report, National Hurricane Center Tropical Cyclone Report.

Walker, N., R. Leben, and S. Balasubramanian, 2005: Hurricane-forced upwelling and chlorophyll a enhancement within cold-core cyclones in the Gulf of Mexico. *Geophysical Research Letters*, **32**.

Walker, N., R. Leben, C. Pilley, M. Shannon, D. Herndon, I.-F. Pun, I.-I. Lin, and C. Gentemann, 2014: Slow translation speed causes rapid collapse of northeast Pacific Hurricane Kenneth over cold core eddy. *Geophysical Research Letters*, **41**, 7595–7601.

Wang, C. and P. Fiedler, 2006: Enso variability and the eastern tropical Pacific: A review. *Progress in Oceanography*, **69**, 239–266.

Wentz, F., C. Gentemann, C. Smith, and D. Chelton, 2000: Satellite measurements of sea surface temperature through clouds. *Science*, **288**, 847–850.

Whitney, L. and J. Hobgood, 1997: The relationship between sea surface temperature and maximum intensities of tropical cyclones in the eastern North Pacific. *Journal of Climate*, **10**, 2921–2930.

Wilson, P., 1991: *Density Cascading: Implications to Carbonate Bank and Periplatform Sedimentation (Northern Bahamas and Southern Florida)*. Master's thesis, Louisiana State University.

Wroe, D. and G. Barnes, 2003: Inflow Layer Energetics of Hurricane Bonnie (1998) near Landfall. *Monthly Weather Review*, **131**, 1600–1612.

Wu, P. and P.-S. Chu, 2007: Characteristics of tropical cyclone activity over the eastern North Pacific: the extremely active 1992 and the inactive 1997. *Tellus*, **59A**, 444–454.

Zelinsky, D. and R. Pasch, 2015: Hurricane Marie (EP13014). Technical report, National Hurricane Center Tropical Cyclone Report.

Zhang, J., P. Black, J. French, and W. Drennan, 2008: First direct measurements of enthalpy flux in the hurricane boundary layer: The CBLAST results. *Geophysical Research Letters*, **35**, 1–4.

Appendix A
Validation of Sea Surface Temperature Data

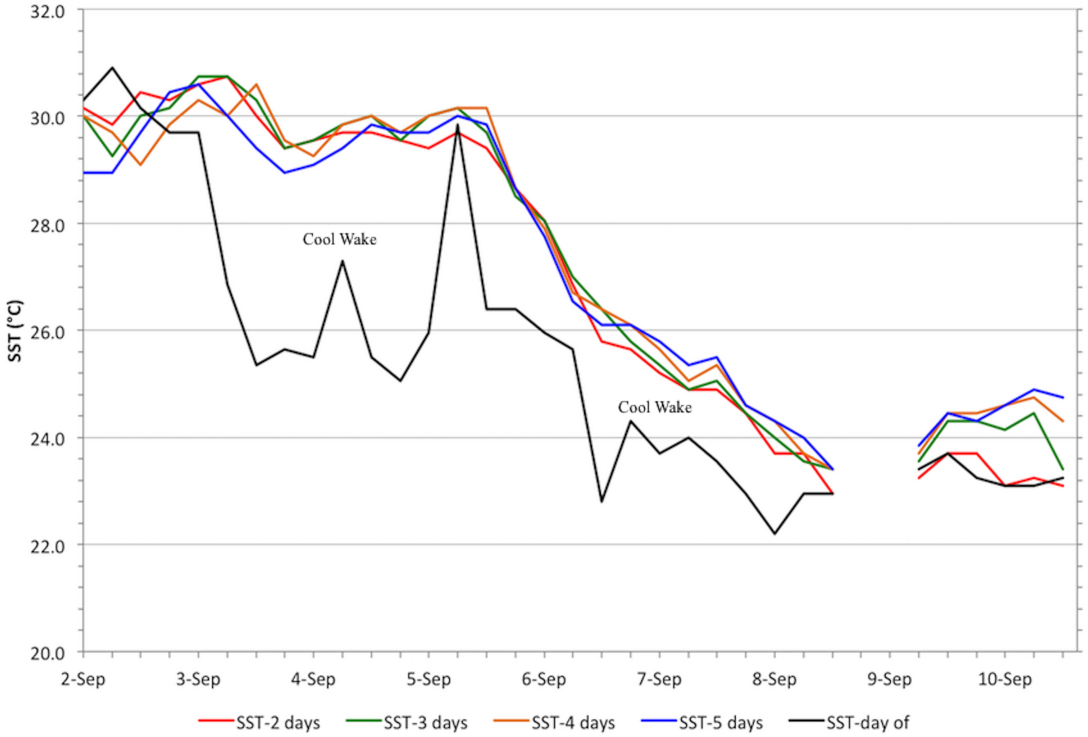

Figure A.1: Validation scheme of the SST dataset during Hurricane Norbert (2014).

Note: Missing values represent storm within 25 km of Isla Guadalupe, Mexico. An approximate 4°C cool wake signature is visible on 3 – 4 September 2014.

Appendix B
Empirical Enthalpy Flux Derivation

The derivation for along-track enthalpy flux via the bulk aerodynamics equations is as follows. Given air temperature (T_a) and hurricane minimum pressure (P), the density of air (ρ_a) can be derived with the Ideal Gas Law (Equation B.1) where R_d is the gas constant for dry air.

$$\rho_a = \frac{P}{R_d T_a} \tag{B.1}$$

Sensible heat flux (Q_H, Equation B.2) can then be solved for, provided SST, hurricane maximum wind speed (U_z), specific heat of air at constant pressure (C_p), and the Stanton exchange coefficient C_H estimated under hurricane strength wind speeds (DeCosmo et al., 1996; Black et al., 2007).

$$Q_H = C_p \rho_a U_z C_H (SST - T_a) \tag{B.2}$$

Next, saturation vapor pressure (e_s) is derived using the Clausius-Clapeyron Equation (Equation B.3), where e_0 is a constant, L_v is the latent heat of vaporization, R_v is the gas constant for moist air, and T_0 is an environmental temperature constant. Vapor pressure (e) can be calculated using the relative humidity relationship (Equation B.4).

$$e_s = e_0 * exp\Big(\Big(\frac{L_v}{R_v}\Big)\Big(\frac{1}{T_0} - \frac{1}{T_a}\Big)\Big) \tag{B.3}$$

$$RH = \frac{e}{e_s} 100\% \tag{B.4}$$

Following similar methods to Hsu (1988) and Wilson (1991), specific humidity for air at 10 m (q_a) is calculated using Equation B.5, where ϵ is the ratio of dry to moist gas constants (R_d / R_v). Similarly, specific humidity at the air-sea surface boundary (q_s, Equation B.6) is solved using a correction factor to account for differences between pure water and seawater (Hsu, 1988).

$$q_a = \epsilon \frac{e}{P} \tag{B.5}$$

$$q_s = 0.98 * \epsilon \frac{e_s}{P} \tag{B.6}$$

Latent heat flux (Q_E, Equation B.7) is calculated with the Dalton exchange coefficient C_E estimated under hurricane strength wind speeds. For these calculations, the Stanton and Dalton exchange coefficients were taken as constant, $C_E = C_H = 1.12x10^{-3}$ (Powell et al., 2003; Black et al., 2007).

$$Q_E = L_v \rho_a U_z C_E (q_s - q_a) \tag{B.7}$$

Lastly, enthalpy flux (Equation B.8) is the addition of sensible heat flux and latent heat flux.

$$Enthalpy = Q_H + Q_E \tag{B.8}$$

Appendix C
Supplemental Regression Analysis

While this research has focused on the importance of SST and UOHC in tropical cyclone intensity variation, it became evident from the regression model results of Section 4.2 that additional linear regression models highlighting the specific influence of storm latitude, longitude, SST, UOHC, and translation speed were needed. The following supplemental models were a series of intensification phase storm-specific simple linear regressions each for SST, UOHC, latitude, longitude, and translation speed. Results from the primary models were reproduced below in Table C.1 and each of the supplemental model results were included in Table C.2.

C.1 Amanda Supplemental Regressions 23 – 27

Regression **23** was a simple linear regression model that utilized SST as an explanatory predictor for U_z variability for Hurricane Amanda (2014). SST proved to be a very significant predictor, with a p-value of <0.001. The model performed somewhat well with an adjusted R-square value of 0.4378, revealing that nearly 44% of along-track U_z variation could be explained by SST. However, this model demonstrated non-normally distributed residuals with several outliers and skewed tails in the data, violating model assumptions. Rejection of the null hypothesis of normality was confirmed with the Shapiro-Wilks test, with a W-value of 0.923 and p-value of <0.001.

Regression **24** was a similar simple linear regression model to **23** in that UOHC was used as an explanatory predictor in SST's place. The oceanic predictor also proved to be highly significant with a p-value of <0.001. However, this model did not perform as well as its SST counterpart, with an adjusted R-squared value of 0.2076. Such results indicate that only 21% of along-track variability could be explained by UOHC. Model residuals

were also non-normally distributed, with several outliers and skewed tails. The normality test revealed a W-value of 0.897 and p-value of <0.001. With these results, the model assumptions were not met and should be treated with caution.

Regression **25** was a simple linear regression model that used translation speed as an explanatory predictor for U_z variability in Hurricane Amanda. The model indicated that translation speed was very significant with a p-value of <0.001. Regression **25** performed poorly with an adjusted R-squared value of 0.1951, indicating that approximately 20% of U_z variability in Amanda could be explained by translation speed. Model residuals were weakly normally distributed with a skewed left tail. The Shapiro-Wilks test rejected normality with a W-value of 0.935 and p-value of <0.001. Low explanatory power was expected as Amanda maintained a relatively constant translation speed.

Regression **26** was a simple linear regression model run for Amanda that incorporated storm latitude as the sole explanatory predictor for U_z variability. The model revealed that latitude was a highly significant parameter with p-value of <0.001. Regression **26** performed well with an adjusted R-squared value of 0.8271, indicating that storm latitude and longitude could account for approximately 83% of variability in Amanda's intensity. However, these results should be treated with extreme caution as plotted model residuals revealed a strong non-normal distribution, with skewed tails, thus violating the model assumptions. The Shapiro-Wilks test confirmed a non-normal distribution with a W-value of 0.888 and p-value of <0.001.

Regression **27** was a simple linear regression model that complemented Regression **26** by the inclusion of longitude in latitude's place. The two variables, while highly coupled, were run separately in order to determine their individual influences on U_z variability. The model revealed longitude to also be a highly significant parameter with a p-value of <0.001.

Regression **27** performed very well with an adjusted R-squared of 0.8406. Compared to the latitude model for Amanda, longitude could explain 2% greater variability in the along-track intensity variation. However, like the latitude regression, Regression **27** exhibited strong non-normality with a significantly skewed left tail and outliers. A normality test indicated a W-value of 0.844 and p-value of <0.001, confirming a lack of normality in the longitude model for Amanda. The supplemental model results revealed that the full combination of predictors in Regression **13** and **14** were the most useful in gleaning explanatory information about Amanda's intensity variation.

C.2 Emilia Supplemental Regressions 28 – 32

Regression **28** was a simple linear regression model for Hurricane Emilia in which SST was the explanatory predictor. SST was revealed to be a highly significant predictor with a p-value of <0.001. The model performed very well, with an adjusted R-squared value of 0.8156, indicating that over 81% of along-track U_z variation could be explained by SST. Model residuals were revealed a weakly normal distribution, however with a few outliers and a slightly skewed right tail. The Shapiro-Wilks normality test revealed that the null hypothesis was rejected, with a W-value of 0.952 and p-value of 0.007.

Regression **29** was a simple linear regression model for Hurricane Emilia that incorporated UOHC as the oceanic explanatory predictor. UOHC also proved to be a highly significant predictor, with a p-value of <0.001. This model did not perform as well as its SST counterpart. The adjusted R-squared value was 0.5869, and plotted residuals revealed a somewhat normal distribution with a few outliers and a skewed left tail in the data. A normality test indicated a non-normal distribution with a W-value of 0.961 and p-value of 0.02. Thus, these results should be interpreted with caution when comparing SST and UOHC influence over U_z in Emilia.

Regression **30** was a simple linear regression model for Hurricane Emilia that employed translation speed as the explanatory predictor. The model indicated that translation speed was a highly significant parameter, with a p-value of <0.001. Regression **30** performed well, with an adjusted R-squared value of 0.7386, indicating that approximately 74% of variability in U_z could be explained by Emilia's translation speed. Plotted residuals revealed a non-normal distribution, with slightly skewed tails. A Shapiro-Wilks normality test resulted in a W-value of 0.952 and p-value of 0.007.

Regression **31** was a simple linear regression model that utilized latitude as the explanatory predictor. Latitude was found to be a highly significant parameter with a p-value of <0.001. Regression **31** performed extremely well, with an adjusted R-squared value of 0.9695. However, plotted residuals revealed a weakly normal distribution, with a skewed right tail in the data. A Shapiro-Wilks normality test confirmed a non-normal distribution with a W-value of 0.951 and p-value of 0.006. Thus, latitude should be treated with caution in analyzing along-track variability in Emilia.

Regression **32** was a simple linear regression model for Emilia that incorporated longitude as the explanatory predictor. Like latitude, longitude also proved to be a highly significant model parameter, with a p-value of <0.001. The model did not perform as well as its latitude counterpart, resulting in an adjusted R-squared value of 0.8955. A Q-Q plot of the model residuals revealed a strongly skewed non-normal distribution, which the Shapiro-Wilks normality test confirmed with a W-value of 0.936 and p-value of 0.001. When Regressions **28** – **32** were analyzed in addition to Regressions **15** and **16**, it was revealed that storm position and translation Due to Emilia's long meridional track, the importance of latitude and longitude as explanatory predictors was unsurprising in the model results.

C.3 Iselle Supplemental Regressions 33 – 37

Regression **33** was a simple linear regression model for Hurricane Iselle that utilized SST as an oceanic explanatory predictor. SST proved to be a highly significant predictor, with a p-value of <0.001. This model performed well, with an adjusted R-squared value of 0.6242, revealing that approximately 62% of U_z variation could be explained. However, this model demonstrated a highly non-normal distribution with highly skewed left and right tails. A normality test confirmed the non-normal distribution with a W-value of 0.898 and p-value of <0.001. Thus, these results are not reliable as they violated model assumptions.

Regression **34** was a simple linear regression model for Hurricane Iselle that employed UOHC in SSTs place as an explanatory predictor. The predictor was shown to be highly significant, with a p-value of <0.001. Similar to the SST model, this model also performed well, with an adjusted R-squared value 0.6210. Unfortunately, this model also revealed a highly non-normal distribution with strongly skewed tails in the data. The Shapiro-Wilks normality test resulted in a W-value of 0.934 and p-value of <0.001, rejecting normality. These results were unsurprising as the SST model also failed to be useful, most likely as Iselle tracked predominately parallel to the 26°C isotherm throughout its lifecycle.

Regression **35** was a simple linear regression model for Hurricane Iselle that used translation speed as the explanatory predictor. The model indicated that translation speed was a somewhat significant parameter with a p-value of 0.002. Regression **35** performed poorly, with an adjusted R-squared value of 0.0693, revealing that approximately 7% of along-track U_z variation could be explained by Iselle's varying translation speed. These results violated model assumptions as plotted residuals revealed a non-normal distribution with skewed tails. A Shapiro-Wilks test resulted in a W-value of 0.941 and p-value of <0.001, confirming a non-normal distribution.

Regression **36** was a simple linear regression model that employed latitude as the sole explanatory predictor. Latitude was found to be a highly significant parameter, with a p-value of <0.001. Regression **36** performed extremely well with an adjusted R-squared value of 0.9584. However, a Q-Q plot of model residuals revealed a non-normal distribution with long skewed tails. A normality test confirmed these findings, with a W-value of 0.961 and p-value of 0.002, thus violating model assumptions.

Regression **37** was a simple linear regression model that complemented Regression **36** by the inclusion of longitude in latitude's place. The model revealed longitude to also be a highly significant parameter with a p-value of <0.001. Regression **37** performed extremely well with an adjusted R-squared of 0.9872. Compared to the latitude model, longitude could explain 3% greater variability in the along-track intensity variation. However, like the latitude regression, Regression **37** exhibited strong non-normality with a significantly skewed right tail. A normality test indicated a W-value of 0.935 and p-value of <0.001, confirming a lack of normality in the longitude model for Iselle. When considering the results from Regressions **33** – **37** with the full model runs in Regressions **17** and **18**, it is suggested that the oceanic predictor, either SST or UOHC, latitude and longitude, in addition to additional predictors could provide further explanatory evidence for along-track U_z variation in Iselle.

C.4 Marie Supplemental Regressions 38 – 42

Regression **38** was a simple linear regression model for Hurricane Marie (2014) that employed SST as an explanatory predictor. SST was not a significant predictor in this model, with a p-value of 0.29. Thus, model results are expected to also not be promising. This model performed extremely poorly, with an adjusted R-squared value of 0.0283. Model residuals were non-normally distributed with a significantly skewed long right tail.

A normality test revealed a W-value of 0.933 and p-value of 0.001, confirming a rejection of the normality hypothesis. As model assumptions failed, these results do not add any usefulness to the model scheme.

Regression **39** was a simple linear regression model for Hurricane Marie that incorporated UOHC in place of SST as the oceanic explanatory predictor. Surprisingly, UOHC proved to be a very significant predictor, with a p-value of <0.001. The model performed much better than its SST counterpart, with an adjusted R-squared value of 0.2081. However, model residuals were again non-normally distributed, with several outliers and a significantly skewed left tail in the data. A Shapiro-Wilks normality test revealed a W-value of 0.922 and p-value of <0.001, thus violating model assumptions.

Regression **40** was a simple linear regression model for Hurricane Marie that utilized translation speed as the explanatory predictor. The model revealed that translation speed was a somewhat significant parameter, with a p-value of 0.002. Regression **40** performed poorly with an adjusted R-squared value of 0.1175, indicating that less than 12% of along-track variability in U_z could be explained by translation speed. A plot of model residuals revealed a highly non-normal distribution with a long skewed left tail in the data, violating model assumptions. A Shapiro-Wilks test confirmed a non-normal distribution, with a W-value of 0.822 and p-value of <0.001. Although Marie's translation speed varied considerably throughout its lifecycle, caution should be applied when using translation speed solely as a predictor for U_z variability.

Regression **41** was a simple linear regression model for Marie that incorporated storm latitude as an explanatory predictor. As the only Category- 5 hurricane included in this research, the need for useful explanatory predictors is critical. The model revealed that latitude was a highly significant parameter, with a p-value of <0.001. Regression **41** per-

formed very well with an adjusted R-squared value of 0.9377. Plotted model residuals indicated a strongly non-normal distribution with skewed tails. A normality test indicated a W-value of 0.906 and p-value of <0.001, confirming the lack of a normal distribution. Thus, model results should be treated with extreme caution.

Regression **42** was a complementary simple linear regression model for Marie that incorporated longitude as the explanatory predictor. Longitude was deemed a highly significant parameter with a p-value of <0.001. The regression performed extremely well, with an adjusted R-squared value of 0.9612. A Q-Q plot of residuals indicated a non-normal distribution with skewed tails and several outliers. The Shapiro-Wilks normality test confirmed these results, with a W-value of 0.936 and p-value of 0.002, thus violating model assumptions. Like the previous storm-specific models, the most usefulness is found with the full variable models of Regressions **19** and **20**.

C.5 Odile Supplemental Regressions 43 – 47

Regression **43** was a simple linear regression model for Hurricane Odile (2014) that incorporated SST as the oceanic explanatory predictor. When considering the strong results from Regressions **21** and **22** for Odile, it was expected that predictors may also may be realistically useful. This model revealed that SST was a significant predictor, with a p-value of 0.037. However, this model performed poorly, with an adjusted R-squared value of 0.0283. Plotted residuals demonstrated a non-normal distribution, with several outliers and a skewed right tail in the data. A normality test indicated a W-value of 0.819 and p-value of <0.001. Thus, model assumptions were violated, and should be treated with caution.

Regression **44** was a simple linear regression model for Hurricane Odile that utilized UOHC as the sole explanatory predictor for along-track U_z variability. The model indi-

cated that UOHC was a highly significant predictor with a p-value of <0.001. This model performed well, with an adjusted R-squared value of 0.4578. Plotted residuals revealed a mostly normal distribution with a few outliers. A normality test confirmed that the null hypothesis was accepted, with a W-value of 0.982 and p-value of 0.108. Such results reveal that approximately 46% of the variability in along-track U_z could be explained by UOHC.

Regression **45** was a simple linear regression model for Hurricane Odile that incorporated translation speed as the explanatory predictor. The model indicated that translation speed was a highly significant parameter with a p-value of <0.001. Regression **45** performed poorly with an adjusted R-squared value of 0.1472, revealing that translation speed could explain less than 15% of variation in along-track U_z. This model suggested a somewhat normal distribution, with a slightly skewed left tail and a few outliers in the data. A normality test rejected the null hypothesis of normality, with a W-value of 0.967 and a p-value of 0.005.

Regression **46** was a simple linear regression model for Odile that used storm latitude as the explanatory predictor for along-track U_z variability. The model revealed that latitude was a statistically significant parameter with a p-value of <0.001. Regression **46** performed very well, with an adjusted R-squared value of 0.9461, indicating that almost 95% of variability in U_z could be explained by storm latitude. However, the Q-Q plot of model residuals demonstrated a strongly non-normal distribution, with an extremely skewed left tail. The Shapiro-Wilks test confirmed the non-normal distribution with a W-value of 0.936 and p-value of <0.001. Thus, model assumptions were violated and these results should be interpreted with caution.

Lastly, Regression **47** was a simple linear regression model for Odile that complements the previous model with longitude as the sole explanatory predictor. The model

demonstrated that longitude was a highly significant parameter with a p-value of <0.001. Regression **47** performed well, with an adjusted R-squared value of 0.8081. However, such results should be treated with caution. A Q-Q plot of model residuals revealed a highly skewed distribution in both tails of the data, violating the model assumption of normality. The Shapiro-Wilks normality test confirmed non-normality, with a W-value of 0.831 and p-value of <0.001. Based on these supplementary model results for Odile, little information was added regarding the usefulness of latitude, longitude, SST, and translation speed in the full regressions. Surprisingly, UOHC was found to be highly reliable within the model scheme for Odile and may benefit from further analysis

Table C.1: Summary of Regression Results. Bold values are considered extremely useful.

Name	Explanatory Variable(s)	Response Variable	# of Obs.	Adjusted R^2 Value
1 – 2012 Majors	SST	U_z	1013	0.5248
2 – 2012 Majors	UOHC	U_z	1013	0.5392
3 – 2014 Majors	SST	U_z	2301	0.0355
4 – 2014 Majors	UOHC	U_z	2301	0.0974
5 – All Majors	SST	U_z	3314	0.0975
6 – All Majors	UOHC	U_z	3314	0.1656
7 – 2012 Majors	SST, Latitude, Longitude, U_H	U_z	1013	0.6453
8 – 2012 Majors	UOHC, Latitude, Longitude, U_H	U_z	1013	0.6410
9 – 2014 Majors	SST, Latitude, Longitude, U_H	U_z	2301	0.2664
10 – 2014 Majors	UOHC, Latitude, Longitude, U_H	U_z	2301	0.2577
11 – All Majors	SST, Latitude, Longitude, U_H	U_z	3314	0.3321
12 – All Majors	UOHC, Latitude, Longitude, U_H	U_z	3314	0.3193
13 – Amanda	SST, Latitude, Longitude, U_H	U_z	81	0.8425
14 – Amanda	UOHC, Latitude, Longitude, U_H	U_z	81	0.8514
15 – Emilia	SST, Latitude, Longitude, U_H	U_z	73	**0.9955**
16 – Emilia	UOHC, Latitude, Longitude, U_H	U_z	73	**0.9960**
17 – Iselle	SST, Latitude, Longitude, U_H	U_z	125	0.9937
18 – Iselle	UOHC, Latitude, Longitude, U_H	U_z	125	0.9946
19 – Marie	SST, Latitude, Longitude, U_H	U_z	67	0.9781
20 – Marie	UOHC, Latitude, Longitude, U_H	U_z	67	0.9822
21 – Odile	SST, Latitude, Longitude, U_H	U_z	118	0.9829
22 – Odile	UOHC, Latitude, Longitude, U_H	U_z	118	0.9812

Table C.2: Summary of Supplemental Regression Results. Bold values are considered extremely useful.

Name	Explanatory Variable(s)	Response Variable	# of Obs.	Adjusted R^2 Value
23 – Amanda	SST	U_z	81	0.4378
24 – Amanda	UOHC	U_z	81	0.2076
25 – Amanda	U_H	U_z	81	0.1951
26 – Amanda	Latitude	U_z	81	0.8271
27 – Amanda	Longitude	U_z	81	0.8406
28 – Emilia	SST	U_z	73	0.8156
29 – Emilia	UOHC	U_z	73	0.5869
30 – Emilia	U_H	U_z	73	0.7386
31 – Emilia	Latitude	U_z	73	0.9695
32 – Emilia	Longitude	U_z	73	0.8955
33 – Iselle	SST	U_z	125	0.6242
34 – Iselle	UOHC	U_z	125	0.6210
35 – Iselle	U_H	U_z	125	0.0693
36 – Iselle	Latitude	U_z	125	0.9584
37 – Iselle	Longitude	U_z	125	0.9872
38 – Marie	SST	U_z	67	0.0023
39 – Marie	UOHC	U_z	67	0.2081
40 – Marie	U_H	U_z	67	0.1175
41 – Marie	Latitude	U_z	67	0.9377
42 – Marie	Longitude	U_z	67	0.9612
43 – Odile	SST	U_z	118	0.0283
44 – Odile	UOHC	U_z	118	**0.4578**
45 – Odile	U_H	U_z	118	0.1472
46 – Odile	Latitude	U_z	118	0.9461
47 – Odile	Longitude	U_z	118	0.8081

Appendix D
Sea Surface Temperature Anomalies

The following figures were obtained from the National Oceanic and Atmospheric Administration's Climate Diagnostics Bulletins, issued every month for 2014. An archive of the monthly reports dates from 1999 through the present year, and are available online at: http://www.cpc.ncep.noaa.gov/products/CDB/CDB_Archive_html/CDB_archive.shtml

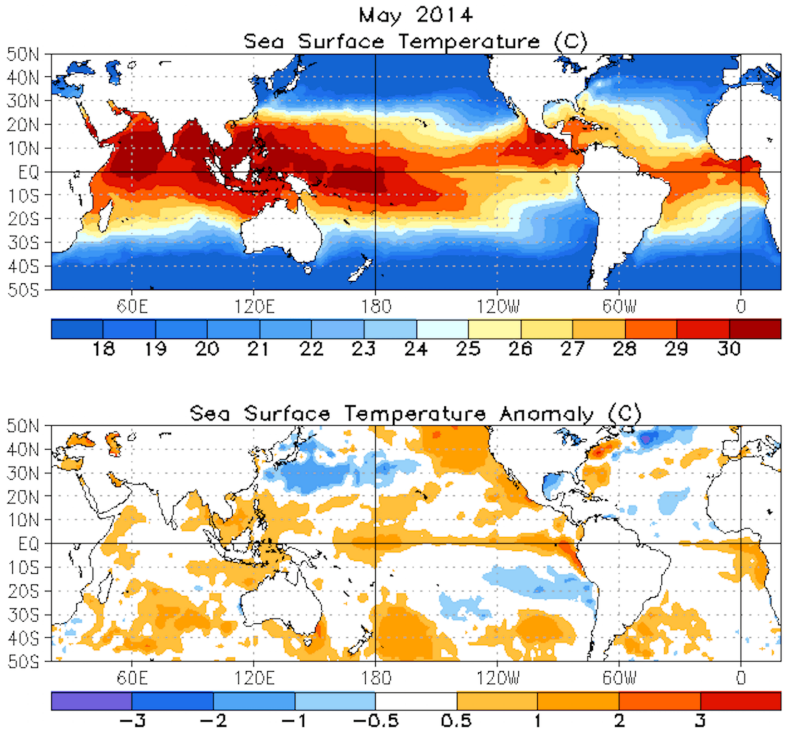

Figure D.1: Average SST and SST anomaly for May 2014.

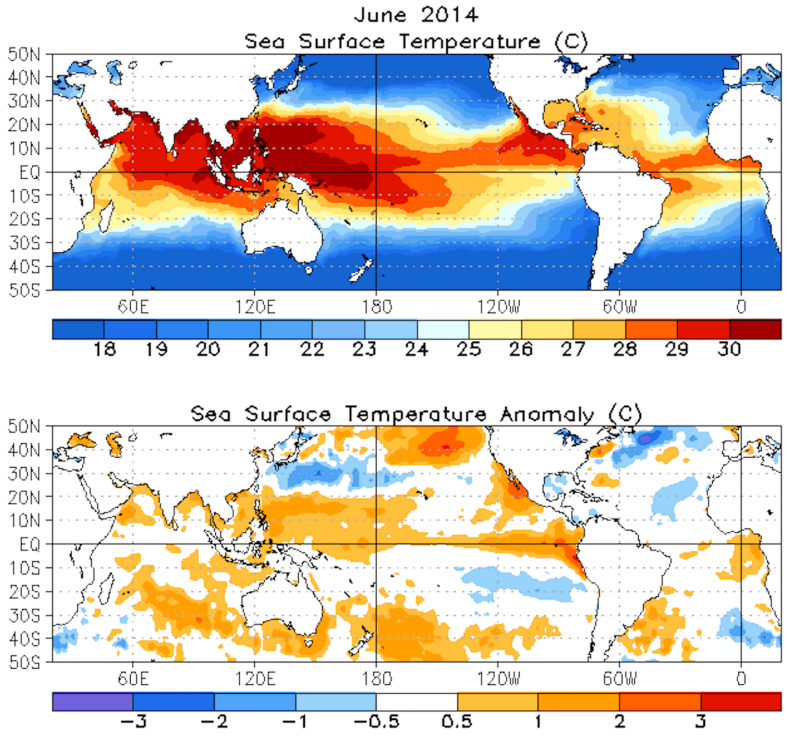

Figure D.2: Average SST and SST anomaly for June 2014.

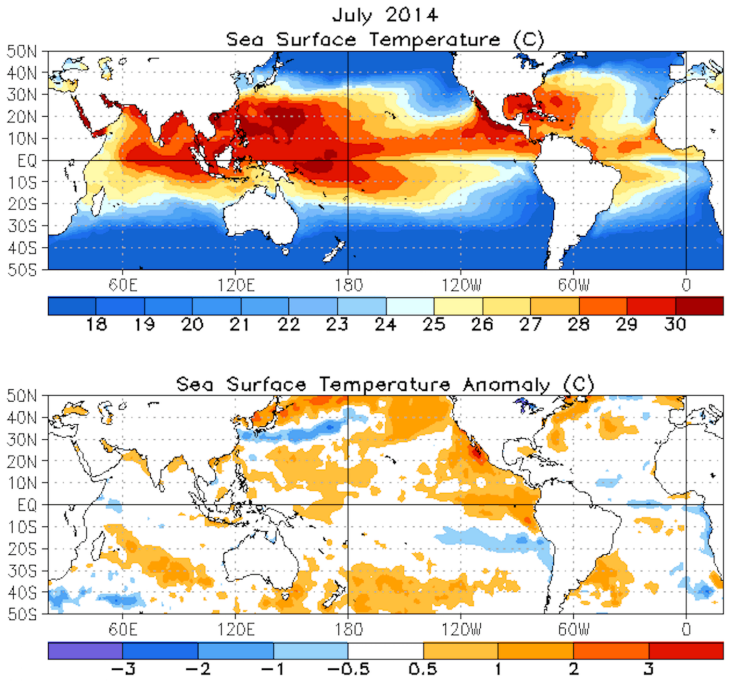

Figure D.3: Average SST and SST anomaly for July 2014.

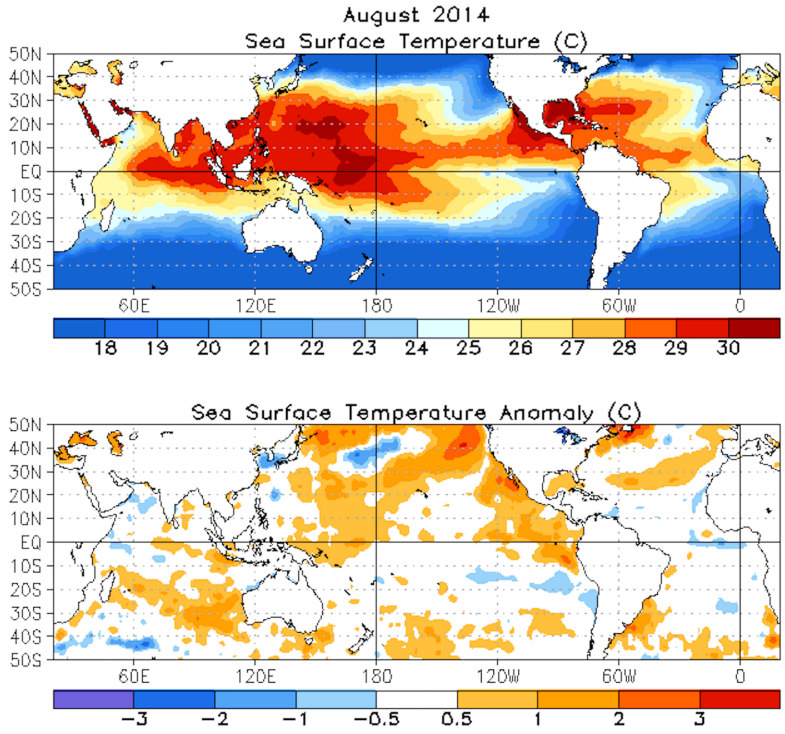

Figure D.4: Average SST and SST anomaly for August 2014.

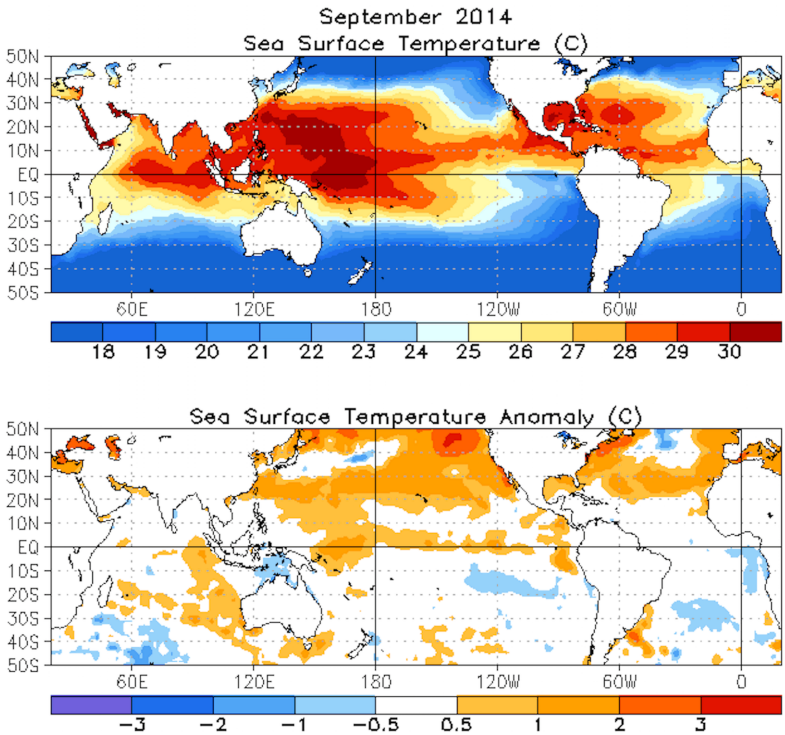

Figure D.5: Average SST and SST anomaly for September 2014.

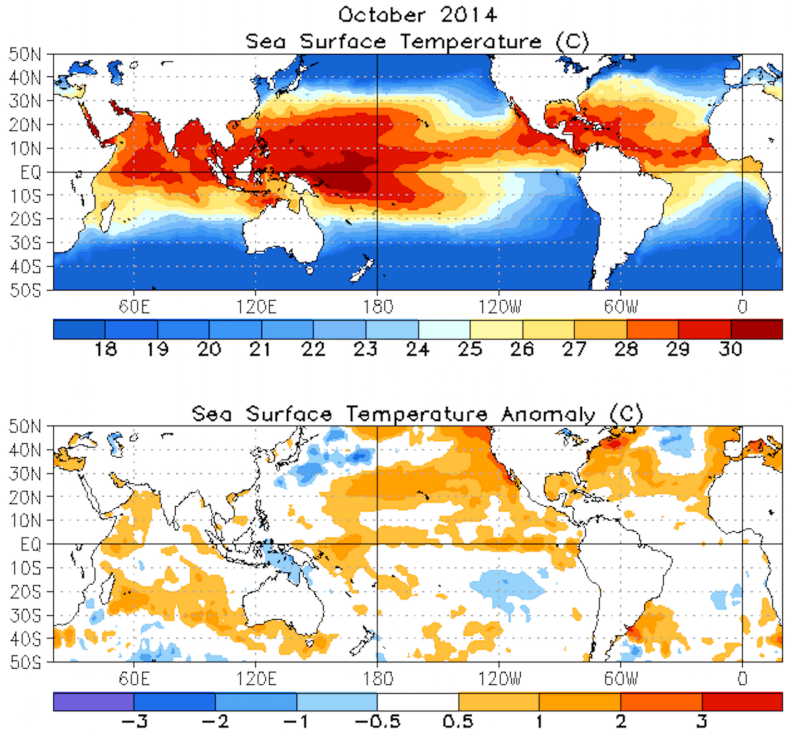

Figure D.6: Average SST and SST anomaly for October 2014.

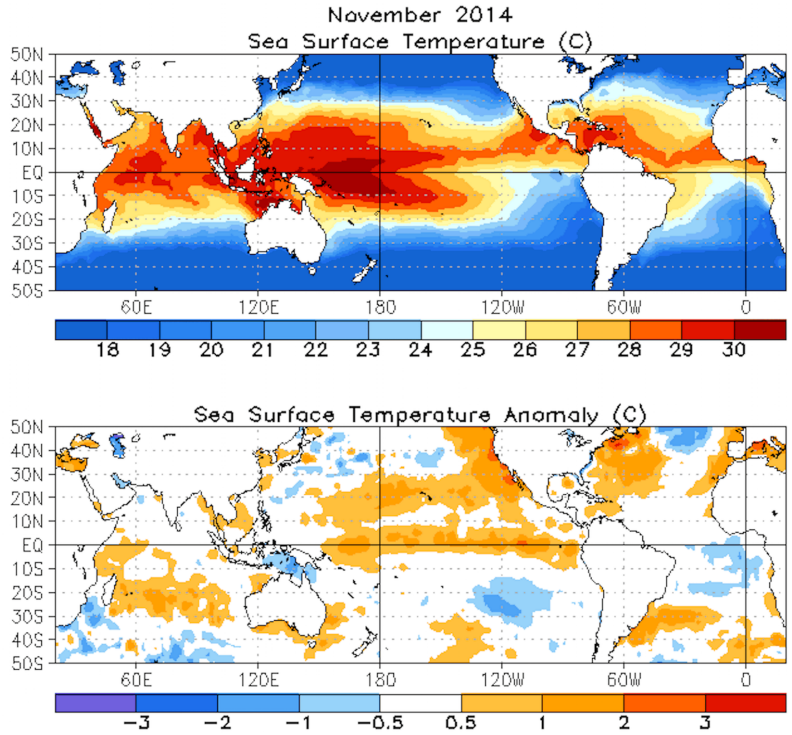

Figure D.7: Average SST and SST anomaly for November 2014.

Vita

Victoria Lauren Ford was born in Wahroonga, Australia in 1991 and attended many schools internationally before graduating from high school in Houston, TX in Spring 2010. At the University of Oklahoma, she pursued a Bachelor of Science (B.S.) in Meteorology and a Minor in Mathematics, graduating with *cum laude* honors in Spring 2014. During her undergraduate career, she worked as an Undergraduate Research Assistant at the Advanced Radar Research Center in Norman, OK. In the Fall of 2014, she started her graduate studies in the Department of Oceanography and Coastal Sciences at Louisiana State University. Her research focused on air-sea-hurricane interactions. While with LSU, she worked in the Earth Scan Laboratory and was elected to Secretary of the Coast and Environment Graduate Organization. She expects to graduate Summer 2016 with a Masters of Science (M.S.) in Oceanography and Coastal Sciences. After graduation, she will begin her Doctorate degree (Ph.D.) in Geography at Texas A&M University.